ABSTRACT

Title of Document: LATERAL LOAD PATTERNS FOR THE CONCEPTUAL SEISMIC DESIGN OF MOMENT-RESISTING FRAME STRUCTURES

Kyungha Park, Ph.D., 2007

Directed By: Assistant Professor, Ricardo A. Medina, Civil and Environmental Engineering

This study deals with the development of lateral load patterns for the conceptual seismic design of moment-resisting frame structures. The proposed lateral load patterns are based on inelastic behavior and are a fundamental component of a proposed seismic design methodology to limit the extent of structural damage in the system and distribute this damage uniformly along the height. These load patterns are expected to provide a uniform distribution of story ductility ratios when compared to the distributions obtained with moment-resisting frames designed based on the code-compliant design lateral load patterns. The implementation of the aforementioned methodology would not only distribute damage along the height of the frame, but also help avoid undesirable dynamic responses that occur once structural damage is concentrated in one or in a few stories, e.g., story drift amplifications caused by P-

delta effects. The family of structural models used in this study is composed of six to eighteen-story moment resisting frame structures with fundamental periods of vibration that vary from 0.6 s. to 3.0 s. On the input side, two basic types of ground motions are used: far-field and near-field ground motions. The proposed design lateral load patterns are a function of the fundamental period of the structural system, the target level of inelastic behavior (or damage), the total height of structures, and the frequency content of the ground motions.

LATERAL LOAD PATTERN FOR THE CONCEPTAUL SEISMIC DESIGN OF MOMENT-RESISTING FRAME STRUCTURES

By

Kyungha Park

Dissertation submitted to the Faculty of the Graduate School of the
University of Maryland, College Park, in partial fulfillment
of the requirements for the degree of
Doctor of Philosophy
2007

Advisory Committee:
Assistant Professor, Ricardo A. Medina, Chair
Professor, Aggour, Sherif M.
Professor, Amde, Amde M.
Research Professor, Fu, Chung C.
Professor, Milke, A. James

Dedication

Dedicated with my gratitude to my parents and my sisters

Namseo Park, Hekyung Lee, Youngha Park, and Chanwook Park

Acknowledgements

I would like to thank all instructors, my family, officemates, classmates, friends, and academic and support staff of the Department of Civil and Environmental Engineering at the University of Maryland.

First of all I would like to express my sincere gratitude to my advisor Dr. Ricardo A. Medina. From the beginning to the end of my Ph.D. study, he was always available when I needed his advice, and provided me with many helpful suggestions, important advice, and constant encouragement. I also wish to express my appreciation to Dr. Sherif M. Aggour, Dr. Amde M. Amde, Dr. Chung C. Fu, and Dr. James A. Milke for serving on my committee and for providing valuable comments and useful discussions.

I feel a deep sense of gratitude for my parents, Namseo Park and Hekyung Lee, who always prayed for me in a long distance from Seoul Korea and encouraged me to concentrate on my study. I would like to thank my sisters and brother-in-law: Youngha Park, Chanwook Park, and Kyuwon Kyung, who always cheered me by phone as well as mail and took care of our family responsibilities. Without their love and support, this journey would not be easy at all.

I would like to thank my former officemates Dr. Ragunath Sankaranarayanan and Dr. Antonio Rigato now who work as professionals for their kind help and invaluable discussions about our research problems. I would also never forget the share of our good and bad times together during the last several years in College Park.

I wish to express my cordial appreciation to Bill Mercado and Candi Anderson who advised me during my internship at Mercado Consultant Inc. I also

thank Dr. Jimmy Yeung, who is the head of Hazard Mitigation Department at Greenhorne & O'Mara (G&O), for his kind support and understanding while I was finishing my dissertation.

I would like thank my uncles Kyusik Lee and Kyuyoung Lee and their families for their constant loving support. I also would like to say big 'thank you' to Magnus Eisele for his loving care and thoughtful understanding. Lastly, I am thankful to my former advisors Dr. Pedro Albrecht and Dr. Soontek Oh; and to all my friends and relatives for their direct and indirect help during my study. Thank you all!

Table of Contents

List of Figures

List of Tables

1 INTRODUCTION

1.1 BACKGROUND AND MOTIVATION

In the United States, lateral-load resisting systems for regular structures may be designed based on the *Equivalent Lateral Force* (ELF) procedure (NEHRP 2003, IBC 2006, and UBC 1997). A fundamental component of the ELF procedure is the utilization of design lateral load patterns to determine the strength, and to some extent, the stiffness characteristics of the structure. These code-compliant design lateral load patterns were established based on the dynamic behavior of elastic structural systems, i.e., story shear demand distributions. Thus, the design lateral load patterns of the ELF procedure do not explicitly account for the inelastic response of the structural system. If the structure is expected to experience significant levels of inelastic behavior, code-compliant lateral load distributions may not provide an accurate representation of the story shear demands imposed on the structural system. Therefore, a designer has certain control on the amount of the total (global) structural damage experienced by the structure based on an appropriate selection of stiffness, strength, and ductility (detailing) requirements in the conceptual seismic design stages of a project. Nevertheless, a designer has limited control over the distribution of damage, which is mainly caused by load redistribution effects characteristic of inelastic structural responses.

In a performance-based earthquake engineering context (see Figure 1.1), the conceptual seismic design of a building or facility is critical for the determination of global strength, stiffness, and ductility requirements necessary to achieve predefined

performance objectives. At this stage of the design process, it is important to estimate the properties of an initial design that will form the basis of an iterative performance-based seismic design process. This iterative process will be ultimately completed once the final design complies with the performance targets of interest. This compliance is evaluated based on seismic performance assessment strategies/criteria. As stated by Krawinkler et al. (2006), a good design is based on concepts that incorporate performance targets up front in the design process, so that performance assessment becomes more of a verification process rather than a design improvement process. In addition, a poor initial conceptual design likely will never become a good design even though the design fulfills the performance targets to some extent.

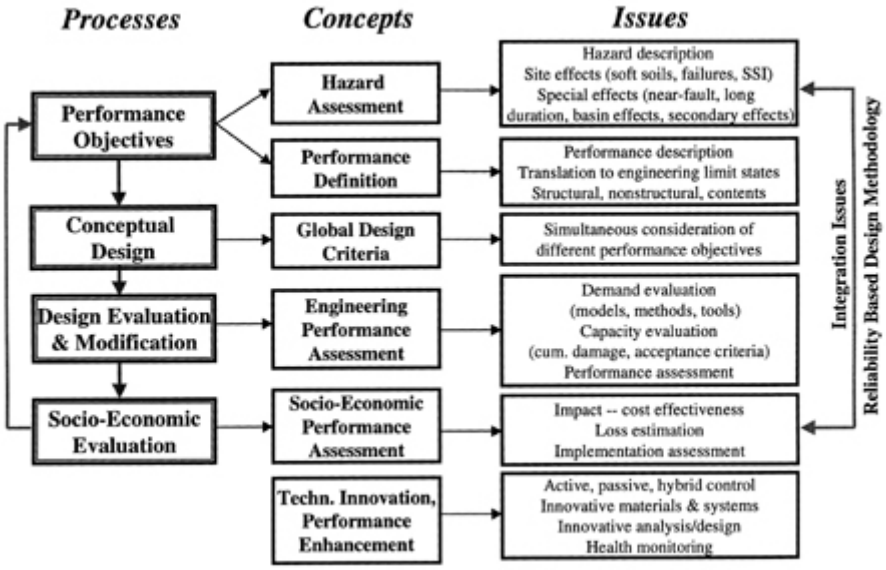

Figure 1.1 Process of performance-based earthquake engineering (Krawinkler 1999)

The design load patterns of the ELF procedure are unable to provide such target performance for moment-resisting frame structures. For instance, Medina (2004) concluded that the distribution of structural damage over the height of the

frame with given fundamental period of vibration (T_1), height (H), and relative intensity ($RI = [Sa(T_1)/g]/\gamma$, where $Sa(T_1)/g$ is the 5% damped pseudo-spectral acceleration at T_1, and $\gamma = V_y/W$ is the based shear coefficient, i.e., design based shear normalized by the seismically effective weight) is very sensitive to the design story shear strength pattern (e.g., patterns 'C' and 'P') and the level of inelastic behavior (e.g., RI = 2 and 4) as shown in Figures 1.2. Each story shear strength pattern is a representative distribution of forty story shear strength values of a 15-story frame structure exposed to a set of ground motions utilized by Medina (2004). Therefore, the distribution of damage along the height of a frame for a given T_1, H, and RI is significantly affected by the design load pattern. In this context, the design load pattern is distinct from the design floor loads. The load pattern designates the relative distribution of the design floor loads without any absolute quantities; whereas, the design floor loads are the combination of the load patterns multiplied by the absolute total strength (e.g., base shear strength) of the system.

Medina (2004) initially introduced new design load patterns to achieve the same amount of structural damage in all stories by tuning structural strength according to design lateral loads. It was assumed that the first mode shape was straight line for all structural models utilized by Medina 2004. However, this study utilizes structural models with a parabolic first mode shape which is a more realistic representation of the deformation profiles experienced by shear-type frame structures. In addition, this study further concentrates on developing the design lateral load patterns for a practical use in the conceptual seismic design stages of a project. The concept of *uniform damage* is still the cornerstone of this study, which indicates only

structural damage measured by using the target story ductility ratio (μ_T). The target story ductility ratio is the ratio of a maximum story drift to a story yield drift and a target performance level of interest in this study.

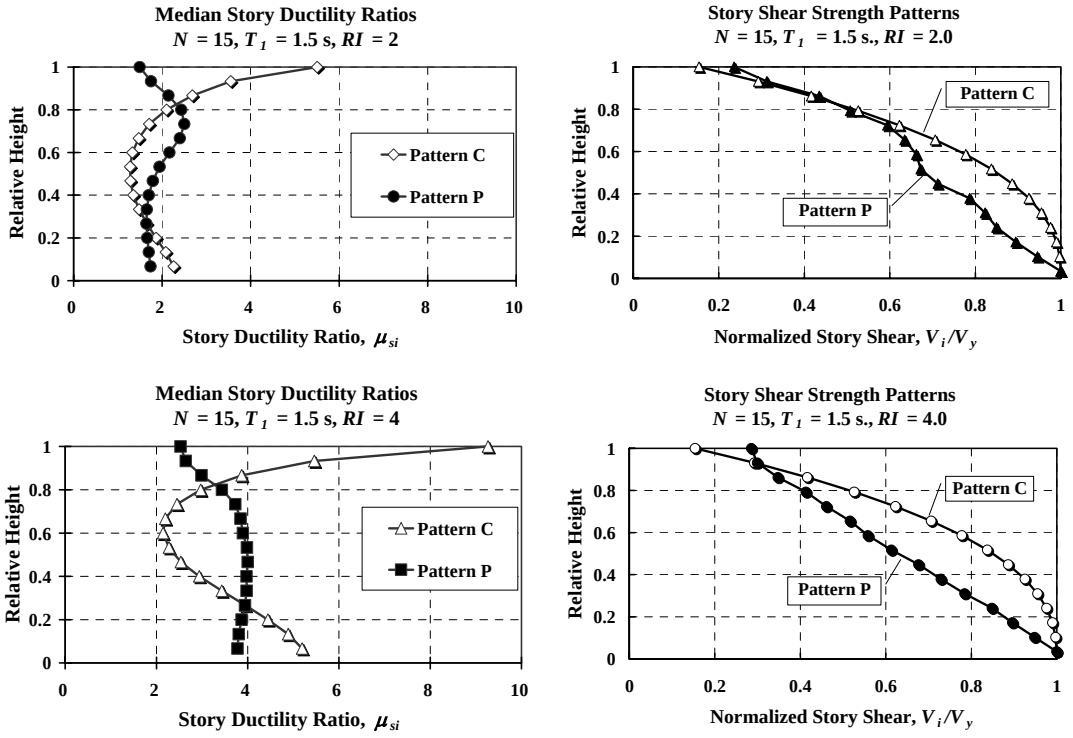

Figure 1.2 Sensitivity of story ductility ratio profiles for a given frame model, *N* = 15, T_1 = 1.5 s., *RI* = 2.0 and 4.0, according to different story shear strength patterns C and P

Many studies have been conducted to develop new design procedures for special moment resisting frames by proposing improved design load patterns. Leelataviwat et al. (1999) developed a new seismic design procedure, using the concept of energy balance applied to moment-resisting frames with a pre-selected yield mechanism. Lee and Goel (2001) also developed a procedure based on plastic design and proposed new seismic lateral load patterns by using high-rise moment-resisting frames (e.g., up to 20-story) with the same concept which Leelataviwat et al. (1999) proposed. Both studies were based on the MDOF inelastic concept of structural behavior and showed quite an improvement to control story drift demands. However, they used SDOF response modification (R_μ) as well as structural ductility factors and dealt with a limited number of ground motions. Their proposed load pattern fundamentally follows the shape of the lateral load pattern in the code provisions (i.e., UBC 1994, 1997) and is a function of mass and the fundamental period of the structure. Moghaddam and Hajirasouliha (2006) also proposed seismic load patterns in which the effects of fundamental periods, target ductility demand, damping ratio, and seismic excitations for truss-like structures and shear-buildings were incorporated. Chao et al. (2007) continued to use the same format of lateral load patterns proposed by Lee and Goel (2001) with a large number of steel moment-resisting frames subjected to more ground motions. P-delta effects were ignored in these previous studies, which may significantly affect the inelastic behavior and dynamic instability of the structure. The procedure developed in this study constitutes a unique approach to limit the extent of structural damage and distribute it uniformly along the height as a function of the target performance level of interest.

1.2 OBJECTIVES AND OUTLINE

The main objective of this study is to develop improved design lateral load patterns for the conceptual design of moment-resisting frame structures. These design lateral load patterns are based on inelastic behavior and are a fundamental component of a proposed seismic design methodology to limit the extent of structural damage in the system and distribute this damage uniformly along the height. These load patterns are expected to provide a uniform distribution of story ductility ratios and a more uniform distribution of story drift ratios when compared to the distributions obtained with moment-resisting frames designed based on code-compliant design lateral load patterns.

Based on the main objective, this study consists of the four following phases:

(1) Development of a procedure to estimate the required shear strength distribution to achieve the same story ductility ratio in all stories for a given system and ground motion.

(2) Establishment of new proposed design lateral load patterns for moment-resisting frames.

(3) Establishment of a conceptual seismic design methodology based on uniform structural damage.

(4) Verification of the proposed conceptual seismic design methodology by comparison of story ductility and drift ratios with structures with member strenghts based on the ELF procedure.

The proposed design lateral load patterns are a function of the fundamental period of the structural system, the target level of inelastic behavior (or damage), and

the frequency content of the ground motions. The performance target of interest for designs based on the proposed lateral load patterns is that of life safety (see Figure 1.3). Based on the fundamental period of a structural system (i.e., T_1 = 0.6 ~ 3.0 s.), the target inelastic levels (i.e., μ_T = 1, 2, 3, 4, 5) and numerous ground motion inputs (e.g., far-field and near-field) utilized in this study, the four phases of this study are presented and discussed in Chapters 3, 4, 5, and 6, respectively.

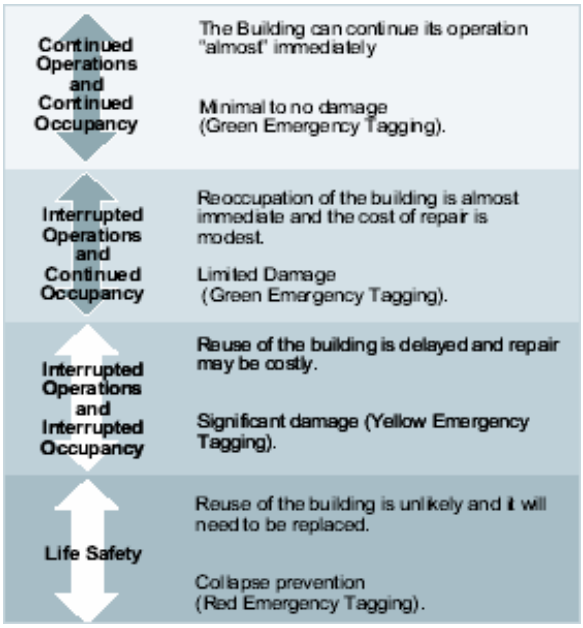

Figure 1.3 Recommended performance choices with discrete levels overlaid (ATC 58-2, 2002)

This dissertation consists of six chapters and one appendix:

Chapter 2 presents a review of the current design lateral load patterns utilized in Europe, Japan, and Mexico, as well as the recent code procedures in the United States (i.e., NEHRP 2003, IBC 2006, UBC 1997) for special moment-resisting frames. The deficiencies and strengths of current code procedures are reviewed and discussed.

Chapter 3 discusses the first phase among four phases. First, the selected ground motions (i.e., ordinary and near-fault) and structural models with various fundamental periods (i.e., T_1 = 0.6 ~ 3.0 s.) are introduced along with the response parameters utilized in this study. The first part of this chapter presents the model of proposed load patterns for various combinations of the total height of structure, the fundamental period of a structure, and the level of inelasticity. The load patterns proposed in this chapter are only applicable to one particular frame, one ground motion, one fundamental period, and a given level of inelasticity.

Chapter 4 presents a general model for proposed load patterns as a function of H, T_1, and μ_T. Statistical regression analyses are utilized to apply the proposed load patterns to frames with different heights (i.e., H = 21.95 m ~ 65.84 m), fundamental periods (i.e., T_1 = 0.6 s. ~ 3.0 s.), and levels of inelasticity (i.e., μ_T = 1 ~ 5). These equations for the proposed load patterns are used in the verification study in Chapter 6.

Chapter 5 presents a proposed conceptual seismic design methodology based on the use of the design lateral load patterns discussed in Chapter 4. The methodology consists of four steps to determine the required story shear strengths based on the relationships between the ground motion hazard at the site, the relative strength, the target story ductility ratio, and the fundamental period of the structure.

Chapter 6 presents results to demonstrate the effectiveness of the methodology introduced in Chapter 5 and also evaluate how designs based on the proposed load patterns compare to those based on the ELF of current U.S. design procedures for a given average structural damage.

Chapter 7 summarizes the main conclusions of this study. Suggestions for future work are also presented. Appendix A presents the verification results for a 15-story generic, regular frame designed based on the U.S. code provision (IBC 2006), and the codes from Europe and Japan, as well as the design load pattern proposed in this study. 174 earthquake ground motions corresponding to NEHRP (NEHRP 2003) Site Class A, B, C, and D are utilized to provide verification results.

2 REVIEW OF CURRENT SEISMIC DESIGN PROCEDURES

2.1 INTRODUCTION

The ELF procedure of seismic code provisions in the United States is based on the notion that structural elements are designed using estimates of expected elastic peak inertial floor load demands. The absolute value of the total design lateral load is estimated from reduced elastic demands experienced by the structure. The distribution of floor loads is determined based on elastic dynamic analysis concepts that are meant to account for the contribution of various modes to the overall structural response. This design approach is especially suitable for relatively small but frequent earthquakes to limit damage to acceptable levels once the system experiences relatively small levels of inelastic behavior. However, when structures are exposed to severe ground shaking, structural elements may be prone to yielding, and consequently, experience significant levels of inelastic behavior. The effects of inelastic behavior on the distribution of peak floor loads are not explicitly accounted for in current US seismic code procedures. This Section provides a review of the equivalent lateral force procedure as described in documents such as NEHRP 2003, UBC 1997, and IBC 2006 and also evaluates seismic lateral force procedures from various places such as Europe, Japan, and Mexico. The objective is to identify the current state of practice and highlight the limitations of such approaches. The response of frame structures designed based on the different load patterns are compared and presented in Appendix A.

2.2 CURRENT PROCEDURES IN THE UNITED STATES

2.2.1 NEHRP (National Earthquake Hazard Reduction Program) 2003-Equivalent Lateral Force Procedure

Estimate of Seismic Base Shear

In the Equivalent Lateral Force Procedure, the total seismic-induced lateral force applied in each orthogonal direction for a three-dimensional structure is equal to the seismic base shear determined in accordance with the following equation (NEHRP 2003):

$$V = C_s \cdot W \qquad [2.1]$$

where C_s is the seismic response coefficient and W is the total dead load and applicable portion of other loads. The applicable portion of other loads includes a minimum of 25% of the floor live load applicable in areas used for storage except for public garages and open parking structures, partition weight or a minimum weight of 10 psf of floor area or greater, total operating weight of permanent equipment, and snow load only exceeding 30 psf (up to 30 psf is negligible).

The seismic response coefficient, C_s, is given by the following expression, Equation 2.2:

$$C_s = \frac{S_{DS}}{R/I} \qquad [2.2]$$

where S_{DS} is the design spectral response acceleration parameter in the short period range. R is the response modification factor (8 for special steel moment resisting frame), and I is the occupancy importance factor (1.0, 1.25, and 1.5 for seismic group

1, 2, and 3, respectively). C_s should not exceed $\frac{S_{D1}}{T(R/I)}$ for $T \le T_L$ and $\frac{S_{D1}T_L}{T^2(R/I)}$ for $T > T_L$ but should not be taken less than 0.01 and $\frac{0.5 \cdot S_1}{R/I}$ when $S_1 \ge 0.6g$ where S_{D1} is the design spectral response acceleration parameter at a period of 1.0 second, T is the fundamental period of the structure (s), and T_L is long-period transition period (s) shown in the US seismic hazard maps provided with the NEHRP 2003 document. The value of S_{DS} and S_{D1} can be obtained as shown below:

$$S_{DS} = \frac{2}{3} \cdot S_{MS} = \frac{2}{3} \cdot F_a \cdot S_s \qquad [2.3]$$

$$S_{D1} = \frac{2}{3} \cdot S_{M1} = \frac{2}{3} \cdot F_v \cdot S_1 \qquad [2.4]$$

where S_{MS} and S_{M1} are the maximum considered earthquake spectral response acceleration parameters which can be adjusted for site class effects; F_a and F_v are site coefficients; and S_S and S_1 are the mapped maximum considered earthquake spectral response acceleration parameters.

It is important to note that estimates of the seismic base shear are obtained by dividing the expected peak elastic response by a response modification factor, *R*, which accounts for the expected level of ductility (inelastic behavior) in the structure. This implies that the total (global) strength of structures is determined by considering different levels of inelastic behavior in an approximate and indirect manner through the parameter *R*, which is not a function of the fundamental period of the structure.

Distribution of Seismic Lateral Forces

The lateral floor load, F_x, is given by the following equation:

$$F_x = C_{vx} \cdot V \qquad [2.5]$$

$$C_{vx} = \frac{w_x h_x^{\,k}}{\sum_{i=1}^{n} w_i h_i^{\,k}} \qquad [2.6]$$

where C_{vx} is vertical distribution vector; V is the total design lateral force or shear at the base of the structure; w_i and w_x are the portion of the total gravity load of the structure located at the level i or x; h_i and h_x is the height from the base to the level i or x; and k is an exponent related to the effective fundamental period of the structure (k = 1 for structures having a period of 0.5 s. or less, k = 2 for structures having a period of 2.5 s. or more, k is determined by linear interpolation between 1 and 2 for structures having a period between 0.5 and 2.5 s.).

When k is equal to 1, this lateral force pattern corresponds to an inverted triangular lateral load distribution. While k = 2, it corresponds to a parabolic lateral load distribution with its vertex at the base (see Figure 2.1). These load patterns are obtained by assuming that the first mode is a straight line. When k = 1, the response of the building is assumed to be controlled primarily by the first mode. When k = 2, the response is assumed to be influenced by higher mode effects. It is important to note that the shape of these load patterns is influenced by the fundamental period of vibration of the structural system, as well as the distribution of mass and stiffness over the height of a structure. The accuracy of the lateral force distribution is much improved by this procedure in structures having only minor irregularity of mass or stiffness over the height (BSSC 2003). The relative distribution of these vibration modes depends on the mass and stiffness distributions, and the level of inelastic behavior is not accounted for in the distribution of lateral loads.

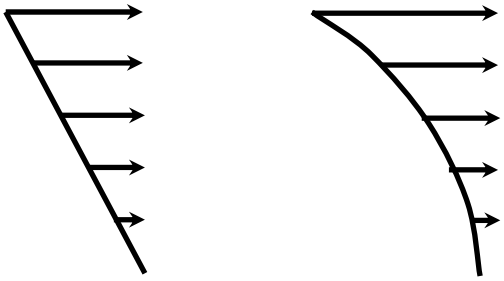

Figure 2.1 Effect of the exponent k on the distribution of seismic lateral load patterns based on NEHRP 2003

2.2.2 IBC (International Building Code) 2006 – Equivalent Lateral Force Procedure

Estimate of Seismic Base Shear

In the Equivalent Lateral Force Procedure, the lateral forces applied in each direction should sum to a total seismic bases shear determined in accordance with the following equation:

$$V = C_s \cdot W \qquad [2.7]$$

where C_s is the seismic response coefficient and W is the total dead load and applicable portion of other loads, which are the same conditions as NEHRP 2003. The seismic response coefficient, C_s, is given by the following expression:

$$C_s = \frac{S_{DS}}{R/I} \qquad [2.8]$$

where all the parameters were defined in Section 2.2.1. C_s should not exceed $\frac{S_{D1}}{T(R/I)}$ and should not be taken less than $0.044 S_{DS} I$. There is no criteria of C_s for long-

period structures (i.e., $T > T_L$) as recommended by NEHRP 2003. S_{D1} is the design spectral response acceleration parameter at a period of 1.0 second, T is the fundamental period of the structure in seconds. The value of S_{DS} and S_{D1} can be obtained as shown in Section 2.2.1. The limitations, briefly discussed in Section 2.2.1, regarding the estimation of the seismic design base shear based on the NEHRP 2003 provisions are equally applicable to the IBC 2006 provisions.

Distribution of Seismic Lateral Forces

The distribution of seismic lateral forces based on the IBC 2006 is identical to that obtained following the NEHRP 2003 provisions. Thus, the limitations of the IBC 2006 approach are consistent with those identified for the NEHRP 2003 provisions as explained in Section 2.2.1.

2.2.3 UBC (Uniform Building Code) 1997 – Static Force Procedure

Estimate of Seismic Base Shear

The total design base shear is given by the following formula:

$$V = \frac{C_v I}{RT} \cdot W \qquad [2.9]$$

where C_v is the seismic coefficient depending on soil type and seismic zones of the site; R is the structural system coefficient representative of the inherent overstrength and global ductility capacity of lateral force-resisting systems (this is in concept analogous to the R factor of the NEHRP 2003 and IBC 2006 provisions); and W is the total seismic dead load and applicable portions of live load.

The total design base shear need not exceed:

$$V = \frac{2.5C_a I}{R} \cdot W \qquad [2.10]$$

where C_a is the seismic coefficient that is determined as a function of soil type and seismic zone factor. The total design base shear should be equal to or greater than:

$$V = 0.11C_a IW \qquad [2.11]$$

In addition, for Seismic Zone 4, the total design base shear should not be less than:

$$V = \frac{0.8ZN_v I}{R} \cdot W \qquad [2.12]$$

where N_v is the near-source factor.

As stated before, the structural system factor, R, is similar to the response modification factor, R, indicated in NEHRP 2003. This implies that the base shear demands are estimated by reducing the expected peak elastic lateral load demands by the factor R in order to consider inelastic levels of interest. In the UBC 1997 provisions, the value of R for special moment-resisting steel frame is equal to 8.5, whereas the value of R for the same frame according to NEHRP 2003 and IBC 2006 is equal to 8.

Distribution of Seismic Lateral Forces

The seismic base shear as a function of the lateral floor loads is given by:

$$V = F_t + \sum_{i=1}^{n} F_i \qquad [2.13]$$

where F_t is the concentrated force at the top of the structure and shall be determined from the following formula:

$$F_t = 0.07 \cdot T \cdot V \qquad [2.14]$$

F_t needs not exceed *0.25V* and may be considered as zero when *T*, the fundamental period of vibration, is 0.7 *s.* or less. The remaining portion of the base shear should be distributed over the height of the structure based on the following expression:

$$F_x = \frac{(V - F_t)w_x h_x}{\sum_{i=1}^{n} w_i h_i} \qquad [2.15]$$

Structural members shall be designed based on the strength and displacements determined by forces F_x and F_t distributed along the height. The lateral load pattern for UBC 1997 is quite different from NEHRP 2003 and IBC 2006 because of the concentrated load at the top as seen in Figure 2.2. However, as it is the case with NEHRP 2003 and IBC 2006, the relative distribution of lateral loads over the height is also based on elastic dynamic analysis concepts without considering the expected level of inelastic behavior in the structure.

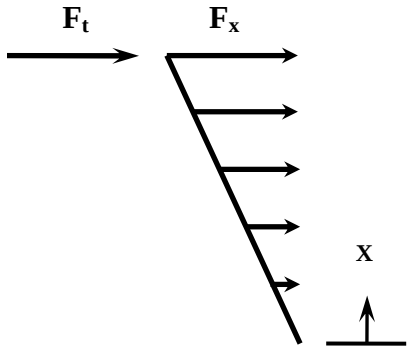

Figure 2.2 Seismic lateral load distribution based on UBC 1997

2.3 STANDARDS FROM OTHER PARTS OF THE WORLD

2.3.1 EuroCode 8 (EC8)

EuroCode 8 (EC8) is a European Standard (EN) and introduces various innovative European seismic design practices for steel buildings (i.e., the capacity design criteria, seismic force reduction factors explicitly correlated with expected ductility of the structure, and others). According to the lateral force method of analysis of EC8, which is equivalent to the ELF (EC8), the ultimate lateral strength of the structure has to be large enough to resist the reference seismic forces representative of strong ground motions. The seismic response of the building may be evaluated by statically applying a set of horizontal forces to the story masses, if the structure itself sufficiently meets the criteria for regularity in elevation and has a fundamental period not larger than $4T_C$ and 2.0. The T_C is one of the characteristic periods of the response spectrum depending on the soil type and equal to 0.4 s. and 0.5 s. for soil types A (hard soils, $V_{S,30} > 800$ m/s) and B (soils with intermediate characteristics in between hard and soft soils, $V_{S,30} = 360$ m/s), respectively. For regular moment-resisting frames, the total seismic design base shear F_b is given by

$$F_b = S_d(T_1) \cdot m \cdot \lambda \qquad [2.16]$$

where m is the total mass of the building. The parameter m is estimated by taking into account the presence of the dead gravity load and a fraction of the live gravity load; S_d is the ordinate of the design spectrum corresponding to the fundamental period of the building T_1; and λ is a reduction factor of the seismic forces based on the effective modal mass of the fundamental mode of vibration. Thus, the value of λ is equal to

0.85 if the building has more than two stories and $T_1 < 2\ T_C$; otherwise, λ is equal to 1.0. The design spectrum parameter S_d is obtained by reducing the ordinates of the reference elastic spectrum based on the behavior factor q. The ductility can be estimated by using this factor q, which is equal to 4.0 and 6.5 for moment-resisting frames corresponding to medium and high ductility classes, respectively. Thus inelasticity is also considered according to the ductility classes when the total seismic design base shear is determined.

The seismic forces F_i, distributed along the height according to an inverted triangular distribution, are evaluated as follows:

$$F_i = F_b \cdot \frac{z_i \cdot m_i}{\sum_{j=1}^{N} z_j \cdot m_j} \qquad [2.17]$$

where N is the number of stories, and m_i and z_i are the i-th floor mass and height measured from the foundation level, respectively. The distribution of lateral loads over the height is a function of floor mass and height, which is based on elastic dynamic analysis concepts without considering the expected level of inelastic behavior in the structure.

2.3.2 Japanese Seismic Design Code (BCJ)

The Japanese seismic design code (BCJ) was adopted in 1981. For regular moment-resisting frame up to 60 m, the seismic design procedure is mostly limited to the static-based design approach which excludes peer-review.

The seismic design shear force in the i-th story, Q_i, is calculated as

$$Q_i = C_i \cdot W_i \qquad [2.18]$$

where W_i is the reactive weight above the *i*-th story, and C_i is the seismic coefficient at each story level. The seismic coefficient at each level C_i is determined as the product of four variables:

$$C_i = Z \cdot R_t \cdot A_i \cdot C_0 \qquad [2.19]$$

where Z represents the seismic zone (e.g., 1.0 for the Kobe region), R_t defines the spectral shape that varies as a function of soil type and $\frac{0.64}{T}$ for hard soil (Type 1) and C_0 represents the peak ground acceleration. Except for wood structures on soft subsoil, C_0 is set equal to 1.0 for the strong ground motions (having a probability of exceedance equal to 10% in 10 years, i.e. a return period equal to 475 years). The value of A_i defines the vertical distribution of seismic force in the building (see Equation 2.20) and takes into account the higher mode effects as a function of T_1 as shown in Figure 2.3.

$$A_i = 1 + \left(\frac{1}{\sqrt{\alpha_i}} - \alpha_i\right) \cdot \frac{2T_1}{1 + 3T_1} \qquad [2.20]$$

$$\alpha_i = \sum_{j=1}^{N} \frac{w_j}{W} \qquad [2.21]$$

where w_j is the weight in *j*-th floor.

For a direct and explicit evaluation of strength and ductility, the ultimate lateral load capacity is computed using plastic analysis. Ultimate seismic demands Q_u are estimated as

$$Q_u = D_s \cdot F_{es} \cdot Q_i \qquad [2.22]$$

where the value of F_{es} is the shape factor according to the distribution of the story stiffness along the height and eccentricity of the plane. For regular frames, F_{es} is

equal to 1.0. To take into account structural characteristics, the factor D_s is established as a function of member ductility for moment-resisting frames. The ductility class depends on the width-to-thickness ratio of beams and columns in moment-resisting frames. The value of D_s is in the range from 0.25 (for members with excellent ductility) to 0.4 (for members with poor ductility). With that said, the ductility class represents the inelastic level of interest, and it is considered when determining the total base shear strength but not the shape of lateral load patterns.

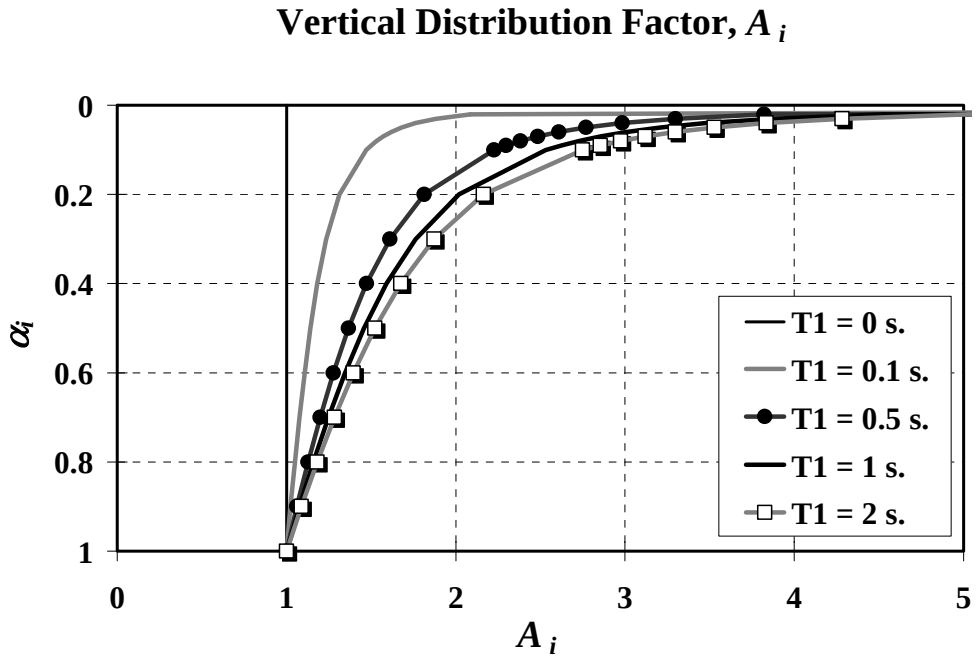

Figure 2.3 Vertical distribution factor A_i

2.3.3 Mexico City Building Code 2003 – Static Method Procedures

The most widely known seismic regulations in Mexico are those of Mexico City. For regular moment-resisting buildings, the static method procedures are mostly applied to the design regular buildings with a height lower than 40 m in the site

classification Zone 1 (i.e., hard ground). The total base shear force V_O as a ratio of the total structural weight W_O is calculated as:

$$\frac{V_0}{W_0} = \frac{c}{Q'} \geq a_0 \qquad [2.23]$$

where, c and a_0 values are a seismic coefficient and horizontal peak-ground acceleration, respectively. Reduction factor Q' can be obtained from following equations:

$$Q' = Q \qquad \text{for } T \text{ unknown or } T \geq T_a \qquad [2.24]$$

$$Q' = 1 + (T / T_a) \cdot (Q - 1) \qquad \text{for } T < T_a \qquad [2.25]$$

where T is a first mode period; and Q can take values of 1, 1.5, 2, 3, and 4 according to structural types, structural materials, and ductility of elements and components. For example, for frames or dual structural types of steel, concrete or steel-concrete composites with frames able to resist 50% of acting seismic force, the value of Q is equal to 4; the Q value is equal to 2 if the structural type is a prefabricated concrete building. Thus, the reduction factor Q is larger for structures designed with elements of high ductility. This implies that there are specific requirements to achieve either high or moderate ductility on the structural members and components for each structural material to determine the total base shear force V_O.

The seismic forces F_i, distributed along the height on each floor of weight W_i (story weight) and height h_i (story height) are given as:

$$F_i = V_0 \cdot \frac{W_i \cdot h_i}{\sum_{j=1}^{N} W_j \cdot h_j} \qquad [2.26]$$

By taking the value of the fundamental period of vibration of the structure into account, the fundamental period T can be calculated by Rayleigh's method as follows:

$$T = 2\pi\sqrt{\frac{\sum W_i \cdot x_i^{\,2}}{g \cdot \sum F_i \cdot x_i}} \qquad [2.27]$$

where x is the shift level of the structure in the direction of force, and g is the acceleration of gravity.

If $T \le T_b$, then $V_0/W_0 = (a/Q')$ and F_i is recalculated with the above equation. However, if $T > T_b$, then the force F_i at each level is the following:

$$F_i = V_0 \cdot (k_1 \cdot h_i + k_2 \cdot h_i^{\,2}) \cdot (a/Q') \qquad [2.28]$$

where $a \ge a_0$ and $k_1 = [1 - 0.5 \cdot r \cdot (1-q)] \cdot \frac{\sum W_i}{\sum W_i \cdot h_i}$, $k_2 = 0.75 \cdot r \cdot (1-q) \cdot \frac{\sum W_i}{\sum W_i \cdot h_i^{\,2}}$, $q = (T_b/T)^r$, where T_b and r are equal to 1.35 and 1.0 in Zone 1 (hard ground), respectively. As the fundamental period of vibration is longer, the value of q becomes smaller, which is the main variable for k_1 and k_2 equations. Since lateral load patterns obtained by Equation 2.28 depend on k_1 and k_2, the load patterns are a function of the fundamental period, site classification, and the weight of structures. However, the inelastic level of structural performance is not considered to determine the seismic lateral load patterns for the static method procedures.

Figure 2.4 shows all the lateral load patterns introduced in this chapter: IBC 2006, UBC 97 (U.S.), EC 8 (Europe), BCJ (Japan), MEXICO 2003. It is interesting to see that all five load patterns shown in Figure 2.4 are comparable except BCJ and UBC 97, which show very similar patterns with a large force at the top. As a function

of the fundamental period of vibration, the shape of IBC 2006 load pattern for this flexible 9-story frame with the fundamental period of 1.8 s. is quite different from that of EC 8 particularly in the upper stories. In addition, the load pattern of Mexico 2003 is very close to the EC8 load pattern if the fundamental period of the structure is less than or equal to 1.35 for Zone 1.

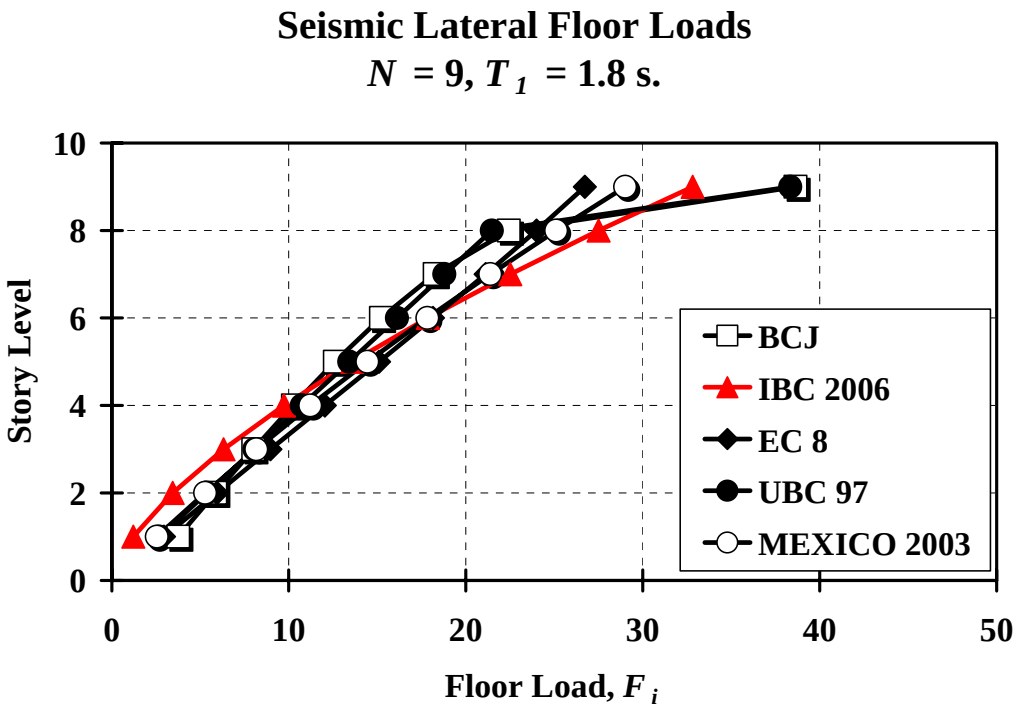

Figure 2.4 Seismic lateral load patterns of various code provisions for a regular 9-story frame with T_1 = 1.8 s

2.4 SUMMARY

- The expected level of ductility in the structure is implicitly accounted for in the seismic base shear, obtained by dividing the expected peak elastic strength (base shear) demand by the response modification factor *R*, the behavior factor *q*, and the reduction factor *Q*. These factors correspond to

U.S. code provisions (i.e., NEHRP 2003, IBC 2006, UBC 1997), EuroCode (EC8), Japanese seismic design code (BCJ), and the Mexico City building code (Mexico 2003), respectively. Therefore, all the building codes reviewed in this study contain specific requirements to achieve some level of inelasticity for the design of structural members and components. However, these requirements mainly influence the global strength of the system and not the strength distribution along the height.

- According to the U.S. code provisions, the shape of the seismic design lateral load patterns is only influenced by the fundamental period of vibration of a structure, as well as the distribution of mass along the height of a structure, up to 72 m (240 feet) high, without considering the expected level of inelastic behavior.
- The shape of the seismic design lateral load patterns corresponding to the EuroCode 8 (EC 8) is a function of mass. For the design of regular moment-resisting frame up to 60 m, Japanese Seismic Design Code (BCJ) is limited to use the static-based design approach. The lateral load patterns along the height of the structure depend on the mass and the fundamental period of the structure. The lateral load patterns from Mexico City Building Code (Mexico 2003), for regular moment-resisting buildings with a height of no more than 40 m, are determined based on the fundamental period of the structure, the site classification, and the weight (mass) of the structure. Thus, specific requirements to vary the

shape of load patterns according to different inelastic levels of interest do not exist. Overall, load patterns from various standards (e.g., U.S., Europe, Japan, and Mexico) reviewed in this study show a very similar shape of load distributions along the height, which are mainly the function of the fundamental period of the structures and their mass, which as stated before, are only based on elastic dynamic analysis concepts.

3 PROCEDURE TO ESTIMATE SHEAR STRENGTH DISTRIBUTIONS FOR UNIFORM DAMAGE

3.1 INTRODUCTION

The design lateral load patterns are a fundamental component of the ELF procedure. Many researchers have developed new design load patterns based on inelastic concepts for regular moment-resisting frames (Leelataviwat et al. 1999; Lee and Goel 2001; Medina 2004; Moghaddamm and Hajirasouliha 2006; Chao, Goel, and Lee 2007). These new design load patterns are mostly a function of structural characteristics (e.g., fundamental period, mass), but do not account for the various levels of inelasticity and different characteristics of ground motions. In this chapter, new design load patterns are proposed as a function of ground motion and structural characteristics as well as the performance level of interest, which is quantified by the target story ductility ratio.

In general, design lateral floor loads consist of two fundamental components: the relative distribution of design floor loads (i.e., story shear strength patterns) and their absolute values (which are determined as a function of the base shear strength). An iterative procedure has been developed to obtain the required story shear strength pattern (absolute and relative values) to achieve uniform damage along the height. The iterative process will be ultimately completed once the final design complies with the performance targets of interest. First, this chapter introduces selected ground motions (i.e., far-field and near-fault), structural models (i.e., with a given mass and stiffness distribution), and response parameters (which would be an indicator to

measure the structural damage: e.g., story drift and ductility ratios) utilized in this study. Since the near-fault ground motions have distinctly different frequency contents with pulse-type characteristics, they are separately classified based on the ratio of pulse period of ground motions to a fundamental period of structures to derive the proposed design load patterns.

An iterative analysis procedure is introduced to estimate the story shear strength distributions for a given structure, a given ground motion, and an inelastic target level of interest. Story shear strength distributions are characterized by a central tendency (i.e., median or mean), as a more representative expression of design load patterns, which can vary with different ground motion frequency content characteristics.

3.2 SELECTION OF GROUND MOTIONS

The ground motions utilized in this study are classified primarily based on their frequency content characteristics. Thus, ordinary (far-field) and near-fault ground motions are used.

3.2.1 Ordinary Ground Motions

Ground motions recorded more than about 15 km from the fault rupture zone without pulse-type characteristics are denoted in this study as ordinary ground motions. The forty ordinary ground motions used in this study correspond to Californian earthquakes with moment magnitudes between 6.5 and 6.9 and distances between 13 km and 40 km ($6.5 < M_w < 7.0$, 13 km $< R <$ 40 km) recorded on soils corresponding to site class D (i.e., stiff soil, IBC 2006). These ground motions were

compiled by Medina (2003) and obtained from the PEER Center Ground Motion Database (http://peer.berkeley.edu/nga/earthquakes.html). These ground motions have characteristics consistent with those that dominate the design level seismic hazard (i.e., 10/50) in the western U.S. The main characteristics of this ground motion set are shown in Table 3.1.

Table 3.1 Ordinary ground motions utilized in this study (Medina 2003)

Record ID	Event	Year	Moment Magnitude	Station	Closest Distance (km)
IV79cal	Imperial Valley	1979	6.5	Calipatria Fire Station	23.8
IV79chi	Imperial Valley	1979	6.5	Chihuahua	28.7
IV79cmp	Imperial Valley	1979	6.5	Compuertas	32.6
IV79e01	Imperial Valley	1979	6.5	El Centro Array #1	15.5
IV79e12	Imperial Valley	1979	6.5	El Centro Array #12	18.2
IV79e13	Imperial Valley	1979	6.5	El Centro Array #13	21.9
IV79nil	Imperial Valley	1979	6.5	Niland Fire Station	35.9
IV79pls	Imperial Valley	1979	6.5	Plaster City	31.7
IV79qkp	Imperial Valley	1979	6.5	Cucapah	23.6
IV79wsm	Imperial Valley	1979	6.5	Westmorland Fire Station	15.1
LP89agw	Loma Prieta	1989	6.9	Agnews State Hospital	28.2
LP89cap	Loma Prieta	1989	6.9	Capitola	14.5
LP89g03	Loma Prieta	1989	6.9	Gilroy Array #3	14.4
LP89g04	Loma Prieta	1989	6.9	Gilroy Array #4	16.1
LP89gmr	Loma Prieta	1989	6.9	Gilroy Array #7	24.2
LP89hch	Loma Prieta	1989	6.9	Hollister City Hall	28.2
LP89hda	Loma Prieta	1989	6.9	Hollister Differential Array	25.8
LP89hvr	Loma Prieta	1989	6.9	Halls Valley	31.6
LP89sjw	Loma Prieta	1989	6.9	Salinas - John & Work	32.6
LP89slc	Loma Prieta	1989	6.9	Palo Alto - SLAC Lab.	36.3
LP89svl	Loma Prieta	1989	6.9	Sunnyvale - Colton Ave.	28.8
NR94cen	Northridge	1994	6.7	LA - Centinela St.	30.9
NR94cnp	Northridge	1994	6.7	Canoga Park - Topanga Can.	15.8
NR94far	Northridge	1994	6.7	LA - N Faring Rd.	23.9
NR94fle	Northridge	1994	6.7	LA - Fletcher Dr.	29.5
NR94glp	Northridge	1994	6.7	Glendale - Las Palmas	25.4
NR94hol	Northridge	1994	6.7	LA - Holywood Stor FF	25.5
NR94lh1	Northridge	1994	6.7	Lake Hughes #1 #	36.3
NR94lv2	Northridge	1994	6.7	Leona Valley #2 #	37.7
NR94lv6	Northridge	1994	6.7	Leona Valley #6	38.5
NR94nya	Northridge	1994	6.7	La Crescenta-New York	22.3
NR94pic	Northridge	1994	6.7	LA - Pico & Sentous	32.7
NR94stc	Northridge	1994	6.7	Northridge - 17645 Saticoy St	13.3
NR94stn	Northridge	1994	6.7	LA - Saturn St	30.0
NR94ver	Northridge	1994	6.7	LA - E Vernon Ave	39.3
SF71pel	San Fernando	1971	6.6	LA - Hollywood Stor Lot	21.2
SH87bra	Superstition Hills	1987	6.7	Brawley	18.2
SH87icc	Superstition Hills	1987	6.7	El Centro Imp. Co. Cent	13.9
SH87pls	Superstition Hills	1987	6.7	Plaster City	21.0
SH87wsm	Superstition Hills	1987	6.7	Westmorland Fire Station	13.3

3.2.2 Near-Fault, Forward-Directivity Ground Motions

Near-fault, forward-directivity ground motions possess characteristics that differ from those of ordinary ground motions. In most cases, near-fault ground motions exhibit stronger acceleration amplitudes and frequency content dominated by a distinct pulse (Somerville et al. 1997). If the site is located in the forward directivity

region of rupture propagation from the hypocenter, the earthquake records consists of a large velocity pulse of motion with relatively large energy content. There are also two components in the orientation of the rupture directivity according to Somerville (2000): strike-normal (ground motion normal to the fault) and strike-parallel components (ground motion parallel to the fault). The strike-normal component mainly contributes to generate a large directivity pulse if the static ground displacement is removed. Therefore, this study utilizes only the forward directivity and strike-normal component of the near-fault ground motions. The set of 64 near-fault ground motions utilized in this study is summarized in Table 2.2. These ground motions were recorded at a horizontal distance to the surface projection of the fault rupture of less than about 15 km, with moment magnitude (M_w) greater or equal to 6, and peak ground velocity (PGV) greater than 20 cm/sec.

The pulse period of a near-fault ground motion is of paramount importance when studying the response of multistory frame structures exposed to such ground motions. For code-compliant structures, this pulse-like ground motion may cause a highly non-uniform distribution of story ductility demands and considerably exceed the level of code expectations (Alavi and Krawinkler 2004). Thus, the approach taken in this study was to classify near-fault ground motions based on the ratio of the fundamental period of the structure to the pulse period of the ground motion (T_1/T_p). As stated by Alavi and Krawinkler (2001), the behavior of a multistory frame structure is strongly dependent on how the fundamental period of the system compares to the pulse period of the ground motion. For example, for structures designed based on story shear strengths consistent with the SRSS load pattern, the

maximum story ductility demands are expected to be larger at the bottom of the frame, if $T_1/T_p < 1$, regardless of the strength of the structure. On the other hand, if $T_1/T_p > 1$, maximum story ductility demands are expected at the top of the frame structure for strong structures; while weak structures will experience larger story ductility demands at the bottom. The near-fault ground motions that correspond to the range $0.35 \le T_1 / T_p \le 3.0$ are utilized in this study. If the ratio T_1/T_p is equal to one, the dynamic amplification of structural behavior is assumed to be very large when the impulsive characterisrics of near-fault ground motions have multiple pulses (Alavi and Krawinkler 2001). Thus, the case of $T_1/T_p = 1$ is included within the range $T_1/T_p < 1$, which has proven to be a more critical case for the ground motions and structural systems utilized in this study. If the ratio T_1/T_p is out of this range, it is unlikely for story drifts to be amplified due to pulse-type characteristics of near-fault ground motions unless significant higher-mode effects are present in the structural response. The main properties of these near-fault ground motions are depicted in Table 3.2.

Table 3.2 Properties of near-fault ground motions used in this study (Fu 2005)

Record ID	Event	Year	Moment Magnitude	Station	Source Mech	Pulse Period (s)
PF66c02	Parkfield	1966	6.1	Station 2 (Cholame #2)	SS	1.88
PF66tmb	Parkield	1966	6.1	Temblor pre - 1969	SS	0.39
MH84and	Morgan Hill	1984	6.2	Anderson Dam	SS	0.49
MH84g06	Morgan Hill	1984	6.2	Gilroy Array # 6	SS	1.04
MH84cyc	Morgan Hill	1984	6.2	Coyote Lake Dam	SS	0.76
IV79bra	Imperial Valley	1979	6.5	Brawley Airport	SS	3.43
IV79ecc	Imperial Valley	1979	6.5	EC County Center FF	SS	4.1
IV79emo	Imperial Valley	1979	6.5	EC Meloland Overpass FF	SS	2.93
IV79e03	Imperial Valley	1979	6.5	El Centro Array # 3	SS	4.55
IV79e04	Imperial Valley	1979	6.5	El Centro Array # 4	SS	4.18
IV79e05	Imperial Valley	1979	6.5	El Centro Array # 5	SS	3.66
IV79e06	Imperial Valley	1979	6.5	El Centro Array # 6	SS	3.63
IV79e07	Imperial Valley	1979	6.5	El Centro Array # 7	SS	3.57
IV79e08	Imperial Valley	1979	6.5	El Centro Array # 8	SS	4.67
IV78e10	Imperial Valley	1979	6.5	El Centro Array # 10	SS	4.01
IV79eda	Imperial Valley	1979	6.5	El Centro Differential Array	SS	4.22
IV79hvp	Imperial Valley	1979	6.5	Holtville Post Office	SS	4.33
SH87icc	Superstition Hills	1987	6.7	El Centro Imp. Co. Cent	SS	2.41
SH87pts	Superstition Hills	1987	6.7	Parachute Test site	SS	2.12
EZ92erz	Erzican	1992	6.9	Erzican	SS	2.31
KB95kjm	Kobe	1995	6.9	KJMA	SS	0.86
KB95prt	Kobe	1995	6.9	Port Island	SS	2.34
KB95tka	Kobe	1995	6.9	Takatori	SS	2.11
KB95jma	Kobe	1995	6.9	JMA	SS	0.9
LD92lnd	Landers	1992	7.3	Lucerne Valley	SS	5.54
KC99dzc	Kocaeli	1999	7.4	Duzce	SS	4.59
KC99gbz	Kocaeli	1999	7.4	Gebze	SS	6.47
KC99ypt	Kocaeli	1999	7.4	Yarimca	SS	4.27
PS86nps	N. Palm Springs	1986	6	North Palm Springs	OB	1.26
PS86dsp	N. Palm Springs	1986	6	Desert Hot Sprongs	OB	1.38
PS86wwt	N. Palm Springs	1986	6	Whitewater Trout Farm	OB	0.63
WN87jab	Whitter Narrows	1987	6	Bell Gardens – Jaboneria	TH	0.71
WN87ejs	Whitter Narrows	1987	6	Santa Fe Springs – E Joslin	TH	0.7
CL83pvy	Coalinga	1983	6.4	Pleasant Valley P.P.-yard	RV/OB	0.7
SF71pcd	San Fernando	1971	6.6	Pacoima dam	RV	1.38
NR94cnp	Northridge	1994	6.7	Canoga Park-Topanga Can	RV	2.02
NR94los	Northridge	1994	6.7	Canyon Cty-W Lost Cany	RV	1.89
NR94jen	Northridge	1994	6.7	Jensen Filter Plant	RV	2.83
NR94nwh	Northridge	1994	6.7	Newhall – Fire Station	RV	0.93
NR94rrs	Northridge	1994	6.7	Rinaldi Receiving	RV	1.16
NR94spv	Northridge	1994	6.7	Sepulveda VA	RV	2.99
NR94scs	Northridge	1994	6.7	Sylmar Converter	RV	2.88
NR94sce	Northridge	1994	6.7	Sylmar Converter East	RV	3.05
NR94syl	Northridge	1994	6.7	Sylmar Olive View	RV	2.53
NR94wpi	Northridge	1994	6.7	Newhall-W.Pico Canyon	RV	2.18
NR94pac	Northridge	1994	6.7	Pacoima Dam Downstreet	RV	0.48
NR94pkc	Northridge	1994	6.7	Pacoima Ragel Canyon	RV	0.72
NR94ldm	Northridge	1994	6.7	LA Dam	RV	1.42
NH85s01	Nahanni	1985	6.8	Site 1	RV	3.25
NH85s02	Nahanni	1985	6.8	Site 2	RV	1.2
LP89gof	Loma Prieta	1989	6.9	Gilroy-Historic Bldg.	RV/OB	1.54
LP89g01	Loma Prieta	1989	6.9	Gilroy Array #1	RV/OB	4.24
LP89g02	Loma Prieta	1989	6.9	Gilroy Array #2	RV/OB	1.43
LP89g03	Loma Prieta	1989	6.9	Gilroy Array #3	RV/OB	1.79
LP89g04	Loma Prieta	1989	6.9	Gilroy Array #4	RV/OB	1.37
LP89gil	Loma Prieta	1989	6.9	Gilroy-Gavilan Coll.	RV/OB	1.77
LP89stg	Loma Prieta	1989	6.9	Saratoga-Aloha Ave.	RV/OB	2.25
LP89wvc	Loma Prieta	1989	6.9	Saratoga-W Valley Coll.	RV/OB	2.16
LP89log	Loma Prieta	1989	6.9	Los Gatos	RV/OB	3.21
LP89lxd	Loma Prieta	1989	6.9	Lexington Dam	RV/OB	1.81
CC99075	Chi-Chi	1999	7.6	TCU075	OB	5.01
CC99129	Chi-Chi	1999	7.6	TCU129	OB	7.41
CC99065	Chi-Chi	1999	7.6	TCU065	OB	4.73
CC99076	Chi-Chi	1999	7.6	TCU076	OB	4.15

Note: SS, strike-slip; OB, oblique; RV, reverse; and DS (dip-slip) includes OB, RV, and RV/OB.

3.3 STRUCTURAL MODELS AND RESPONSE PARAMTERS

3.3.1 Structural Models

The structural models used in this study correspond to a set of two dimensional single-bay, moment-resisting frames (MRFs) with number of stories from 6 to 18 and fundamental periods from 0.6 s. to 3.0 s. (Figure 3.1). Story heights are equal to 12 ft (3.6 m) and beam spans are equal to 24 ft (7.2 m) with the same mass at all floor levels. Frames are designed based on the strong column-weak girder philosophy; i.e., plastification is confined only at the beam ends and the bottom of the first story columns. A peak-oriented (stiffness degrading) model with 3% hardening in the moment-rotation relationship is used to represent the hysteretic response at plastic hinge locations. Member strengths are tuned so that simultaneous yielding at all plastic hinge locations occurs when the frame is subjected to the design lateral load patterns, i.e., the same amount of overstrength is assumed at all story levels. This allows the calculation of story yield drifts, which are used in the computation of story ductility ratios. These frames are similar to those used by Medina and Krawinkler (2005) with the exception that the first mode shape is nonlinear (see Figure 3.2). Five percent Rayleigh damping was assigned to the first mode and to those modes where the cumulative mass participation exceeds 95%.

In order to evaluate the sensitivity of the response to the type of hysteretic behavior, a bilinear hysteretic model was also utilized in the development of the proposed lateral load patterns in this study. As seen in Figure 3.3, the required lateral load distribution to achieve a uniform distribution of damage over the height of non-deteriorating moment-resisting frames is weakly dependent on the type of hysteretic

model. Thus, the peak-oriented hysteretic model was used to model the hysteretic behavior at plastic hinge locations throughout the entire study.

It is also important to note that the single-bay frames used in this study are adequate to represent the global inelastic behavior of more complex multi-bay frames, as shown in Medina and Krawinkler (2005).

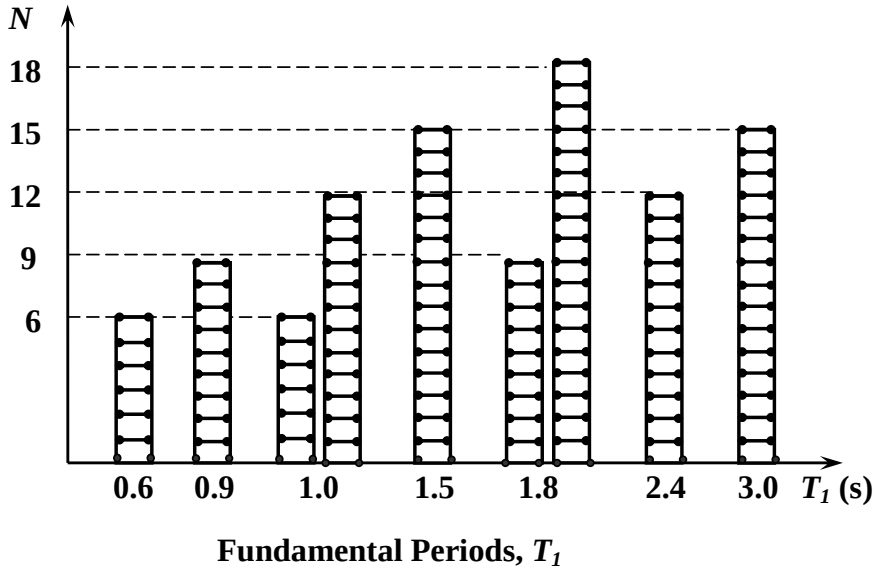

Figure 3.1 Single-bay, moment-resisting frames with N = 6 to 18 and T_1 = 0.6 s. to 3.0 s

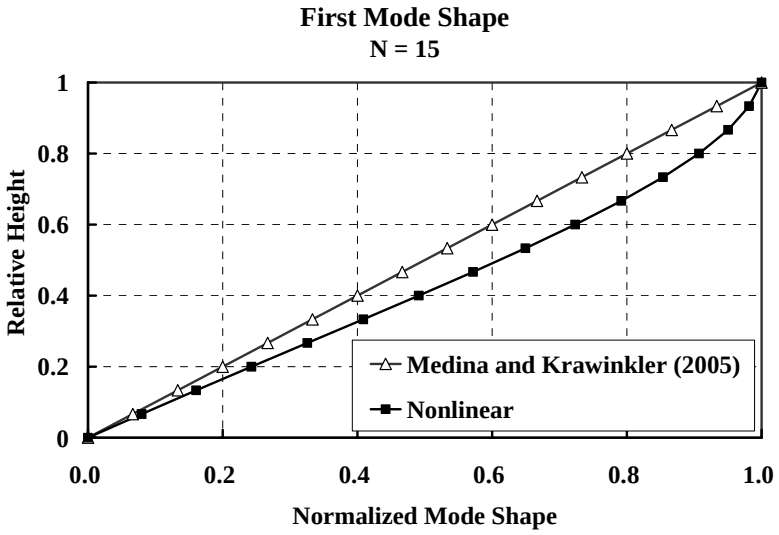

Figure 3.2 First mode shape, fifteen-story frame structure

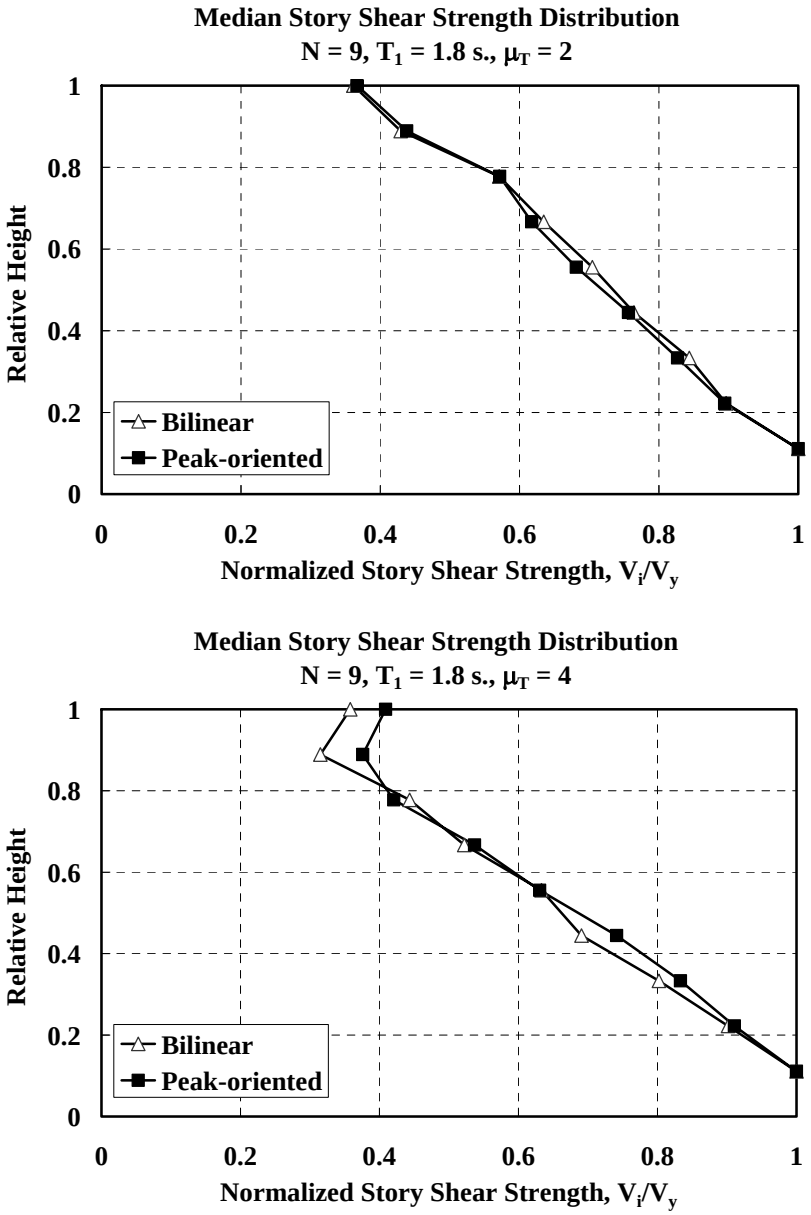

Figure 3.3 Story shear strength distributions corresponding to the bilinear and peak-oriented hysteretic models for 9-story frame with T_1 = 1.8 s, 40 far-field ground motions, for target ductilities 2 and 4

3.3.2 Primary Response Parameters

Since limiting and distributing structural damage along the height of a moment-resisting frame is the main target performance level in this study, it is important to select appropriate response parameters (or engineering demand parameters, EDPs) to quantify the extent of damage of the system. There are several EDPs commonly used to quantify structural damage (Krawinkler and Nassar 1992, Teran 1997, Teran 2005), story ductility ratio, maximum story drift ratio, cyclic story ductility, the number of cycles of yielding, and the normalized hysteretic energy among others.

The story ductility ratio, defined as the peak story drift normalized by the story yield drift, as well as the maximum story drift ratio, defined as the peak relative displacement between adjacent floor levels normalized by the story height, are considered appropriate parameters to quantify structural damage for non-deteriorating structural systems. The cyclic story ductility, defined as the maximum plastic story drift divided by the story yield drift, is used for assessing cumulative structural damage. The number of cycles of yielding may be utilized to measure damage, if an engineering component contains a crack. For example, if a cyclic load is applied, the crack is likely to grow slowly with increasing number of load cycles. This process is commonly called fatigue crack growth. The normalized hysteretic energy is also used to quantify the cumulative inelastic/ plastic response (damage) of a structural system. The normalized hysteretic energy is a useful parameter to characterize the cumulative structural damage especially if a structural member is ductile. However, if cyclic deterioration of a structural component is not a critical issue, a structure can be

assumed as a non-deteriorating structure. A non-deteriorating structure (i.e., a structure with ductile structural members with no deterioration in strength, steel in particular) can resist forces and take further loading before complete loss of load-carrying capacity.. In order to capture large deformation of structures, story ductility and peak story drift ratios might be suitable parameters to measure structural damage. Miranda (1997) also pointed out several advantages: story ductility and peak story drift ratios (a) are very simple parameters; (b) structural engineers are familiar with them; (c) many experimental research is based on these parameters. Thus, those parameters are sufficient EDPs to assess the structural damage and are utilized as the primary indicators of structural damage in this study.

3.4 ESTIMATION OF STORY SHEAR STRENGTH DISTRIBUTION FOR UNIFORM DAMAGE

Since the uniform distribution of story ductility ratios over the height of structures represents a uniform distribution of structural damage, the main goal of this Section is to illustrate the proposed procedure to obtain the required story strength pattern to achieve the same target story ductility ratio in all stories. As mentioned in Section 3.1, design load patterns have two fundamental components: the relative distribution of design floor loads and their absolute values. These two components are updated during the iteration process (see Figure 3.4) until the target story ductility ratio, μ_T, is achieved in all stories.

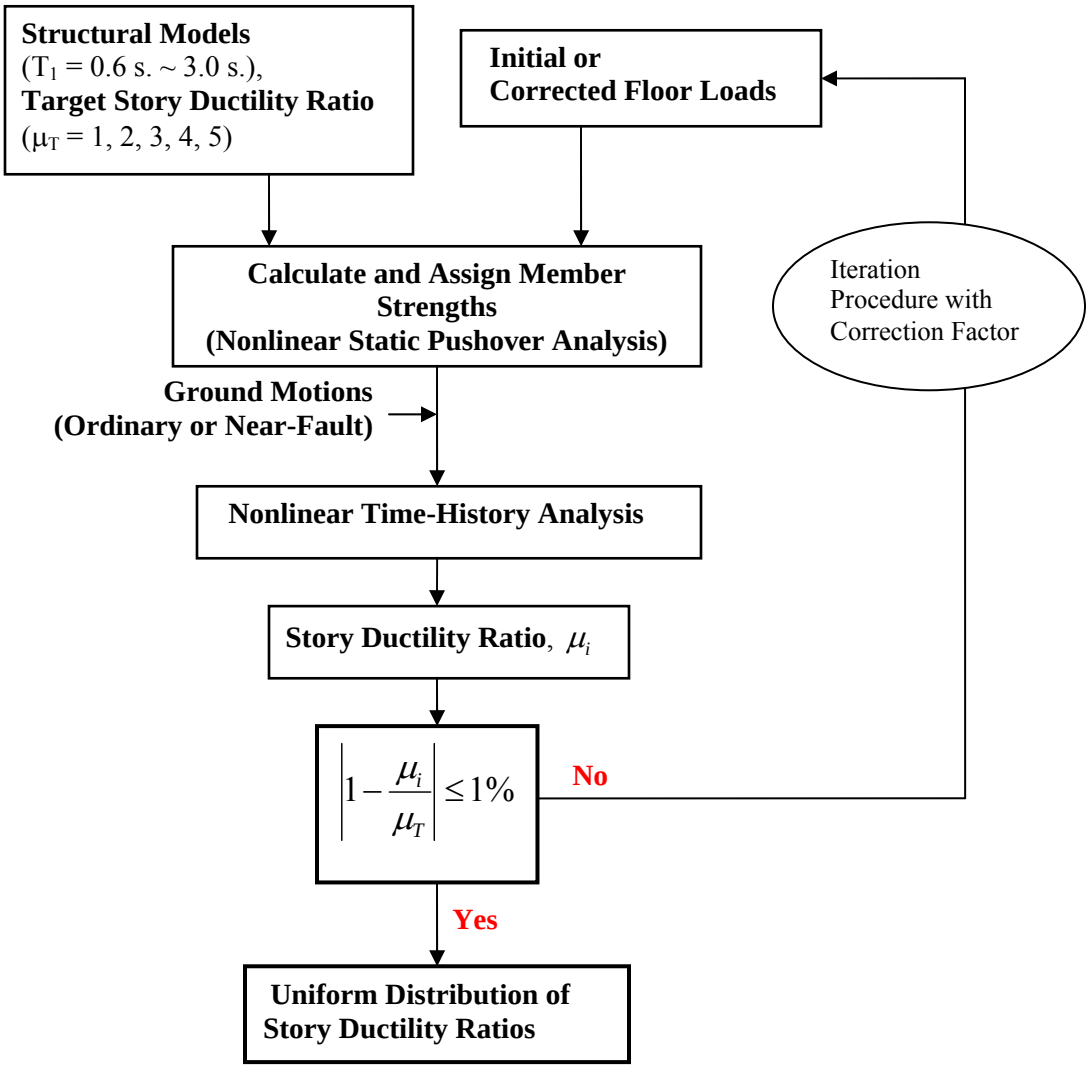

Figure 3.4 Iteration procedures to obtain design lateral load patterns to achieve uniform story ductility ratio over the height in all stories of regular moment-resisting frames

As shown in Figure 3.4, the procedure begins by assigning member strengths based on an assumed seismic design lateral load distribution. A nonlinear time history analysis is conducted and story ductility ratios, μ_i, are calculated. Member strengths are tuned so that simultaneous yielding occurs when the structure is designed based on the lateral load distribution. Thus, the yield story drift ratios necessary to estimate μ_i can be readily calculated. Values of μ_i are compared to the target value to

determine if the computed story ductility ratio in all stories is within 1% of μ_T. If this is the case, the story shear strength at story *i* is then modified by a correction factor that is a function of the ratio μ_i/μ_T. A nonlinear time history analysis is conducted with the updated story shear-strength distribution and the process is repeated until story ductility ratios are within 1% of the target value. The target story ductility ratios of interest are 1, 2, 3, 4, and 5. The solutions (i.e., proposed load patterns) for ordinary and near-fault ground motions are independently obtained corresponding to a given structure, a given ground motion record, and given target story ductility ratios.

3.4.1 Uniform Damage – Absolute Value of Shear Strength

For regular structures, seismic design lateral loads are computed based on the base shear strength and its distribution along the height of the structure and are characterized by two components: the relative intensity and the relative distribution of story shear strength distribution, as previously mentioned in this chapter. The relative distribution of story shear strength along the height is obtained by normalizing the story shear strength at a given level, V_i, with the base shear strength. Based on a given ground motion hazard level ($S_a(T_1)/g$) and a given effective seismic weight (W), the base shear strength, V_y, can be calculated to achieve the target story ductility ratio. The seismic hazard depends on the seismicity of an individual region. For example, the 10/50 ground motion hazard level, which is defined as that corresponding to 10 percent probability of exceedance (PE) of a given ground motion intensity measure in 50 years, is utilized herein for the set of ordinary ground motions. On the other hand, near-fault ground motions tend to control the 2/50 hazard level in relativel high seismic region in the U.S., with is defined as that corresponding to 2 percent

probability of exceedance (PE) of a given ground motion intensity measure in 50 years. Nevertheless, ground shaking calculated at a 2 percent probability of exceedance in 50 years would be much larger than which would be expected based on the characteristic magnitudes of earthquakes on known active faults (BSSC 2003). For these regions, according to BSSC 2003, it is considered more appropriate to directly determine maximum considered earthquake ground motions based on the characteristic earthquakes of these defined faults. Hence, in order to capture the effect of pulse-type ground motion characteristics in the required distribution of story shear strengths to achieve a constant story ductility ratio, the 10/50 hazard level is also selected to estimate the spectral values of the near-fault ground motions used in this study. The design response spectrum required by NEHRP 2003 and IBC 2006 is presented in Figure 3.5 for both ordinary and near-fault ground motions.

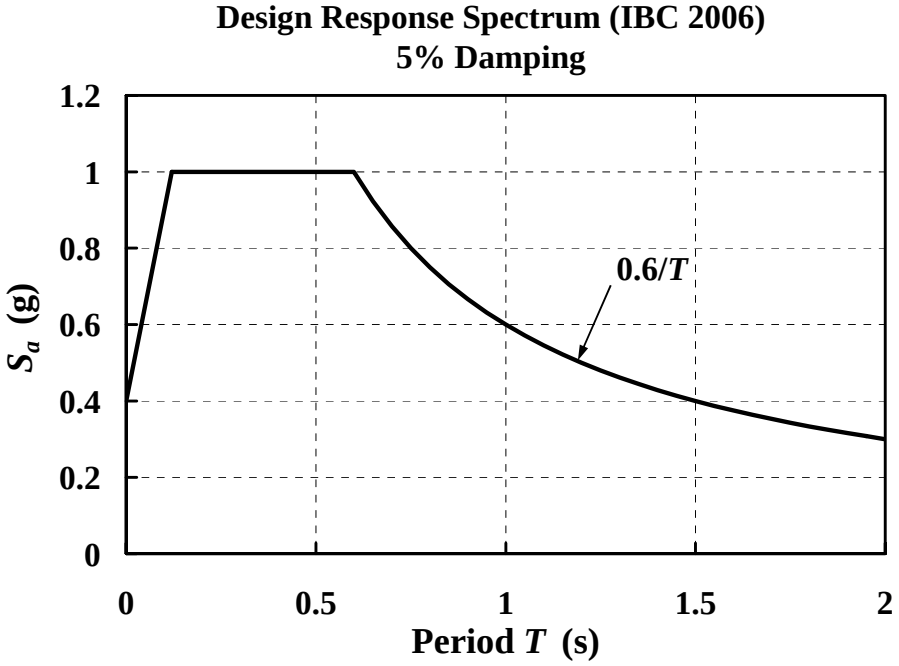

Figure 3.5 Design acceleration response spectrum for the area in Los Angeles, California

Representative results obtained from this iterative procedure are shown in Figure 3.6 for the 15-story regular frame model with the fundamental period of 1.5 s, exposed to the set of 40 ordinary ground motions (OGMs) described in Table 3.1 and the set of near-fault ground motions (NFGMs) described in Table 3.2, respectively. Each data point in Figure 3.6 corresponds to the required relative intensity to achieve a target story ductility ratio, $\mu_T = 4$, for an individual ground motion. This relative intensity is denoted herein as RI_P. It is notable that the resulting data points are closely scattered around at $RI_P = 4$; however, the relative intensity was slightly overestimated (above 4.0 for $\mu_T = 4$) when the 15-story frame was exposed to near-fault ground motions for $T_1/T_p > 1$. This implies that a smaller base shear strength is required for the frame to achieve uniform story ductility ratios along the height for near-fault ground motions with $T_1/T_p > 1$.

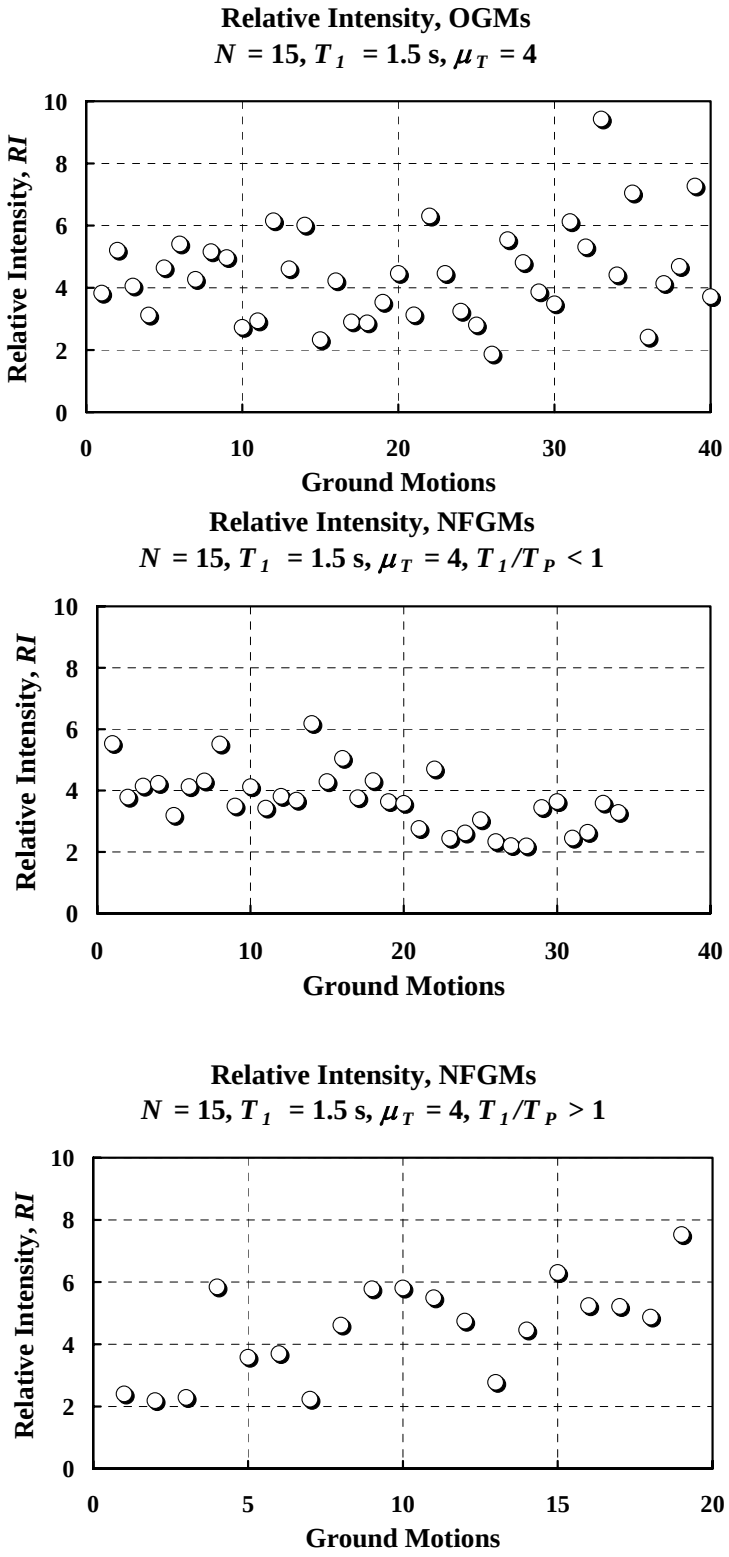

Figure 3.6 Relative intensity for OGMs; for NFGMs, $T_1/T_p < 1$ and $T_1/T_p > 1$ required to achieve a target story ductility of 4, 15-story frame

3.4.2 Uniform Damage - Relative Distribution of Story Shear Strength

The relative distribution of story shear strength is the second component necessary to characterize seismic design lateral loads. After implementing the iterative procedure in which the relative intensity and story shear strength pattern are determined simultaneously (see Figure 3.4), the story shear strength patterns are obtained as shown in Figure 3.7. Each gray line in the figure corresponds to the relative distribution necessary to achieve a target story ductility ratio of 4 for an individual ground motion in conjunction with one of the relative intensity values of Figure 3.6. For a given target inelastic performance level (μ_T = 4), story shear strength distributions are significantly different from the design story shear strength pattern based on the equivalent lateral force procedure of the IBC 2006. This process was carried out for all frames (T_1 = 0.6 s. ~ 3.0 s.) and target story ductility ratios of interest (μ_T = 1 ~ 5).

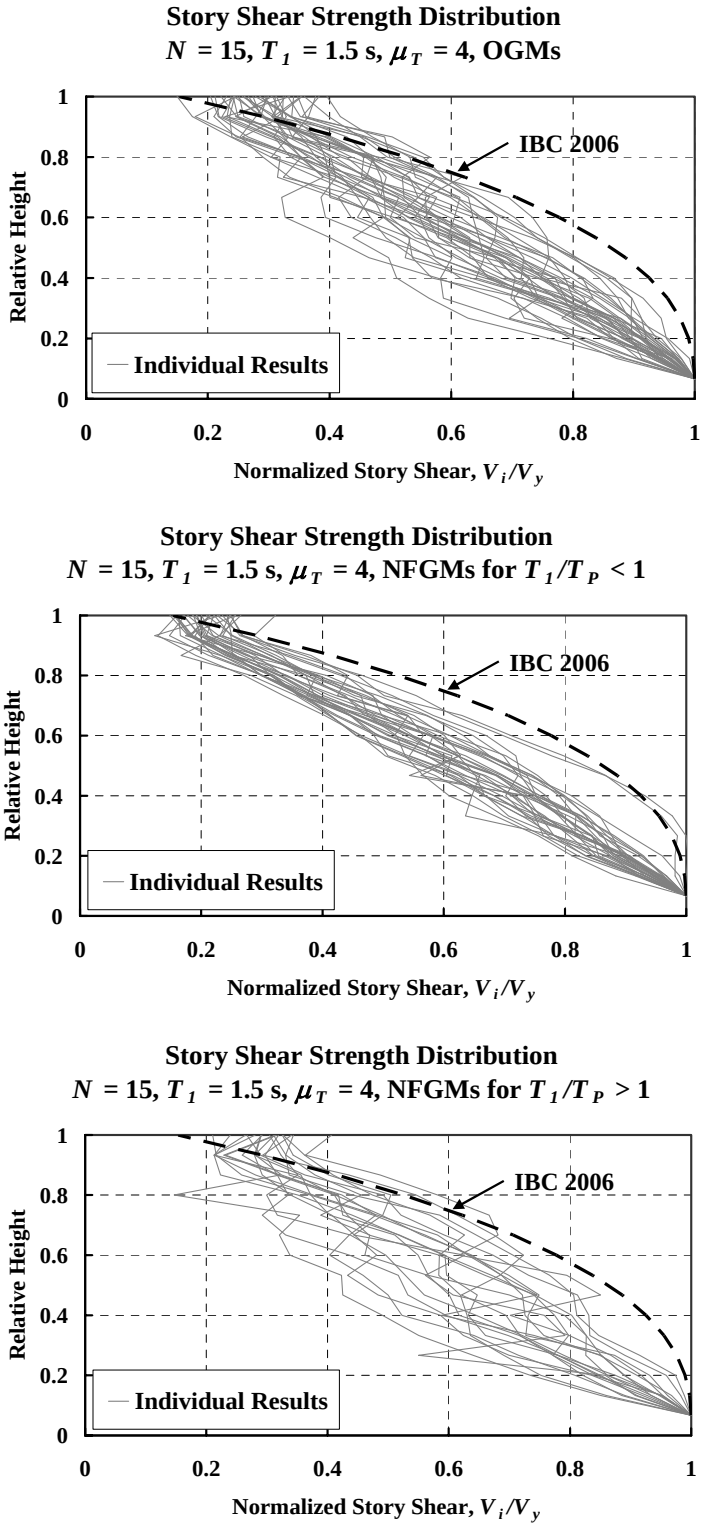

Figure 3.7 Normalized shear story strength distributions for OGMs; for NFGMs, $T_1/T_p < 1$ and $T_1/T_p > 1$ required to achieve a target story ductility of 4, 15-story frame

3.5 CHARACTERIZATION OF STORY SHEAR STRENGTH DISTRIBUTIONS FOR UNIFORM DAMAGE

The determination of a story shear strength distribution needs to take record-to-record variability in ground motion data into account to provide data for a uniform distribution of story ductility ratios over the height for similar structures and ground motions. In this study, the target story ductility ratios of interest are 1, 2, 3, 4, and 5 for structures exposed to ordinary ground motions and near-fault ground motions. For example, for a regular 15-story moment-resisting frame structure with a fundamental period of vibration of 1.5 s, a set of 40 ordinary (far-field) ground motions and a set of near-fault ground motions (see Table 3.3) are utilized. In Figure 3.8, the median (or mean) distribution of story shear strength distributions (each gray line) is estimated as a central tendency of a given frame model exposed to a given set of ground motions. This central tendency is a representative value of the overall behavior in the presence of the record-to-record variability in ground motion data for a given frame model subjected to a set of ground motions with characteristics similar to those utilized in this study. As the target story ductility ratio is increased from 1 to 4 as shown in Figure 3.9, this central tendency of the required distribution of story shear strengths varies significantly. The shape of the distribution of story shear strengths over the height depends strongly on the level of inelastic behavior, i.e., target story ductility (see Figure 3.9). Similar conclusions were obtained by Alavi and Krawinkler (2000) when studying the effect of simplified pulses on the response of regular frames. These observations are also consistent with those obtained from the rest of the frames analyzed in this study.

Both median and mean are two types of measures of central tendency in this study. A set of ordinary ground motions has 40 records, where as sets of near-fault ground motions contains fewer recordings, e.g., 3, 10, 14, or 19 depending on the fundamental period of structures and the pulse period of the ground motion (see Table 3.3). In this study, median is defined as the geometric mean (exponential of the average of the natural logarithm of the values) of the data points. The median is an appropriate representation of the central tendency of data that is lognormally distributed and reduces the amount of skewing due to outliers in the data points. However, if enough data points are not present to assess distribution types (e.g., normal or lognormal), the mean values provide a reasonable representation of the central tendency because of the data points. Because a sufficient number of data points are available for the statistical analysis of the response due to ordinary ground motions, the median is suitable to represent the central tendency of all the data points, especially when the distribution of story ductility ratios can be described by a lognormal distribution. However, because of the smaller number of data points available in the statistical analysis of the response due to near-fault ground motions, the mean may be considered a more accurate measure of "average" (or central tendency). Median values could be obtained for near-fault ground motions as long as additional near-fault ground motion records are included in the analysis.

Table 3.3 Lower and upper limits of frames, target story ductility ratios and near-fault ground motions

T_1 (s)	Number of NFGMs	
	$T_1/T_P < 1$	$T_1/T_P > 1$
0.6	19	3
0.9	27	10
1.2	31	14
1.5	34	19
1.8	38	20
2.4	28	26
3.0	24	28

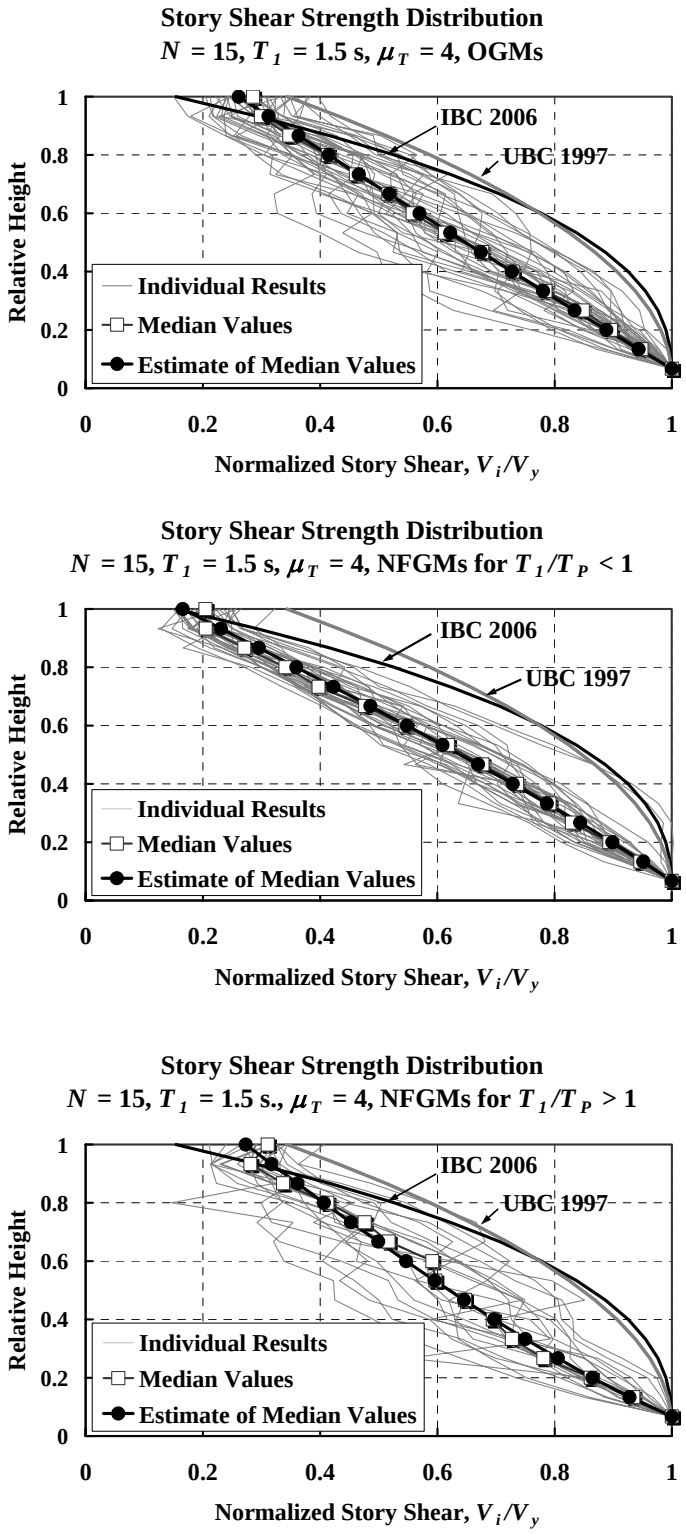

Figure 3.8 Estimated median and mean story shear strength distributions for a 15-story frame with T_1 = 1.5 s. and μ_T = 4 exposed to OGMs; and to NFGMs, $T_1/T_p < 1$ and $T_1/T_p > 1$

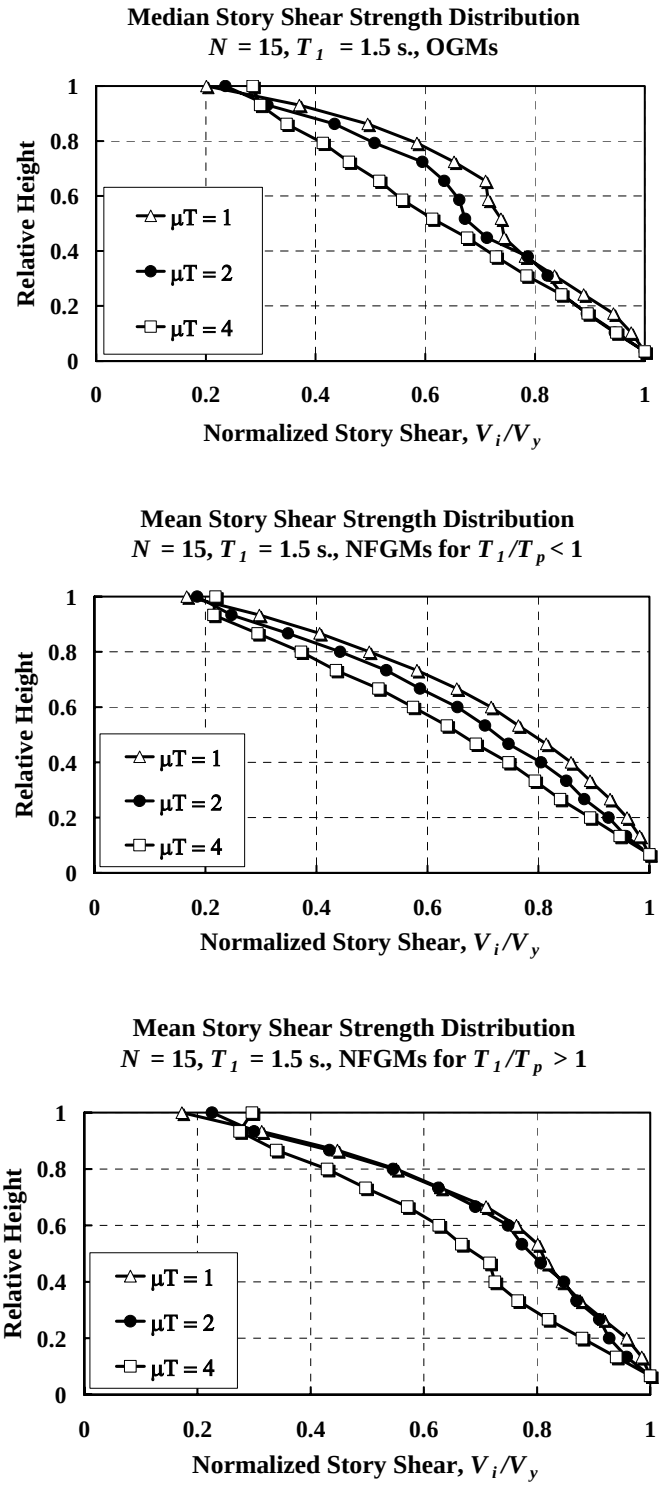

Figure 3.9 Median and mean story shear strength distributions for 15-story frame with T_1 = 1.5 s. for μ_T = 1, 2, and 4 exposed to OGMs; and to NFGMs, $T_1/T_p < 1$ and $T_1/T_p > 1$

Relative distribution of story shear strength

Proposed lateral load patterns are developed in this study to characterize the distribution of seismic lateral loads along the height. These proposed lateral load patterns are depicted in Figure 3.10 and are given by the following expression (Park and Medina 2007):

$$F_x = \frac{(V_y - F_{top})w_x h_x^{\ k}}{\sum_{i=1}^{N} w_i h_i^{\ k}}; \text{ for } x = 1, 2, 3, ...,N \qquad [3.1]$$

where F_x is the lateral load at level x; F_{top} is the portion of the base shear that is applied as a concentrated force at the top of the structure; k is an exponent that defines the relative distribution of lateral loads (Figure 3.11); w_i, w_x are the portions of the total seismic effective weight of the structure located at levels i, x; and h_i, h_x are the heights from the base to levels i, x. Equation 3.1 with $F_{top} = 0$ is equivalent to the design lateral load pattern of the equivalent lateral force procedure of the IBC 2006. Equation 3.1 with $k = 1$ is equivalent to the design lateral load pattern of the static force procedure of the 1997 Uniform Building Code (UBC 1997, see Figure 2.4).

For the structural models utilized in this study, which have a regular distribution of mass along the height (same mass at all floor levels), the shape of the design lateral load patterns is controlled by two parameters: k and F_{top}/V_y. The parameter F_{top}/V_y represents the fraction of the design seismic base shear, V_y, that is allocated at the roof level as an additional lateral load (Figure 3.10). In addition, an expression for the static story shear strength, based on Equation 3.1, is given by:

$$V_x = V_y \left[\left(1 - \frac{F_{top}}{V_y} \right) \sum_{i=x}^{N} \left(\frac{w_i h_i^{\,k}}{\sum_{z=1}^{N} w_z h_z^{\,k}} \right) + \frac{F_{top}}{V_y} \right]; \text{ for x = 1, 2, 3, ...,N} \quad [3.2]$$

where V_x is the story shear at level x; w_z is the portion of the seismic effective weight located at level z; and h_z is the height from the base to level z.

The parameters, k and F_{top}/V_y, are determined based on an optimization procedure that minimize the error between the median (or mean) story shear strength patterns (such as those shown in Figure 3.8). These optimized distributions (i.e., estimate of median or mean values in Figure 3.8) are computed based on Equation 3.1. Although the general shapes of the 16th and 84th percentile results differ from the shape of the median (or mean) results, median (or mean) values are used to represent the central tendencies of the results. The uncertainty of the optimization procedure is computed by:

1. Calculating the square of the difference between the median (or mean) normalized story shear strength pattern and the normalized story shear strength pattern based on Equation 3.2 for each story.
2. Adding the square of the differences over the height of the frame to estimate a total error for a given value of k and F_{top}/V_y.

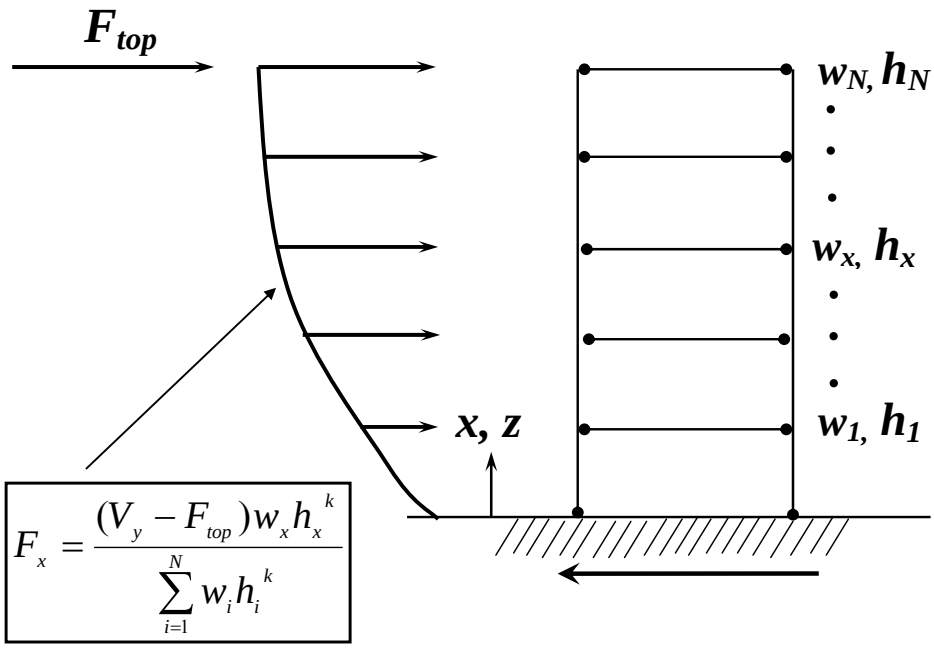

Figure 3.10 Proposed design lateral load pattern (Park and Medina, 2007)

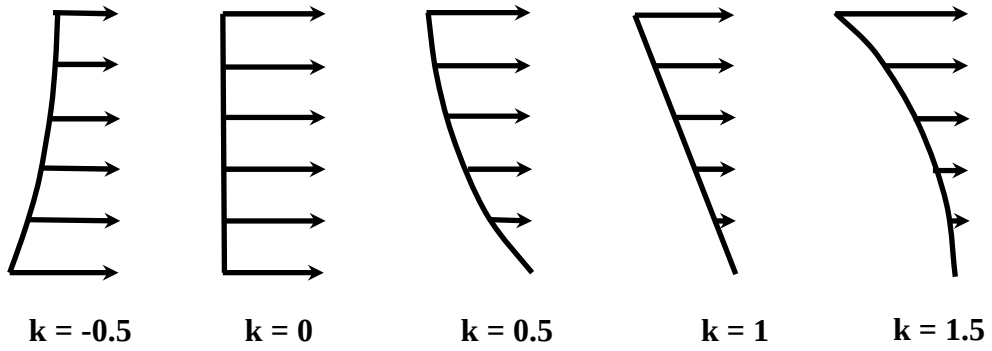

Figure 3.11 Effect of parameter '*k*' on the proposed distribution of seismic design lateral loads (Park and Medina, 2007)

In concept, the parameters k and F_{top}/V_y provide a story shear strength distribution. Each story shear strength distribution would produce, on average, constant story ductility ratios over the height when a frame is designed with member strengths tuned to the design lateral load pattern and the frame is exposed to a ground

motion with its frequency content characteristics similar to those utilized in this study. The results from this optimization procedure are discussed in Chapter 4.

3.6 SUMMARY

- 40 ordinary ground motions ($6.5 < M_w < 7.0$, 13 km $< R <$ 40 km, NEHRP site class D) and near-fault ground motions ($6.0 < M_w$, $R <$ 17 km) characterized by the ratio T_1/T_p ($0.35 \le T_1 / T_p \le 3.0$) are selected. Single-bay moment-resisting frames with number of stories from 6 to 18 and fundamental periods from 0.6 s to 3.0 s are used as representative structural models.
- The story ductility ratio (μ_i) and the peak story drift ratio (θ_{max}) are utilized as primary parameters, and structural damage is quantified by the story ductility ratio for non-deteriorating structural systems. Because the structural systems utilized in this study are non-deteriorating, the story ductility ratios are similar over the height, which translates into a uniform distribution of damage over the height of the structure.
- The story strength distributions required to achieve a constant story ductility ratio along the height are significantly different from the code-compliant story shear strength distributions and are strongly dependent on the level of inelastic behavior, i.e., target story ductility ratio.
- For uniform damage along the height, the required design floor loads are estimated based on the combination of required base shear strength and a story shear strength distribution. The required base shear strength controls

the total strength level of the structure to target story ductility ratios. In order to account for the presence of record-to-record variability in ground motion data, the central tendency is utilized to represent the required story shear strength distribution for a given frame model. This central value of story shear strength distributions is quantified by a model proposed by Park and Medina (2007), which is a function of two parameters k and F_{top}/V_y.

4 DESIGN LATERAL LOAD PATTERNS FOR MOMENT-RESISTING FRAMES

4.1 INTRODUCTION

In Chapter 3, the required relative distribution of design floor loads and their absolute values to achieve uniform damage along the height for a given structural model, a selected target inelastic level of interest, and a given ground motion, were estimated. In order for these result to be of practical use, it is necessary to develop general relationships for absolute values and relative distribution of seismic forces. These relationships should be applicable to any frame models within the range T_1 = 0.6 s. ~ 3.0 s. and H = 72 ft ~ 216 ft (20 m ~ 60 m) for the target values of interest (μ_T = 1 ~ 5). Because of the record-to-record variability in ground motions and frame models with different fundamental periods and various target story ductility ratios, it is necessary to characterize seismic design lateral load patterns statistically. This chapter presents and discusses regression models to estimate values of: (a) relative intensity, and (b) k and F_{top}/V_y, required achieving uniform damage along the height of frame structures.

4.2 DESIGN LATERAL LOAD PATTERNS FOR MOMENT-RESISTING FRAMES EXPOSED TO ORDINARY GROUND MOTIONS

4.2.1 Seismic Base Shear Strength

In order to estimate the base shear strength, the statistical evaluation of the relative intensity, RI_p, which is required to achieve a target story ductility ratio, is conducted. For each frame structure, ground motion, and target story ductility ratio, a unique RI_P value is available to provide the absolute values of story shear strengths V_y, as shown in Figure 3.10. In order to generalize these values, a statistical model is developed to estimate RI_P as a function of the target story ductility ratio, which permits an estimation of the required base shear strength for a given ground motion hazard level (when this latter one is expressed in terms of the spectral acceleration at the first-mode period of the structure).

Various research studies on strength-reduction factors, (R_μ), have been conducted over the last 40 years, and many researchers carried out numerous analyses and simplified expressions of strength-reduction factors to estimate inelastic design spectra as functions of ductility ratios. Newmark and Hall (1973) presented their observations that resulted in the recommendation of a procedure to construct inelastic spectra from the elastic spectra based on target ductility and damping ratios. Moreover, Lai and Biggs (1980) proposed design inelastic response spectra based on mean inelastic spectra computed for 20 artificial ground motions. Riddell and Newmark (1979) conducted a statistical analysis to develop inelastic response spectra

of real ground motion records for elasto-plastic systems. Other researchers: Elghadamsi and Mohraz (1987); Riddell et al. (1989); Arias and Hidalgo (1990); Nassar and Krawinkler (1991); Vidic, Fajfar and Fischinger (1992); Miranda (1993) also proposed inelastic response spectra based on recorded ground motions with different structural period of vibrations, yield levels, hysteretic behaviors, and site conditions. However, the expressions of strength-reduction factors from those studies were only based on Single-Degree-Of-Freedom (SDOF) structures. In addition, for SDOF systems with 5 percent damping and T_1 equal or greater than 0.6 s., Miranda (1993) and Riddell (1995) concluded that the coefficient of variation (COV) of R_μ is approximately independent of period and that the dispersion increases with increasing displacement ductility ratio. Nassar and Krawinkler (1991) and Miranda (1993) also studied the influence of earthquake magnitude and epicentral distance on the strength-reduction factors and concluded that the effect of both parameters on R_μ was negligible.

Based on the knowledge obtained from the behavior of SDOF systems and statistical studies with the data obtained from this dissertation, Park and Medina (2007) proposed a 'ductility-strength reduction factor' type relationship, μ_T - RI_P, applicable to MDOF systems with fundamental periods from 0.6 to 1.8 s:

$$RI_P = 1.10 \cdot \mu_T^{0.996} \qquad [4.1]$$

where $1 \leq \mu_T \leq 5$ and 0.6 s. $\leq T_1 \leq$ 1.8 s. This relationship was obtained by conducting a weighted least squares (WLS) regression analysis with the natural logarithms of RI_P and μ_T. The correlation coefficient and the standard error are 0.902 and 1.02, respectively (see Figure 4.1). The need for a weighted least squares approach arose

from the variation in the dispersion of RI_P values with μ_T. For this period range, the results were weakly dependent on the fundamental period of vibration, which is consistent with previous studies conducted with SDOF structures.

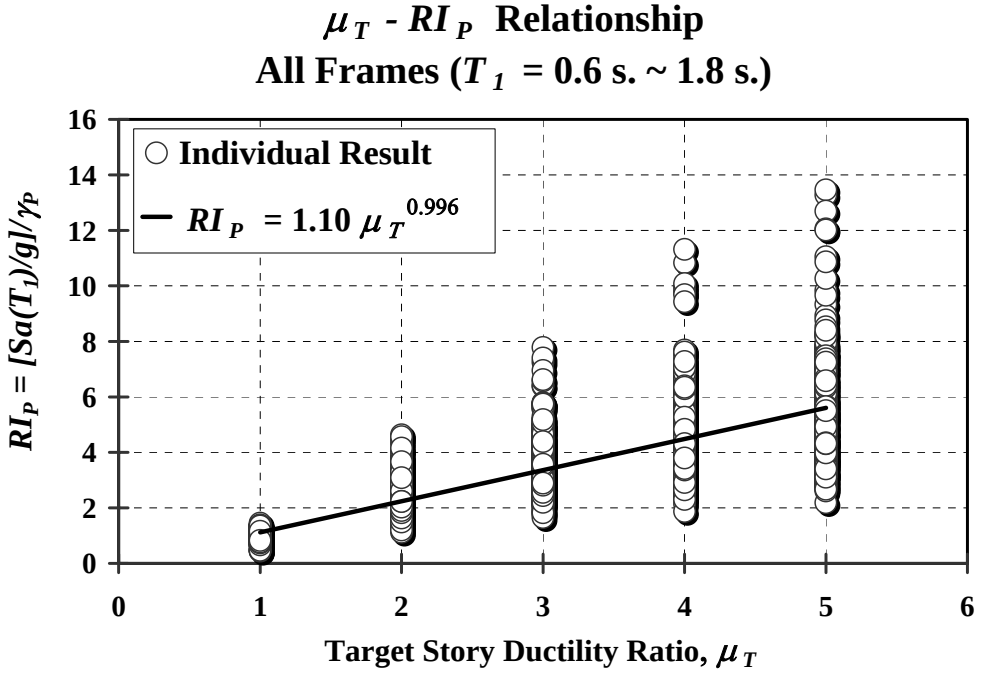

Figure 4.1 μ_T-RI_P relationship for moment-resisting frames with T_1 = 0.6 s. ~ 1.8 s. (Park and Medina, 2007)

However, by expanding the range of fundamental periods from (0.6 s. ~ 1.8 s.) to (0.6 s. ~ 3.0 s.), RI_P is more strongly dependent on T_1 for the same target story ductility ratio utilized by Park and Medina (2007). The correlation coefficient of the dependent variable RI_P with T_1 is 0.119 when the parameter T_1 is in the range (T_1 = 0.6 s. ~ 3.0 s.) compared to 0.066 from the $T_1 - RI_P$ relationship for the range (T_1 = 0.6 s. ~ 1.8 s.). For the expanded range T_1 = 0.6 s. ~ 3.0 s., the proposed μ_T - T_1 - RI_P relationship is of the form:

$$RI_P = 1.13 \cdot \mu_T^{0.993} \cdot T_1^{-0.160} \qquad [4.2]$$

where $1 \leq \mu_T \leq 5$ and 0.6 s. $\leq T_1 \leq$ 3.0 s. A weighted least squares (WLS) multiple regression analysis with the natural logarithm of independent and dependent variables is necessary in order to account for the dependence of the variance of RI_P on the target story ductility ratio (see Figure 4.2). Through a weight estimation procedure, the more precise observations (with less variability) are given greater weight in determining the regression coefficients. For Equation 4.2, the weight is estimated from the relationship $Weight = \frac{1}{Variance}$, and the correlation coefficient and the standard error are 0.908 and 0.986, respectively. Note that the range of periods is also considered (from 0.6 s to 3.0 s) in the μ_T - T_1 - RI_P relationship, which provides a slightly better fit for Equation 4.2 when compared to Equation 4-1: for example, from Equation 4.1 to Equation 4.2, the correlation coefficient is increased from 0.902 to 0.908, and the standard error is decreased from 1.02 to 0.986. This implies that the fundamental period of vibration becomes more important to represent the μ_T - T_1 - RI_P relationship when flexible frames are included (e.g., frames with T_1 = 2.4 s. and 3.0 s.). Figure 4.2 shows a graphical representation of the proposed μ_T - T_1 - RI_P relationship. Equation 4.2 is utilized for the new methodology and the verification results which will be discussed later in this study.

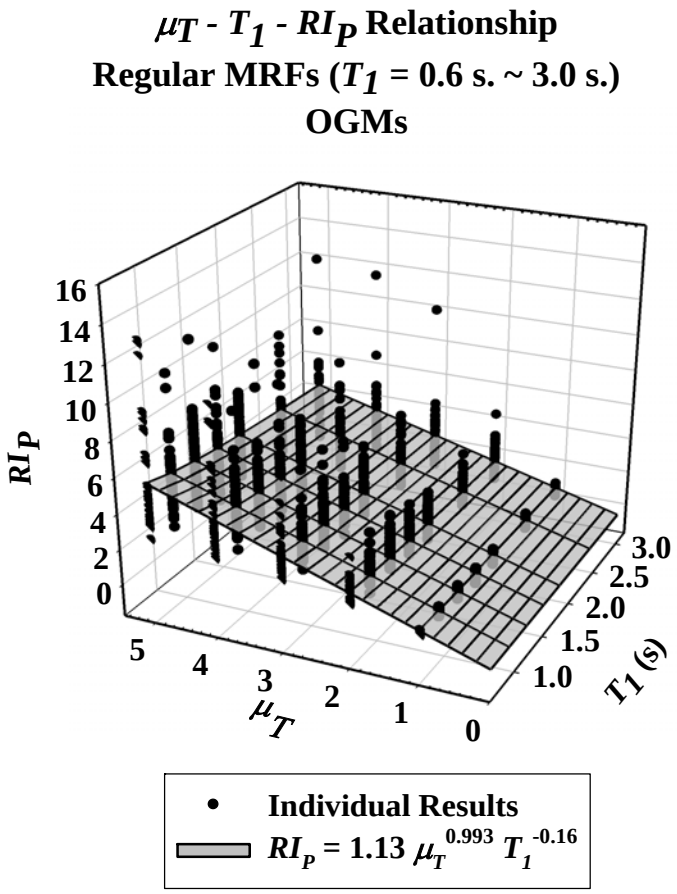

Figure 4.2 μT- T_1 - RI_P relationship in 3-D for frames designed based on the lateral load patterns proposed in this study

As shown in Figure 4.3, especially for long fundamental periods (1.2 s. ~ 3.0 s.), Equation 4.2 is consistent with 'the equal displacement' rule of SDOF systems, in which inelastic peak displacements remain almost the same as elastic peak displacements. In other words, on average, the ductility-dependent strength reduction factor (R_μ) is directly proportional to the SDOF displacement ductility ratio in the range of periods of interest in this study. It is noted that Equation 4.2 is utilized for (a) ground motions recorded on stiff soil sites that do exhibit neither near-fault nor soft-soil characteristics, and (b) structural systems designed to develop a beam-hinge mechanism. For the assessment of nonlinear behavior of structures, these factors

make the dynamic response of the structural systems similar to that of SDOF systems which have periods of vibrations between 1.2 s and 3.0 s and are exposed to ground motions consistent with those used in this study.

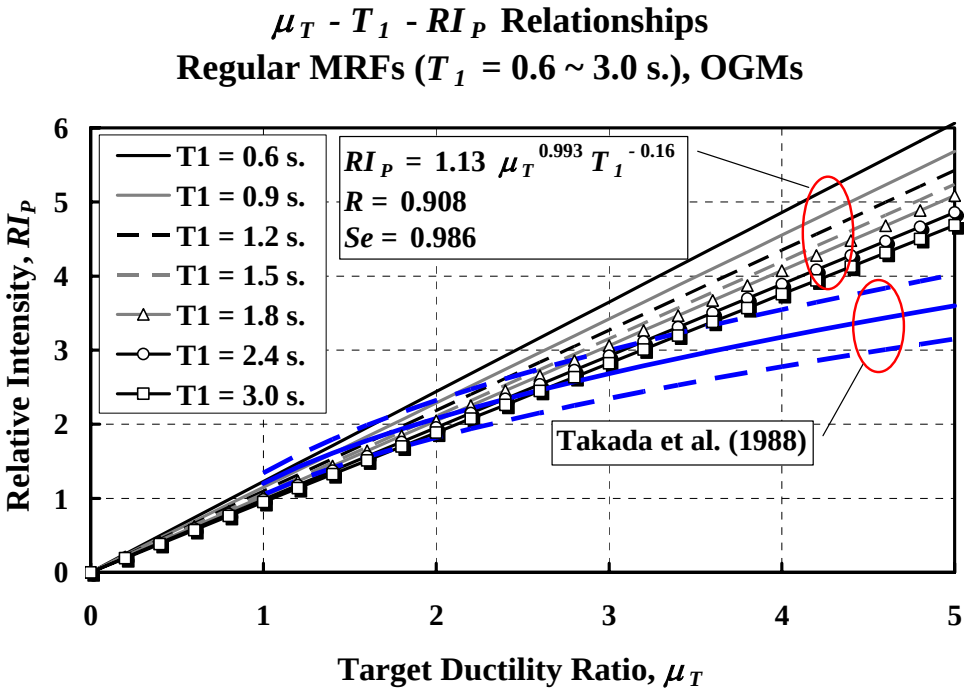

Figure 4.3 μ_T - T_1 - RI_P relationships in 2-D for frames designed based on the lateral load patterns proposed in this study

It is important to note that the best estimate of the relationship between RI_P (or R_μ) and ductility ratio μ_T (or μ) obtained in this study differs from those proposed in past studies for MDOF systems with a uniform distribution of stiffness over the height. For instance, Takada et al. (1988) recommended the use of a period-independent $\mu - R_\mu$ relationship for MDOF systems of the form $R_\mu = \varepsilon\sqrt{2\mu - 1}$, where the adjustment factor, ε, was approximately equal to 1.2 (i.e., the average of the range between 1.05 and 1.34, see Figure 4.3). This adjustment factor represented the degree

of deviation of the μ -R_μ relationship from the 'equal energy expression' $\sqrt{2\mu - 1}$. The difference in the form of the relationship used by Takada et al. (1988) and the one proposed in this study is attributed mainly to differences in the range of fundamental periods of vibration utilized: 0.6 s. to 3.0 s. and 0.5 s. to 1.0 s. respectively. However, as shown in Figure 4.3, the μ -R_μ relationship proposed by Takada et al. (1998) differs from the proposed μ_T - T_1 - RI_P relationship even for the period range used by them (i.e., T_1 = 0.5 s. ~ 1.0).

4.2.2 Relative Distribution of Story Shear Strength

For a given structural system and a given set of ground motions, Equation 3.2 is used to fit the story shear strength patterns of the type shown in Figure 3.10 and simultaneously obtain the required estimates of k and F_{top}/V_y in order to achieve a predefined target story ductility ratio. For each structure, fundamental period of vibration, and target story ductility ratio, the parameters k and F_{top}/V_y are determined by fitting the normalized story shear strength distribution based on Equation 3.2 into the median of the story shear strength distribution (see Table 4.1). In concept, these parameters provide a story shear strength pattern that would produce, on average, a constant story ductility ratio along the height when the frames are exposed to the ground motions utilized in this study.

Table 4.1 Parameters k and F_{top}/V_y for frames exposed to OGMs

N = 6, T_1 = 0.6 s.					
μ_T	1	2	3	4	5
k	0.52	0.32	0.11	-0.12	-0.22
F_{top}/V_y	0.11	0.15	0.21	0.29	0.34
N = 6, T_1 = 1.2 s.					
μ_T	1	2	3	4	5
k	0.42	-0.05	-0.4	-0.64	-0.68
F_{top}/V_y	0.25	0.37	0.4	0.44	0.44
N = 9, T_1 = 0.9 s.					
μ_T	1	2	3	4	5
k	0.74	0.58	0.32	0.02	-0.09
F_{top}/V_y	0.12	0.18	0.23	0.29	0.3
N = 9, T_1 = 1.8 s.					
μ_T	1	2	3	4	5
k	0.16	-0.06	-0.16	-0.19	-0.25
F_{top}/V_y	0.31	0.31	0.3	0.27	0.27
N = 12, T_1 = 1.2 s.					
μ_T	1	2	3	4	5
k	0.6	0.54	0.19	0.01	-0.9
F_{top}/V_y	0.2	0.22	0.25	0.25	0.25
N = 12, T_1 = 2.4 s.					
μ_T	1	2	3	4	5
k	-0.04	-0.24	-0.28	0.55	0.24
F_{top}/V_y	0.24	0.22	0.2	0.23	0.23
N = 15, T_1 = 1.5 s.					
μ_T	1	2	3	4	5
k	0.55	0.24	0.05	-0.04	-0.08
F_{top}/V_y	0.23	0.23	0.23	0.21	0.2
N = 15, T_1 = 3.0 s.					
μ_T	1	2	3	4	5
k	-0.24	-0.34	-0.39	0.53	0.25
F_{top}/V_y	0.2	0.17	0.15	0.23	0.23
N = 18, T_1 = 1.8 s.					
μ_T	1	2	3	4	5
k	0.53	0.25	-0.02	-0.09	-0.15
F_{top}/V_y	0.23	0.23	0.21	0.18	0.17

Strictly speaking, the design load patterns consisting of the above parameters are only applicable for those designated frame models, so these values are not readily applicable to the design of frame structures with fundamental periods of vibration (or number of stories) that lie between those included in Table 4.1. To generalize the use of parameters k and F_{top}/V_y for the design of moment-resisting frames with a fundamental period in the range of T_1 = 0.6 s. ~ 3.0 s. for the aforementioned target ductility levels, statistical regression analyses are conducted. Statistical models are developed for the estimation of the design lateral load pattern (e.g. k, F_{top}/V_y) as a function of relevant structural properties (e.g. fundamental period, total height) and target story ductility ratios.

Before using the regression models, two options were evaluated in order to determine the values of parameters k and F_{top}/V_y necessary for the regression analyses: (1) first option (*Option 1*) was used to fit median of story shear strength distribution with the normalized story shear strength distribution based on Equation 3-2 ; (2) second option (*Option 2*) was used to fit the individual story shear strength distributions based on Equation 3-2 and determine the average value of the fitted parameters k and F_{top}/V_y. The results from both approaches, *Option 1* and *Option 2*, are shown to be very similar as presented in Figures 4.4 and 4.5, respectively. Because the median values are less sensitive to the record-to-record variability of story shear strength distributions (see Figure 4.4) and the objective is to develop design load patterns tha provide median story ductility ratios along the height that are the same in each story, *Option 1* was selected to determine parameters k and F_{top}/V_y as representative values for a given frame model and a target story ductility ratio.

Parameter k (*Option 1* vs. *Option 2*)
MRFs (T_1 = 0.6 s. ~ 3.0 s.), OGMs

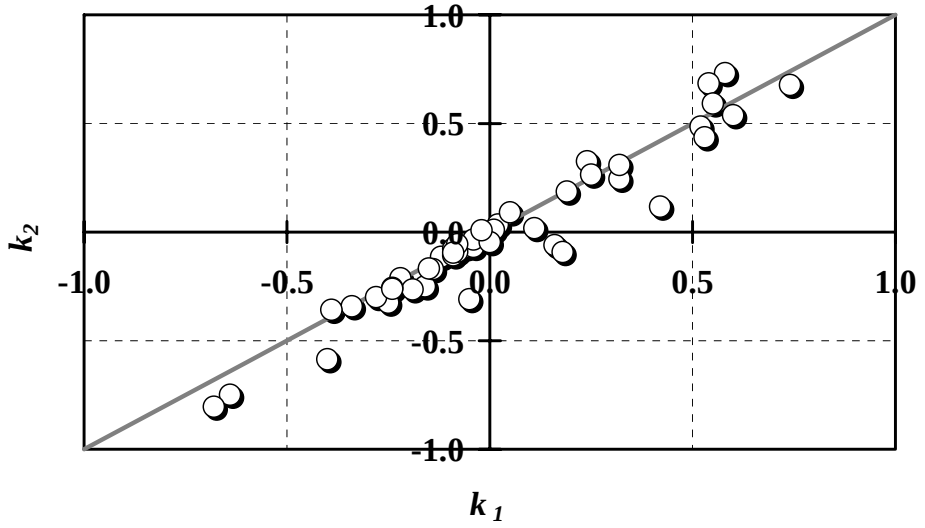

Figure 4.4 Comparison of k_1 and k_2 for moment-resisting frames utilized in this study

Parameter F_{top}/V_y (*Option 1* vs. *Option 2*)
MRFs (T_1 = 0.6 s. ~ 3.0 s.), OGMs

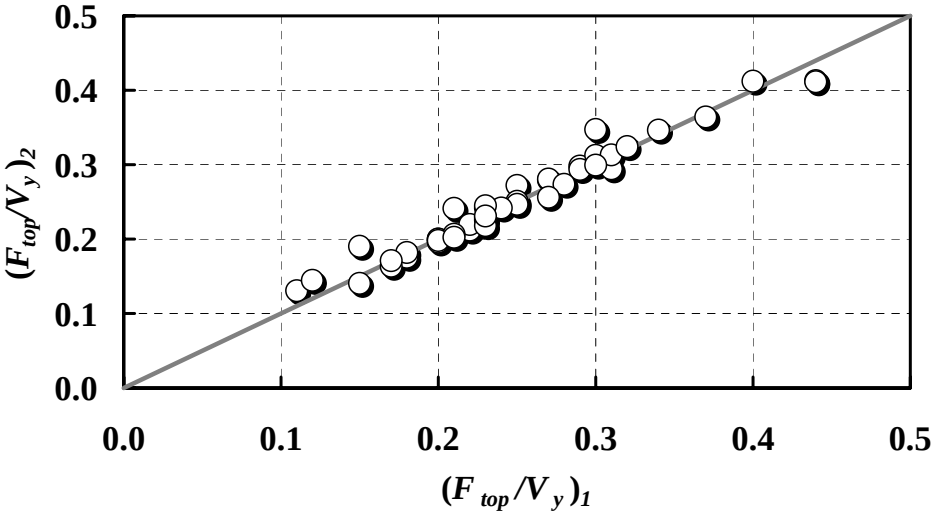

Figure 4.5 Comparison of $(F_{top}/V_y)_1$ and $(F_{top}/V_y)_2$ for moment-resisting frames utilized in this study

Statistical analyses were conducted to evaluate the relationships between k, F_{top}/V_y, μ_T, and the total height of the frame, H. The correlation between pairs of variables was evaluated first to quantify their relationships. The analyses demonstrated that a positive correlation existed between the parameters k and μ_T. Therefore, the following linear model is proposed to estimate values of the exponent k in Equations 4.3 as a function of the desired level of inelastic behavior, μ_T (see Figure 4.6):

$$k = 0.53 - 0.17 \cdot \mu_T \text{, where } \quad 1 \leq \mu_T \leq 5 \qquad [4.3]$$

This linear model was presented by Park and Medina (2007), and is valid for the fundamental period from 0.6 s. to 1.8 s., and the coefficients of the model from Park and Medina (2007) were modified based on the range of fundamental periods as presented in Equation 4.3. In this study, the correlation coefficient and standard error for Equation 4.3 are equal to 0.736 and 0.225 for the range T_1 from 0.6 s. to 3.0 s, respectively, as compared to 0.686 and 0.053 in the model utilized by Park and Medina (2007). From a physical point of view, the implementation of Equation 4.3 implies that the relative distribution of seismic lateral forces over the height of the frame depends explicitly on the target level of inelastic behavior in the design, which is a feature that is lacking in current seismic code provisions.

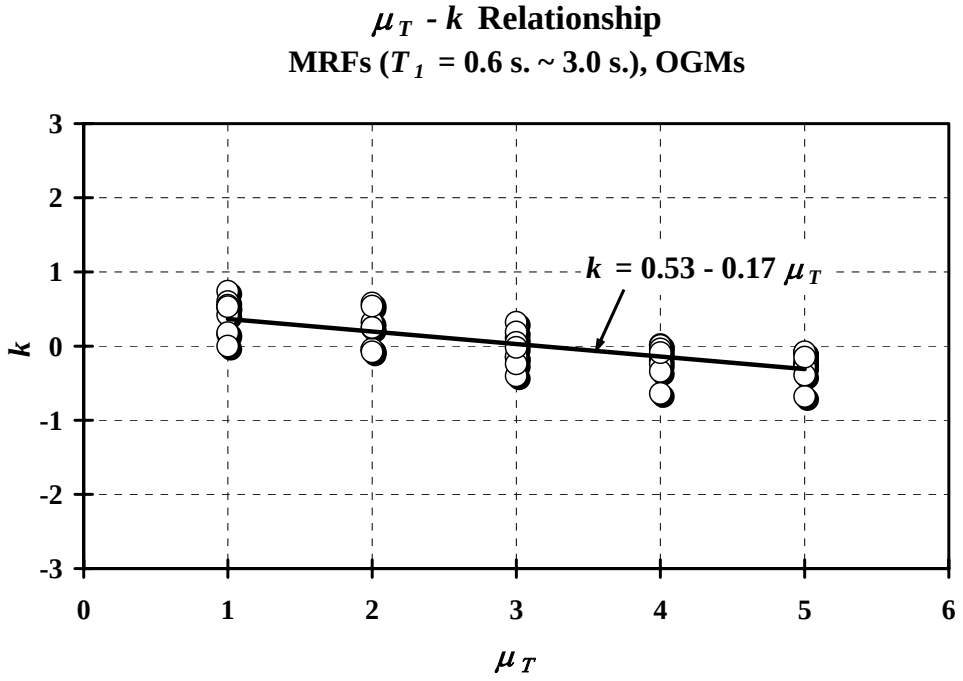

Figure 4.6 μ_T – k relationship for all frame models utilized in this study

Because statistical analyses demonstrated that F_{top}/V_y depends on both H and k, a model that provides estimates of F_{top}/V_y is provided by:

$$\frac{F_{top}}{V_y} = 0.34 - 0.002 \cdot H - 0.11 \cdot k \text{ , where } 22 \text{ m} \le H \le 66 \text{ m} \qquad [4.4]$$

The correlation coefficient is 0.649 and the standard error is 0.0576. Figure 4.7 presents a graphical representation of Equation 4.4 for all moment-resisting frames utilized in this study. It is also noted that Equations 4.3 and 4.4 are only applicable to moment-resisting frames exposed to ordinary ground motions which do neither exhibit near-fault nor soft-soil characteristics.

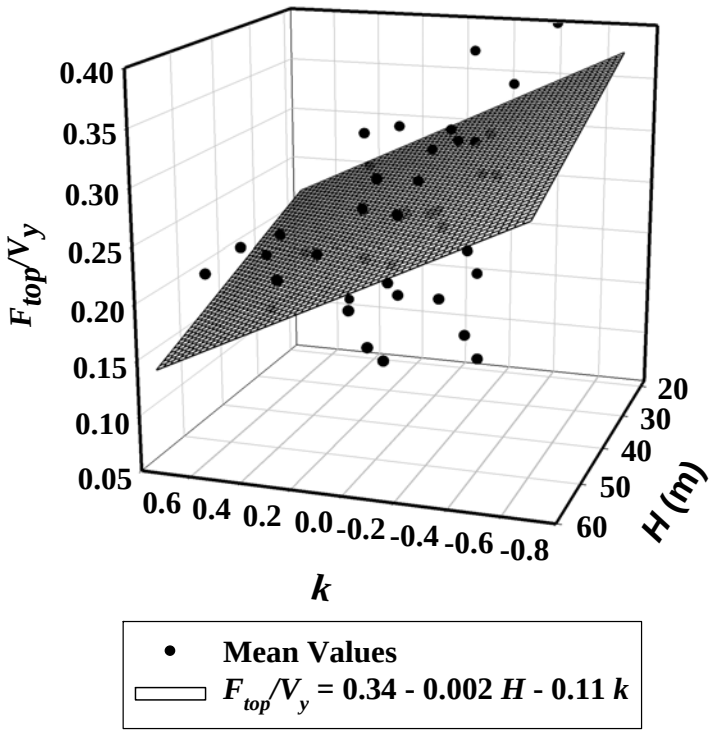

Figure 4.7 $H - k - F_{top}/V_y$ relationship for all frame models exposed to OGMs utilized in this study

4.3 DESIGN LATERAL LOAD PATTERNS FOR MOMENT-RESISTING FRAMES EXPOSED TO NEAR-FAULT GROUND MOTIONS

4.3.1 Seismic Base Shear Strength

The same regression model used for ordinary ground motions is utilized for the μ_T - T_1 - RI_P relationships corresponding to frames exposed to near-fault ground motions. A Weighed-Least-Squares multiple regression was also utilized and the proposed μ_T - T_1 - RI_P relationships for $T_1/T_p < 1$ and $T_1/T_p > 1$ are of the forms:

$$\text{For } T_1/T_p < 1: \; RI_P = 1.21\, \mu_T^{\,0.789}\, T_1^{\,-0.092} \qquad [4.5]$$

$$\text{For } T_1/T_p > 1: \; RI_P = 1.34\, \mu_T^{\,0.913}\, T_1^{\,-0.349} \qquad [4.6]$$

Equations 4-5 and 4-6 present RI_P as a function of target story ductility ratio, the fundamental period, as well as the ratio T_1/T_p. The correlation coefficients and the standard errors for Equations 4.5 and 4.6 are (0.767, 0.0744) and (0.821, 0.117), respectively. The graphical representations for Equations 4.5 and 4.6 are shown in Figure 4.8.

μ_T -*RI* relationships for frames exposed to near-fault ground motions, previously proposed by Park and Medina (2006), were of the form:

$$RI = \alpha\, \mu_T \qquad [4.7]$$

where the parameter α was a function of the ratio T_1/T_p as well as the fundamental period of structures. Since a limited number of fundamental periods was used (e.g., T_1 = 1.2 s., 1.5 s., 1.8 s.) by Park and Medina (2006), the dependency of *RI* on T_1 was relatively weak. This dependency was accounted for through the parameter α as shown in Figure 4.9. It is important to note that, for the range $T_1/T_p > 1$, the proposed load patterns for a frame exposed to near-fault ground motions are similar to the proposed load patterns for frame structures exposed to ordinary ground motions. As shown in Figures 4.3 and 4.10, this observation is limited to the fundamental period range from 1.2 s. to 1.8 s. for the same performance target of interest. For flexible frames with T_1 = 2.4 s. and 3.0 s, the μ_T - T_1 - RI_P relationships for $T_1/T_p > 1$ are more comparable to those relationships for $T_1/T_p < 1$. In this study, structural strength is tuned based on the lateral floor loads, and the base shear strength is as a function of fundamental period of structures. Thus, the responses of flexible frame structures

with T_1 = 2.4 s. and 3.0 s are more influenced by higher mode effects (e.g., 2nd and 3rd).

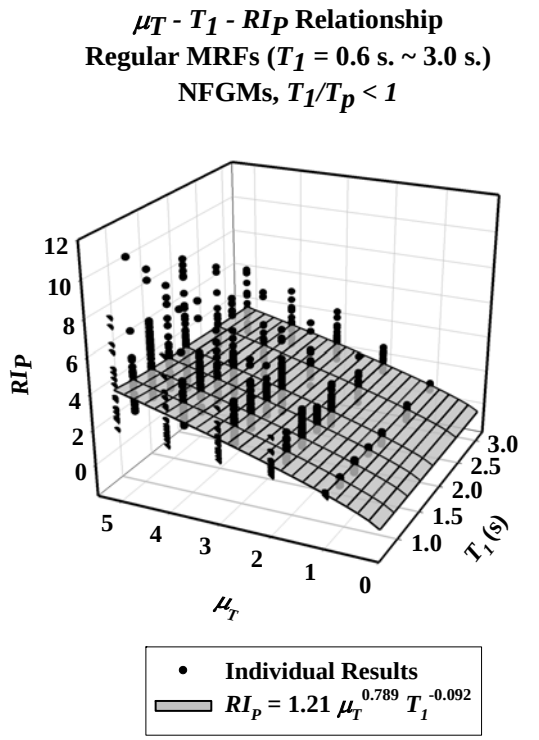

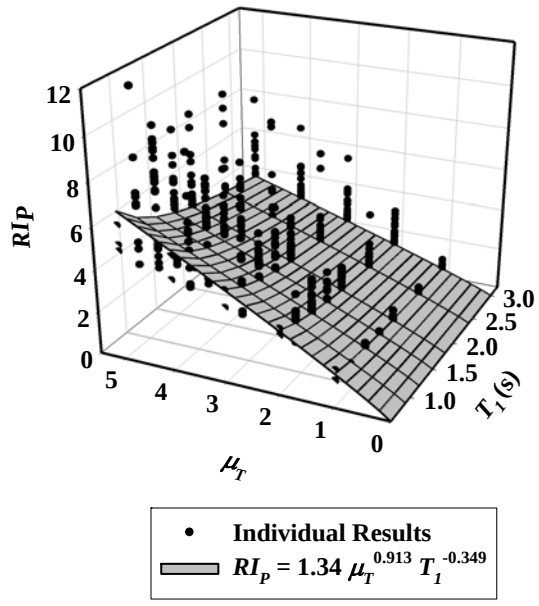

Figure 4.8 μ_T - T_1 - RI_P relationships for frames designed based on the proposed lateral load patterns and exposed to NFGMs for $T_1/T_p < 1$ and $T_1/T_p > 1$

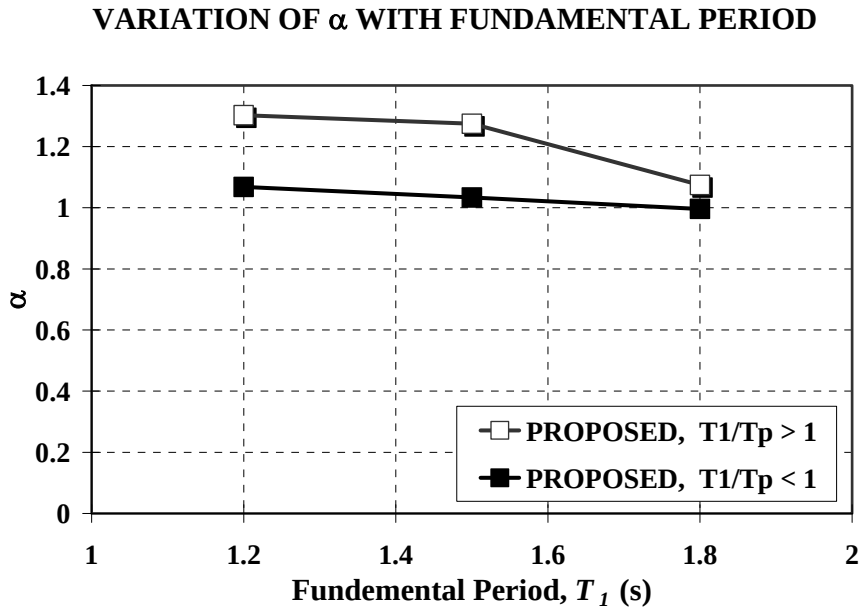

Figure 4.9 Variation of coefficient α in Equation 4.7 with fundamental period

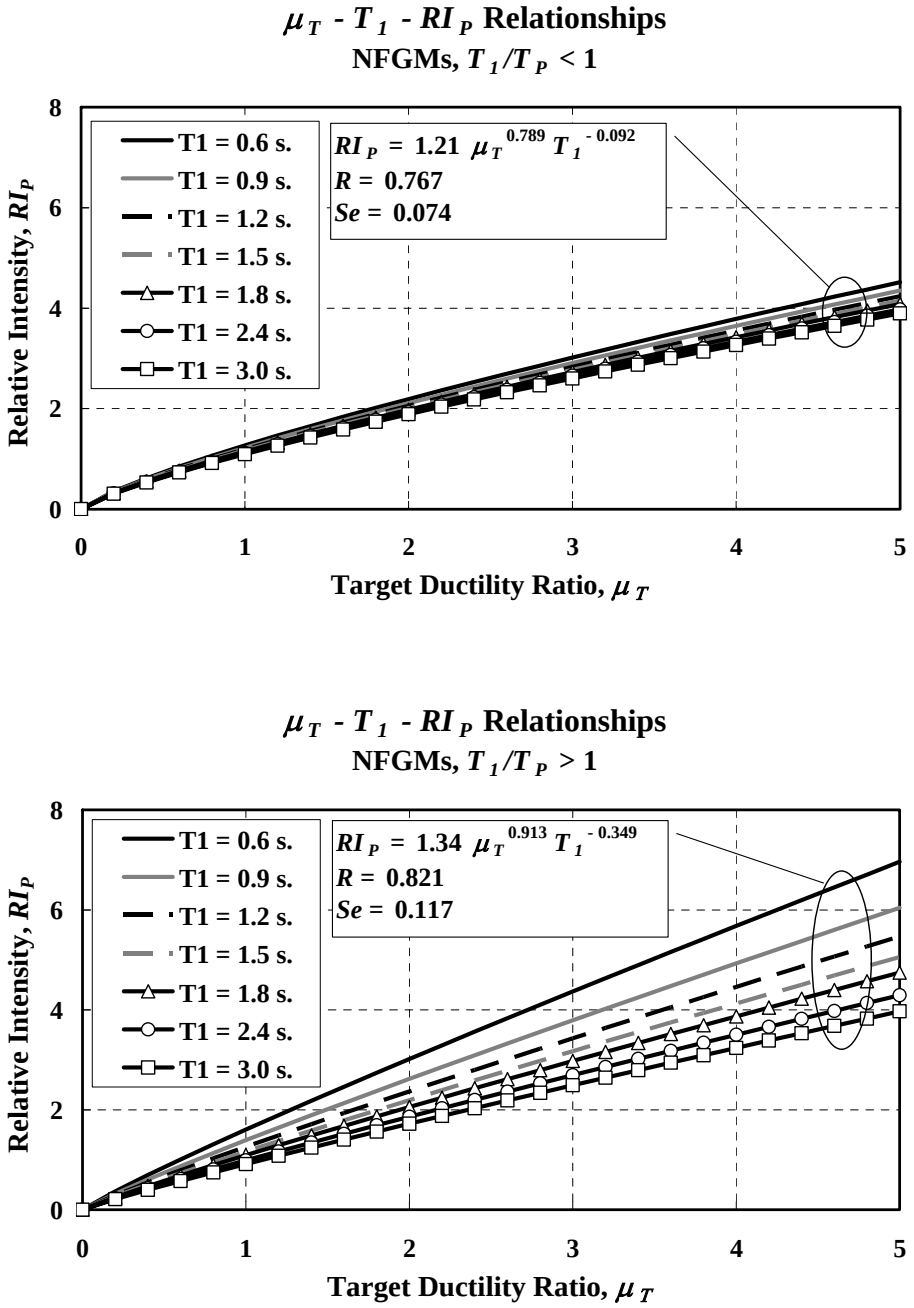

Figure 4.10 μ_T - T_1 - RI_P relationships in 2-D for frames designed based on the proposed lateral load patterns and exposed to NFGMs for T_1/T_p < 1 and T_1/T_p > 1

The best estimate of the relationships between RI_P, T_1, and μ_T for frames exposed to near-fault ground motions depends on the ratio T_1/T_p. To better illustrate the variation

of the relationships with respect to the fundamental period of vibration, Figure 4.8 is re-plotted in 2-D as shown in Figure 4.10. It is found that for a given T_1/T_p ratio, RI_P is strongly dependent on the fundamental period of vibration, as well as the target story ductility ratio when the T_1/T_p ratio is greater than 1.0. Figure 4.10 shows results that are more consistent with "the equal displacement" rule of SDOF systems for $T_1/T_p < 1$; however, the shorter T_1, the larger RI_P for the case of $T_1/T_p > 1$. Because $RI_P = [S_a(T_1)/g]/\gamma_P$, for $T_1/T_p < 1$, a larger base shear strength is required when compared to the case for $T_1/T_p > 1$. This implies that the 'period elongation' for the first mode (when the fundamental period is smaller than the pulse period) produces larger inelastic deformations than those produced by the tuning of the higher modal periods with the pulse period of the ground motion (when $T_1/T_p > 1$).

4.3.2 Relative Distribution of Story Shear Strength

The same procedure utilized in Section 4.2.2 to determine the parameters k and F_{top}/V_y is utilized for moment-resisting frames exposed to near-fault ground motions. The values of k and F_{top}/V_y are estimated for all frame structures with T_1 = 0.6 s. ~ 3.0 s. and target story ductility ratios from 1 to 5. For each structure, ground motion sets are assembled based on the ratio of the fundamental period of the structure to the pulse period of the ground motion, T_1/T_p, i.e., one set corresponding to $T_1/T_p < 1$ and another one corresponding to $T_1/T_p > 1$ (see Tables 4.2 and 4.3). The lower and upper limits of the number of stories (N), target story ductility ratios (μ_T), structural periods (T_1), and the number of near-fault ground motions (No. of NFGMs) utilized in this study corresponding to the ratio T_1/T_p are shown in Table 3.3.

Table 4.2 Parameters k and F_{top}/V_y for all frames and for all target story ductility ratios exposed to near-fault ground motions based on $T_1/T_p < 1$

N = 6, T_1 = 0.6 s.					
μ_T	1	2	3	4	5
k	0.81	0.14	-0.1	-0.17	-0.32
F_{top}/V_y	0.08	0.15	0.21	0.26	0.32
N = 6, T_1 = 1.2 s.					
μ_T	1	2	3	4	5
k	0.5	0.17	-0.05	-0.12	-0.25
F_{top}/V_y	0.16	0.2	0.23	0.25	0.28
N = 9, T_1 = 0.9 s.					
μ_T	1	2	3	4	5
k	0.63	0.4	0.3	0.12	0.05
F_{top}/V_y	0.12	0.12	0.14	0.18	0.2
N = 9, T_1 = 1.8 s.					
μ_T	1	2	3	4	5
k	0.3	0.15	0.05	-0.07	-0.06
F_{top}/V_y	0.16	0.16	0.15	0.16	0.15
N = 12, T_1 = 1.2 s.					
μ_T	1	2	3	4	5
k	0.74	0.5	0.3	0.23	0.14
F_{top}/V_y	0.11	0.11	0.13	0.13	0.14
N = 12, T_1 = 2.4 s.					
μ_T	1	2	3	4	5
k	0.39	0.17	0.09	0.03	-0.02
F_{top}/V_y	0.16	0.12	0.11	0.1	0.09
N = 15, T_1 = 1.5 s.					
μ_T	1	2	3	4	5
k	0.8	0.35	0.2	0.11	0.02
F_{top}/V_y	0.1	0.11	0.11	0.1	0.11
N = 15, T_1 = 3.0 s.					
μ_T	1	2	3	4	5
k	0.49	0.21	0.08	-0.04	-0.09
F_{top}/V_y	0.11	0.11	0.09	0.09	0.08
N = 18, T_1 = 1.8 s.					
μ_T	1	2	3	4	5
k	0.46	0.28	0.11	0.05	0.03
F_{top}/V_y	0.13	0.12	0.11	0.1	0.09

Table 4.3 Parameters k and F_{top}/V_y for all frames and for all target story ductility ratios exposed to near-fault ground motions based on $T_1/T_p > 1$

N = 6, T_1 = 0.6 s.					
μ_T	1	2	3	4	5
k	2.28	1.58	0.3	-0.27	-0.71
F_{top}/V_y	0	0.1	0.36	0.46	0.54
N = 6, T_1 = 1.2 s.					
μ_T	1	2	3	4	5
k	-0.21	-0.45	-0.61	-0.85	-1.14
F_{top}/V_y	0.48	0.51	0.5	0.53	0.54
N = 9, T_1 = 0.9 s.					
μ_T	1	2	3	4	5
k	0.55	0.8	0.24	-0.07	-0.23
F_{top}/V_y	0.24	0.22	0.33	0.35	0.37
N = 9, T_1 = 1.8 s.					
μ_T	1	2	3	4	5
k	0.18	-0.05	-0.42	-0.52	-0.56
F_{top}/V_y	0.42	0.41	0.36	0.31	0.28
N = 12, T_1 = 1.2 s.					
μ_T	1	2	3	4	5
k	0.44	0.55	0.19	-0.04	-0.21
F_{top}/V_y	0.32	0.26	0.28	0.3	0.31
N = 12, T_1 = 2.4 s.					
μ_T	1	2	3	4	5
k	-0.01	0.13	-0.13	-0.23	-0.31
F_{top}/V_y	0.35	0.25	0.21	0.17	0.16
N = 15, T_1 = 1.5 s.					
μ_T	1	2	3	4	5
k	0.59	0.52	0.12	-0.19	-0.32
F_{top}/V_y	0.3	0.24	0.25	0.23	0.22
N = 15, T_1 = 3.0 s.					
μ_T	1	2	3	4	5
k	0.03	0.08	-0.27	-0.36	-0.42
F_{top}/V_y	0.34	0.23	0.16	0.12	0.1
N = 18, T_1 = 1.8 s.					
μ_T	1	2	3	4	5
k	0.77	0.34	-0.13	-0.28	-0.36
F_{top}/V_y	0.3	0.28	0.22	0.18	0.15

For regular moment-resisting frames exposed to near-fault ground motions, statistical analyses were conducted to evaluate the relationships between k, F_{top}/V_y, μ_T, and the total height of the frame, H. The analyses also demonstrated that a positive correlation existed between the parameters k and μ_T with a linear regression model. Forms of $\mu_T - k$ relationships for the range ($\mu_T = 1 \sim 5$) are presented in Equations 4.8 and 4.9. Correlation coefficients and the standard errors are (0.810, 0.157) and (0.617, 0.516) for Equations 4.8 and 4.9, respectively.

For $T_1/T_p < 1$: $k = 0.63 - 0.15 \cdot \mu_T$ [4.8]

For $T_1/T_p > 1$: $k = 0.86 - 0.28 \cdot \mu_T$ [4.9]

From the statistical results shown in Figure 4.11, the parameter k strongly depends on the target story ductility ratio, especially when the pulse period is greater than the fundamental period of structures (i.e., $T_1/T_p < 1$). For $T_1/T_p > 1$, the dependency of μ_T on k is somewhat weaker than the dependency for $T_1/T_p < 1$ because of two data points above $k = 1.0$ at $\mu_T = 1$ and 2, which belong to the 6-story frame with $T_1 = 0.6$ s (see Figure 4.11). Excluding those two values, Equation 4.9 becomes very similar to Equation 4.3 for ordinary ground motions (i.e., $k = 0.54 - 0.2\ \mu_T$).

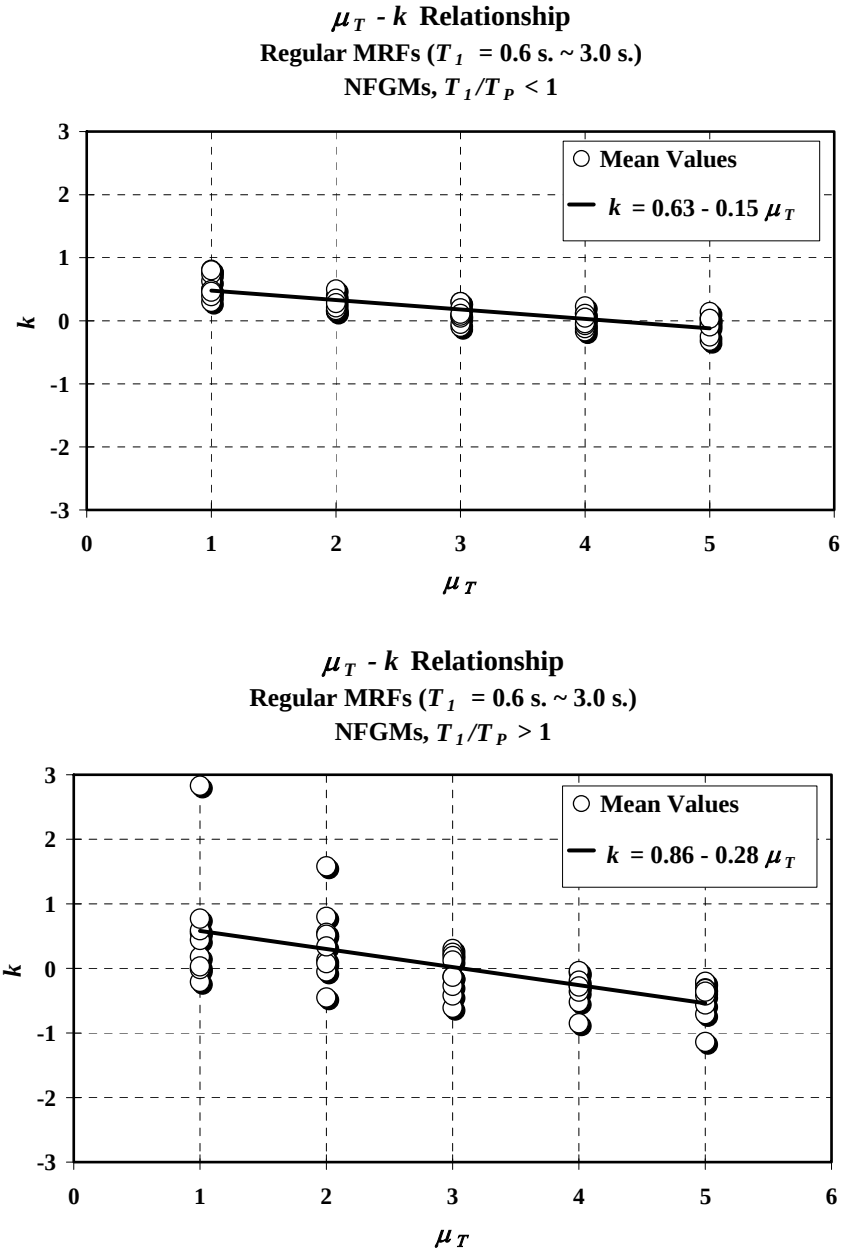

Figure 4.11 μ_T – k relationship for the frames exposed to NFGMs for T_1/T_p < 1 and T_1/T_p > 1

The parameter F_{top}/V_y provides a concentrated load at the top of a frame (see Figure 3.10) as a function of the parameter k and the total height of a structure. Statistical analyses demonstrated that F_{top}/V_y depends on both H and k, and a model was developed to provide estimates of F_{top}/V_y as follows:

For $T_1/T_p < 1$: $\frac{F_{top}}{V_y} = 0.26 - 0.003 \cdot H - 0.082 \cdot k$ [4-10]

For $T_1/T_p > 1$: $\frac{F_{top}}{V_y} = 0.49 - 0.005 \cdot H - 0.10 \cdot k$ [4-11]

where the height varies from 72 ft (22 m) to 216 ft (66 m). Correlation coefficients and standard errors are (0.800, 0.157) and (0.617, 0.516) for Equations 4.10 and 4.11, respectively, which show that the parameter F_{top}/V_y is more strongly dependent on H and k when the fundamental period of the structure is less than the pulse period (i.e., $T_1/T_p < 1$). Figures 4.12 present a graphical representation of Equations 4.10 and 4.11, respectively. These two parameters, k and F_{top}/V_y, provide a story shear strength pattern that would produce, on average, a constant story ductility ratio along the height when the moment-resisting frames are exposed to near-fault ground motions characterized by the ratio T_1/T_p.

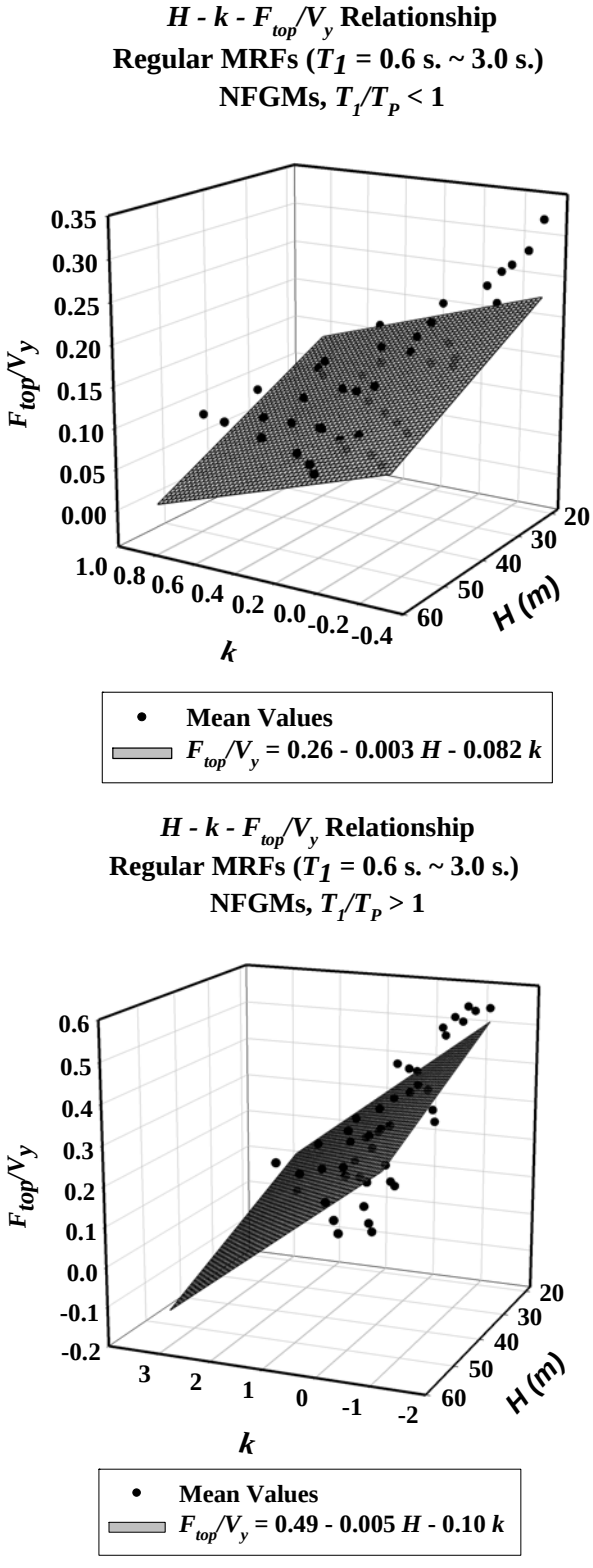

Figure 4.12 $H - k - F_{top}/V_y$ relationship for all frame models exposed to NFGMs for $T_1/T_p < 1$ and $T_1/T_p > 1$

For the same performance target of interest, the proposed load patterns for a frame exposed to near-fault ground motions within the range $T_1/T_p > 1$ are very similar to the proposed load patterns for frame structures exposed to the ordinary ground motions. This is true especially for the large portion of the base shear strength at the top, (see Figure 4.13). This implies that for this family of generic frames, the structural response when $T_1/T_p > 1$ is not significantly affected by the pulse-type characteristics of near-fault ground motions.

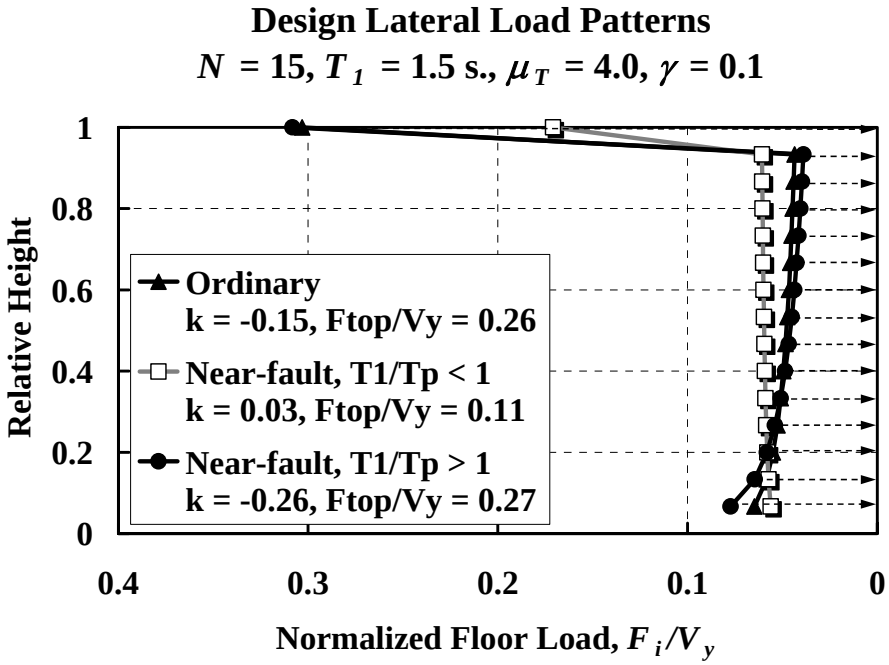

Figure 4.13 Lateral load patterns for 15-story frame with T_1 = 1.5 s. and γ = 0.1 for μ_T = 4

4.4 SUMMARY

- The seismic base shear strength for moment-resisting frames exposed to ordinary ground motions is obtained from the relative intensity (RI_P) estimated from the μ_T-T_1-RI_P relationship. The relative intensity obtained from the iterative procedure for the uniform story ductility ratio along the height of structure strongly depends on the target story ductility ratio (μ_T = 1 ~ 5) and the fundamental period of structures (T_1 = 0.6 s. ~ 3.0 s.). This relationship is consistent with the equal displacement rule of SDOF systems, especially for longer fundamental periods (T_1 = 1.2 s. ~ 3.0 s.). In addition, the best estimates of the proposed μ_T-T_1-RI_P relationship of MDOF systems are significantly different from those from previous studies for MDOF systems.
- Proposed load patterns for moment-resisting frames exposed to ordinary ground motions are determined by the parameters k and F_{top}/V_y. Parameter k strongly depends on the target level of inelastic behavior, and F_{top}/V_y strongly depends on the parameter k and the story height of structure, H.
- For moment-resisting frames (T_1 = 0.6 s. ~ 3.0 s.) exposed to near-fault ground motions, the seismic base shear strength is obtained from RI_P values estimated from μ_T-T_1-RI_P relationships. For a given frame and a selected target story ductility ratio, the variation of the proposed μ_T-T_1-RI_P relationship strongly depends on the ratio of the fundamental period of the structure to the pulse period of the ground motion, T_1/T_p.

- The relative distribution of story shear strength for moment-resisting frames exposed to near-fault ground motions also depends on the ratio T_1/T_p, as well as the target level of inelastic behavior and the story height.
- For the same performance target of interest and the fundamental period range 1.2 s. and 1.8 s, the proposed load patterns for a frame exposed to near-fault ground motions within the range $T_1/T_p > 1$ are similar to the proposed load patterns for frame structures exposed to ordinary ground motions. This implies that for this family of generic frames with this fundamental period range, the structural response is not significantly affected by the pulse-type characteristics of near-fault ground motions.

5 CONCEPTUAL SEISMIC DESIGN METHODOLOGY BASED ON UNIFORM STRUCTURAL DAMAGE

5.1 INTRODUCTION

In Chapter 4, design lateral load patterns to obtain a uniform distribution of damage along the height were proposed by using the combination of a seismic base shear strength obtained through the relative intensity parameter (RI_P) and a relative shear strength distribution (see Equation 4.2). The proposed relative intensity was obtained by using Equations 4.2, 4.5, and 4.6 for ordinary ground motions and near-fault ground motions, respectively, corresponding to a given target story ductility ratio (μ_T). As mentioned earlier, this study utilizes story ductility ratios as a damage indicator and the main parameter to quantify structural damage. Thus, this chapter deals with proposing a conceptual seismic design methodology based on the use of the design lateral load patterns developed in Chapter 4.

The new conceptual seismic design methodology is based on the notion that the total seismic-induced damage to structural components is equivalent to the damage experienced by systems designed based on current seismic design procedures for a given seismic hazard level (mainly 10/50). The main advantage is that, on average, designs based on the proposed approach would exhibit a more uniform distribution of damage over the height. The global damage parameter is quantified by the average of story ductility ratios along the height of a structure (μ_{avg}). This implies that the proposed seismic lateral loads can be used to design systems which

experience μ_{avg} demands consistent with those experienced by systems designed based on current approaches.

As part of the proposed approach, story strengths are assigned such that story ductility ratios over the height are approximately equal to μ_{avg}, i.e., uniform damage along the height. Figure 5.1 shows an example of median story ductility ratios (computed as geometric mean) for two 15-story frame structures exposed to the 40 ordinary ground motions provided in Table 3.1. Story shear strengths are tuned to values estimated based on the equivalent lateral force procedure of the IBC 2006 (denoted as "CURRENT" in Figure 5.1) and the approach based on Equations 4.3 and 4.4 (denoted as "PROPOSED" in Figure 5.1). The global damage for both frames corresponds to an average story ductility ratio over the height approximately equal to 4. However, the structure designed based on the proposed approach exhibits a more uniform distribution of story ductility ratios over the height. It is important to note that limiting the story ductility ratio to a target story ductility ratio over the height also results in a smoother distribution of maximum story drift ratios (see Figure 5.1). This issue will be discussed in more detail in Chapter 6.

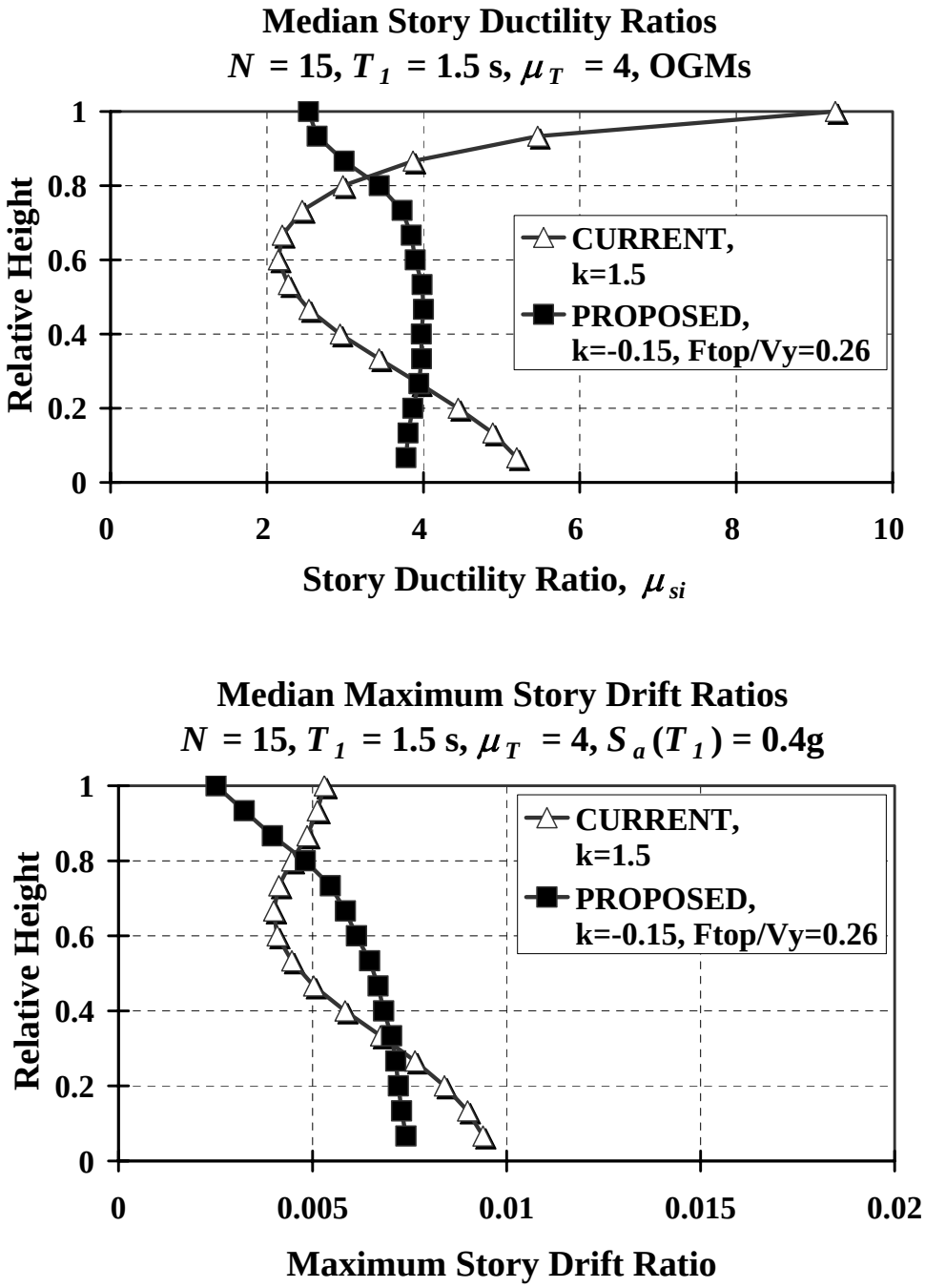

Figure 5.1 Fifteen-story frame structure median distribution of story ductility ratios; median maximum story drift ratios over the height

5.2 CONCEPTUAL SEISMIC DESIGN METHODOLOGY

The proposed approach to achieve a uniform distribution of structural damage over the height consists of the following steps (Park and Medina 2007):

1. For a given height and type of lateral-load resisting system (i.e., moment-resisting frame), select the response modification factor (R), estimate the global system overstrength (Ω), and determine the relative intensity (RI_C) of frames designed based on current U.S. seismic provisions, where $RI = R / \Omega$ as shown in Figure 5.2.
2. Estimate the expected average of the story ductility ratios over the height of frames designed based on current procedures, i.e., μ_{avg}, for a given RI_C.
3. Make μ_{avg} equal to the target story ductility ratio, μ_T, and estimate the story shear-strength distribution required to achieve this target story ductility ratio.
4. Utilize the story shear strength distribution of Step 3 to design the moment-resisting frame followed by the seismic performance evaluation of the design.

These general steps are depicted in Figure 5.3 and discussed in subsequent Sections in this chapter.

.

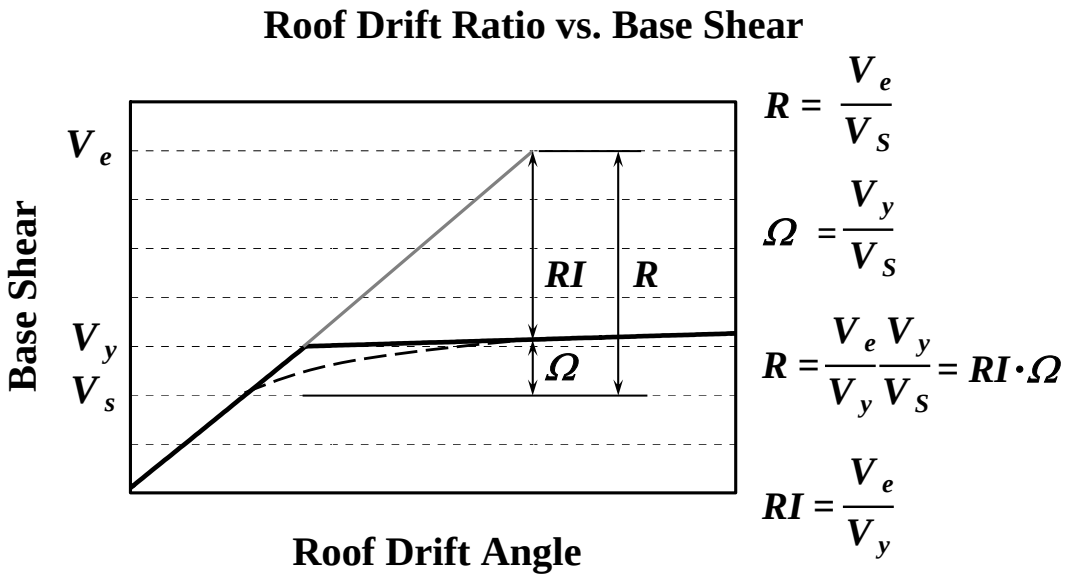

Figure 5.2 Relationship between response modification factor, global overstrength, and relative intensity (Park and Medina, 2007)

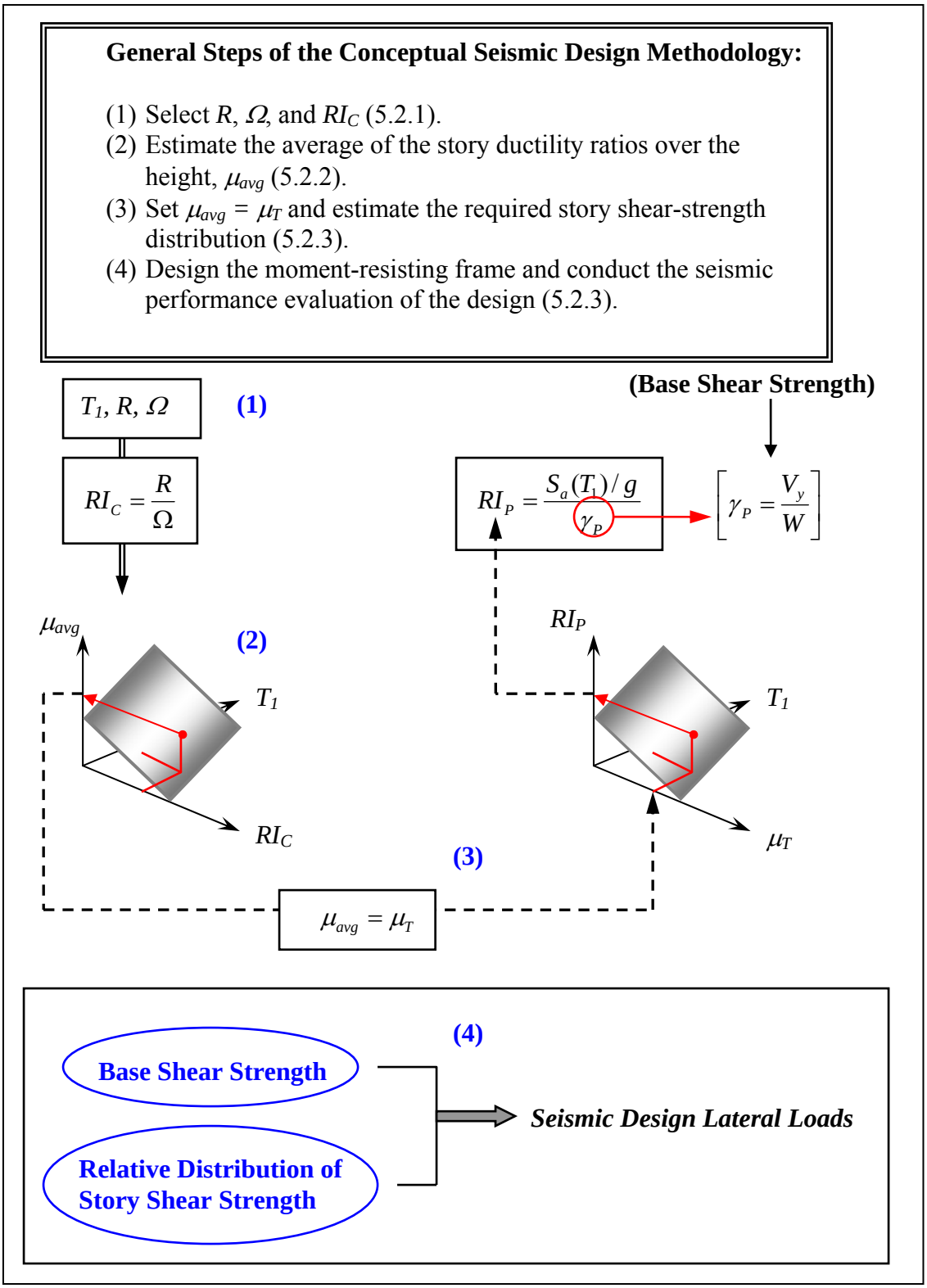

Figure 5.3 Procedure of the proposed conceptual seismic design methodology for special moment-resisting frames

5.2.1 Response Modification Factors (R) and Global Overstrength (Ω), and Relative Intensity (RI_C)

Response modification factors in current U.S. seismic code provisions are based on the type of lateral-load resisting systems. The value of the response modification factor, recommended for concrete and steel special moment-resisting frame structures, is 8 (IBC 2006). Those special moment-resisting frames are detailed to ensure ductile behavior of the beam-to-column joints and are normally used in zones of higher seismicity. Since values of relative intensity (RI) depend on both R and Ω, the challenge is to have a reasonable estimate of the global overstrength parameter. However, there is no simple way to estimate the actual overstrength of structures because it is a function of a variety of factors such as the effect of gravity loads on member strengths, member overstrength due to discrete choices of member sizes, member overstrength due to drift requirements, et cetera (Osteraas and Krawinkler 1990).

All structures possess their structural and nonstructural built-in strength capacities. These capacities are mostly determined by the combination of code-compliant loading conditions: dead load, live load, seismic lateral load, wind load, etc. If the actual strength of the structure is equal to the ultimate strength of the structure, the overstrength is defined as the difference between the actual strength and the design strength level from the code provisions (see Figure 5.2). The overstrength factor is determined in accordance with a variety of sources as shown in Table 5.1. Thus more research is needed to quantify representative values of overstrength factors. Based on limited data and the information presented in several previous studies

(Osteraas and Krawinkler 1990; Uang 1991; Gupta and Krawinkler 1999; Masumi et al. 2004), global overstrength factors between 1.45 and 4 are adopted in this study for moment-resisting frames with fundamental periods from 0.6 s. to 3.0 s. The corresponding number of stories is in between 6 to 18, and the structures are exposed to two different sets of ground motions: ordinary and near-fault ground motions. Ordinary and near-fault ground motions corresponding to spectral values consistent with the 10/50 seismic hazard level in the western U.S. (see Section 3.2). Since the relative intensity is estimated based on the ELF procedure, *RI* values are designated as RI_C in the calculation of average of story ductility ratios and estimated based on the relationship $RI_C = R / \Omega$ in this study, where $R = 8$ and Ω is assumed to vary between 1.45 and 4.

In practice, an alternative to obtain an overstrength factor for a moment resisting frame is to design the structure and conduct a nonlinear static or modal pushover analysis which can be viewed as a method for predicting seismic force and deformation demands (Krawinkler and Seneviratna 1998; Chopra and Goel 2002; Goel and Chopra 2005). From the static pushover curve, the global overstrength factor of the system designed based on the code provisions can be approximately estimated from the ratio of the fully yielded strength (V_y) to the design strength (V_s) as shown in Figure 5.2.

Table 5.1 Sources of overstrength (Osteraas and Krawinkler 1990)

	Source Type	Description
Local Overstrength	(a) Implied code strength	The difference between design level and required member strength which includes the effects of the material "factor of safety" and, for flexure, the section shape factor.
	(b) Controlling design condition	Member selection is typically controlled by a strength or serviceability criterion that involves other than seismic strength, such as gravity loading alone, combined gravity and lateral loading, wind loading, live load deflection control, or drift control.
	(c) Actual vs. norminal yield strength	The actual average yield strength of A36 rolled sections is greater than 36 ksi.
	(d) Actual vs. design loads	Actual floor live loads are typically significantly less than the reduced code minimum design live load.
	(e) Code minimum requirements	Under some circumstances, design will be governed by specific code requirements unrelated to strength or serviceability.
	(f) Discrete size selection	A design procedure will indicate a theoretical section requirement based on a controlling loading condition. The section selected will typically be somewhat larger than theoretically necessary.
	(g) Uniformity for constructability	Member sections will be typically more uniform than required.
	(h) Architectural considerations	Member sizes are greater than required for structural requirements (e.g., shear walls, spandrel beams).
Global Overstrength	(i) Structural elements not considered in design	In many cases, only certain portions of the structure will be designated as part of the lateral load system; the lateral strength and stiffness of the remainder of the structure is neglected.
	(j) Non-structural elements	Non-structural elements (e.g., partitions, stairways, cladding) all contribute to the ultimate lateral strength of any structure.

5.2.2 Average Story Ductility Ratio (μ_{avg})

The average value of story ductility ratios, μ_{avg}, is an indicator of global damage nondeteriorating frame structures. In the proposed approach, μ_{avg} values are estimated based on RI_C. RI_C-μ_{avg} relationships depend on a variety of factors such as ground motion frequency content and fundamental period. Thus, it is necessary to quantify RI_C-μ_{avg} relationships statistically to develop a model to predict central values of μ_{avg} for a given RI_C, which will be used to evaluate the expected global damage of frame structures designed based on current seismic code provisions. It is important to remember that, in this study, story shear strength values are tuned to the story shear demands based on the lateral-load patterns, which implies that the same amount of overstrength is assumed at all story levels. This assumption is made based on the large variations in story overstrength exhibited by moment-resisting frame structures (Jain and Navin 1993) and the inability to determine the actual distribution along the height of story overstrength *a priori*. Moreover, an accurate prediction of the expected distribution of story overstrength may not be warranted in the preliminary stages of the design.

Nonlinear time history analyses are conducted with the family of frames used in this study exposed to the ensemble of ground motions. Story shear strengths are tuned based on design lateral-load patterns proposed as part of the equivalent lateral force procedure of the IBC 2006. These design load patterns are determined based on Equations 2.5 and 2.6 in Chapter 2.

Average story ductility ratio (μ_{avg}) for moment-resisting frames exposed to ordinary ground motions

For each structure and ground motion, the average story ductility ratio is calculated as a function of the relative intensity as shown in Figure 5.4. The dots in Figure 5.4(a) represent median average story ductility ratio demands as a function of the relative intensity (RI_C). A RI_C-μ_{avg} relationship was initially proposed by Park and Medina (2007) for moment-resisting frames with the fundamental period T_1 = 0.6 s. ~ 1.8 s. in the form:

$$\mu_{avg} = 0.908\, RI_C^{\,1.02} \qquad [5.1]$$

The overstrength factor in the range between 1.45 and 4 is utilized to compute RI_C. For the range T_1 = 0.6 s. ~ 1.8 s., the RI_C - μ_{avg} relationship is not sensitive to the fundamental period and a relatively strong correlation existed between RI_C and μ_{avg}: the correlation coefficient is equal to 0.759. However, the variance of μ_{avg} is also affected when data points from more flexible structures, 12- and 15-story frames (i.e., T_1 = 2.4 s. and 3.0 s.), are included. The correlation coefficients of the relationship between μ_{avg} and T_1 are equal to 0.07 and 0.11 for fundamental periods in the range of 0.6 s. ~ 1.8 s. and 0.6 s. ~ 3.0 s., respectively. Even though the difference of correlation coefficients is not very significant, the fundamental period of vibration is also included in the relationship in order to estimate more accurate values of the average of story ductility ratios.

If the frames are designed with member strengths tuned to the design lateral load patterns corresponding to the ELF of the U.S. code provisions, the average of

story ductility ratios (i.e., total damage of the system) can be estimated from the regression model of the RI_C-T_1-μ_{avg} relationship as shown below:

$$\mu_{avg} = 0.94\ RI_C^{\ 0.99}\ T_1^{-0.05} \qquad [5.2]$$

A weighted least-squares multiple regression was conducted with the natural logarithms to quantify the RI_C - T_1- μ_{avg} relationship (see Figure 5.4) for regular frame structures with periods between 0.6 s. and 3.0 s. exposed to ordinary ground motions. The overstrength factor in the range between 1.45 and 4 was utilized to compute RI_C. This relationship is weakly dependent on the fundamental period of vibration as shown in Figure 5.4, but this dependency is not negligible. Note that Equation 5.2 is only applicable to obtain the average story ductility ratio (i.e., average damage) along the height of structures when exposed to ordinary ground motions ignoring pulse characteristics. The correlation coefficient and the standard error for this regression are 0.738 and 0.997, respectively.

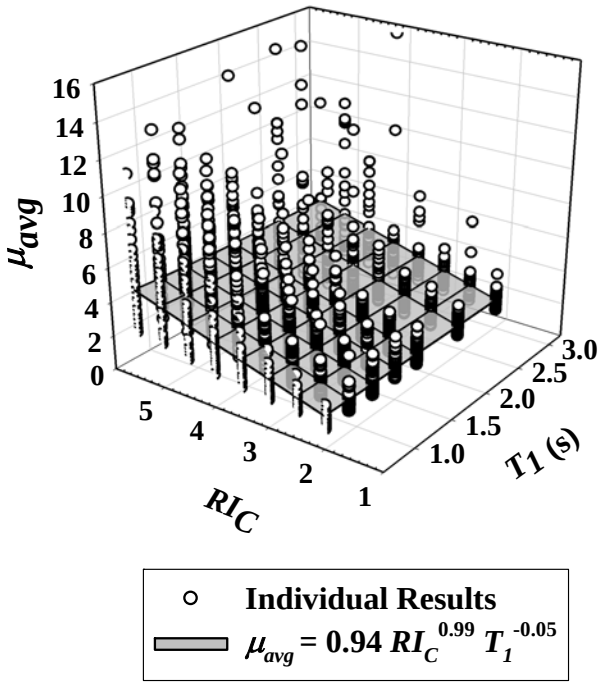

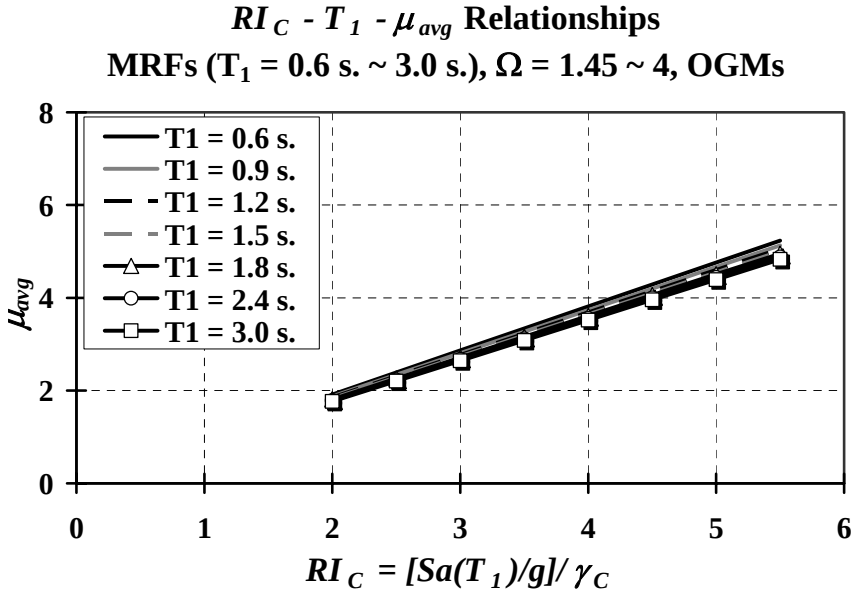

Figure 5.4 RI_C-T_1-μ_{avg} relationships in 3-D and 2-D for frames designed based on the lateral load patterns of the IBC 2006 ELF procedure

Average story ductility ratio (μ_{avg}) for moment-resisting frames exposed to near-fault ground motions

For moment-resisting frames exposed to near-fault ground motions, a weighted least-squares regression analysis was also conducted with natural logarithms to quantify the RI_C-T_1-μ_{avg} relationship for moment-resisting frames with a fundamental period from 0.6 s. to 3.0 s. It is noted that RI_C-T_1-μ_{avg} relationships were significantly sensitive to the fundamental period of the structural system as well as the ratio T_1/T_P. The overstrength factor in the range between 1.45 and 4 was utilized to compute RI_C for frame structures subjected to two different sets of near-fault ground motions: $T_1/T_P < 1$ and $T_1/T_P > 1$.

$$\text{For } T_1/T_p < 1: \ \mu_{avg} = 0.788\, RI_C^{\,1.17}\, T_1^{-0.109} \qquad [5.3]$$

$$\text{For } T_1/T_p > 1: \ \mu_{avg} = 1.20\, RI_C^{\,0.821}\, T_1^{-0.105} \qquad [5.4]$$

These RI_C-T_1-μ_{avg} relationships are presented in Figures 5.5 and 5.6. The correlation coefficient and the standard error of each regression equation are equal to (0.785, 0.989) and (0.699, 0.988) for $T_1/T_p < 1$ and $T_1/T_p > 1$, respectively, which demonstrates a relatively strong statistical correlation. For a predetermined RI_C, the average of ductility ratios for $T_1/T_p < 1$ increases as the value of RI_C increases (see Figure 5.5) when compared to μ_{avg} for $T_1/T_p > 1$ (see Figure 5.6). This implies that, for a predetermined relative intensity (i.e., a function of base shear strength) and ground motion hazard level, moment-resisting frames exposed to near-fault ground motions with pulse period greater than the fundamental period ($T_1/T_p < 1$) are expected to have more total (or average) damage on the system than the frames exposed to near-fault ground motions corresponding to $T_1/T_p > 1$. In addition, the RI_C-

T_1-μ_{avg} relationships for both $T_1/T_p < 1$ and $T_1/T_p > 1$ vary significantly with respect to the fundamental period of structures (see Figures 5.5 and 5.6). Therefore, for a given average of story ductility ratio, the base shear strength varies according to the ratio T_1/T_p and the fundamental period of structures exposed to near-fault ground motions when the frame is designed such that member strengths are tuned based on the U.S. ELF procedure seismic design loads.

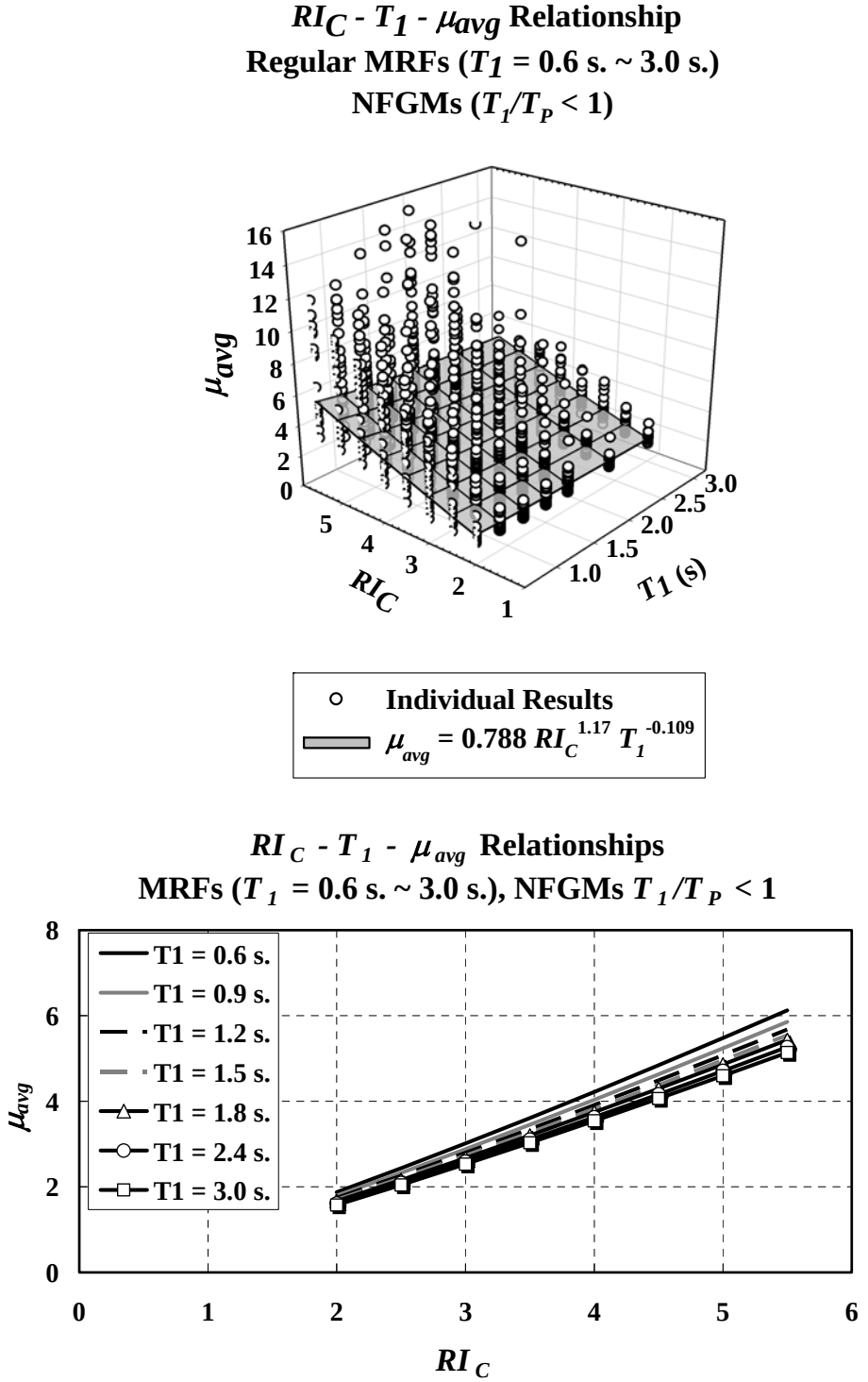

Figure 5.5 RI_C - T_1 - μ_{avg} relationships in 3-D and 2-D for frames designed based on IBC 2006 lateral load patterns for T_1/T_p < 1

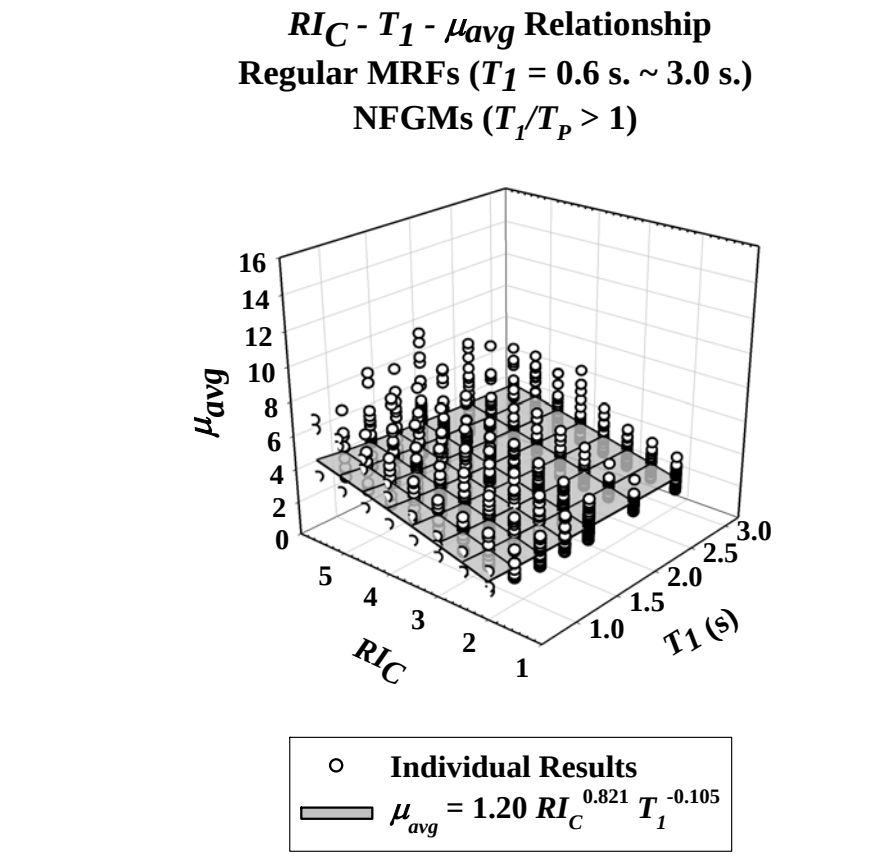

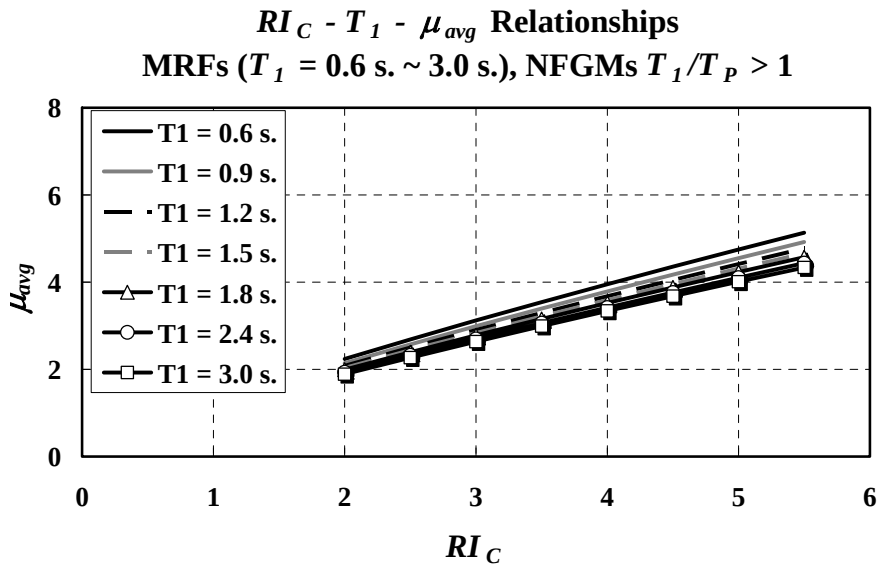

Figure 5.6 RI_C - T_1 - μ_{avg} relationships in 3-D and 2-D for frames designed based on IBC 2006 lateral load patterns for T_1/T_p > 1

5.2.3 Required Story Shear Strength Distribution

This study mainly focuses on distributing the expected total damage level of a system designed based on current U.S. seismic provisions so that a uniform distribution of damage over the height is obtained, and hence, the concentration of damage in a few stories is avoided. Thus the total damage of structures designed based on the proposed lateral load patterns is required to be equal to that of frames designed based on the current code provisions. Since the average story ductility ratio is presented as a measure of global damage, the estimated value of μ_{avg} based on structures designed following current code procedures is set equal to the target story ductility ratio (i.e. $\mu_{avg} = \mu_T$), which now becomes the expected average damage of the structure designed based on the proposed approach.

Once the target story ductility ratio is defined, the total seismic story shear strength of structures can be estimated by using results from the statistical evaluation of the relative intensity required to achieve a target story ductility ratio for frames designed based on the proposed load patterns, i.e., RI_P in Chapter 4. Once an estimated value of RI_P is obtained, the required base shear strength, V_y, can be computed by using the relationship $\gamma_P = V_y/W$. In order to obtain the same total structural damage estimated from moment-resisting frames designed based on the current procedure, the corresponding base shear strength has to be estimated separately based on results for ordinary and near-fault ground motions by using Equations (4.2) and (4.5 and 4.6) respectively. With the combination of relative distribution of story shear strength (see Table 5.3, calculated by using Equations 4.8, 4.9, 4.10, and 4.11) and the base shear strength of structures, seismic design lateral

loads can be provided for the seismic design of regular moment-resisting frames to achieve uniform damage along the height.

Table 5.2 Computed values of parameters k and F_{top}/V_y for the relative distribution of story shear strength

			Ordinary		Near-fault, $T_1/T_P < 1$		Near-fault, $T_1/T_P > 1$	
	μ_T	H (m)	k	F_{top}/V_y	k	F_{top}/V_y	k	F_{top}/V_y
N = 6	1	19.68	0.36	0.26	0.78	0.14	0.58	0.33
	2	19.68	0.19	0.28	0.33	0.17	0.3	0.36
	3	19.68	0.02	0.30	0.18	0.19	0.02	0.39
	4	19.68	-0.15	0.32	0.03	0.20	-0.26	0.42
	5	19.68	-0.32	0.34	-0.12	0.21	-0.54	0.45
N = 9	1	29.52	0.36	0.24	0.48	0.13	0.58	0.28
	2	29.52	0.19	0.26	0.33	0.14	0.3	0.31
	3	29.52	0.02	0.28	0.18	0.16	0.02	0.34
	4	29.52	-0.15	0.30	0.03	0.17	-0.26	0.37
	5	29.52	-0.32	0.32	-0.12	0.18	-0.54	0.40
N = 12	1	39.36	0.36	0.22	0.48	0.10	0.58	0.23
	2	39.36	0.19	0.24	0.33	0.11	0.3	0.26
	3	39.36	0.02	0.26	0.18	0.13	0.02	0.29
	4	39.36	-0.15	0.28	0.03	0.14	-0.26	0.32
	5	39.36	-0.32	0.30	-0.12	0.15	-0.54	0.35
N = 15	1	49.2	0.36	0.20	0.48	0.07	0.58	0.19
	2	49.2	0.19	0.22	0.33	0.09	0.3	0.21
	3	49.2	0.02	0.24	0.18	0.10	0.02	0.24
	4	49.2	-0.15	0.26	0.03	0.11	-0.26	0.27
	5	49.2	-0.32	0.28	-0.12	0.12	-0.54	0.30
N = 18	1	59.04	0.36	0.18	0.48	0.04	0.58	0.14
	2	59.04	0.19	0.20	0.33	0.06	0.3	0.16
	3	59.04	0.02	0.22	0.18	0.07	0.02	0.19
	4	59.04	-0.15	0.24	0.03	0.08	-0.26	0.22
	5	59.04	-0.32	0.26	-0.12	0.09	-0.54	0.25

Seismic base shear strength for moment-resisting frames exposed to ordinary ground motions

For a given target story ductility ratio (μ_T), the relative intensity values for the current and proposed approaches are shown in Table 5.3. Because the average story ductility ratio is exactly the same as the target story ductility ratio, the values of both RI_P (from Equation 4.2) and RI_C (from Equation 5.2) can be compared as shown in Figure 5.7 for a given target story ductility ratio and a fundamental period of vibration. In Figure 5.7, *RI* values above the dividing grey line translate into RI_C values that are greater than RI_P values. This implies that frames designed based on the current U.S. code provisions require less seismic design base shear strength when compared to the frames designed based on the proposed load patterns for uniform damage along the height. Note that both RI_P and RI_C are a function of the inverse of the base shear strength coefficient.

As the structural system becomes more flexible (e.g., with the fundamental period greater than 1.2 s), structural systems designed based on the proposed approach require more strength to provide uniform damage along the height of the structure. For example, for a given target story ductility ratio of 2.0, the relative intensity for a 12-story frame with T_1 = 2.4 s. designed based on the current U.S. provisions (i.e., RI_C for IBC 2006 in this study) is equal to 2.24 when compared to 1.96 for RI_P. The difference of the relative intensity values between RI_P and RI_C implies that a frame designed based on the proposed design load pattern requires 18% (0.13/0.11*100) more base shear strength of the frame designed based on the current approach. This observation is based on the assumption that the same amount of

overstrength in both current and proposed approaches is distributed over the height of frame structures. In addition, this difference in required based shear strengths is due to the increase in story drift ratios caused by gravity loads acting on the deformed configuration of the frames.

Table 5.3 Computed relative intensity values of frames designed based on the proposed and current design load patterns when exposed to ordinary ground motions

T_1 (s)	$\mu_{avg} = \mu_T$	RI_P	RI_C
0.6	2	2.44	2.09
	3	3.65	3.14
	4	4.86	4.20
	5	6.06	5.25
0.9	2	2.29	2.13
	3	3.42	3.21
	4	4.55	4.28
	5	5.68	5.36
1.2	2	2.18	2.16
	3	3.27	3.25
	4	4.35	4.35
	5	5.43	5.44
1.5	2	2.11	2.19
	3	3.15	3.29
	4	4.20	4.40
	5	5.24	5.50
1.8	2	2.05	2.21
	3	3.06	3.32
	4	4.07	4.44
	5	5.09	5.55
2.4	2	1.96	2.24
	3	2.92	3.37
	4	3.89	4.50
	5	4.86	5.63
3.0	2	1.89	2.27
	3	2.82	3.41
	4	3.75	4.55
	5	4.69	5.70

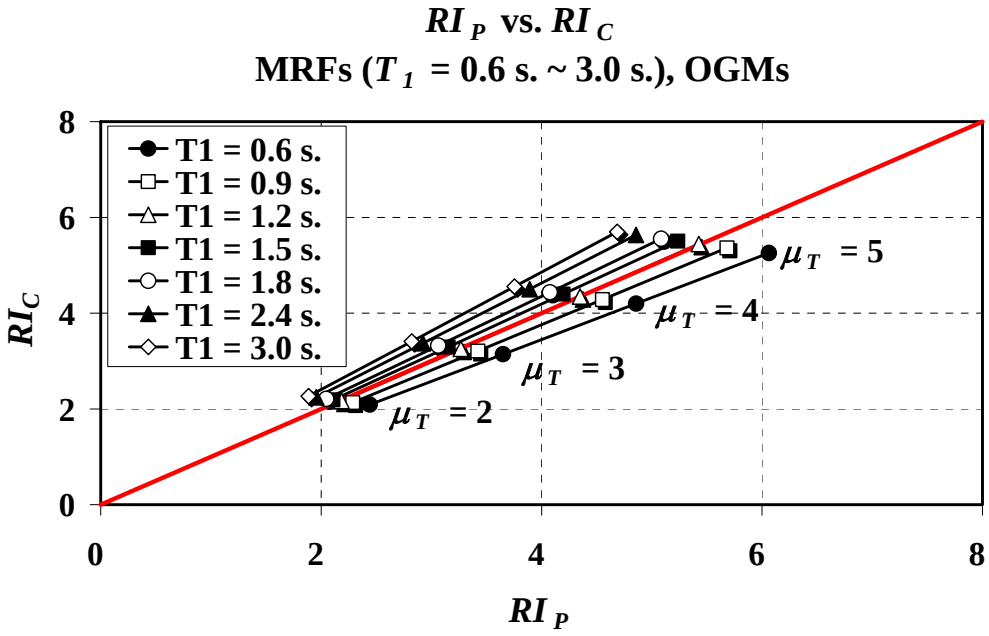

Figure 5.7 Comparison of relative intensity values, RI_P and RI_C, for frames exposed to ordinary ground motions

Seismic base shear strength for moment-resisting frames exposed to near-fault ground motions

When frames are exposed to near-fault ground motions, the relative intensity values for the current and proposed approaches are shown in Table 5.4. For a given target story ductility ratio (μ_T) and fundamental period of vibration (T_1), required relative intensity values were separately computed according to the ratio T_1/T_p: relative intensity values for the proposed load patterns and the current approach are obtained from Equations (4.5 and 4.6) and (5.3 and 5.4), respectively, and also depicted in Figures 5.5 and 5.6. It is notable that, for a given fundamental period of vibration, the variation of relative intensity values (i.e., RI_P and RI_C) for $T_1/T_p < 1$ are different from the variation of those values for $T_1/T_p > 1$.

In Figure 5.8, the relative intensity value for the current approach is consistently greater than or equal to the value for the proposed load pattern for any given target story ductility ratio and fundamental period of vibration. This implies that the structural system designed based on the proposed method should exhibit a greater base shear strength to distribute the story ductility ratio uniformly along the height when it is exposed to near-fault ground motions for $T_1/T_p < 1$. In addition, as shown in Figure 5.8, the variation of relative intensity values is very sensitive to the fundamental period of vibration (T_1) and the target story ductility ratio when the ratio T_1/T_p is greater than one. Thus, the frame designed based on the proposed load pattern requires more total strength on the system if the fundamental period of a structure is in the range 1.2 s. ~ 3.0 s. when compared to the range 0.6 s. ~ 1.2 s. This later statement is consistent with the behavior observed when the frames were exposed to ordinary ground motions (see previous Section). Figure 5.8 also shows that the determination of base shear strength is also very sensitive to the ratio T_1/T_p for a given frame and predefined target story ductility ratio. Thus, when designing moment-resisting frames exposed to near-fault ground motions, it is necessary to account for ground motion characteristics such as the predominant pulse period of the ground motion recording.

Table 5.4 Computed relative intensity values of frames designed based on the proposed and current design load patterns when exposed to near-fault ground motions

		$T_1/T_P < 1$		$T_1/T_P > 1$	
T_1 (s)	$\mu_{avg} = \mu_T$	RI_P	RI_C	RI_P	RI_C
0.6	2	2.19	2.11	3.02	1.75
	3	3.02	2.99	4.37	2.86
	4	3.79	3.82	5.68	4.06
	5	4.52	4.63	6.96	5.33
0.9	2	2.11	2.20	2.62	1.84
	3	2.91	3.10	3.79	3.01
	4	3.65	3.97	4.93	4.28
	5	4.35	4.80	6.04	5.61
1.2	2	2.06	2.25	2.37	1.91
	3	2.83	3.19	3.43	3.12
	4	3.55	4.08	4.46	4.44
	5	4.24	4.93	5.47	5.82
1.5	2	2.01	2.30	2.19	1.96
	3	2.77	3.26	3.17	3.22
	4	3.48	4.16	4.12	4.56
	5	4.15	5.04	5.06	5.99
1.8	2	1.98	2.34	2.06	2.01
	3	2.73	3.31	2.98	3.29
	4	3.42	4.23	3.87	4.67
	5	4.08	5.12	4.74	6.13
2.4	2	1.93	2.41	1.86	2.08
	3	2.66	3.40	2.69	3.41
	4	3.33	4.35	3.50	4.85
	5	3.97	5.26	4.29	6.36
3.0	2	1.89	2.46	1.72	2.14
	3	2.60	3.47	2.49	3.51
	4	3.27	4.44	3.24	4.99
	5	3.89	5.37	3.97	6.55

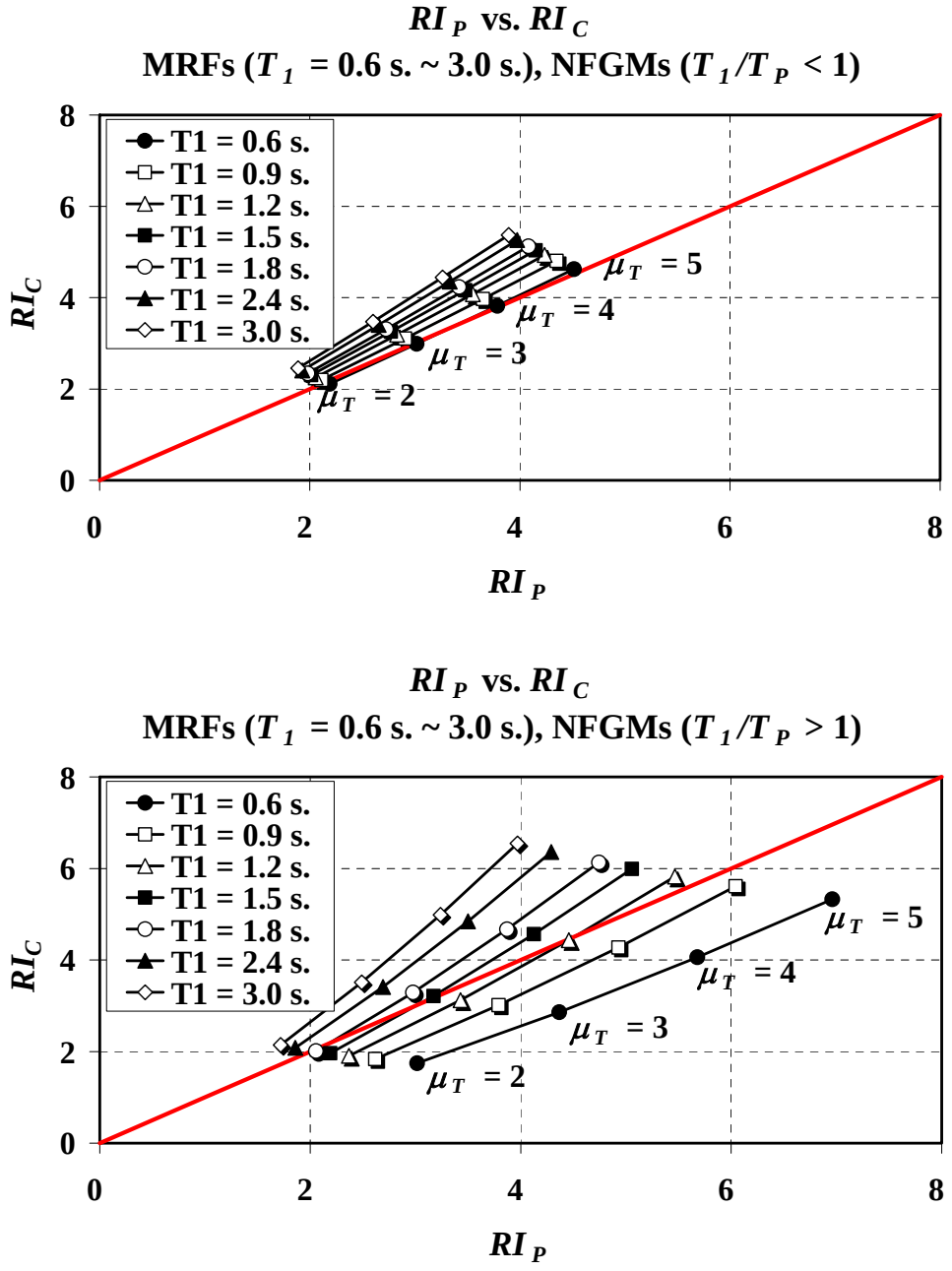

Figure 5.8 Comparison of relative intensity values, RI_P and RI_C, for frames exposed to near-fault ground motions for $T_1/T_P < 1$ and $T_1/T_P > 1$

5.3 SUMMARY

The conceptual seismic design methodology proposed in this study is used to estimate story shear strength patterns for the preliminary design of regular moment-resisting frames exposed to ordinary and near-fault ground motions. A major advantage of the proposed approach is that performance objectives for the design of inelastic frame structures can be explicitly considered in the conceptual design stages of a project.

- For a given hazard level and the fundamental period of vibration, the basic premise of the new conceptual seismic design methodology is that the total damage in a structural system design based on this methodoloty is approximately equal to the total damage quantified by using the ELF procedure.
- For the seismic design based on the current U.S. code provisions (i.e., IBC 2006), global overstrength factors between 1.45 and 4 were adopted and utilized for moment-resisting frames with fundamental periods from 0.6 s. to 3.0 s., and number of stories from 6 to 18, exposed to ordinary and near-fault ground motions corresponding to spectral values consistent with the 10/50 seismic hazard levels in the western U.S.
- For ordinary ground motions, global damage (i.e., average damage) is primarily a function of the relative intensity and the fundamental period, while for near-fault ground motions, global damage is primarily controlled by the relative intensity, fundamental period of vibration, and the ratio T_1/T_p. When regular frame structures are exposed to ordinary

ground motions for a given hazard level, average story ductility ratios are strongly dependent on the base shear strength of the structural system and weakly dependent on the fundamental period of the structure.

- If regular moment-resisting frames are exposed to ordinary ground motions, the frames designed based on the proposed load pattern require stronger base shear strength especially when the fundamental period of a structure is in the range (1.2 s. ~ 3.0 s), when compared to the frames designed based on the current U.S. code provisions. This behavior is attributed to the presence of P-delta loads that tend to increase the story drift ratios of flexible structures, particularly at the bottom stories. In addition, when the pulse period of the near-fault ground motion is greater than the fundamental period of structures, the use of proposed load pattern mostly requires greater base shear strength as compared to designs with member strengths tuned to seismic loads based on current U.S. code provisions.

6 APPLICATION OF PROPOSED METHODOLOGY TO SPECIAL MOMENT-RESISTING FRAMES

6.1 INTRODUCTION

From the review of the ELF procedure in the U.S. code provisions (Chapter 2), it can be seen that the code-prescribed seismic design load patterns are based on elastic dynamic analysis. However, because of the philosophy to design structural systems to dissipate energy through inelastic action once they are exposed to strong ground motions, accounting for inelastic behavior in the determination of seismic lateral loads appears to be an adequate component of performance-based design approaches. This can be achieved by using the methodology proposed in this study, which is based on distributing structural damage caused by inelastic action along the height of structures.

Verification studies are conducted in this chapter to demonstrate the effectiveness of the design methodology proposed in Chapter 5 and evaluate: (1) whether, on average, the proposed load patterns are able to provide a uniform distribution of story ductility ratios over the height; and (2) for a given average structural damage, how designs based on the proposed load patterns compare to those based on the ELF of U.S. design procedures. Because the equations of the proposed lateral load patterns are developed based on the central values (i.e., median or mean values) of story shear strength distributions corresponding to each set of ground motions, the verification results are focused on median or mean EDP values for the same set of ground motions utilized in this study.

For given fundamental period and target story ductility ratio, the story ductility ratios and maximum story drift ratios are quantified to evaluate the effectiveness of the proposed methodology on given moment-resisting frame structures when exposed to ordinary and near-fault ground motions. The seismic hazard for scaling the ground motion acceleration records is represented by the elastic spectral acceleration at the first mode period of the frame, which is obtained from a 2006 International Building Code design spectrum corresponding to site classification D and a location in a California costal region. These spectral values are deemed to be close to those corresponding to the 10/50 hazard level. This implies that the performance target of interest is life safety.

6.2 EXAMPLES OF THE PROPOSED METHODOLOGY FOR ORDINARY GROUND MOTIONS

To evaluate the effectiveness of the proposed methodology, single-bay multi-story frame structures are utilized to quantify the story ductility ratios and story drift ratios when exposed to the ensemble of 40 ordinary ground motions. Within the range of target story ductility ratios from 1 to 5, the value of 1 is representative of elastic and relatively small inelastic behavior, while μ_T = 5 represents a more extreme case for seismic design applications. Thus, two middle values equal to 2 and 4 are selected as example cases. Performance levels correspond to μ_{avg} values 2 and 4 with assumed overstrength factors, Ω, equal to 3.7 and 1.85, respectively. For a given fundamental period, the response modification factor (R = 8 for special moment-resisting frames), overstrength factor, and target story ductility ratio, Equation 4.2 was utilized to

determine RI_P value as shown in Figure 6.1. Once the base shear strength γ_P is determined, story shear strength patterns to achieve average target story ductility ratios of 2 and 4 are estimated with k and F_{top}/V_y values, computed from Equations 4.3 and 4.4. By conducting a time history analysis, story ductility ratios and story drift ratios quantified for a given frame structure designed based on the proposed load patterns are compared to those corresponding to the frame designed based on the ELF of the IBC 2006. As stated earlier, the response of frame structures whose story shear strengths are tuned to those in the equivalent lateral force procedure of the IBC 2006 are denoted as 'CURRENT', whereas results corresponding to frame structures with story shear strengths tuned to the proposed load patterns are denoted as 'PROPOSED'. It is important to note that the lateral load patterns based on IBC 2006 are a function of fundamental period of vibration (T_1) and the floor masses (m); whereas story ductility ratios (μ_T), the total height of structures (H), and the floor masses (m) are the main components to determine the shape of proposed load patterns.

Seismic demand evaluation studies were conducted in three different domains: (a) story ductility ratio profiles; (b) maximum story drift ratio profiles; (c) incremental dynamic analysis (see Figure 6.1). In these analyses, member strengths were tuned to the seismic design lateral loads.

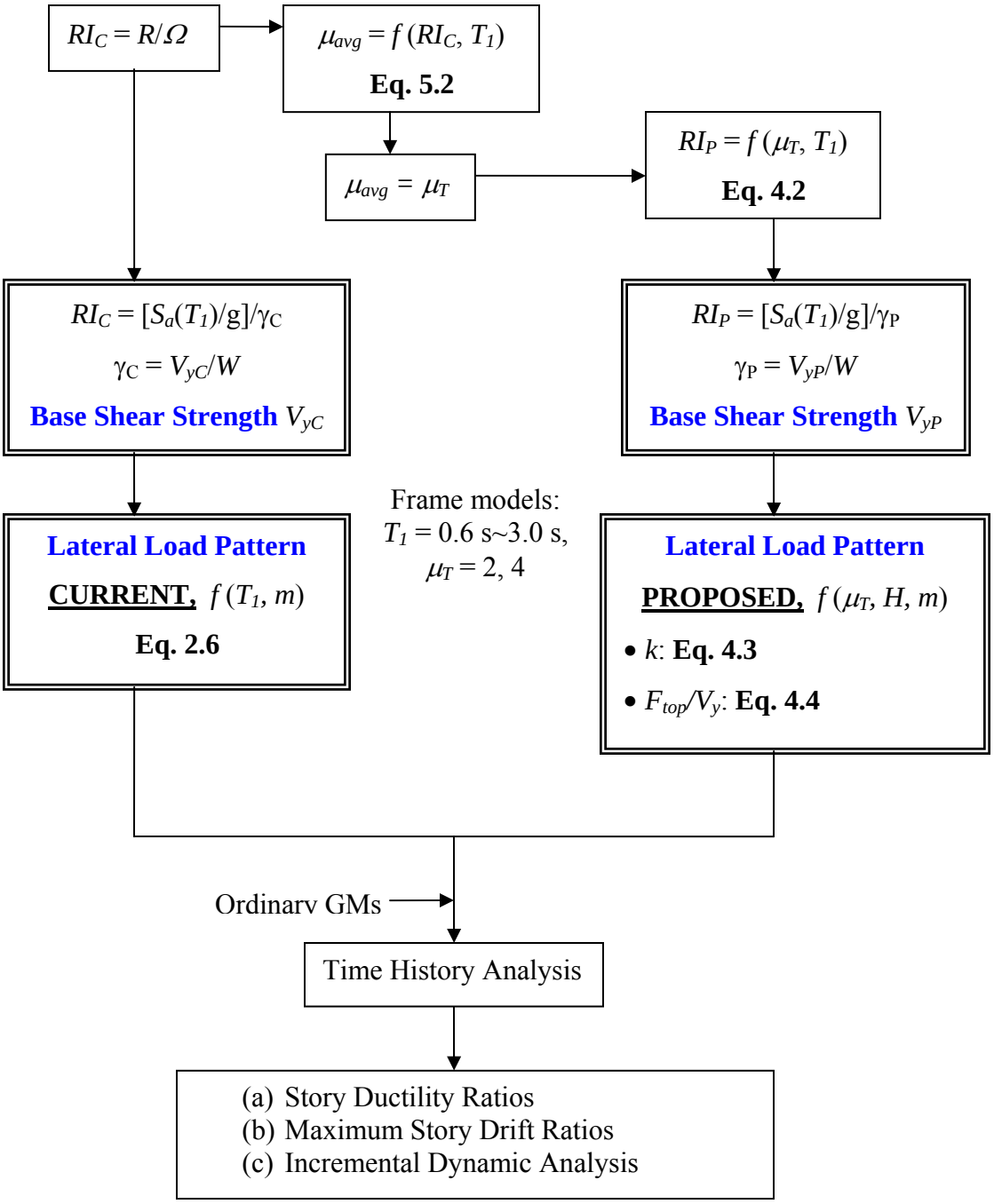

Figure 6.1 Verification process for moment-resisting frame structures exposed to ordinary ground motions

6.2.1 Story Ductility Ratios

Median story ductility ratios for the aforementioned structures are presented in Figures 6.2 through 6.6. On average, frame structures designed based on the proposed approach provide a more uniform distribution of story ductility ratios over the height and about the same average story ductility as those designed based on current seismic code provisions in the United States. The overestimation and underestimation of target story ductility values at the top stories of the six- and eighteen-story frames with a target story ductility ratio of 4 (see Figures 6.2 and 6.6) are due to the fact that the use of F_{top}/V_y from the regression equation, Equation 4.4, does not provide a strong positive correlation with individual values of F_{top}/V_y (the correlation coefficient is 0.649). However, compared to the distributions of CURRENT, the frames designed corresponding to the proposed approach provide a more uniform distribution of story ductility ratios as presented in Figures 6.2 through 6.6.

The shape of CURRENT median story ductility ratio distributions significantly varies along the height, depending on the total height of structure as well as target story ductility ratios. For example, as a frame structure is taller, the values of story ductility ratios are amplified at top and bottom stories. In addition, for the target story ductility ratio of 4, structural damage is more severe in top and bottom stories when compared to μ_T = 2. These observations show that the distribution of story ductility ratios for CURRENT is significantly affected by different levels of target story ductility ratios. For regular frame structures, the load patterns mostly change with the variation of the fundamental period of structures and the mass in each story level.

For flexible frame structures designed based on the ELF procedure of building codes, large story ductility ratios are found notably in the bottom stories when compared to story ductility ratios obtained from stiff frame structures. Figures 6.2 to 6.5 show that story ductility ratios at bottom stories of flexible frame structures (i.e., T_1 = 0.2 N) are much larger than those at bottom stories of stiff frame structures (i.e., T_1 = 0.1 N) for a given structural height and a given target story ductility ratio. This implies that dynamic P-delta effects play an important role in the inelastic dynamic behavior of flexible frames. Given that the fundamental period of the structure and the floor masses are the main parameters that determine the shape of the lateral load pattern when the ELF procedure is applied, the inelastic level of interest, μ_T, and the total height of structures appear to be more relevant parameters to determine the seismic lateral load patterns in order to minimize the structural damage in certain story levels. These observations are found mostly in the bottom stories of medium to tall frame models (i.e., $N = 9 \sim 18$).

For frame structures with T_1 = 2.4 s. and 3.0 s, unreasonably large values of story ductility ratios (e.g., $\mu_{si} > 20$) are obtained in some cases from both CURRENT and PROPOSED when $\mu_T = 4$. These values are the byproduct of the inability of the models to simulate large-displacement responses in the presence of second order nonlinearities and material degradation. Because of the presence of significant P-delta effects, very flexible frames with relatively large target story ductility ratios (e.g., μ_T = 4) may be prone to experience dynamic instability when the frames are exposed to certain ground motions. This implies that the use of both methodologies is sensitive to the different frequency content characteristics of ground motions when used to design

very flexible frames for high inelastic levels of interest. However, median values for the distributions of PROPOSED are still more uniform when compared to those distributions of CURRENT for approximately the global damage represented by the average story ductility ratio.It is noted that the strength of structures for PROPOSED is tuned based on the load patterns determined by using the regression equations of the parameters k and F_{top}/V_y. Thus the distributions of PROPOSED along the height of structures are not expected to be perfectly uniform. In addition, despite a greater amount of structural damage in the middle stories in the PROPOSED distributions, less damage at the bottom stories is an advantage for tall buildings, which may be prone to experience dynamic instability.

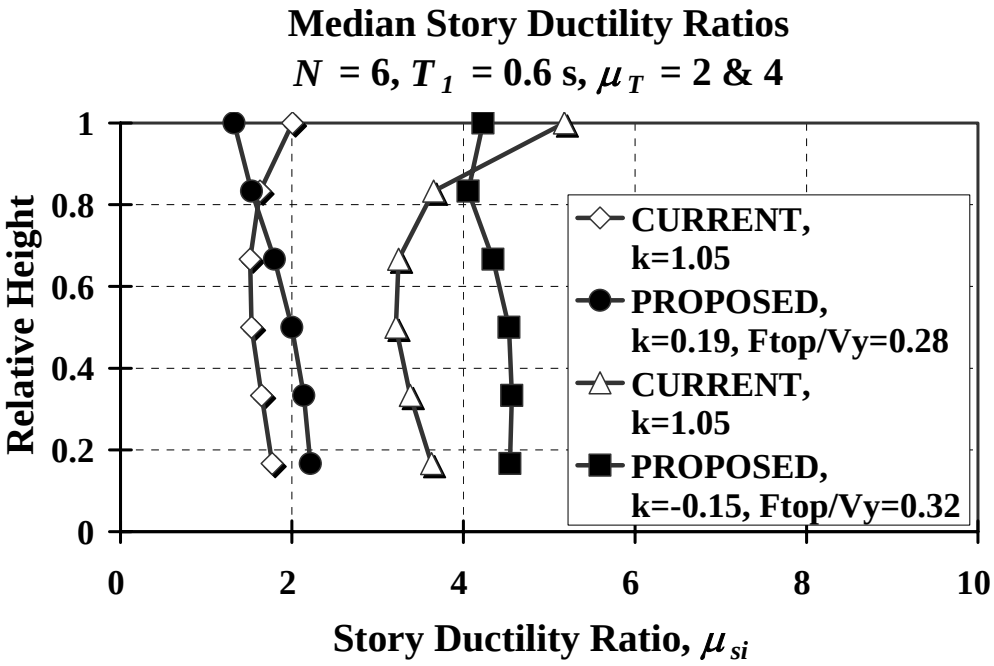

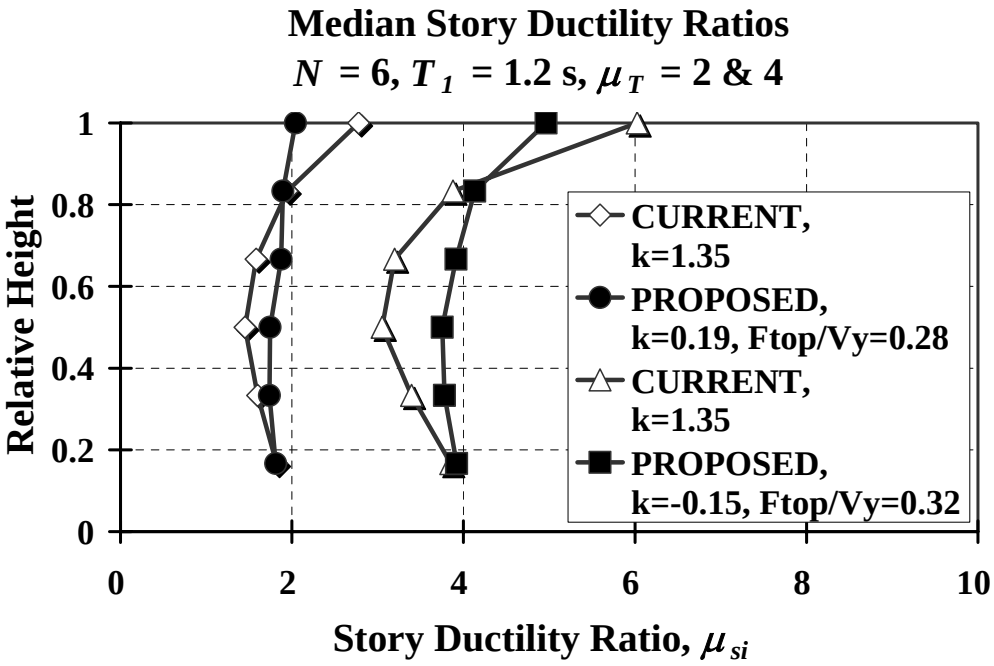

Figure 6.2 Median story ductility ratio profiles, 6-story frame structures with T_1 = 0.6 s. and 1.2 s. for μ_T = 2 and 4

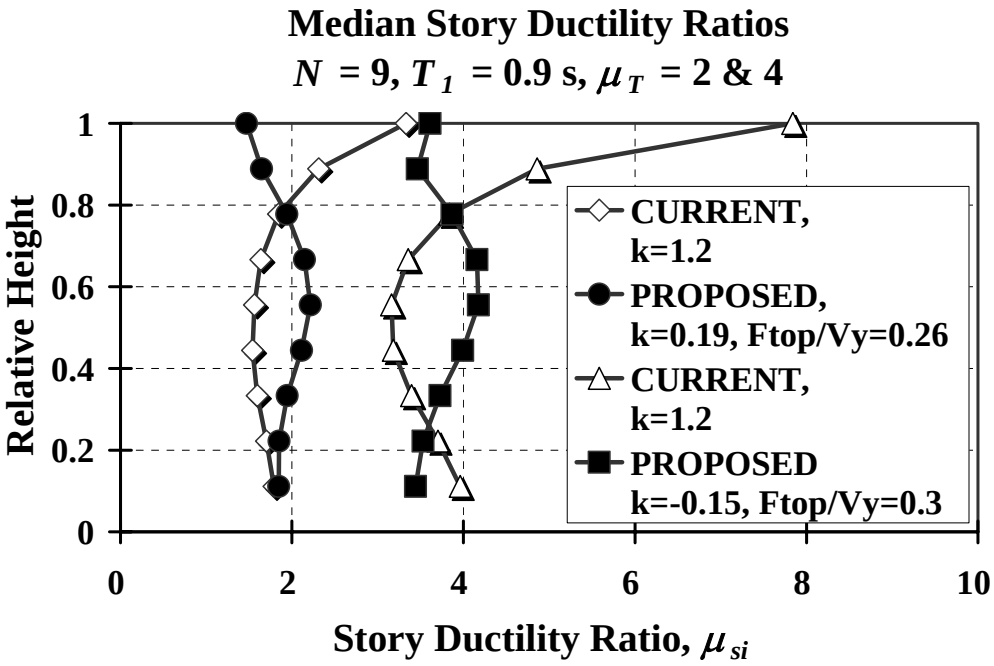

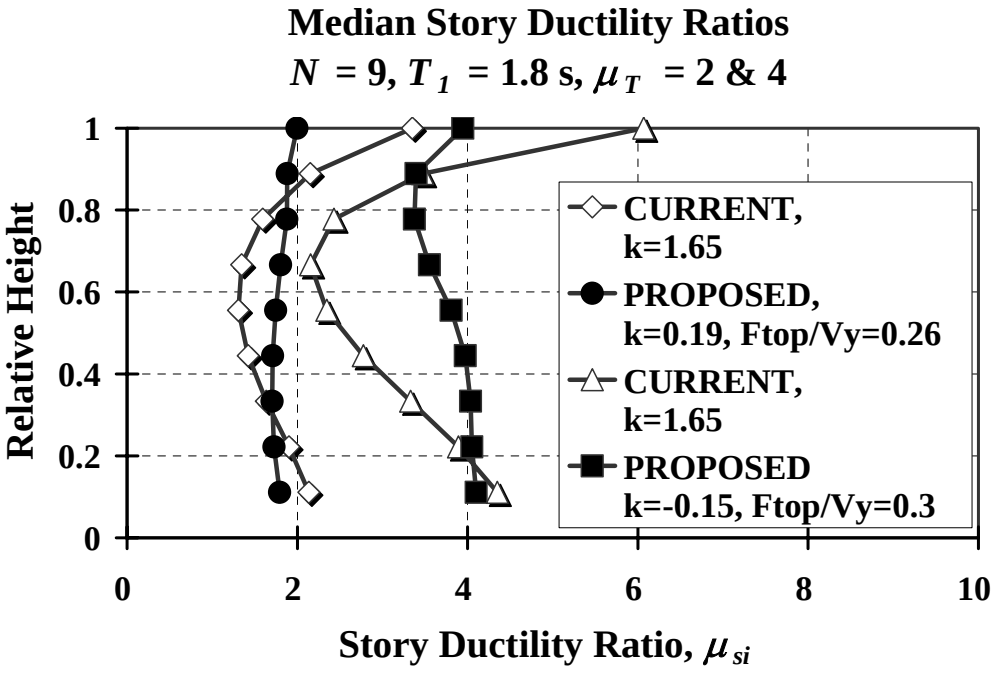

Figure 6.3 Median story ductility ratio profiles, 9-story frame structures with T_1 = 0.9 s. and 1.8 s. for μ_T = 2 and 4

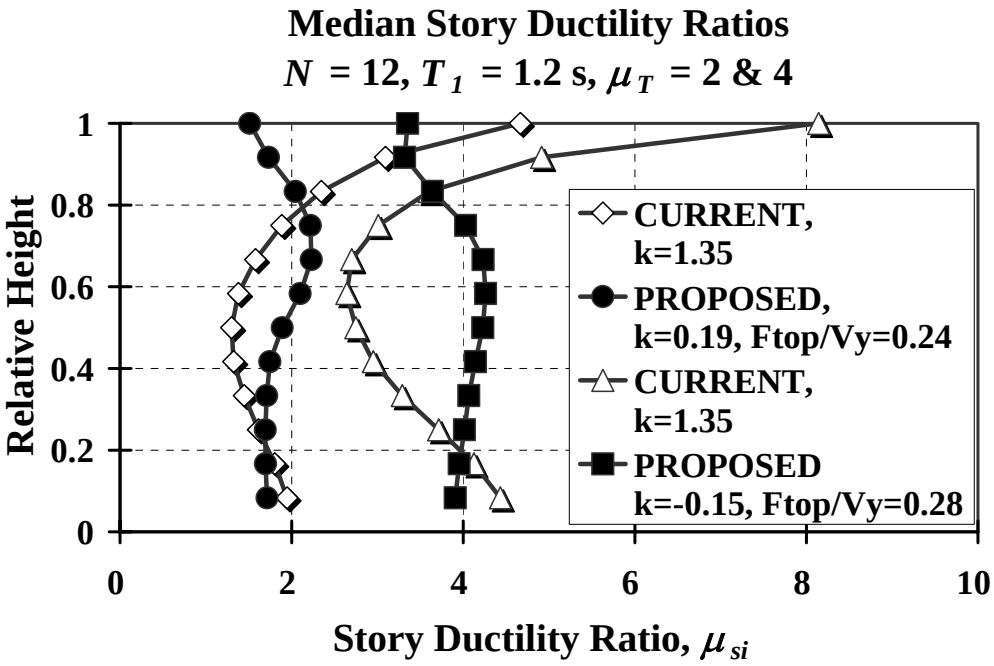

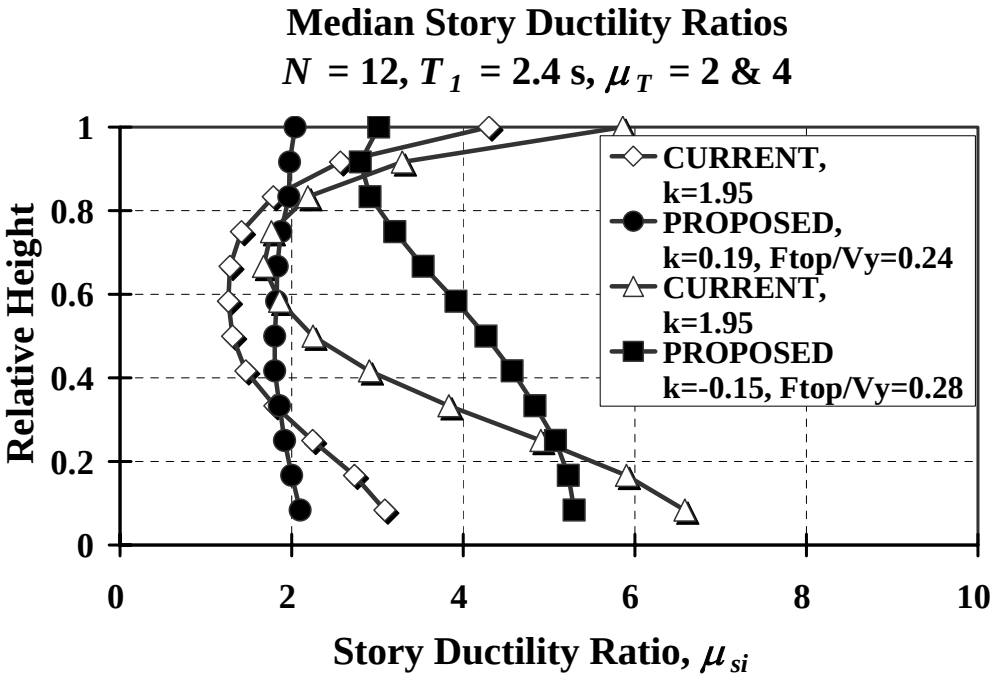

Figure 6.4 Median story ductility ratio profiles, 12-story frames with T_1 = 1.2 s. and 2.4 s. for μ_T = 2 and 4

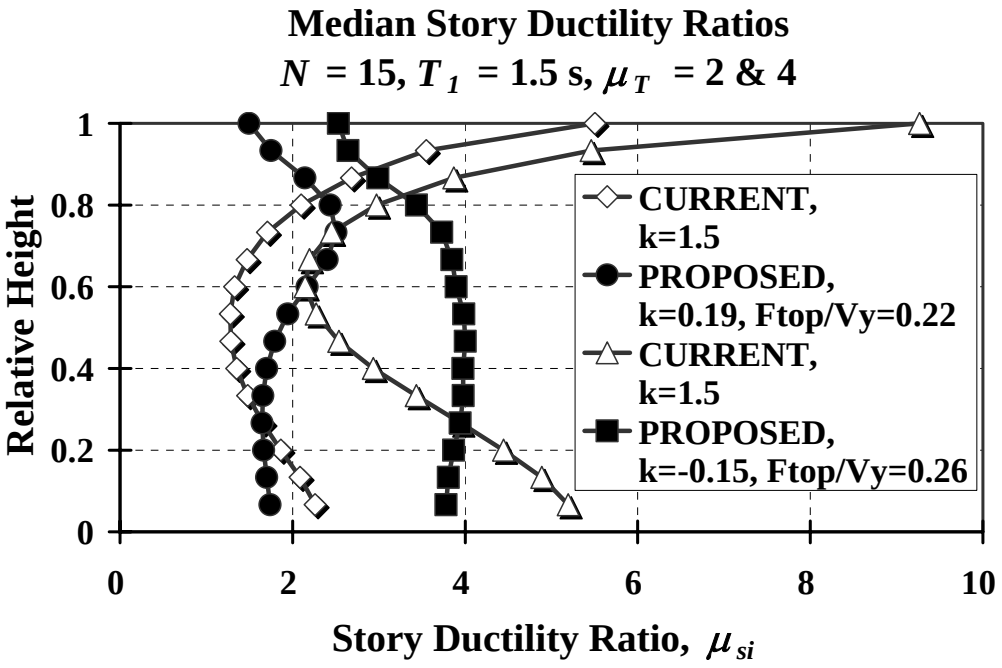

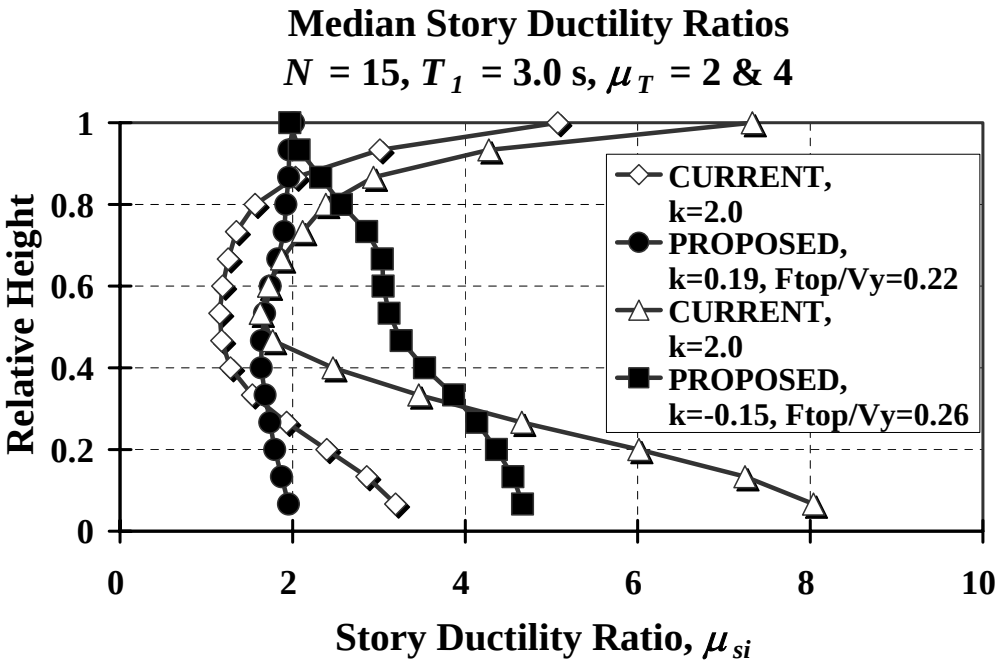

Figure 6.5 Median story ductility ratio profiles, 15-story frames with T_1 = 1.5 s. and 3.0 s. for μ_T = 2 and 4

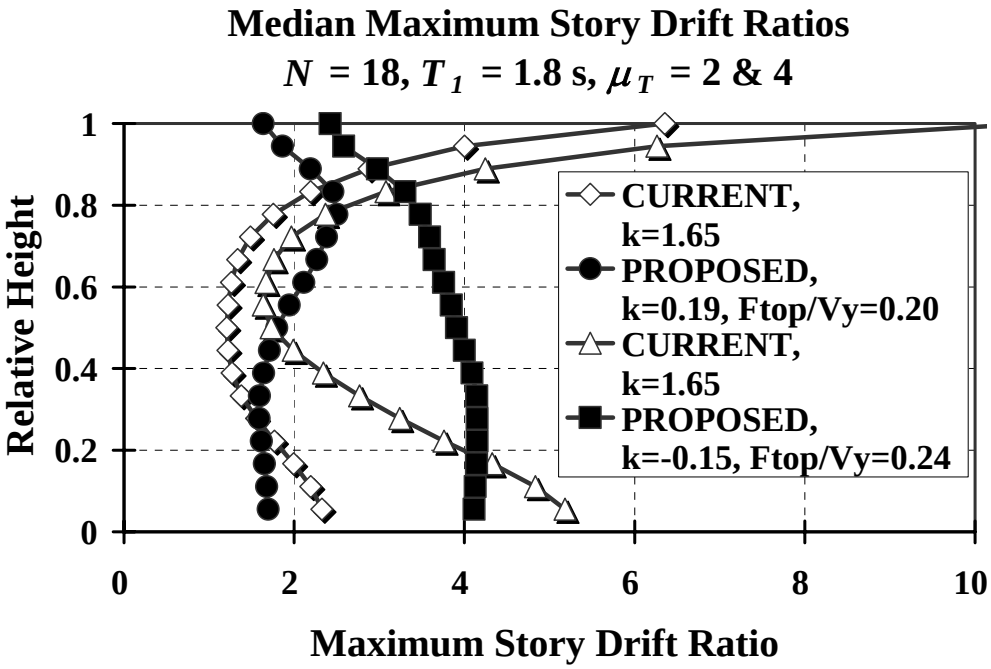

Figure 6.6 Median story ductility ratio profiles, 18-story frames with T_1 = 1.8 s. for μ_T = 2 and 4

6.2.2 Story Drift Ratios

Median story drift ratios are depicted in Figures 6.7 to 6.15 for the same frames that are evaluated in Figures 6.2 to 6.6, with target story ductility ratios of 2 and 4. As generally shown in the figures, frame structures designed based on the proposed methodology exhibit smaller story drift ratios at the top and bottom stories when compared to structures whose member strengths are tuned to code-compliant story shear strength distributions in the case of tall structures. Moreover, a more uniform distribution of story drift ratios is also achieved for frame structures designed based on the proposed methodology.

The distributions of median story drift ratios for short frames (i.e., the six-story structure) are similar in both cases as shown in Section 6.2.1. For the same stiffness distribution, base shear strength, and seismic hazard level, the distribution of story drift ratios is expected to be less dependent on the distribution of shear strengths as the height of the frame decreases (see Figures 6.7 and 6.8). Therefore, for regular short-frame structures, the proposed methodology does not appear to provide a significant improvement over the ELF procedure. For regular medium to tall-story structures (i.e., number of stories greater than or equal to 9), the proposed methodology helps control story drift ratios at the top and bottom stories when compared to those experienced by frames designed based on current code procedures. Thus, an advantage of implementing the proposed seismic design methodology is that, for a given ground motion hazard level, frame structures are expected to exhibit smaller story drift ratios at the bottom stories. These smaller story drift ratios translate

into an increased capacity against global collapse due to P-delta effects, which is discussed in Section 6.2.3.

The median values of maximum story drift ratios for $\mu_T = 2$ are very similar to those for $\mu_T = 4$ (see Figures 6.7 to 6.15). For a given T_1, N, and $S_a(T_1)$, the strength of frame structures utilized in this study are tuned by using the base shear strength and the relative strength distribution. In other words, the same frame structures for different target story ductility ratios are designed based on different story shear strength distributions with a constant stiffness distribution. Thus, the fundamental period of a structure is unchanged while the strength of structure is tuned to various load patterns which are a function of target story ductility ratios. For this constant stiffness distribution, the median maximum story drift ratios remain nearly constant for different target values of story ductility ratios. This corroborates the well-known fact that the peak inelastic displacements of inelastic structural systems are more influenced by the modal period of vibrations rather than the global strength of the system. Therefore, the distribution of maximum story drift ratios is more affected by the change in stiffness distribution, which implies that a procedure used to control the absolute value of story drift ratios should focus on the variation of the stiffness along the height of the frame.

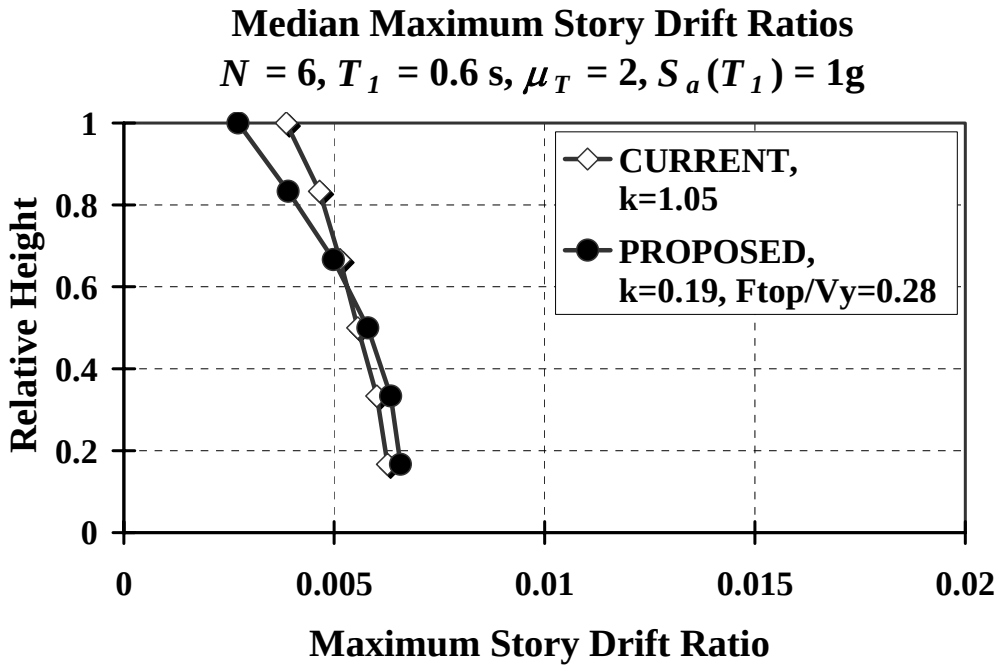

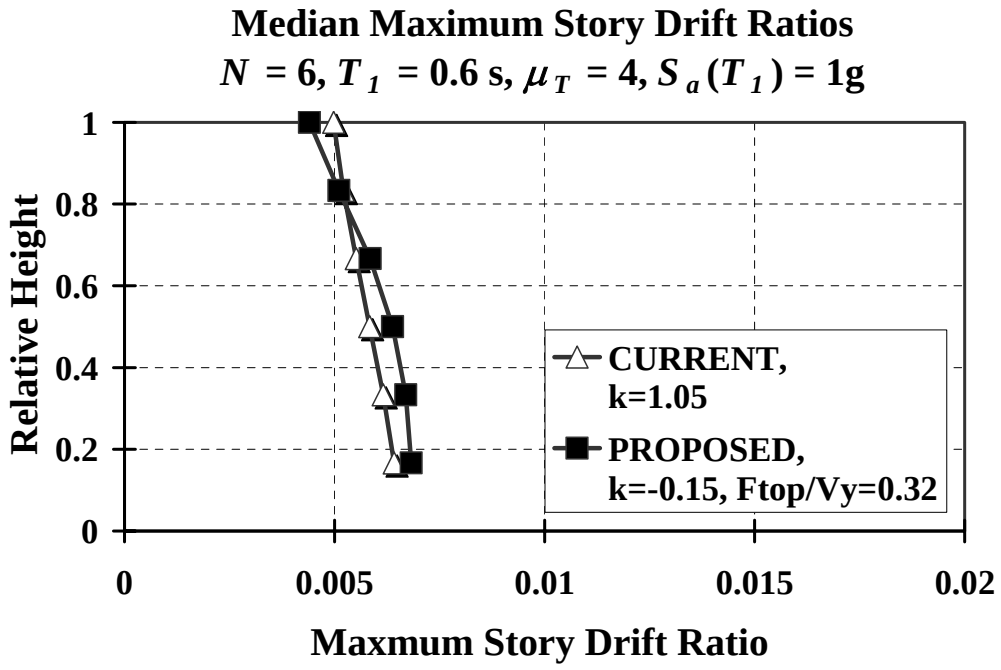

Figure 6.7 Median maximum story drift ratio profiles, 6-story frame structure with T_1 = 0.6 s. for μ_T = 2 (γ_C = 0.48 and γ_P = 0.41) and 4 (γ_C = 0.24 and γ_P = 0.21)

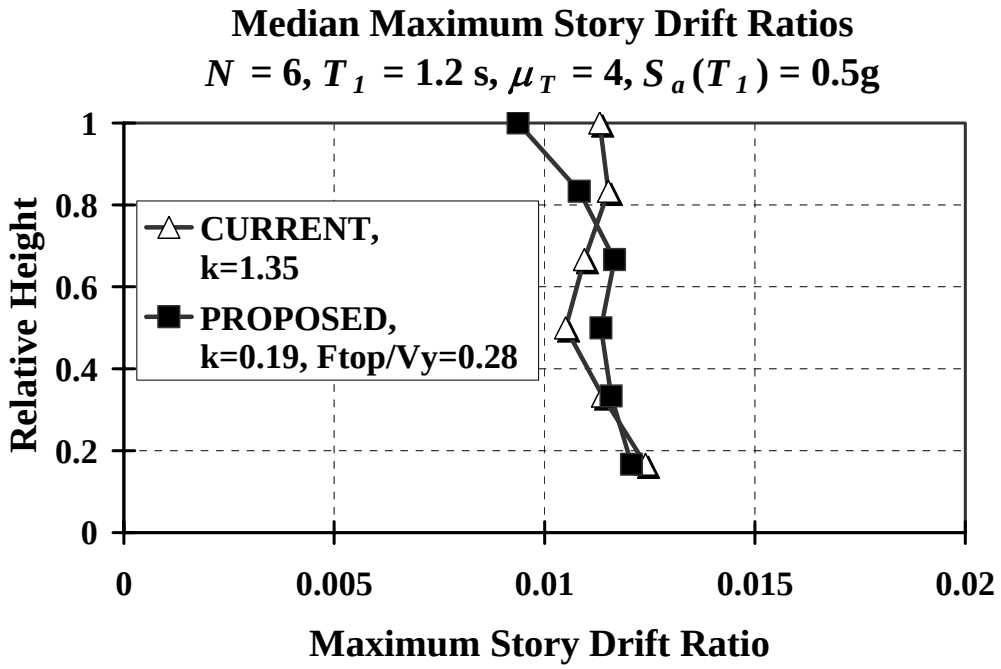

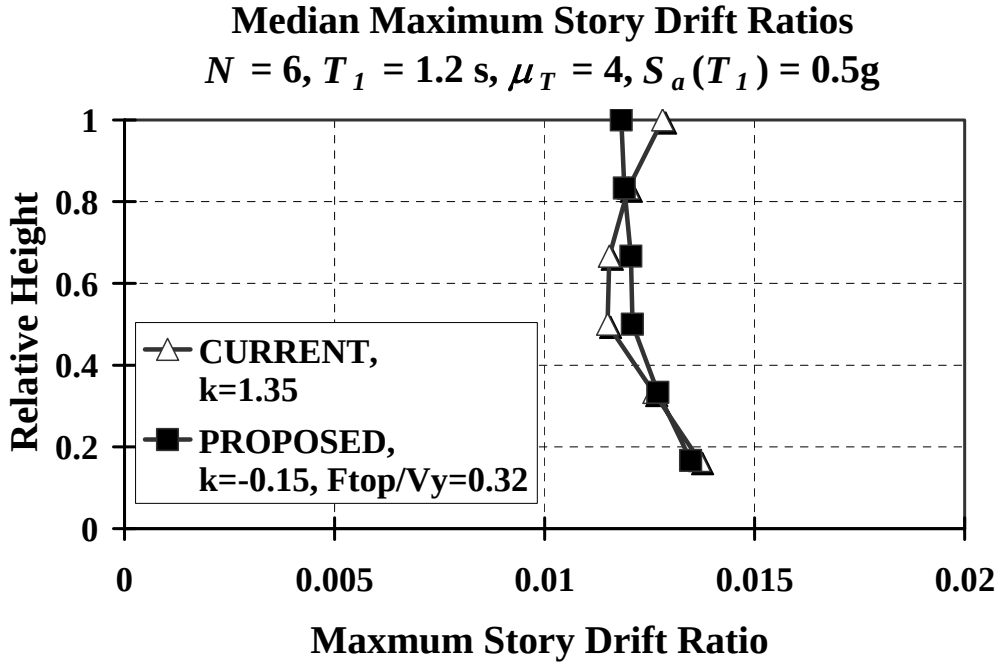

Figure 6.8 Median maximum story drift ratio profiles, 6-story frame structure with T_1 = 1.2 s. for μ_T = 2 (γ_C = 0.23 and γ_P = 0.23) and 4 (γ_C = 0.12 and γ_P = 0.12)

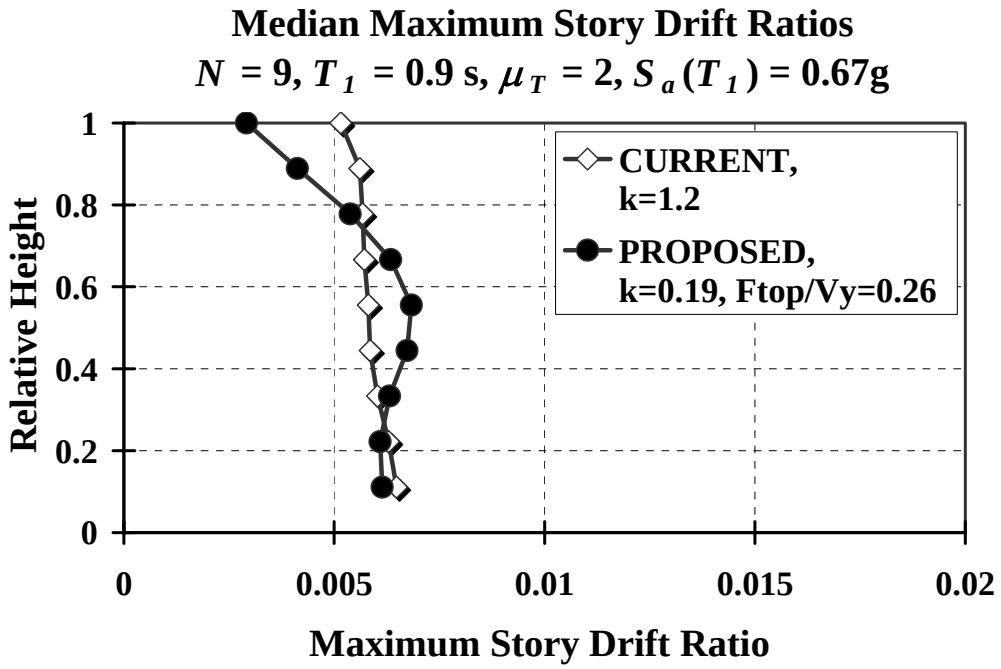

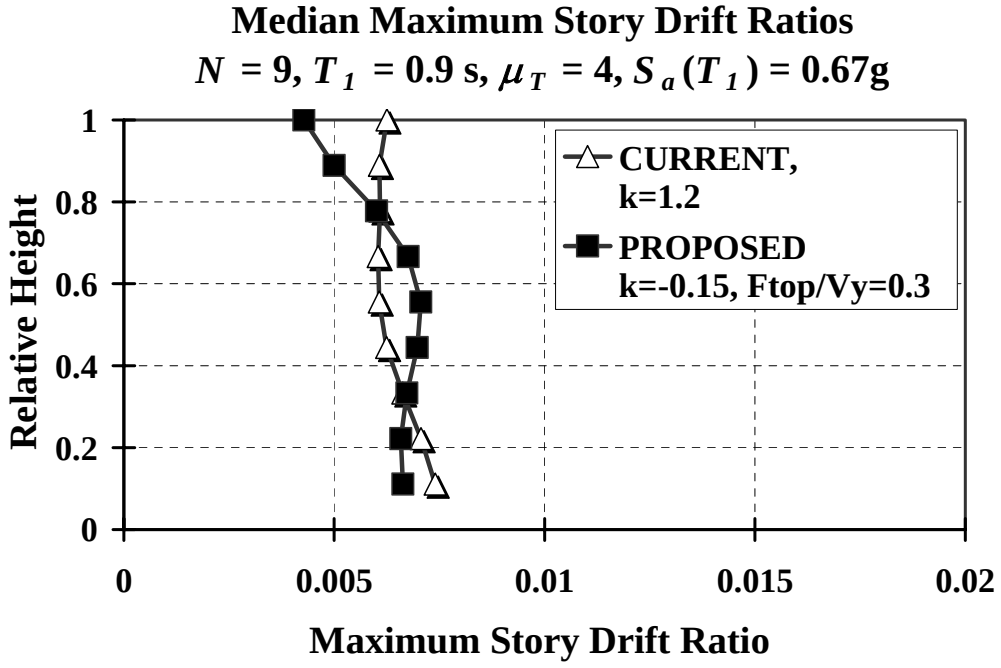

Figure 6.9 Median maximum story drift ratio profiles, 9-story frame structure with T_1 = 0.9 s. for μ_T = 2 (γ_C = 0.31 and γ_P = 0.29) and 4 (γ_C = 0.16 and γ_P = 0.15)

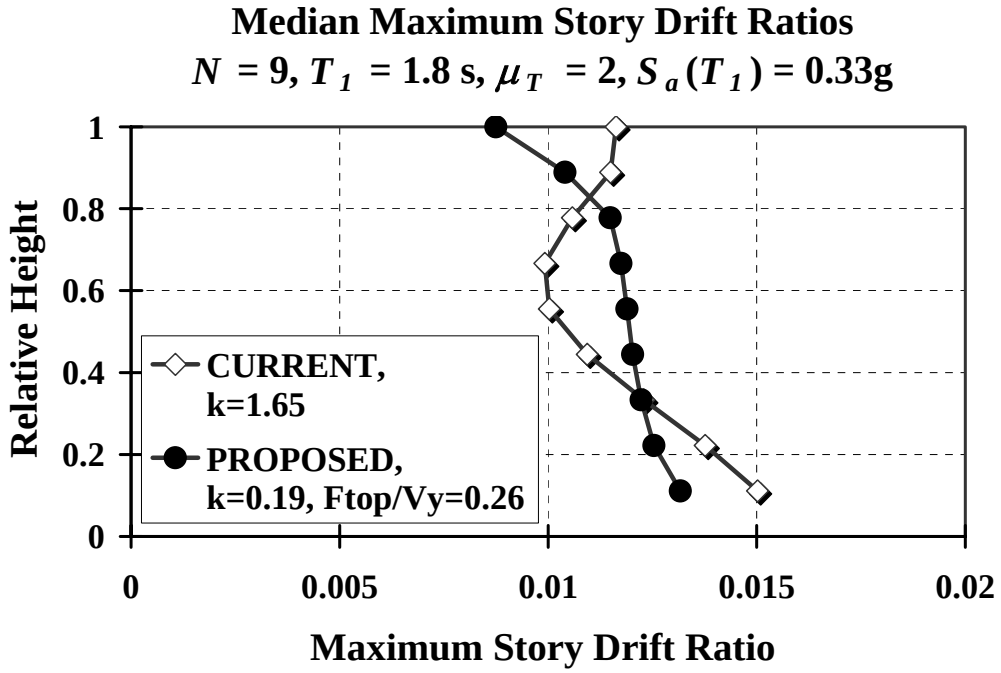

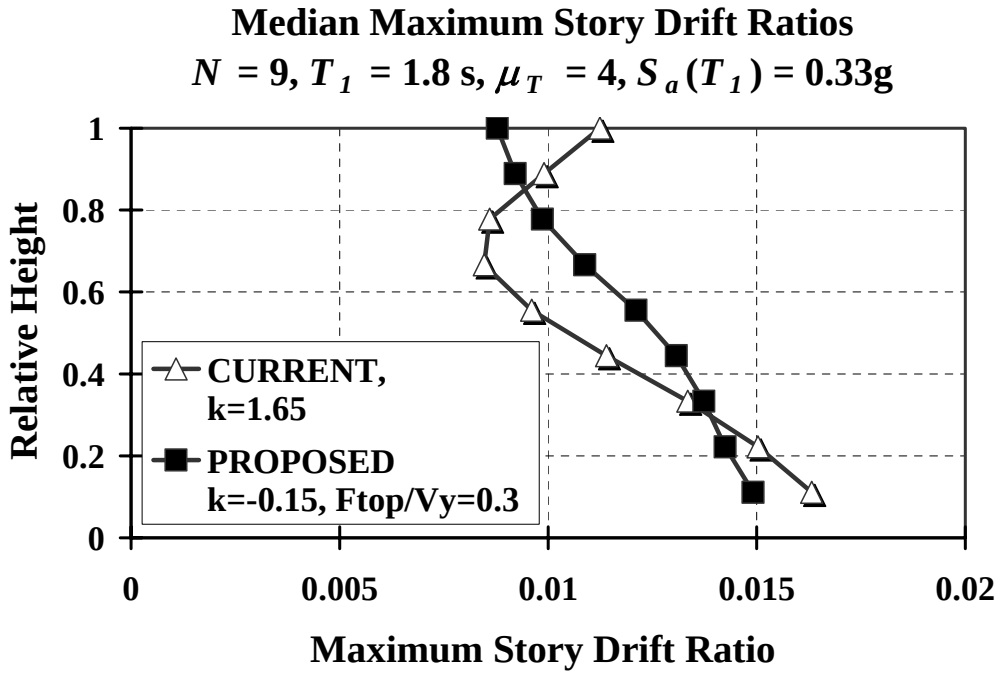

Figure 6.10 Median maximum story drift ratio profiles, 9-story frame structure with T_1 = 1.8 s. for μ_T = 2 (γ_C = 0.15 and γ_P = 0.16) and 4 (γ_C = 0.08 and γ_P = 0.08)

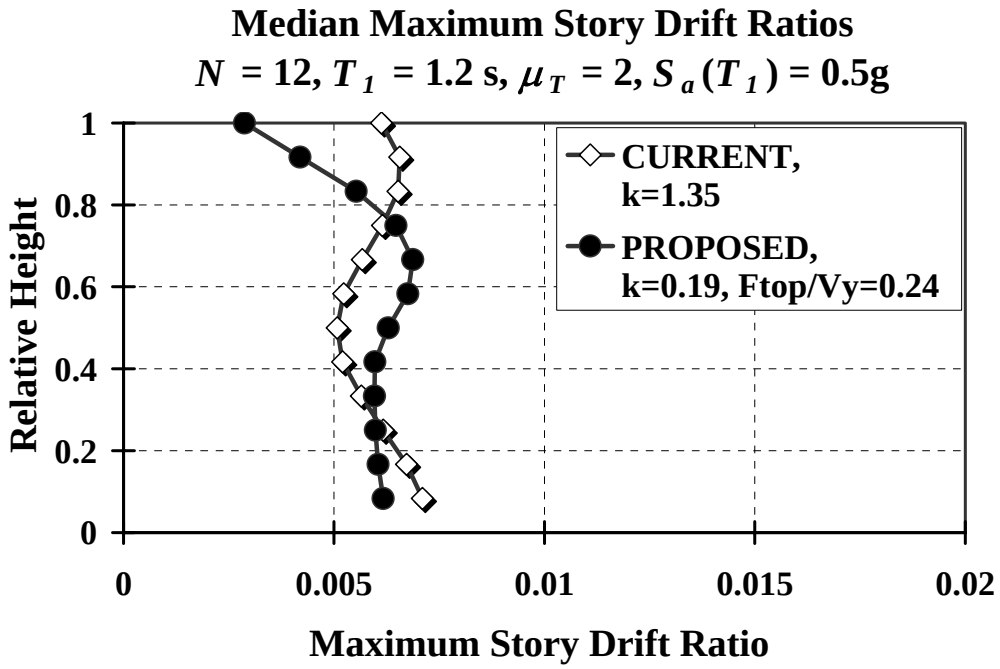

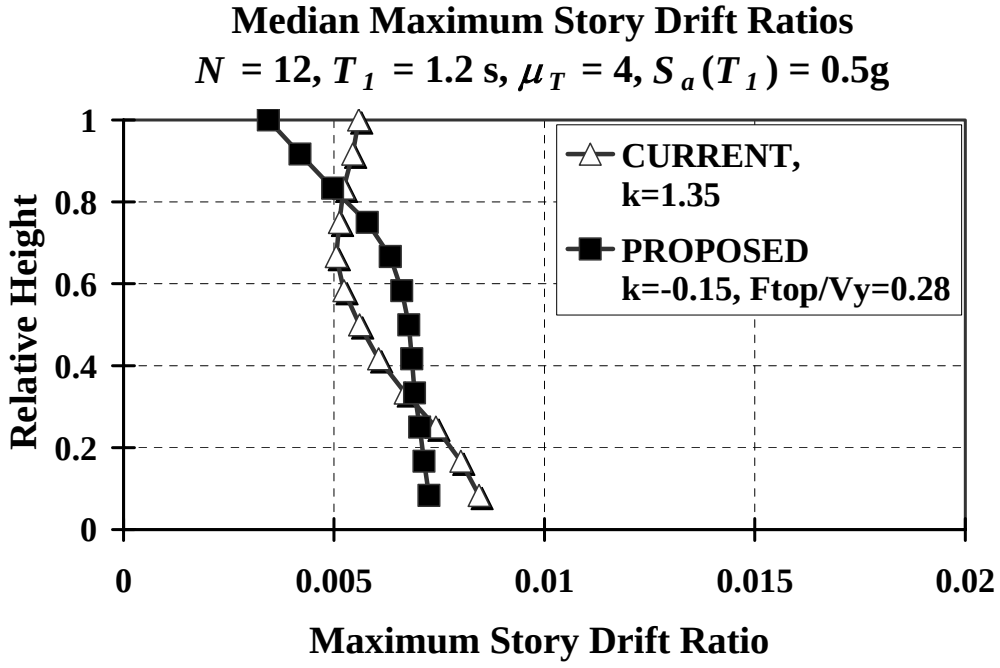

Figure 6.11 Median maximum story drift ratio profiles, 12-story frame structure with T_1 = 1.2 s. for μ_T = 2 (γ_C = 0.23 and γ_P = 0.23) and 4 (γ_C = 0.12 and γ_P = 0.12)

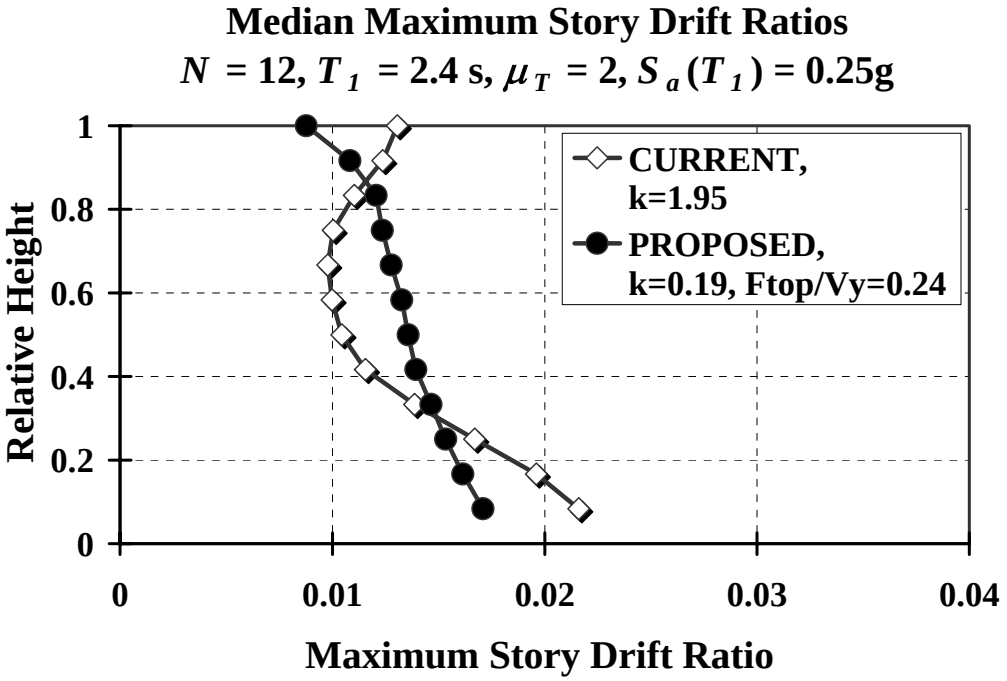

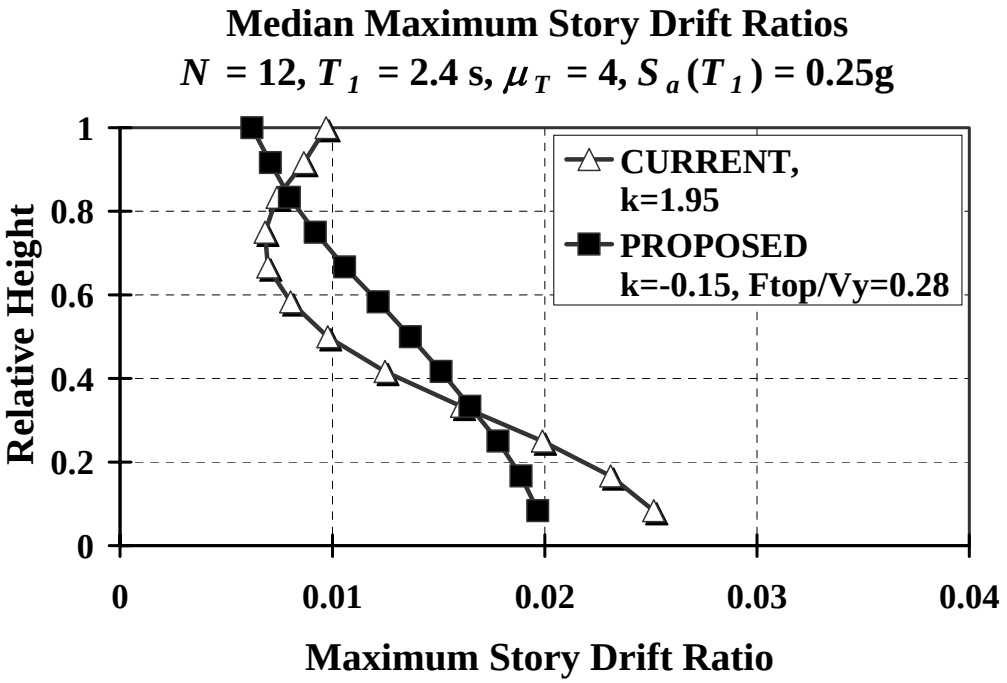

Figure 6.12 Median maximum story drift ratio profiles, 12-story frame structure with T_1 = 2.4 s. for μ_T = 2 (γ_C = 0.11 and γ_P = 0.13) and 4 (γ_C = 0.06 and γ_P = 0.06)

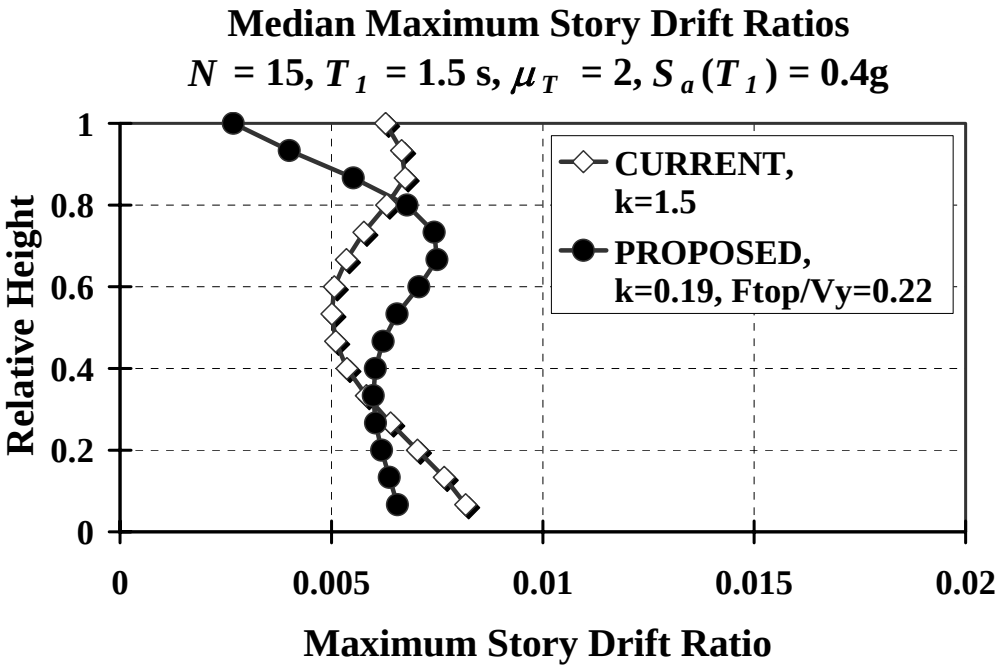

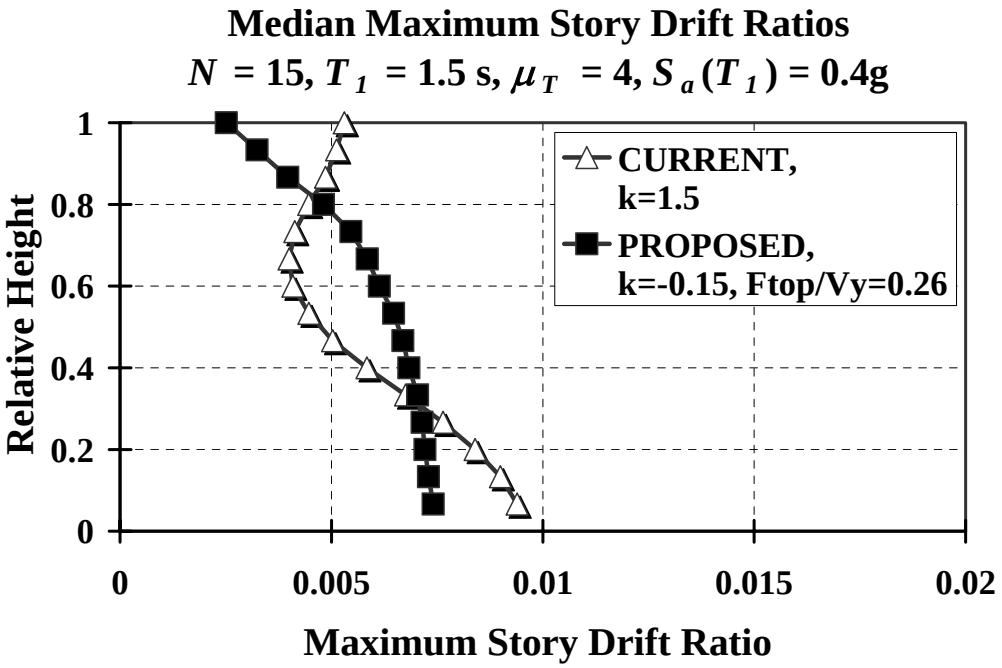

Figure 6.13 Median maximum story drift ratio profiles, 15-story frame structure with T_1 = 1.5 s. for μ_T = 2 (γ_C = 0.18 and γ_P = 0.19) and 4 (γ_C = 0.09 and γ_P = 0.1)

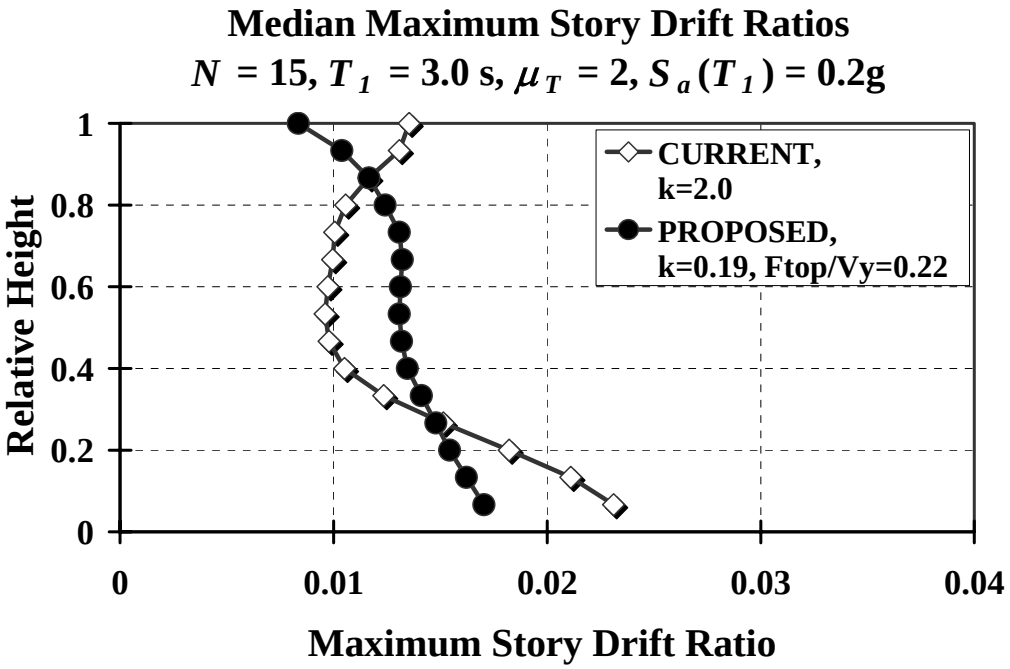

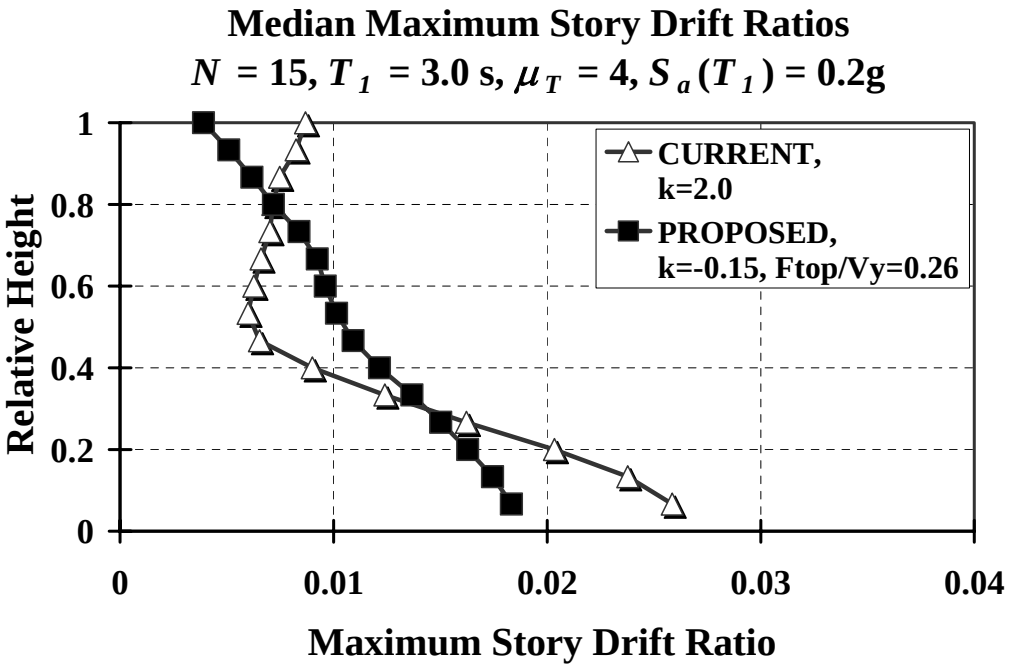

Figure 6.14 Median maximum story drift ratio profiles, 15-story frame structure with T_1 = 3.0 s. for μ_T = 2 (γ_C = 0.09 and γ_P = 0.11) and 4 (γ_C = 0.04 and γ_P = 0.05)

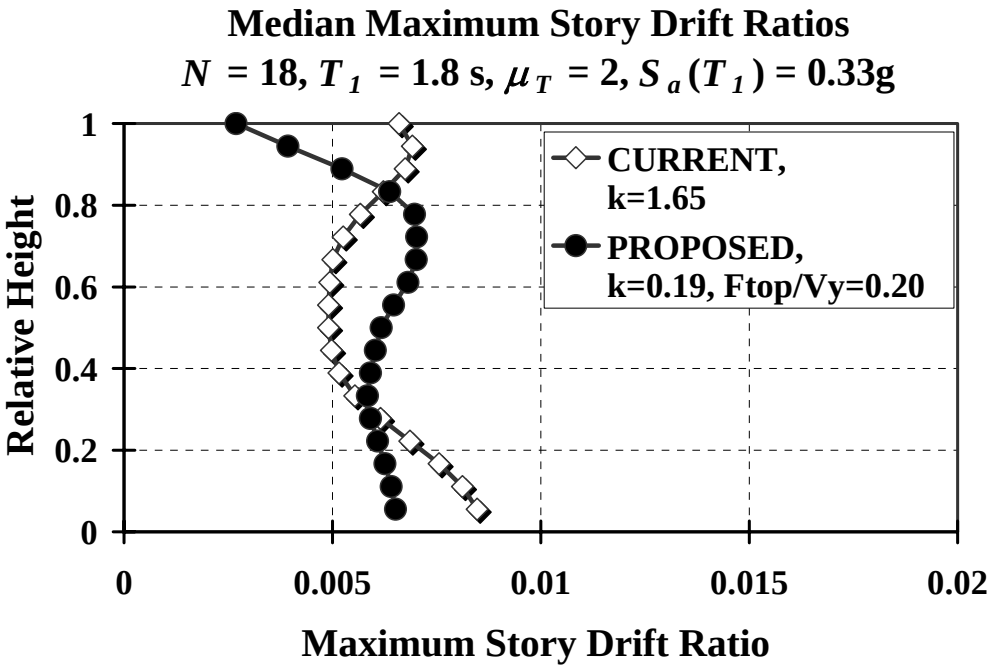

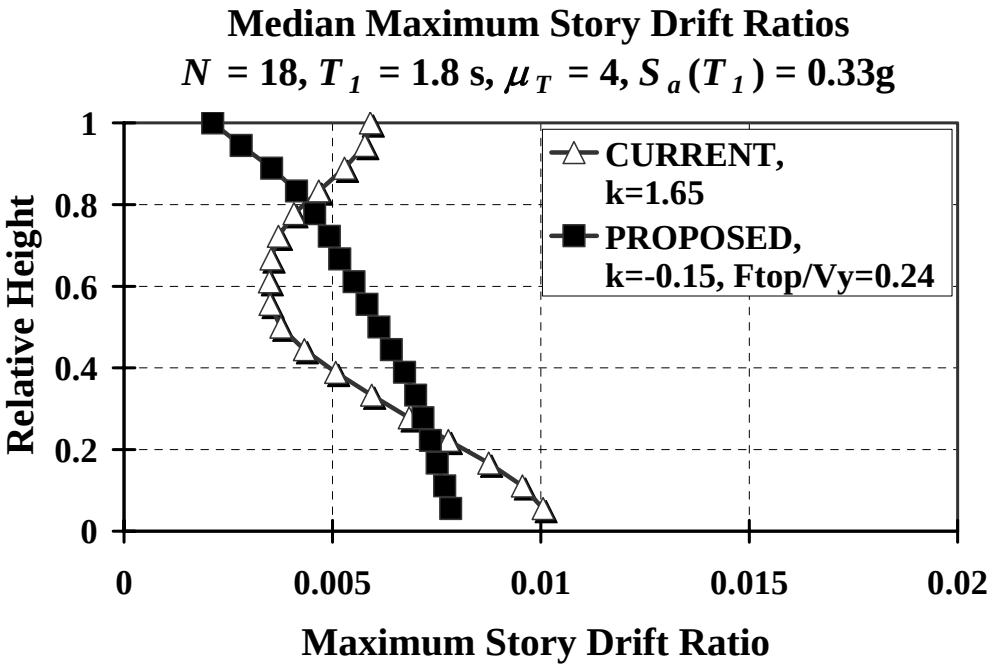

Figure 6.15 Median maximum story drift ratio profiles, 18-story frame structure with T_1 = 1.8 s. for μ_T = 2 (γ_C = 0.15 and γ_P = 0.16) and 4 (γ_C = 0.08 and γ_P = 0.08)

6.5.3 Incremental Dynamic Analysis (IDA)

Because of the presence of P-delta effects, dynamic instability, and hence, global collapse, can be expected in the flexible and relatively long-period structural systems (i.e. $T_1 = 0.2\,N$, $N = 9 \sim 15$) designed based on both current and proposed design approaches when those frame models are exposed to strong ground motions. In order to see the complete picture of structural behavior from elasticity to yielding and global collapse, Incremental Dynamic Analyses (IDA) are conducted to provide a better understanding of structural response corresponding to the ground excitation. Incremental dynamic analysis is a well known and widely utilized seismic evaluation tool, as originally proposed by Vamvatsikos and Cornell (2002). An IDA involves a series of time history analyses by increasing the severity of the record until a collapse limit state is reached. The IDA curve characterizes the variation of engineering demand parameters (e.g., maximum story drift ratio) with changes in ground motion intensity measures and provides a general idea of the 'capacity' of the structure against global collapse.

The intensity of the ground motion, i.e., spectral acceleration at the first mode period of the structure, $S_a(T_1)$/g is increased and the maximum story drift ratio is computed for each value of $S_a(T_1)$/g. Flexible nine-, twelve-, and fifteen-story frame models with fundamental periods of 1.8 s, 2.4 s, and 3.0 s respectively, are utilized to estimate the dynamic response of the structural systems for the target story ductility ratio equal to 2.

Median IDA profiles for CURRENT and PROPOSED are presented in Figures 6.16 to 6.18 along with individual values of maximum story drift angles. In these three figures, the moment-resisting frame designed based on the proposed

methodology exhibits approximately the same peak story drift ratios for smaller values of $S_a(T_1)$/g. However, it can be observed that both CURRENT and PROPOSED tend to approach the onset of dynamic instability at different value of $S_a(T_1)$/g: median PROPOSED curves, shown in Figures 6.16, 6.17, and 6.18, more slowly approach the onset of dynamic instability. This is clearly shown when the number of stories and the fundamental period of vibration are increased for the same target story ductility ratio of 2. It is noted that each maximum story drift ratio is obtained by computing the maximum of peak story drift ratios along the height. Thus, these values may not always occur at the bottom story and can be different from the values of maximum story drift ratios depicted in Section 6.2.2.

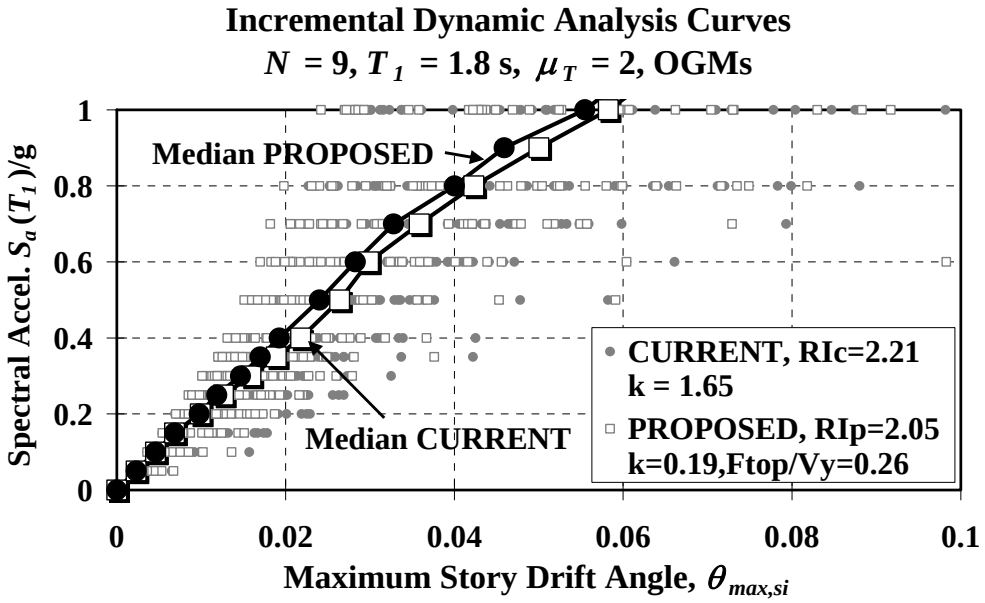

Figure 6.16 Incremental dynamic analysis profiles for flexible 9-story structure with T_1 = 1.8 s. for μ_T = 2

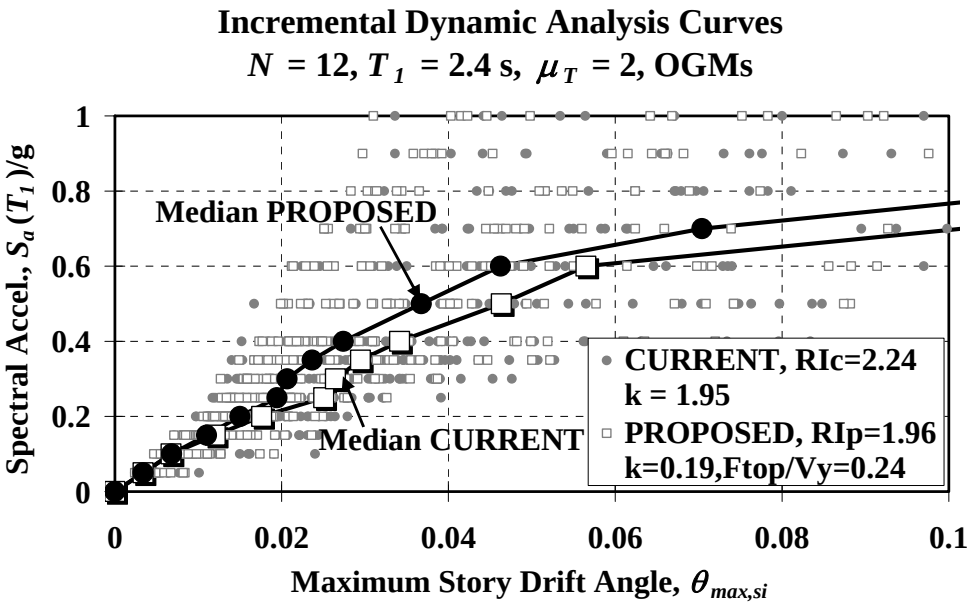

Figure 6.17 Incremental dynamic analysis profiles for flexible 12-story structure with T_1 = 2.4 s. for μ_T = 2

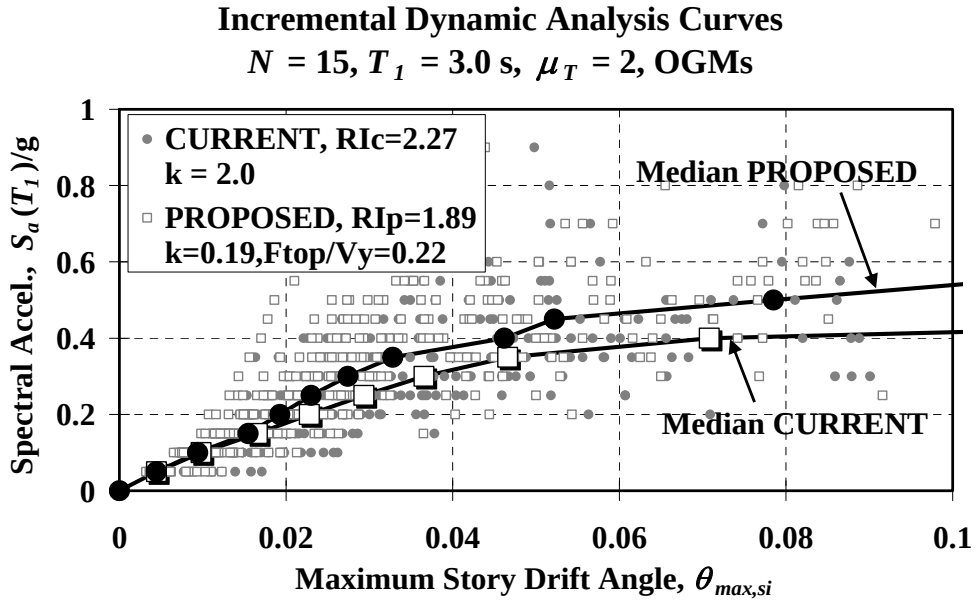

Figure 6.18 Incremental dynamic analysis profiles for flexible 15-story structure with T_1 = 3.0 s. for μ_T = 2

6.3 EXAMPLES OF THE PROPOSED METHODOLOGY FOR NEAR-FAULT GROUND MOTIONS

The same verification process for moment-resisting frame structures exposed to ordinary ground motions was conducted for frames with fundamental periods from 0.6 s. to 3.0 s exposed to near-fault ground motions designated in Table 3.2. As mentioned earlier in Chapter 3, near-fault ground motions possess different characteristics from ordinary ground motions: strong velocity amplitudes and frequency contents dominated by a distinct pulse (Somerville et al. 1997). Recent seismic code provisions provide the same lateral load patterns, applicable for frame structures exposed to ordinary ground motions, for the design of moment-resisting frame structures exposed to near-fault ground motions. Thus the verification results from this Section demonstrate: (1) how the lateral load patterns from the current U.S. code provisions provide different inelastic behavior for frame structures exposed to pulse-type near-fault ground motions when it is compared to the behavior of frame structures exposed to ordinary ground motions; (2) that the proposed load patterns are able to provide a more uniform distribution of story ductility and story drift ratios over the height; (3) for a given average structural damage, how structural design based on the proposed load patterns compares to those based on the current seismic design procedures for different ranges $T_1/T_p < 1$ and $T_1/T_p > 1$.

Moment-resisting frame models from 6- to 18-story with fundamental periods from 0.6 s. to 3.0 s. are utilized as representative frame models to test the proposed methodology for the target story ductility ratios of 2 and 4. The relative intensity values corresponding to $T_1/T_p < 1$ and $T_1/T_p > 1$ for PROPOSED are estimated based on Equations 4.5 and 4.6, respectively, as shown in Figure 6.19.

The regressed parameters k and F_{top}/V_y are utilized as computed by using Equations 4.8 and 4.10 for the range $T_1/T_p < 1$. For the range $T_1/T_p > 1$, Equations 4.9 and 4.11 are utilized to calculate a second set of parameters k and F_{top}/V_y, respectively. Member strengths are tuned to the predefined seismic design lateral loads. As shown in Figure 6.19, the lateral load patterns for CURRENT (i.e., as a function of T_1, m) are not changed from Figure 6.1, which is used for ordinary ground motions. However, lateral load patterns for PROPOSED are different from ordinary ground motions depending on the ratio T_1/T_p as well as a function of μ_T, and H.

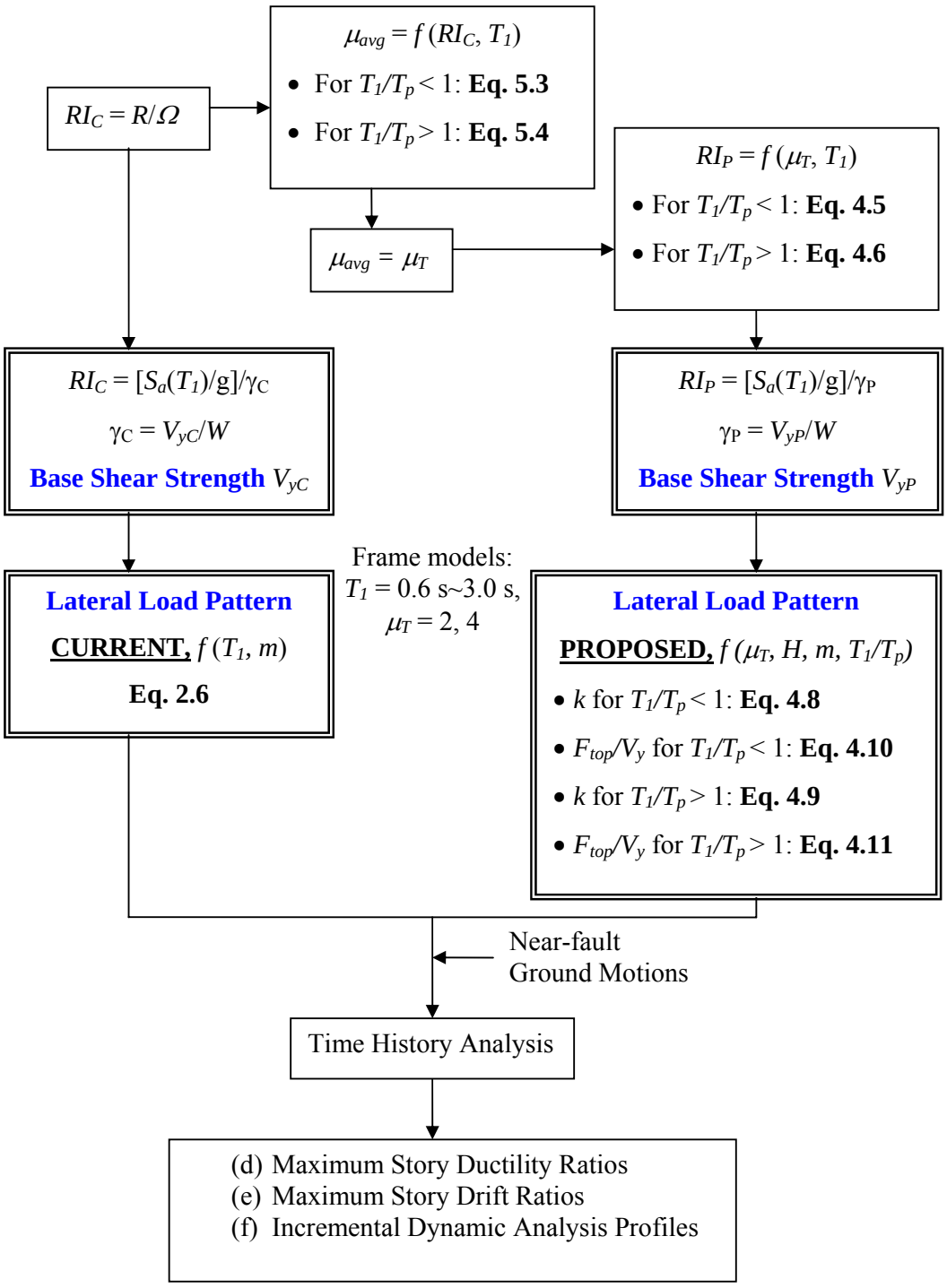

Figure 6.19 Verification process for moment-resisting frame structures exposed to near-fault ground motions

6.3.1 Story Ductility Ratio

Because of the small number of ground motion records for several frame models (see. Table 3.3), averaged story shear strength distributions are used to obtain the main parameters k and F_{top}/V_y of the proposed load patterns as presented in Chapter 4. Thus, average (mean) story ductility ratio profiles are depicted in Figures 6.20 through 6.28 for moment-resisting frame structures with fundamental periods from 0.6 s. to 3.0 s. and target story ductility ratios of 2 and 4. The frame structures are designed based on the current and proposed approaches and exposed to near-fault ground motions in the ranges $T_1/T_p > 1$ and $T_1/T_p < 1$. Results mainly demonstrate that the distribution of story ductility ratios along the height of frames with member strength tuned to the proposed seismic lateral load patterns is rather uniform and close to the target values of 2 and 4. However, for $\mu_T = 4$, average of story ductility ratios over the height are overestimated or underestimated in some cases because of the following reasons: First, μ_{avg} values are computed from the regression equations (i.e., Equations 5.3 and 5.4 for $T_1/T_p < 1$ and $T_1/T_p > 1$, respectively) and are used to estimate the base shear strength for PROPOSED by using additional regression equations, i.e., Equations 4.5 and 4.6 for $T_1/T_p < 1$ and $T_1/T_p > 1$, respectively. Hence, the determination of μ_{avg} strongly depends on how accurately the regression models fit a given set of individual data points. For very flexible frame structures (T_1 = 2.4 s. and 3.0 s.) and $T_1/T_p > 1$, Figure 6.29 shows significant difference between the story shear strength distributions produced by the equations with the estimated values (open square symbol line) and the proposed equations determined by the statistical regression analyses (solid circle symbol line). This case highlights some of the limitations of the proposed equations.

An average value is used as the representative quantity of the central tendency for frame structures exposed to large numbers of near-fault ground motions with different frequency content characteristics. For example, Figures 6.23, 6.26, and 6.28 show that median profiles (grey symbols and lines) are closer to the target value of 4 than average profiles because individual results in those cases exhibit a relatively large dispersion about the mean and the corresponding data points follow a lognormal distribution more closely. For μ_T = 4, this observation is particularly applicable to cases in which a relatively large number of near-fault ground motions (e.g., 34 and 38) exist.

Although the mean of the average story ductility ratios for frames with member strengths tuned to the 2006 IBC design load patterns are identical to those based on the proposed lateral load patterns, the distribution of story ductility ratios varies significantly with height. Frames designed based on the proposed story shear strength distributions have smaller story ductility ratio demands at the bottom stories, when exposed to near-fault ground motions in most cases, regardless of the ratio T_1/T_p. This is desirable to prevent excessive story displacement amplification for flexible systems that may be prone to experience dynamic instability. For $T_1/T_p > 1$, the resultant maximum story ductility ratios for the frame model with longer periods (e.g., T_1 = 1.5 s. ~ 3.0 s.) of frame structures designed based on CURRENT in the top and bottom stories are considerably greater than 4, as shown in Figures 6.23, 6.26, 6.27, and 6.28. Alavi and Krawinkler (2004) support the results from this study by stating that early yielding occurs in higher stories but high ductility demands migrate to the bottom stories as ground motions become more severe for structures designed based on the current

load patterns when the fundamental period of the structure is greater than the pulse period of the ground motion.

The distribution of average story ductility ratios for CURRENT is presented in Figures 6.21 to 6.28. It can be seen that large values are found in bottom stories when the fundamental period is smaller than the pulse period (see part (a) of each figure). On the other hand, large values of CURRENT story ductility ratios are observed in top stories when the fundamental period is greater than the pulse period. This implies that frame structures designed based on the current U.S. code provisions (i.e., IBC 2006) behave differently in response to the ratio T_1/T_p, and the design load patterns for CURRENT do not account for the pulse-type characteristic of near-fault ground motions (see Figure 6.19). Contrary to the distributions of CURRENT, the proposed load patterns consistently provide quite uniform distributions of story ductility ratios along the height of frame structures for both ranges: $T_1/T_p < 1$ and $T_1/T_p > 1$.

As mentioned in Chapter 4, for the same performance target of interest, proposed load patterns for frames exposed to near-fault ground motions within the range $T_1/T_p > 1$ are very similar to the proposed load patterns for frame structures exposed to ordinary ground motions. Distributions of story ductility ratios along the height of frame structures designed based on the current and proposed lateral load patterns exposed to near-fault ground motions, $T_1/T_p < 1$ and $T_1/T_p > 1$, are compared to the distribution for ordinary ground motions in Figure 6.30. Symbols and lines utilized in Figure 6.30 are designated as follows:

- (a-2): Ordinary ground motions, median profiles for $\mu_T = 2$
- (b-2): Near-fault ground motions, $T_1/T_p < 1$, average profiles for $\mu_T = 2$
- (c-2): Near-fault ground motions, $T_1/T_p > 1$, average profiles for $\mu_T = 2$
- (a-4): Ordinary ground motions, median profiles for $\mu_T = 4$
- (b-4): Near-fault ground motions, $T_1/T_p < 1$, average profiles for $\mu_T = 4$
- (c-4): Near-fault ground motions, $T_1/T_p > 1$, average profiles for $\mu_T = 4$

As an example, a 15-story frame structure with the fundamental period T_1 = 1.5 s. is utilized to demonstrate story ductility ratio profiles for comparison. As shown in the profiles, for both story ductility ratios of 2 and 4, CURRENT and PROPOSED story ductility ratio profiles of (a-2) and (a-4) are very similar to those of (c-2) and (c-4), respectively. Figure 6.30 shows that the structural response is not significantly affected by the pulse-type characteristics of near-fault ground motions when $T_1/T_p > 1$. This implies that the inelastic dynamic response of these frames is primarily influenced by the contribution of the fundamental mode of vibration to the overall response.

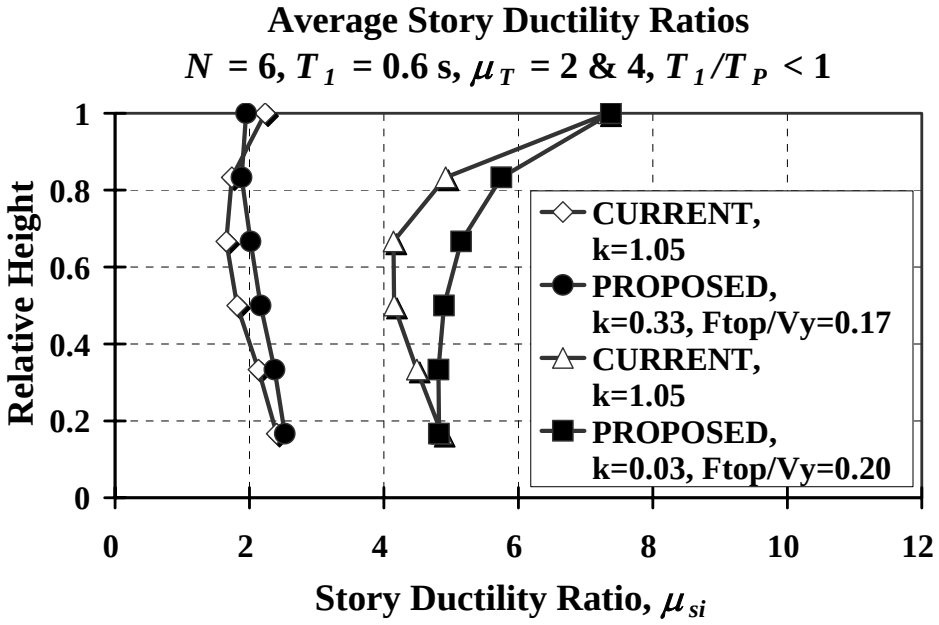

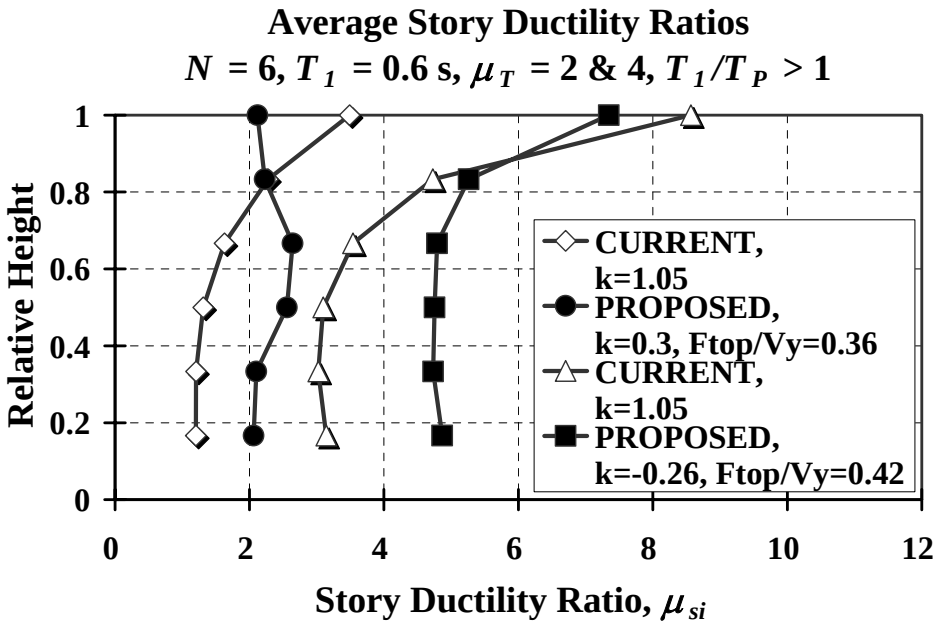

Figure 6.20 Average story ductility ratio profiles, 6-story frame structure with T_1 = 0.6 s. for μ_T = 2 and 4 for T_1/T_p < 1 and T_1/T_p > 1

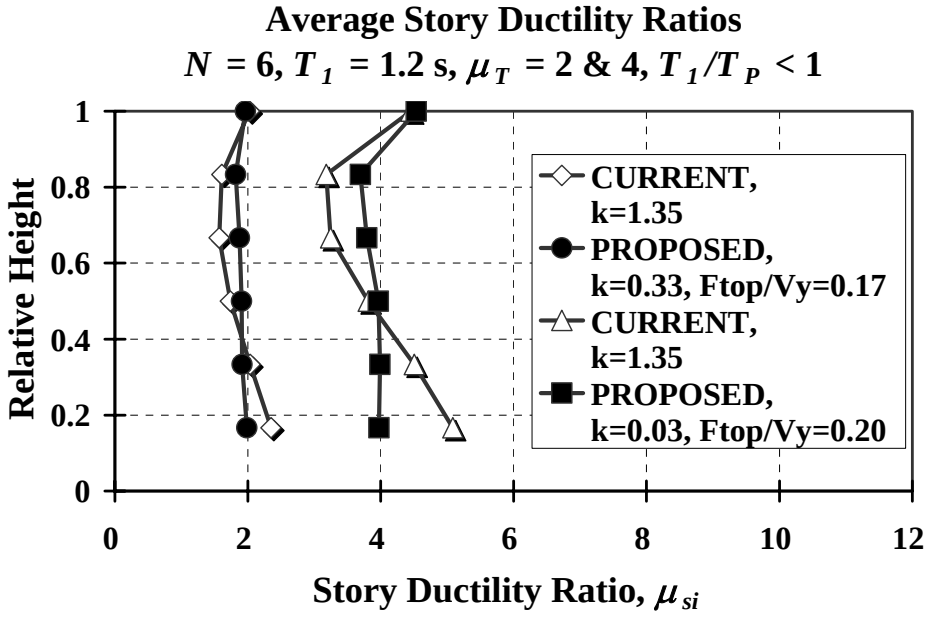

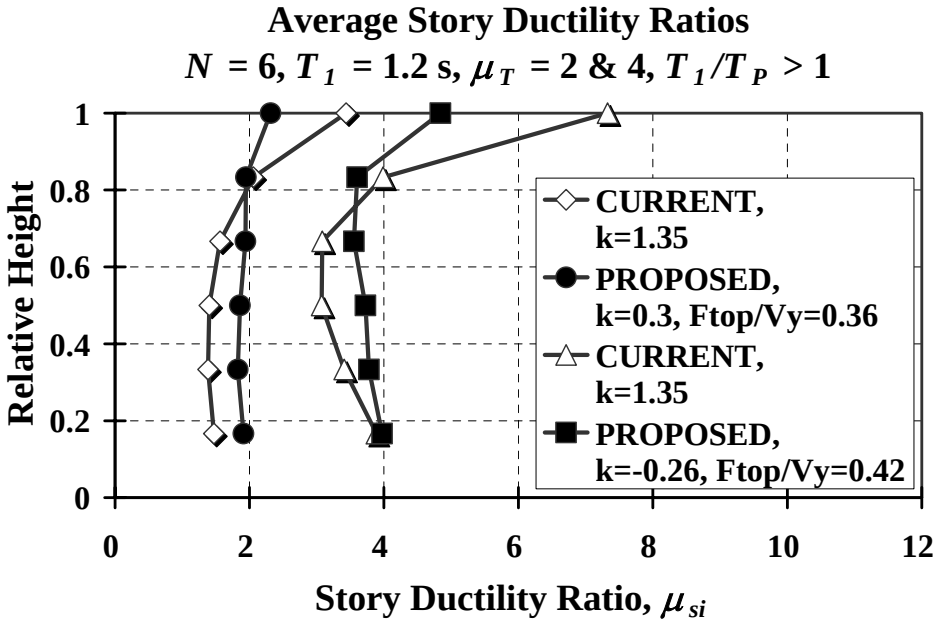

Figure 6.21 Average story ductility ratio profiles, 6-story frame structure with T_1 = 1.2 s. for μ_T = 2 and 4 for T_1/T_p < 1 and T_1/T_p > 1

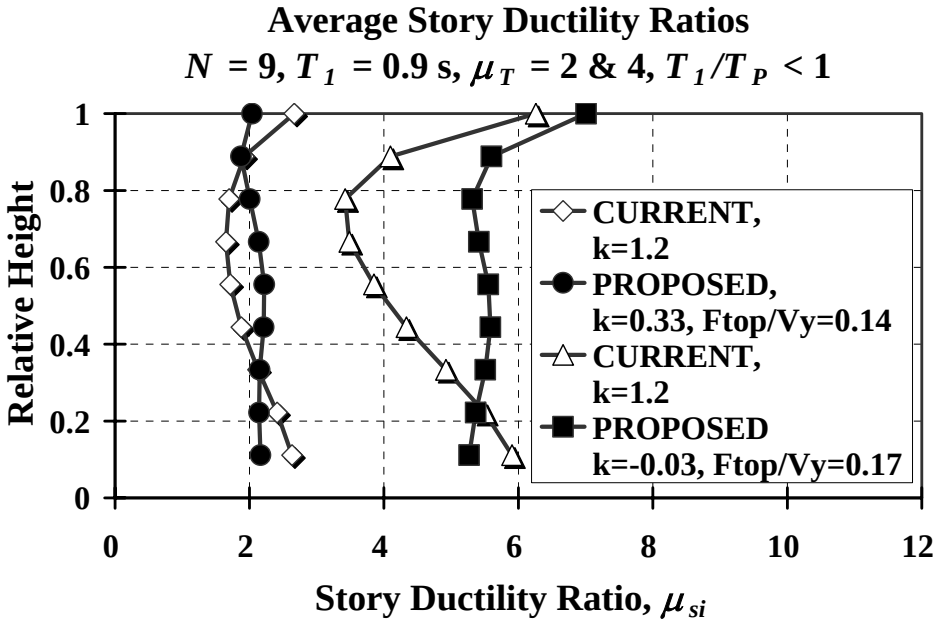

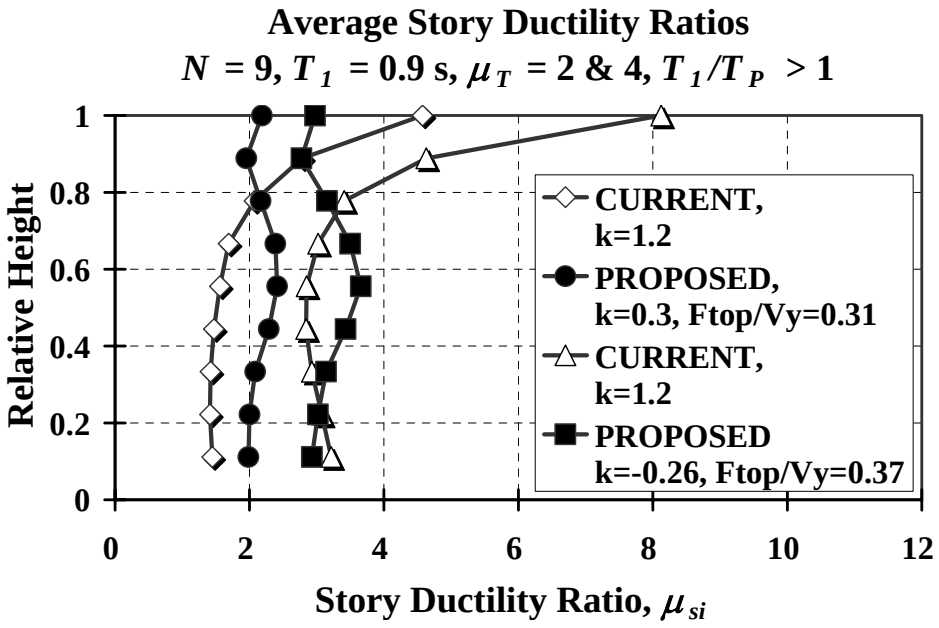

Figure 6.22 Average story ductility ratio profiles, 9-story frame structure with T_1 = 0.9 s. for μ_T = 2 and 4 for T_1/T_p < 1 and T_1/T_p > 1

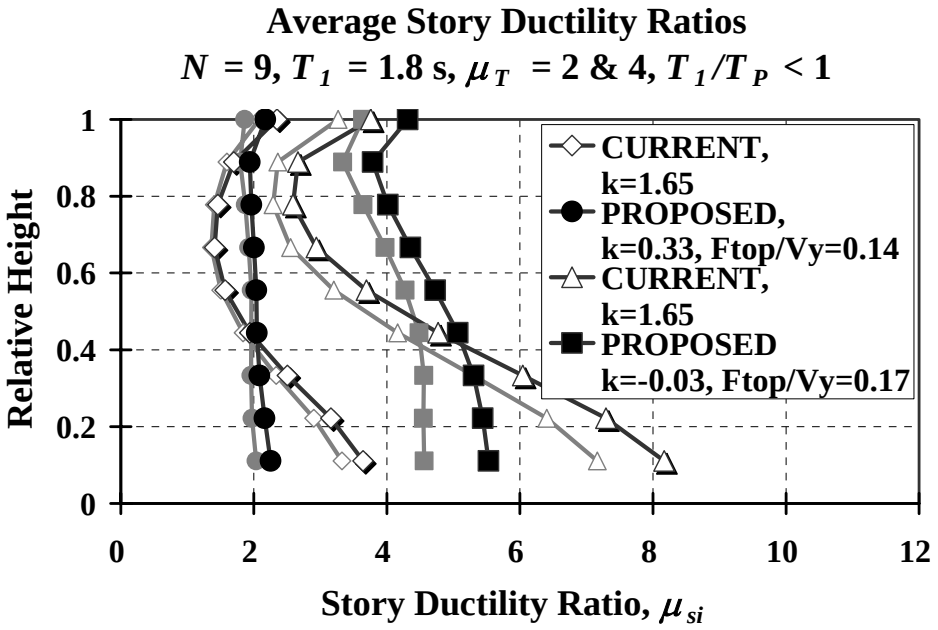

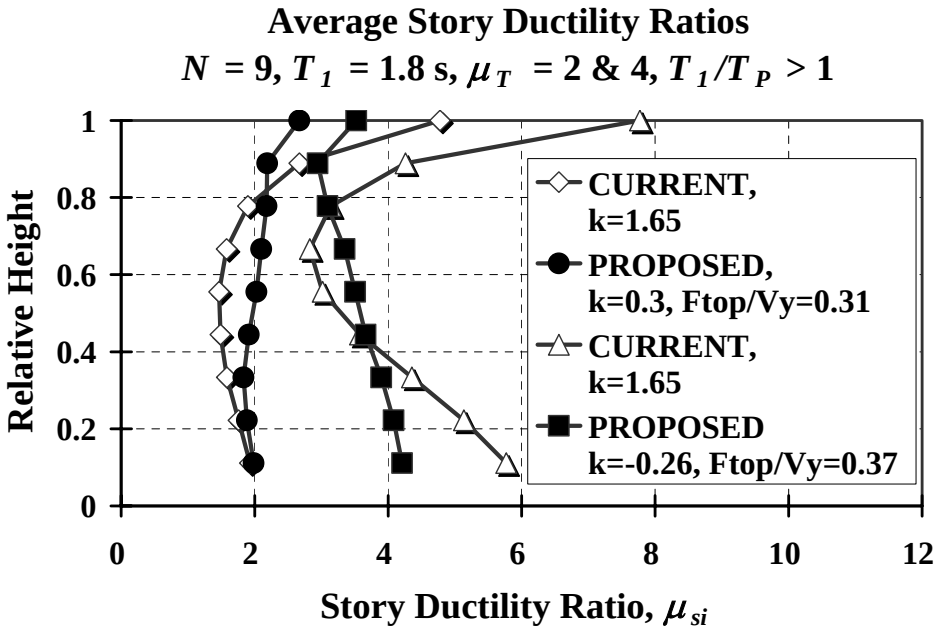

Figure 6.23 Average story ductility ratio profiles, 9-story frame structure with T_1 = 1.8 s. for μ_T = 2 and 4 for T_1/T_p < 1 and T_1/T_p > 1

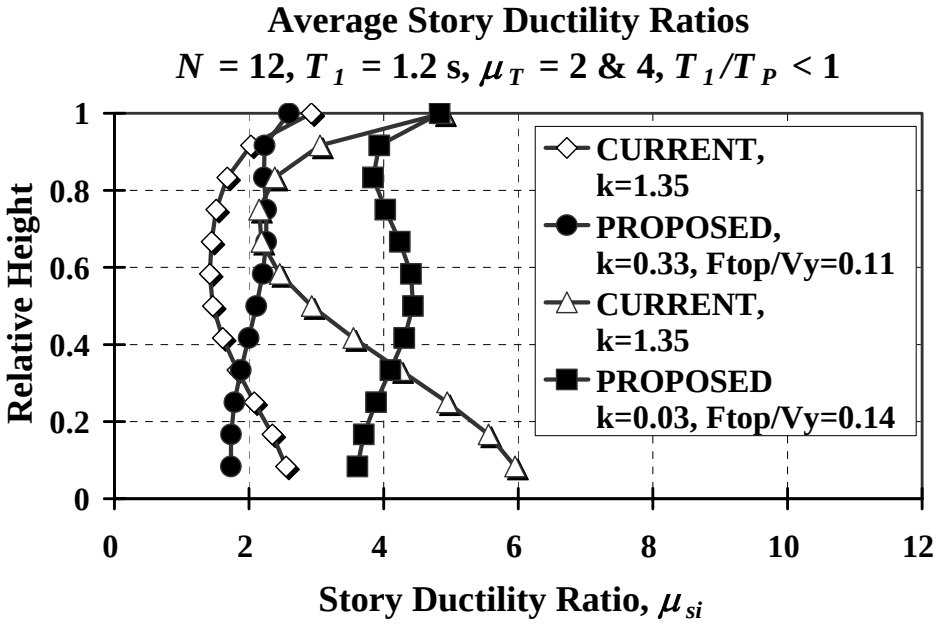

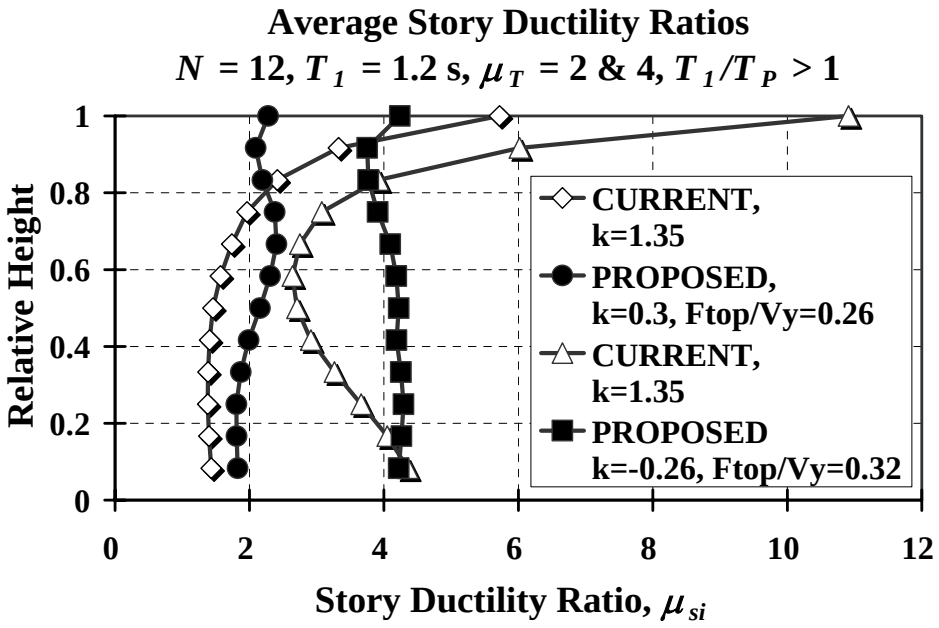

Figure 6.24 Average story ductility ratio profiles, 12-story frame structure with T_1 = 1.2 s. for μ_T = 2 and 4 for $T_1/T_p < 1$ and $T_1/T_p > 1$

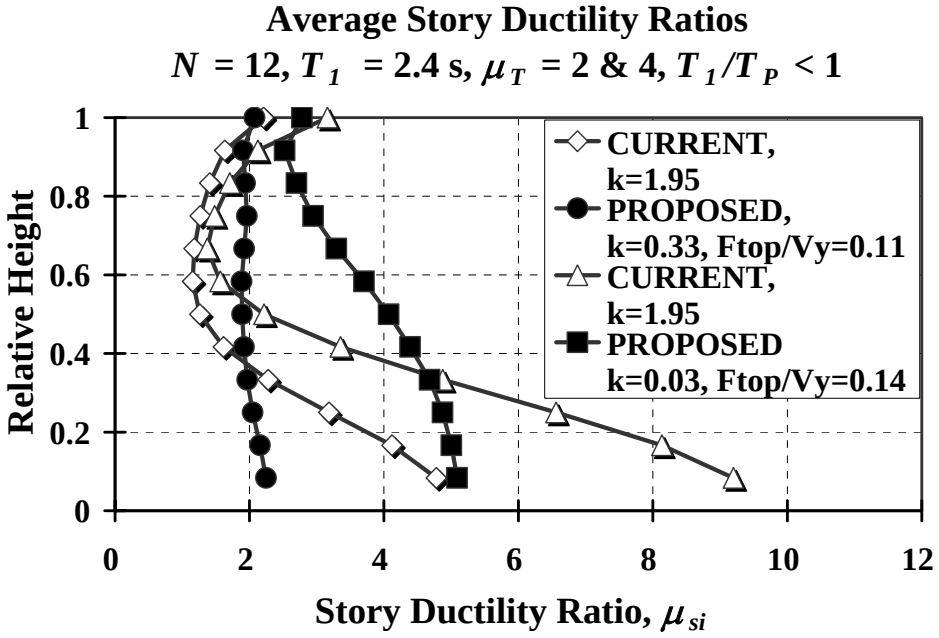

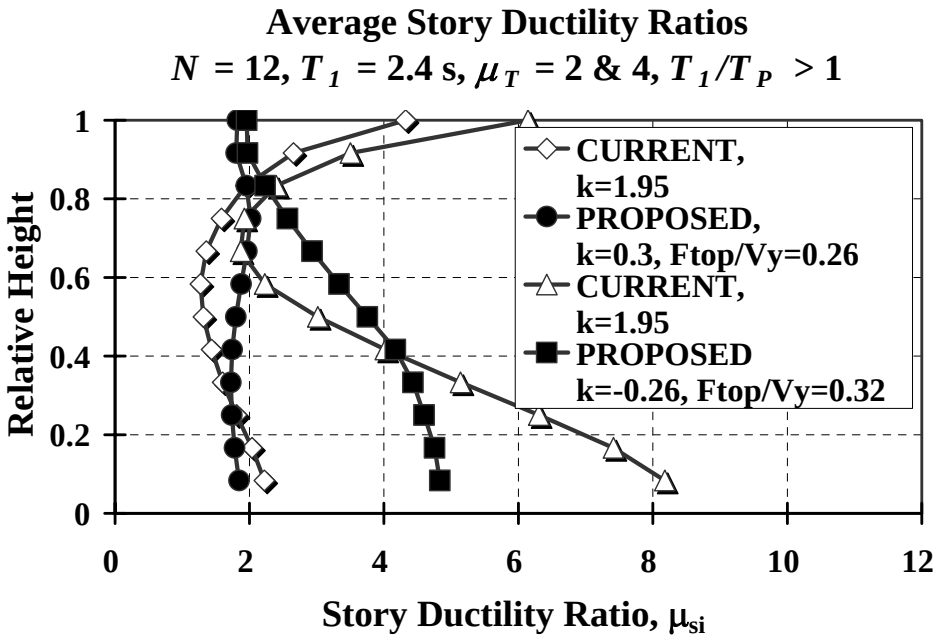

Figure 6.25 Average story ductility ratio profiles, 12-story frame structure with T_1 = 2.4 s. for μ_T = 2 and 4 for $T_1/T_p < 1$ and $T_1/T_p > 1$

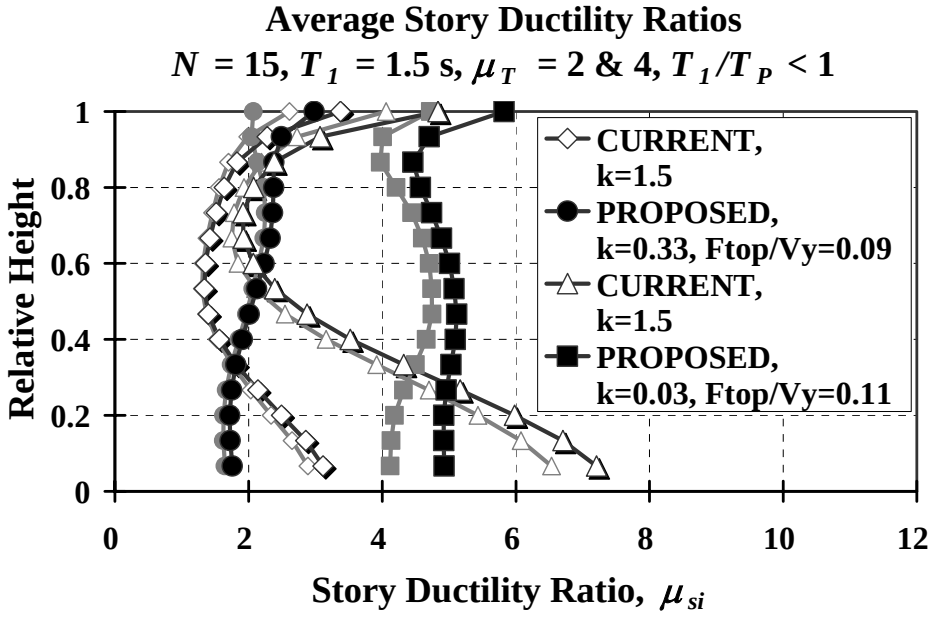

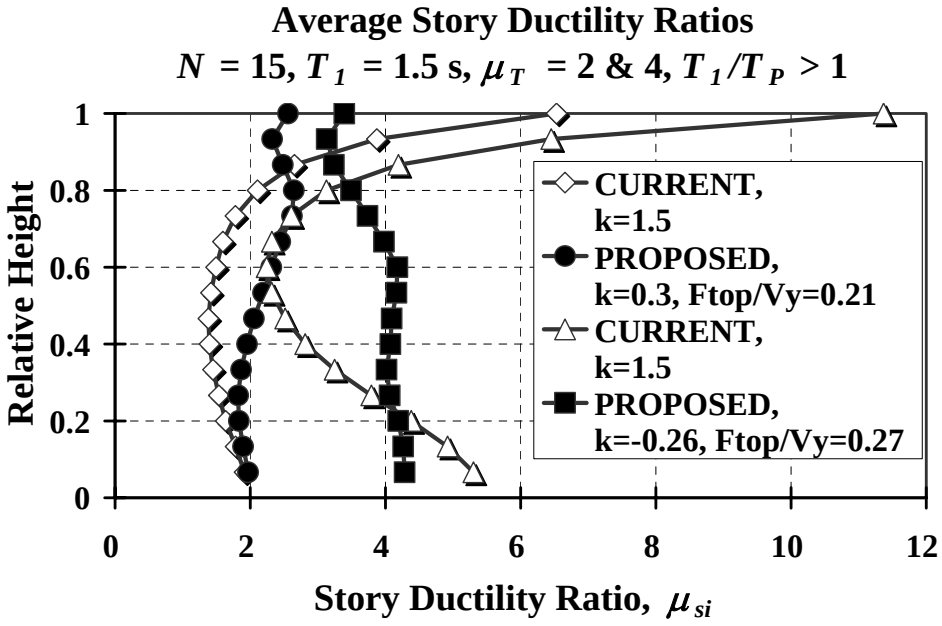

Figure 6.26 Average story ductility ratio profiles, 15-story frame structure with T_1 = 1.5 s. for μ_T = 2 and 4 for T_1/T_p < 1 and T_1/T_p > 1

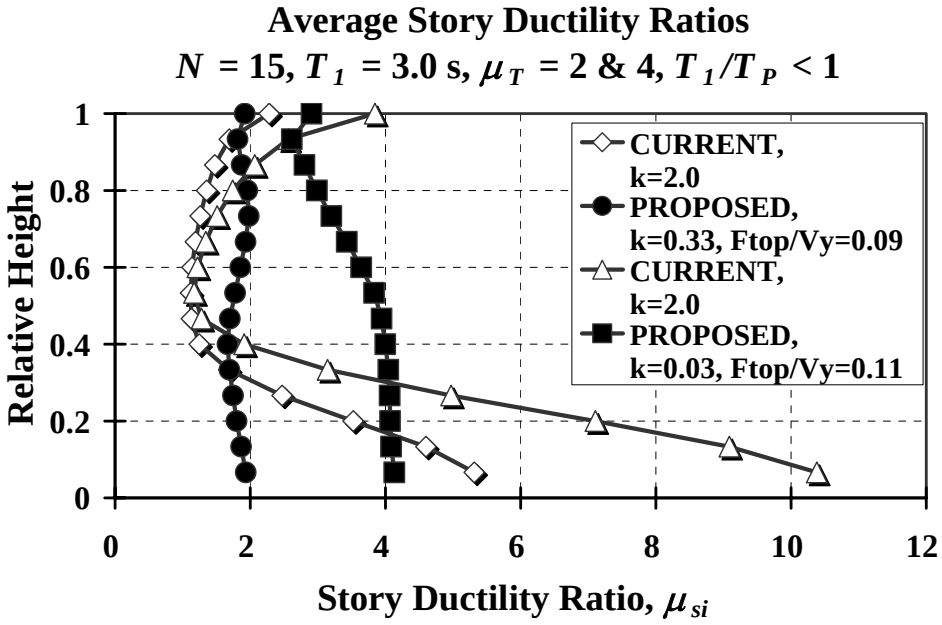

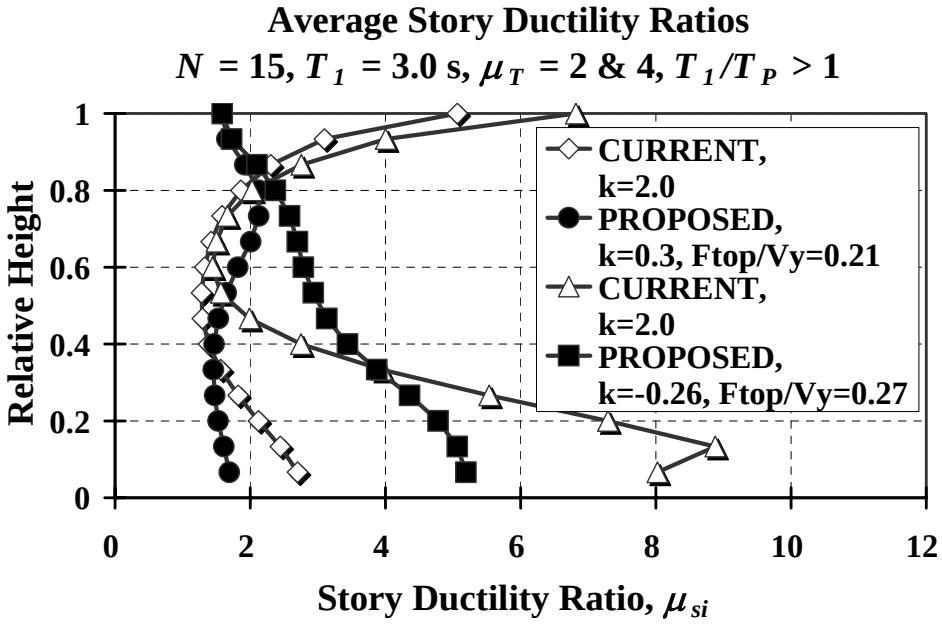

Figure 6.27 Average story ductility ratio profiles, 15-story frame structure with T_1 = 3.0 s. for μ_T = 2 and 4 for T_1/T_p < 1 and T_1/T_p > 1

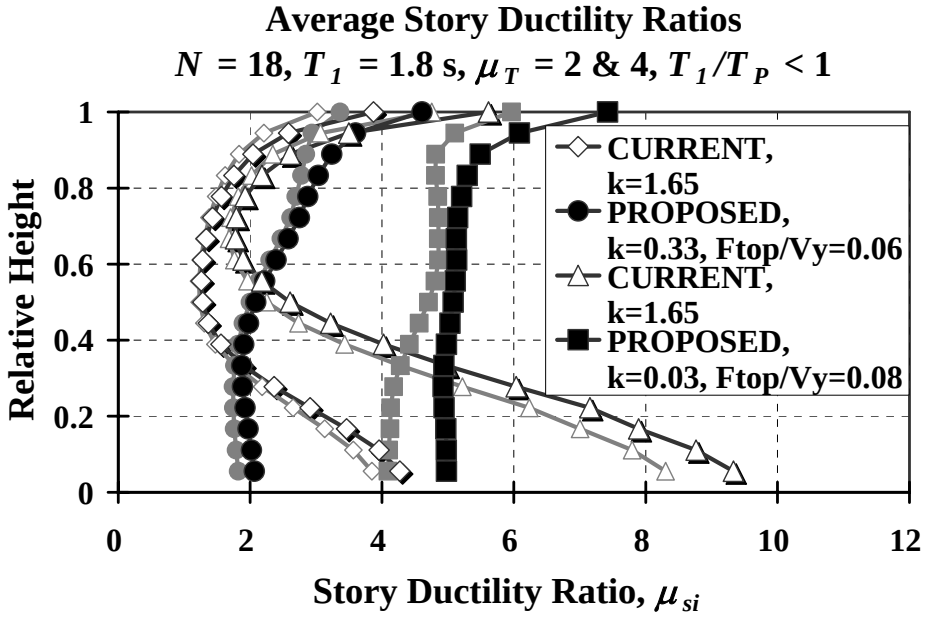

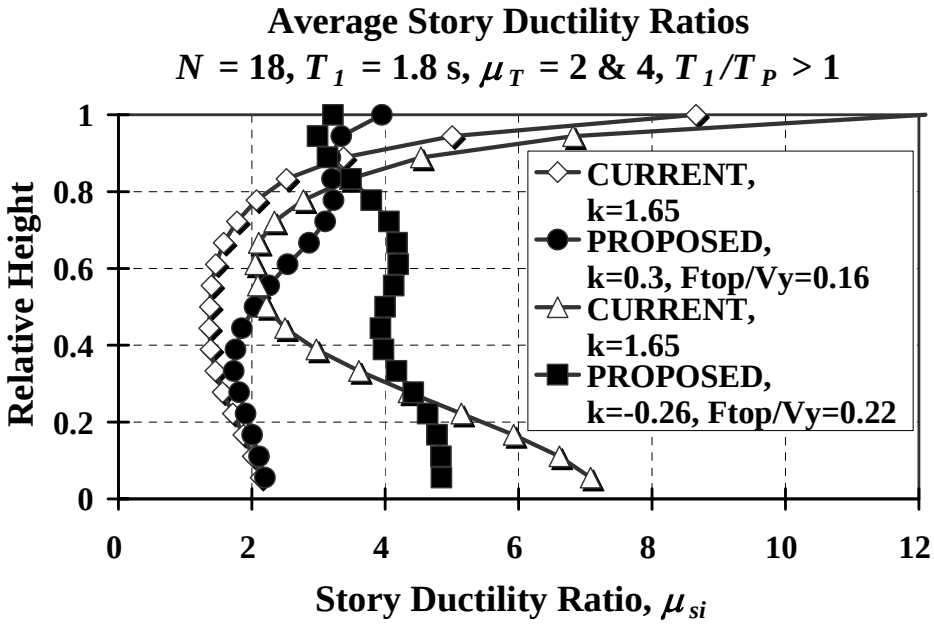

Figure 6.28 Average story ductility ratio profiles, 18-story frame structure with T_1 = 1.8 s. for μ_T = 2 and 4 for T_1/T_p < 1 and T_1/T_p > 1

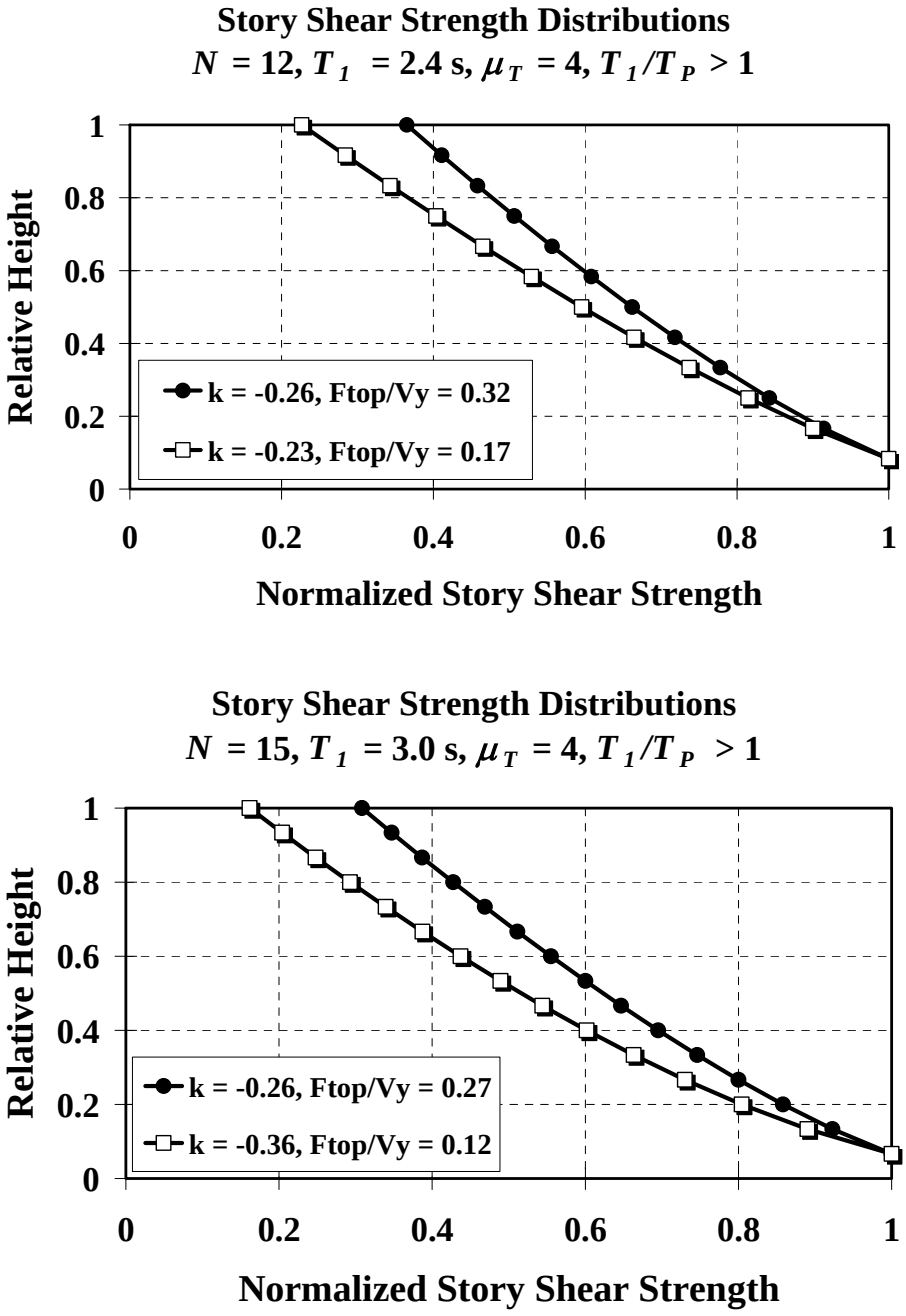

Figure 6.29 Difference of normalized story shear strength distributions of flexible 12-story and 15-story frame models for $T_1/T_p > 1$

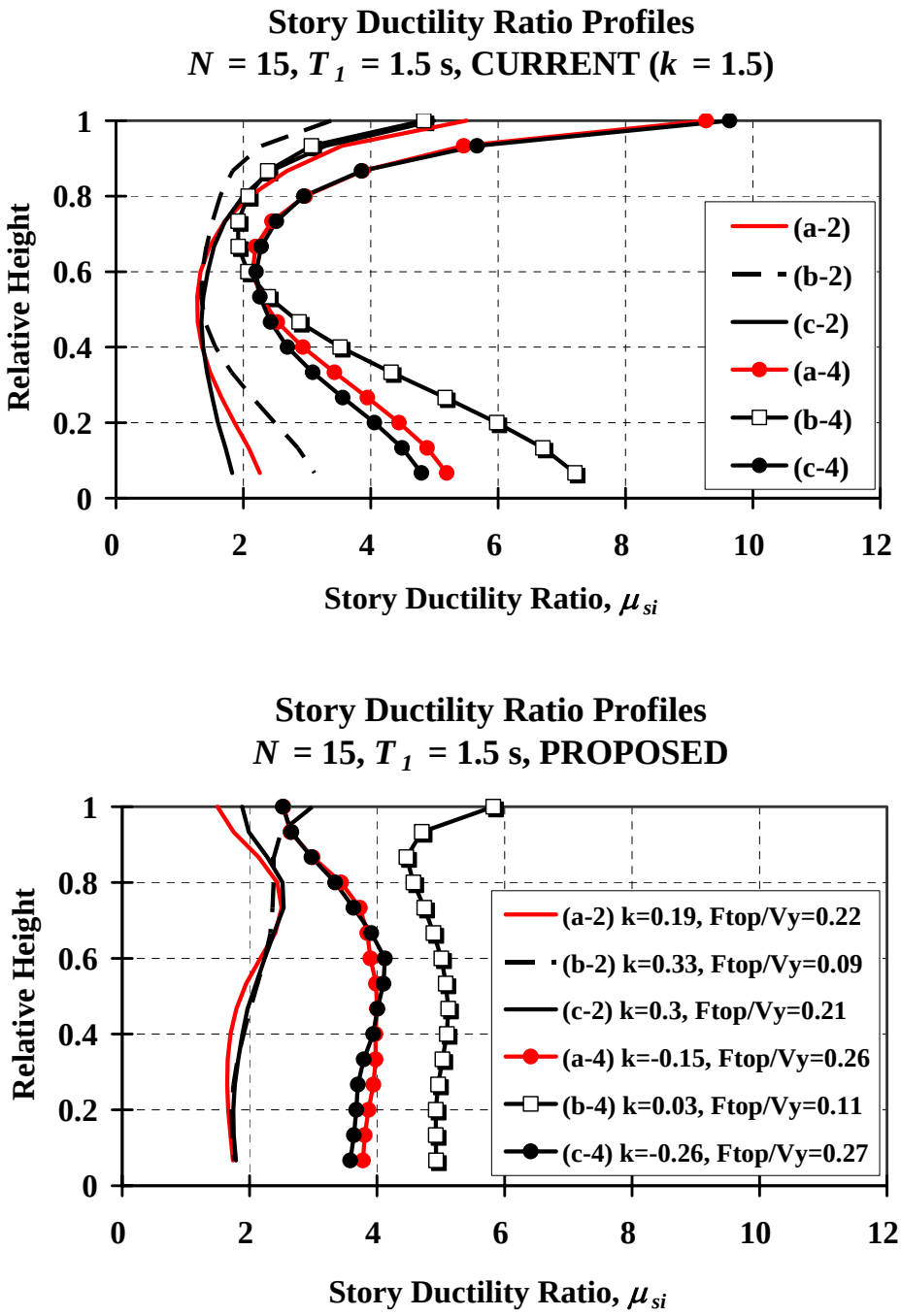

Figure 6.30 CURRENT and PROPOSED story ductility ratio profiles for ordinary and near-fault ground motions, 15-story frames with T_1 = 1.5 s. for μ_T = 2 and 4

6.3.2 Story Drift Ratio

Mean story drift ratios are also depicted in Figures 6.31, 6.33, and 6.35 for the flexible 9-, 12-, and 15-story frames with a target story ductility of 2. In these figures, the mean of average of maximum story drift ratios for a given frame structure designed based on PROPOSED is approximately equal to the mean of maximum story drift ratios for the frame designed based on CURRENT. However, the distribution of average story drift ratios for the frame model designed based on CURRENT varies significantly along the height and presents much larger story drift demands in the bottom stories than the distribution of maximum story drift ratios for the frame designed based on PROPOSED in the range $T_1/T_p < 1$.

The story drift ratio profiles for different target story ductility ratio of 4 are also evaluated and shown in Figures 6.32, 6.34, and 6.36. These results exhibit very similar story drift ratios along the height when compared to the story drift ratios for flexible frame models in the range $T_1/T_p < 1$ as shown in Figures 6.31, 6.33, and 6.35. As a result, frames designed based on the proposed lateral load patterns are also expected to exhibit smaller story displacement amplification at the bottom stories when compared to frames with member strengths tuned to the ELF procedure of building codes. It is important to note that the shape of the distribution of CURRENT average maximum story drift ratios along the height are dissimilar between $T_1/T_p < 1$ and $T_1/T_p > 1$. However, the distribution of PROPOSED story drift ratios along the height of frames for the range $T_1/T_p < 1$ is comparable to the distribution for the range $T_1/T_p > 1$. Thus, for near-fault ground motions with pulse-type characteristics, moment-resisting frames should be designed separately corresponding to the ratio T_1/T_p.

It is also interesting to see that the largest difference between CURRENT and PROPOSED maximum story drift ratios for $T_1/T_p < 1$ occurs in the bottom story of all frame structures utilized in this study. This difference is present with various fundamental periods within the range from 0.9 s. to 3.0 s. as shown in Figure 6.37. The difference in maximum story drift ratios between CURRENT and PROPOSED increases with an increase in the fundamental period for target story ductility ratios 2 and 4, especially when the pulse period of near-fault ground motions is greater than the fundamental period of the structure. This implies that, for a given ground motion hazard level, medium-to-long period frame structures designed based on the ELF procedure of building codes (i.e., T_1 = 0.9 s. to 3.0 s.) are expected to exhibit larger story drift ratios in the bottom stories when compared to the story drift ratios of frames designed based on the proposed approach. These relatively large story drift ratios translate into a decreased capacity against global collapse due to P-delta effects.

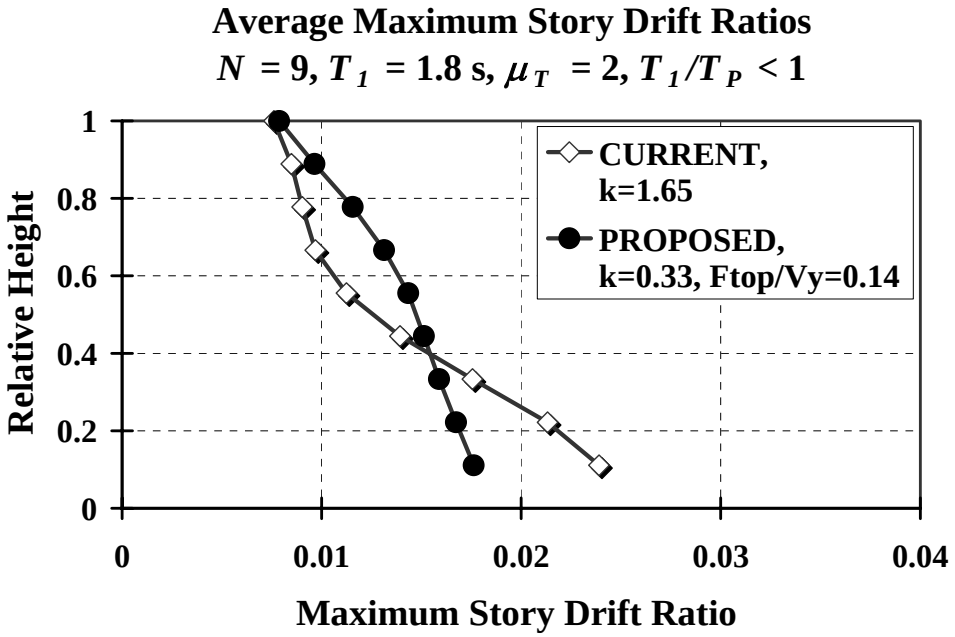

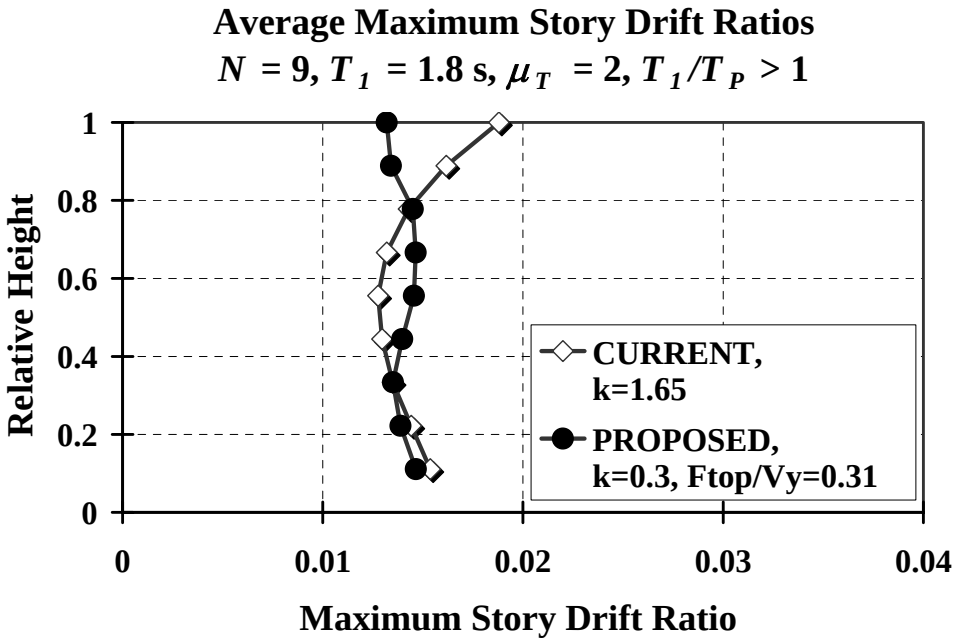

Figure 6.31 Figure 6.31 Average maximum story drift ratio profiles, 9-story frame with T_1 = 1.8 s. for μ_T = 2 for $T_1/T_P < 1$ (γ_C = 0.14 and γ_P = 0.17) and $T_1/T_P > 1$ (γ_C = 0.17 and γ_P = 0.16)

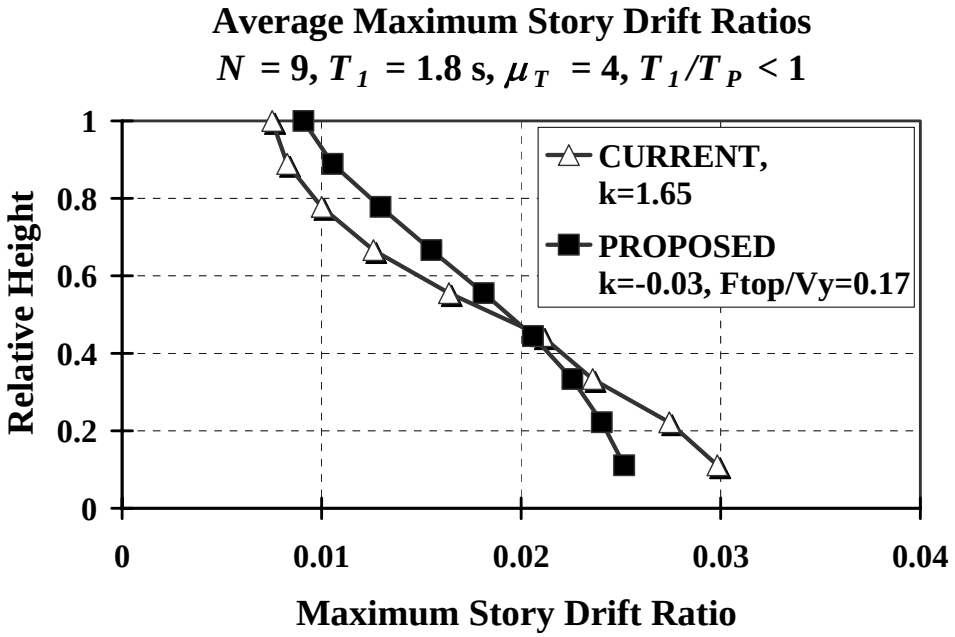

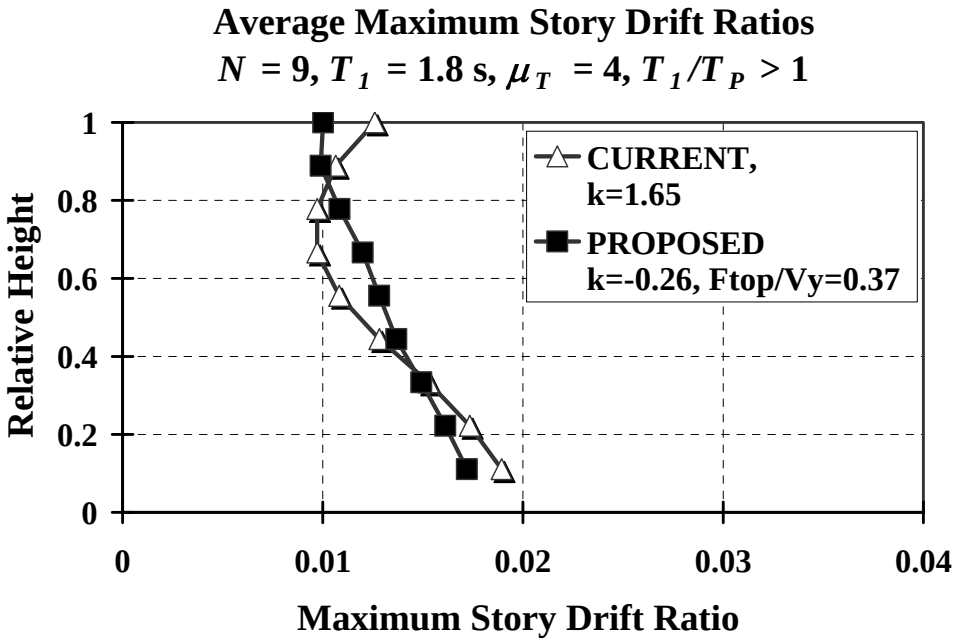

Figure 6.32 Average maximum story drift ratio profiles, 9-story frame with T_1 = 1.8 s. for μ_T = 4 for T_1/T_P < 1 (γ_C = 0.08 and γ_P = 0.10) and T_1/T_P > 1 (γ_C = 0.07 and γ_P = 0.09)

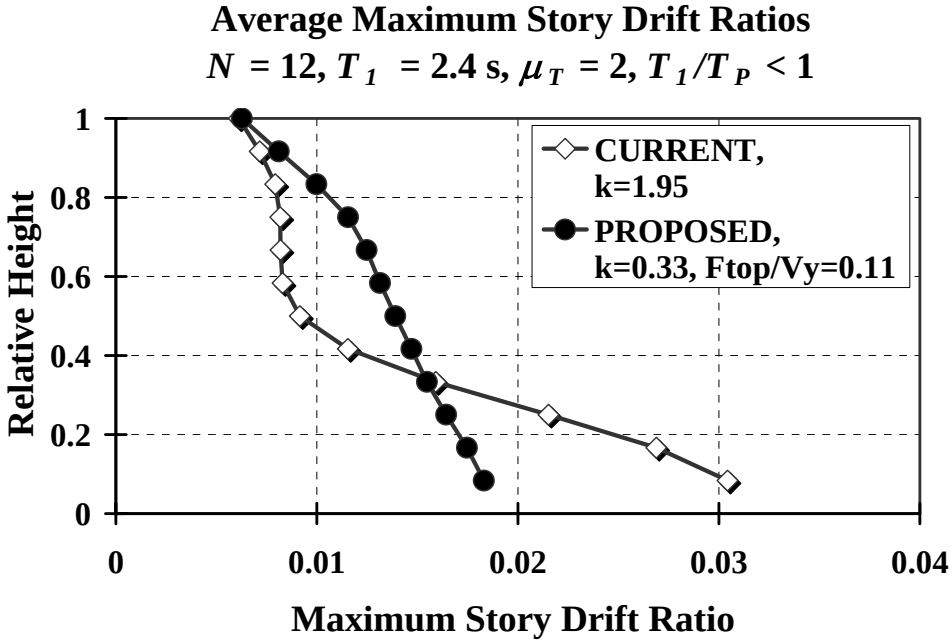

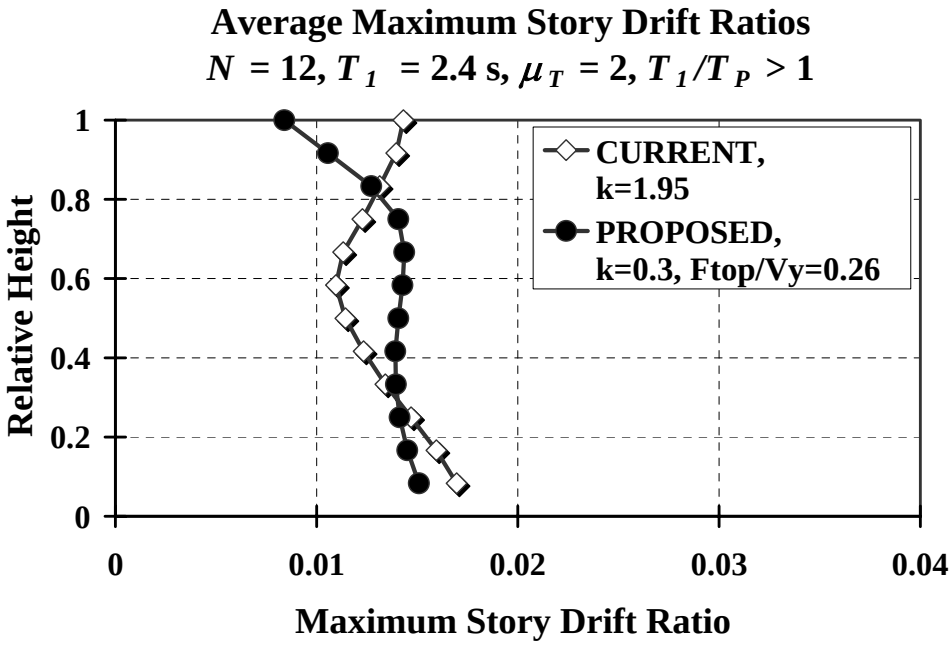

Figure 6.33 Average maximum story drift ratio profiles, 12-story frame with T_1 = 2.4 s. for μ_T = 2 for $T_1/T_P < 1$ (γ_C = 0.10 and γ_P = 0.13) and $T_1/T_P > 1$ (γ_C = 0.12 and γ_P = 0.13)

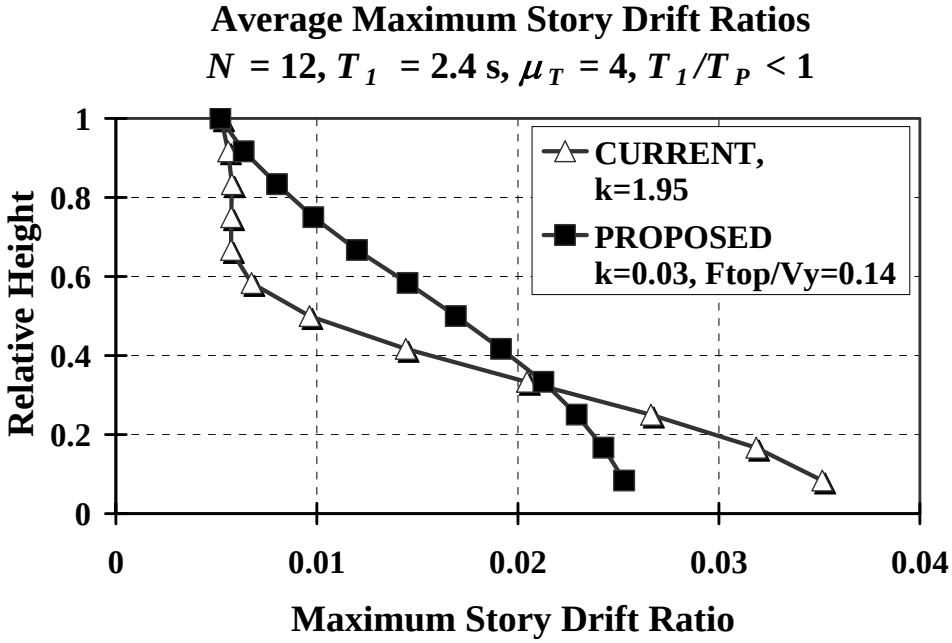

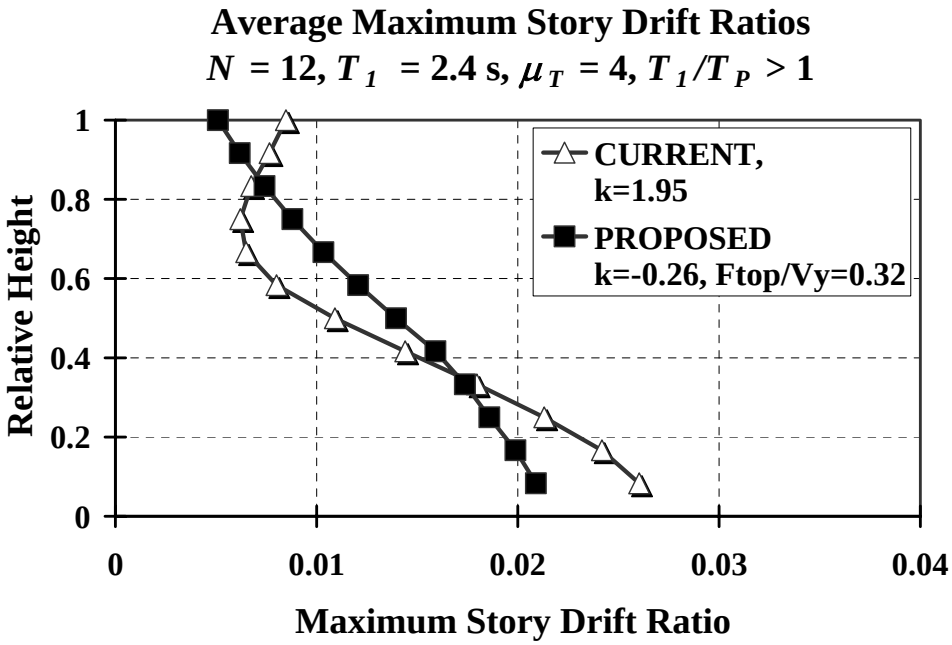

Figure 6.34 Average maximum story drift ratio profiles, 12-story frame with T_1 = 2.4 s. for μ_T = 4 for $T_1/T_P < 1$ (γ_C = 0.06 and γ_P = 0.08) and $T_1/T_P > 1$ (γ_C = 0.05 and γ_P = 0.07)

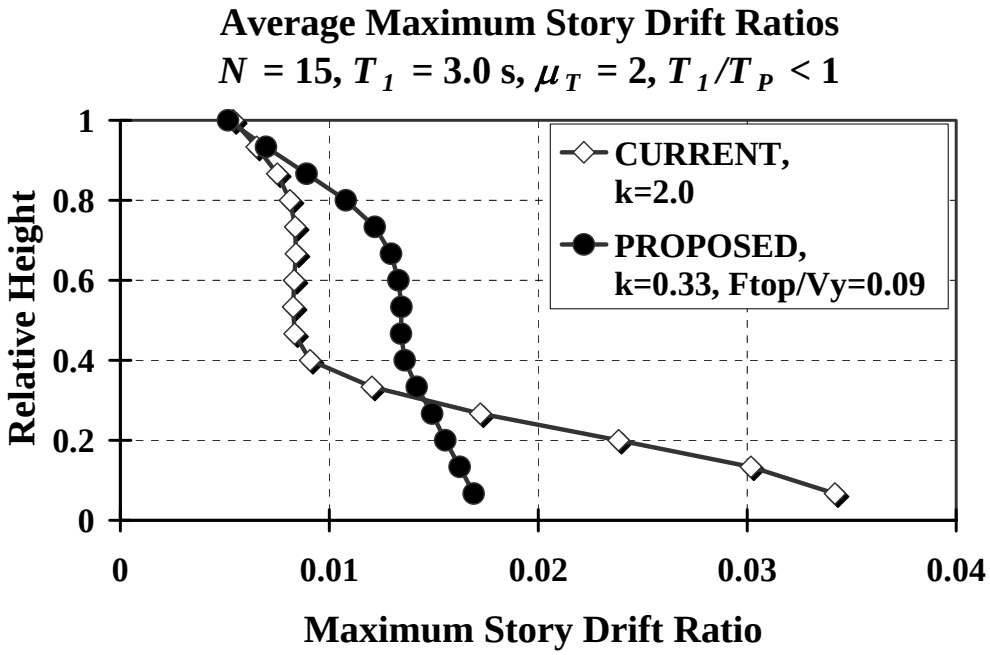

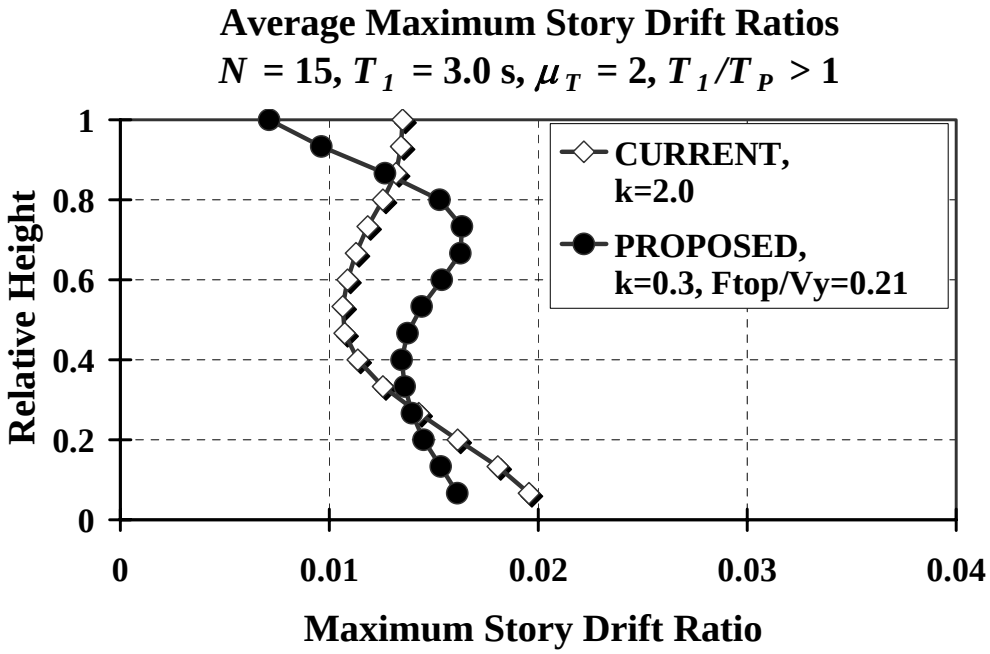

Figure 6.35 Average maximum story drift ratio profiles, 15-story frame with T_1 = 3.0 s. for μ_T = 2 for T_1/T_P < 1 (γ_C = 0.08 and γ_P = 0.11) and T_1/T_P > 1 (γ_C = 0.19 and γ_P = 0.12)

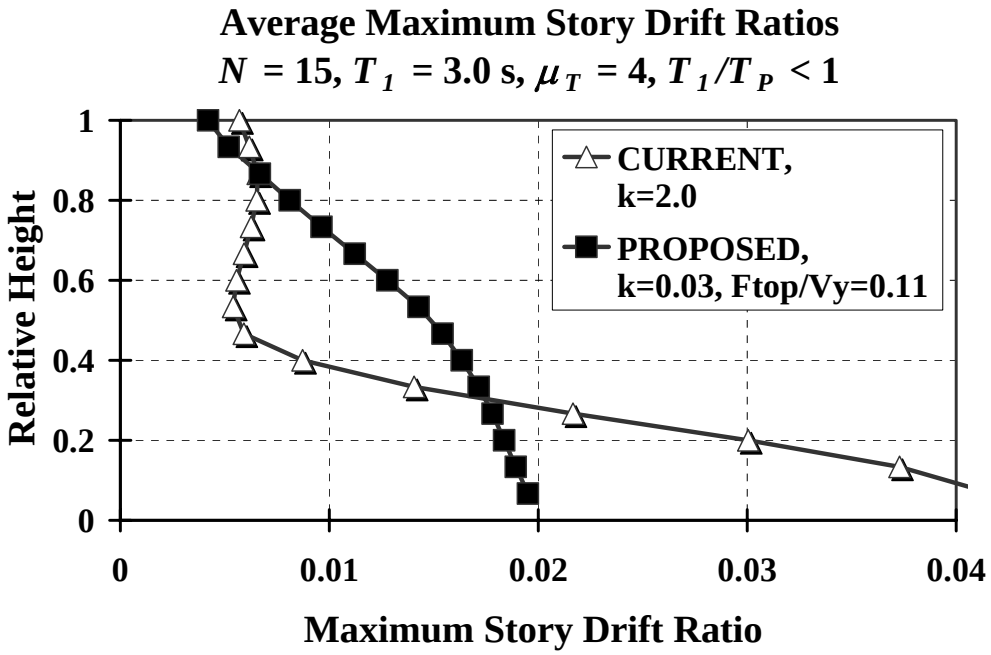

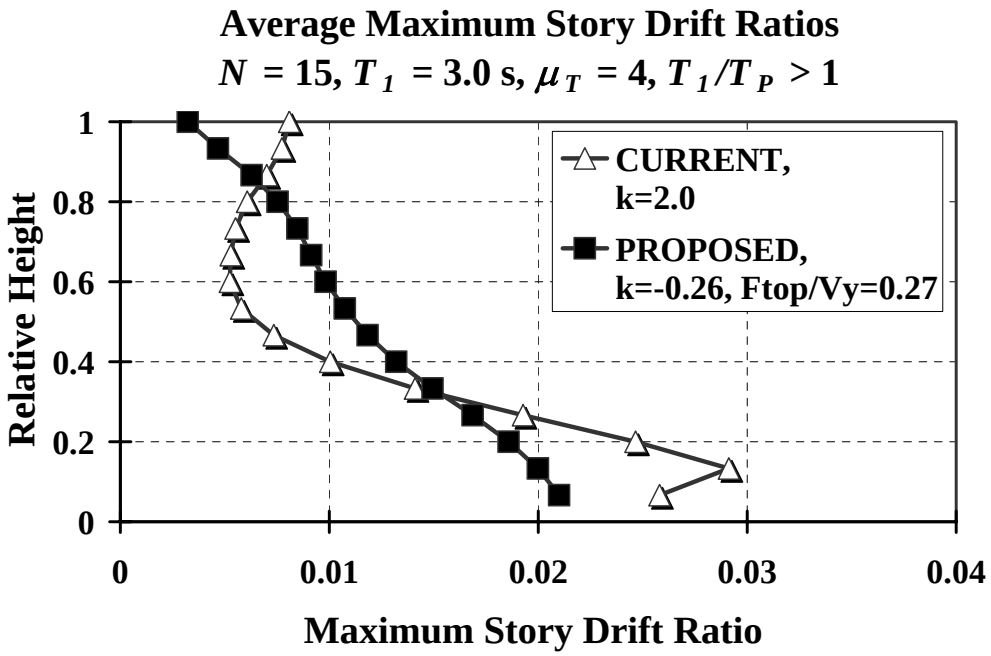

Figure 6.36 Average maximum story drift ratio profiles, 15-story frame with T_1 = 3.0 s. for μ_T = 4 for $T_1/T_P < 1$ (γ_C = 0.05 and γ_P = 0.06) and $T_1/T_P > 1$ (γ_C = 0.04 and γ_P = 0.06)

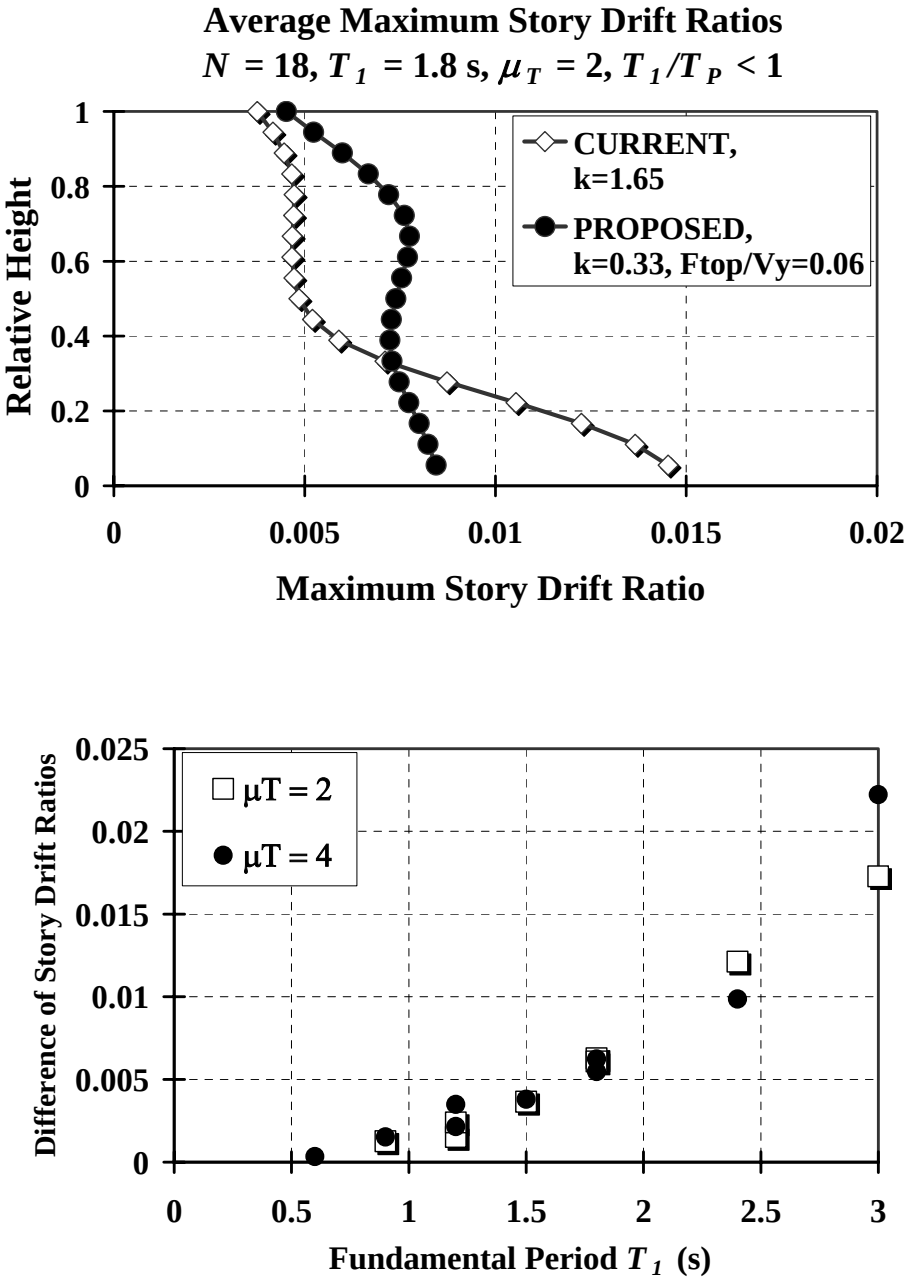

Figure 6.37 Average story drift ratio, T_1/T_p < 1, 18-story frame, T_1 = 1.8 s., μ_T = 2 (γ_C = 0.14 and γ_P = 0.17), and difference of first story drift ratios between CURRENT and PROPOSED

6.3.3 Incremental Dynamic Analysis (IDA)

Distinct from ordinary ground motions, each frame model is exposed to a different number of near-fault ground motions corresponding to the ratio T_1/T_p (see Table 3.3). A previous study by Shome and Cornell (1999) demonstrates that ten to twenty data points are usually enough to provide sufficient accuracy in the estimation of median or average seismic demands when a relatively efficient intensity measure such as $S_a(T_1)$ is used. For flexible 9-, 12-, and 15-story frame structures, the number of each set of ground motions is greater or equal to twenty. As shown in Figures 6.38, 6.39, and 6.40 for the target story ductility ratio of 2, the maximum story drift ratio values conditioned on the spectral acceleration at the first mode period are not normally distributed. These distributions are mostly lognormal and the median (the geometric mean) is typically used for "best estimate" of the post-elastic damage measure (Shome and Cornell 1998). Therefore, the median values shown in Figures 6.38 to 6.40 are adequate to represent the central tendency of IDA results.

The median IDA curves of CURRENT and PROPOSED for the 9-story frame structure approach dynamic instability in a very similar fashion, except within certain $S_a(T_1)$ range: approximately 0.3 g ~ 0.7 g and 0.4 g ~ 0.8 g for $T_1/T_p < 1$ and $T_1/T_p > 1$, respectively, as shown in Figure 6.38. In spite of small differences between CURRENT and PROPOSED, frame structures designed based on the proposed load patterns can prevent early dynamic instability when exposed to given ground motions. For other flexible 12- and 15-story frame structures and a given ground motion intensity level, Figures 6.39 and 6.40 show that the maximum of the peak story drift ratios along the height of the frame designed based on the current code provisions is constantly greater than that of the

frame designed based on the proposed lateral load patterns when exposed to the near-fault ground motions with $T_1/T_p < 1$. This observation is more obvious when the fundamental period of structures increases, from 1.8 s. to 3.0 s. This confirms that the variation of story drift ratios is strongly dependent on the fundamental period of structures.

Based on the results provided in this Section, frames designed based on the proposed approach provide 'capacites' against global collapse that are greater than or at equal to those obtained for frames designed based on the current code provisions. However, when the pulse period of near-fault ground motions is smaller than the fundamental period of the structure, both moment-resisting frame structures designed according to the current and proposed approaches reach the onset of global dynamic instability in a similar fashion. This implies that structural capacity against collapse is also strongly dependent on the ratio T_1/T_P.

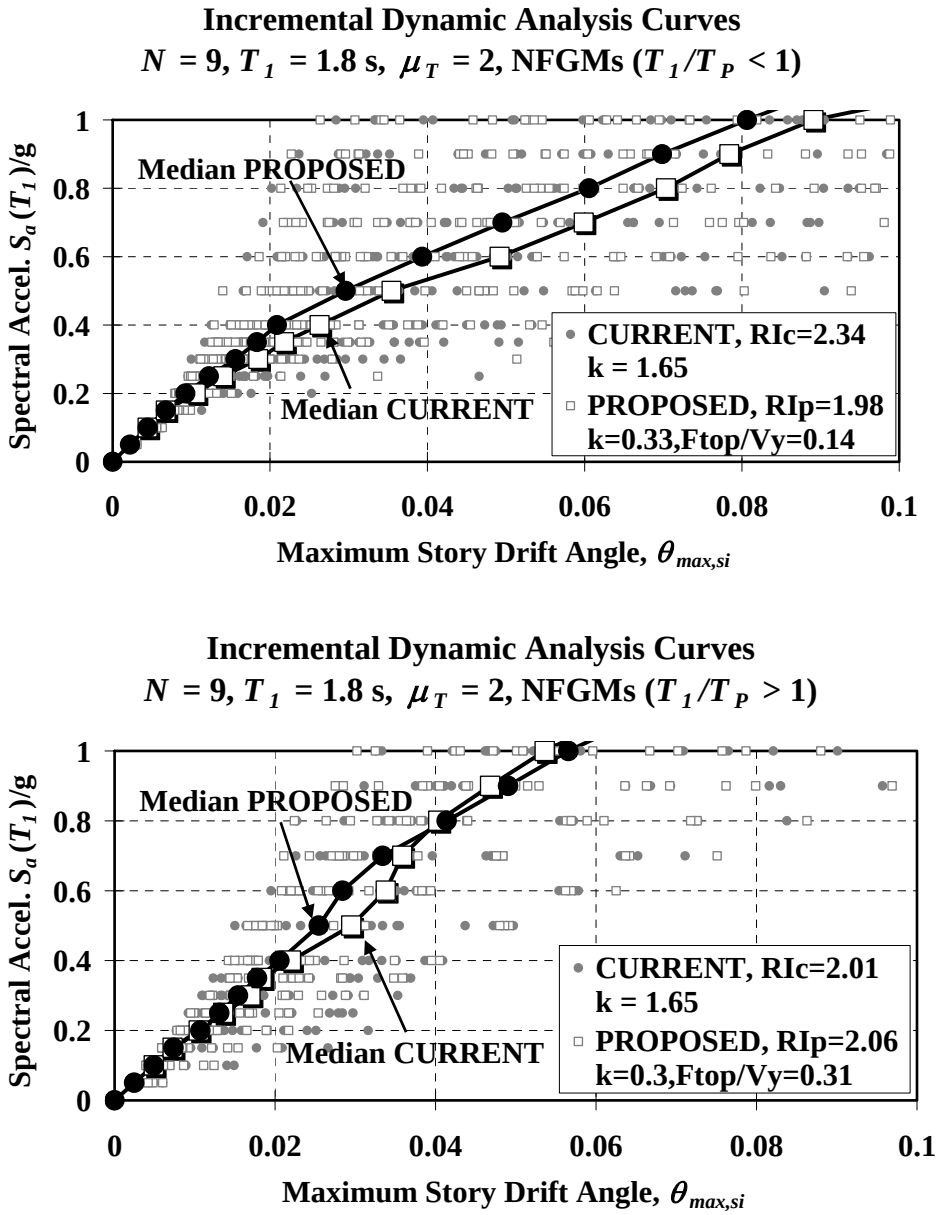

Figure 6.38 Median incremental dynamic analysis profiles for 9-story frame with T_1 = 1.8 s. for μ_T = 2 for T_1/Tp < 1 and T_1/Tp > 1

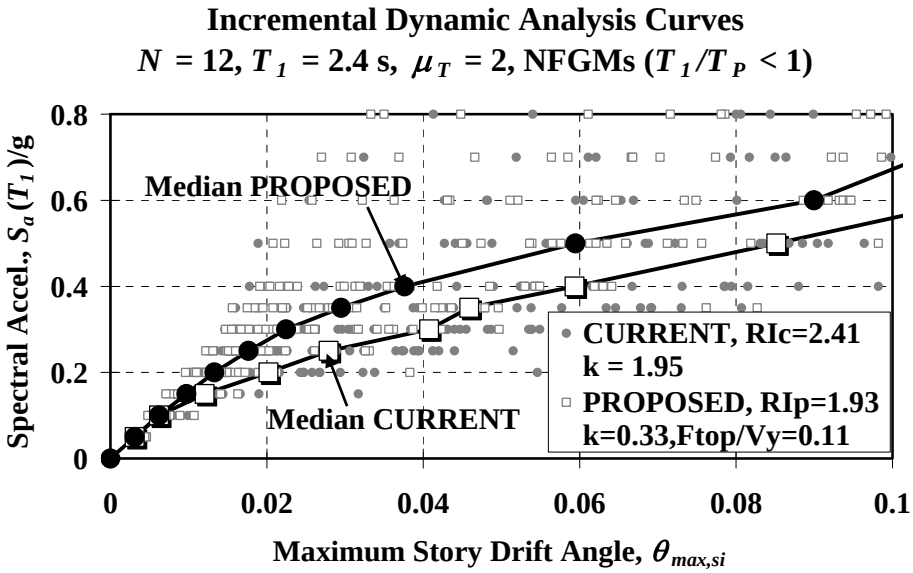

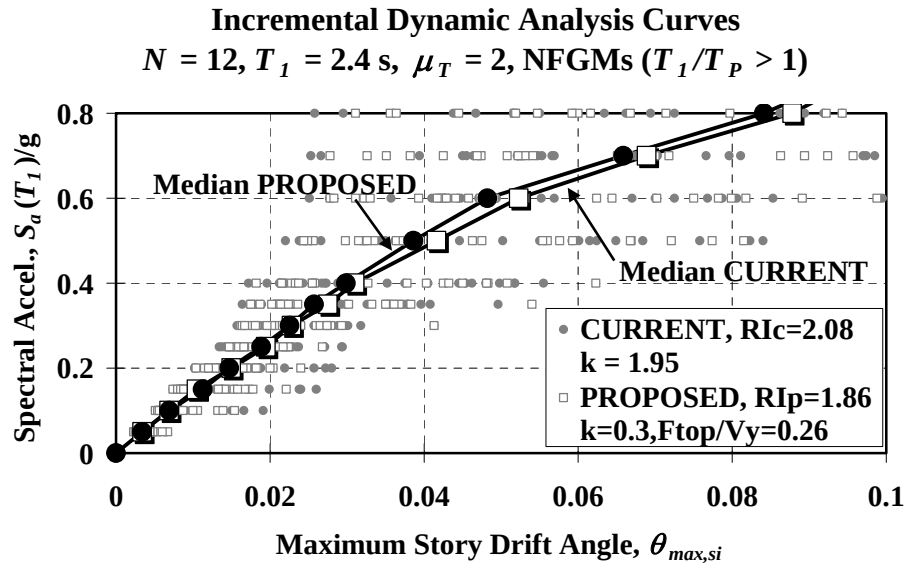

Figure 6.39 Median incremental dynamic analysis profiles for 12-story frame with T_1 = 2.4 s. for μ_T = 2 for T_1/Tp < 1 and T_1/Tp > 1

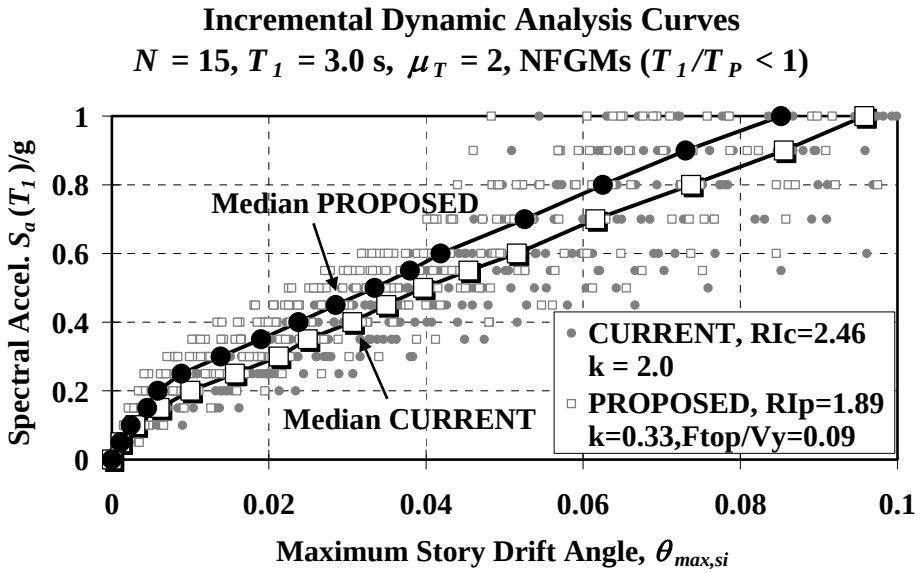

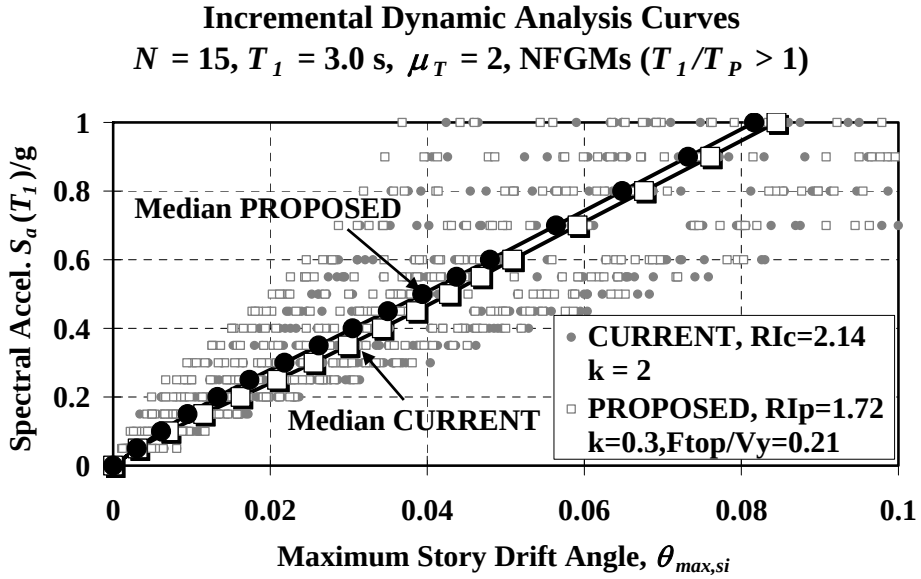

Figure 6.40 Median incremental dynamic analysis profiles for 15-story frame with T_1 = 3.0 s. for μ_T = 2 for T_1/Tp < 1 and T_1/Tp > 1

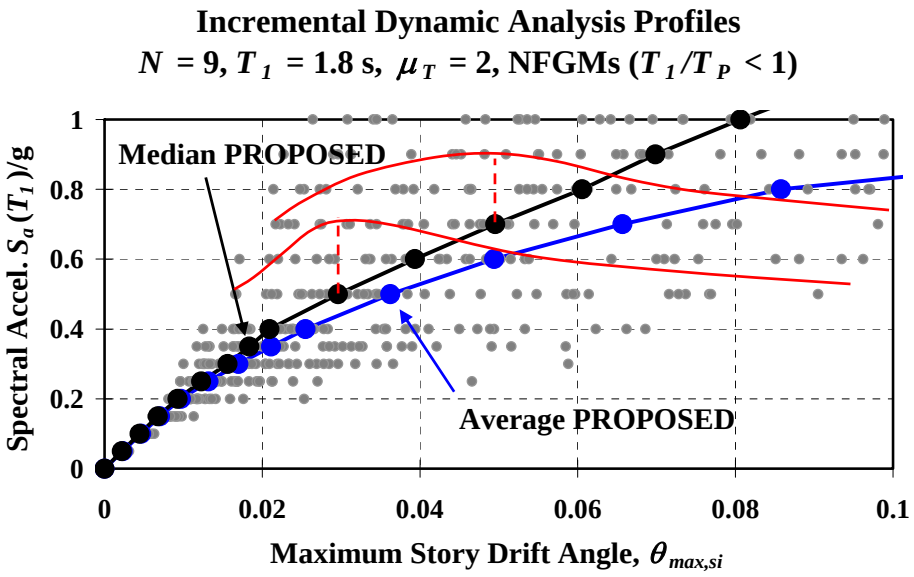

Figure 6.41 Median and average incremental dynamic analysis profiles for 9-story frame with T_1 = 1.8 s. for μ_T = 2

6.4 SUMMARY

- For the same average structural damage for ordinary ground motions, frames with member strengths tuned to proposed seismic design lateral loads provide a rather uniform (constant) distribution of story ductility and story drift ratios when compared to the distributions obtained using the current seismic code provisions in the United States. The shape of story ductility ratio distributions of frame structures designed based on the current approach significantly varies along the height as a function of the total height of the structure as well as the target story ductility ratio. In addition, relatively large story ductility ratios are found in bottom stories, but smaller story ductility ratios are found in middle stories of flexible frame structures (i.e., $T_1 = 0.2\ N$) designed based on the current approach. Nevertheless,

the small story ductility ratios at the bottom stories of frames designed based on the proposed load patterns translates into an advantage for tall buildings because of the mitigation of potential second-order, P-delta effects. The main difference between current and proposed lateral load patterns is that the current load patterns are a function of the fundamental period of the structure and the floor masses ; whereas, the story ductility ratio and the total height of the structure are additional components of the proposed load patterns.

- For regular medium-to-tall frame structures (i.e., number of stories greater than or equal to 9), the proposed conceptual seismic design methodology helps control story drift ratios at the top and bottom stories when compared to those experienced by frames designed based on current code procedures.
- The IDA curves for frame models designed based on the proposed approach more slowly the onset of dynamic instability as the ground motion intensity increases. This observation shows that less damage is experienced by flexible structural systems (e.g., 2.4 s. and 3.0 s.) that are exposed to ordinary ground motions when their member strengths are tuned to the proposed lateral load patterns.
- The proposed lateral load patterns for frames designed based on the set of near-fault ground motions with $T_1/T_p < 1$ provide an increased protection for the bottom stories by limiting the story ductility ratio to values close to the target value. In most cases, story ductility ratios at the bottom stories of frame models designed based on the proposed approach show smaller demands when compared to those from frame

models designed based on the current load patterns. For longer periods frame structures designed based on the current procedure (e.g., T_1 = 1.5 s. ~ 3.0 s.) that are exposed to near-fault ground motions for T_1/T_P > 1, relatively large values of story ductility ratios are found in the higher stories. Distributions of story ductility ratios for frame structures designed based on the current procedure mainly depend on the ratio T_1/T_P, whereas a distribution for frames designed according to the proposed approach is more uniform and close to the target story ductility ratio. In addition, for the same performance target of interest, the proposed load patterns for a frame exposed to near-fault ground motions within the range T_1/T_P > 1 are very similar to the proposed load patterns for frame structures exposed to ordinary ground motions.

- The distribution of maximum story drift ratios for the frame model designed based on the current load patterns varies widely along the height with large story drift demands in the bottom stories, which depends on the ratio T_1/T_P. However, the proposed approach provides a more uniform distribution of maximum story drift ratios regardless of the ratio T_1/T_P. For a given target story ductility ratio, amplified story drift ratios are also found in the bottom stories of the maximum story drift ratio profiles for the current procedure, particularly for the fundamental period of structure within the range from 0.9 s. to 3.0 s. In these cases, the story drift ratios are controlled by the variation of stiffness over the height of structures.
- For near-fault ground motions for T_1/T_P < 1, the use of proposed load patterns for flexible frame structures (e.g., T_1 = 2.4 s. and 3.0 s.) has

shown to mitigate the potential for dynamic instability for a given hazard level and a given target inelastic level, as compared to near-fault ground motions for $T_1/T_P > 1$.

7 SUMMARY AND CONCLUSIONS

7.1 SUMMARY

The major objective of the study was to develop improved design lateral load patterns for the conceptual seismic design of moment-resisting frame structures. Seismic design load patterns of the Equivalent Lateral Force (ELF) procedure are used for the design based on National Earthquake Hazard Reduction Program (NEHRP 2003), Uniform Building Code (UBC 1997), ASCE 7-05, and International Building Code (IBC 2006). Among them, IBC 2006 is the primary code provision of interest in this study, and it widely used for the design of buildings in the United States. The relative force distributions as described in the Equivalent Lateral Force (ELF) procedure are based on elastic dynamic behavior. This procedure is in concept more accurate when the structure is expected to remain nearly elastic for a certain level of ground motions and it is meant to produce a relatively uniform distribution of structural damage along the height. However, the seismic design philosophy for conventional structures requires buildings to undergo inelastic deformations when subjected to strong ground motions. This philosophy results in story shear strength demands different from the ones obtained from the siemsic design lateral loads, and hence, a distribution of structural damage along the height that is not constant. Thus, this study proposes new design load patterns based on inelastic behavior of structures, which can limit the extent of structural damage in the system and distribute this damage uniformly along the height. These lateral load patterns are expected to provide a uniform distribution of damage to structural members when compared to the distribution obtained from the load patterns of the ELF procedure.

Many researchers have recommended improved seismic design load patterns for multistory structures: Leelataviwat et al. 1999; Lee and Goel (2001); Medina (2004); Moghaddamm and Hajirasouliha (2006); Chao, Goel, and Lee (2007). These researchers focused on incorporating inelastic dynamic behavior into their proposed lateral loads with the objective of reducing structural damage to a reasonable amount when the buildings are exposed to strong earthquakes. The work summarized in this dissertation differs from those presented elsewhere in that the focus is not only on reducing the overall damage but also on optimizing the energy dissipation capacity of the structural components in the system. In the development of this work, numerous ground motions (i.e., 104) with different frequency contents, intensities, and durations were utilized. These ground motions were already selected by other researchers (Medina 2003 and Fu 2005) to capture reasonable intensity, frequency content, and duration of ground motions by considering various seismic hazard levels (i.e., 10/50 and 2/50). In addition, previous studies have focused on relating global strength with global structural damage based on analyses with Single-Degree-Of-Freedom (SDOF) systems. The conceptual design methodology developed in this study relies on relationships between relative intensity (*RI*), which is analogous to strength-reduction factors for SDOF systems, and story ductility ratios (μ_{si}). These relationships were developed specifically for MDOF systems. Another important contribution of this study is the incorporation of second-order, P-delta effects into the development of the proposed lateral load patterns. These second order effects have the potential to compromise the dynamic instability of tall and flexible structures. The incorporation of these effects is a characteristic lacking in previous research works in this area.

Multistory frame structures with 6-, 9-, 12-, 15-, and 18-stories with the same mass at each floor level were utilized. These frame models represented stiff ($T_1 = 0.1\ N$) and flexible ($T_1 = 0.2\ N$) behavior with fundamental periods of vibration that varied from 0.6 s. to 3.0 s. Member strengths were tuned to predefined lateral load patterns, which implies that the same amount of overstrength was assumed at each story level. Because the structural systems utilized in this study are non-deteriorating frame structures, the story ductility ratio and the maximum story drift ratio were selected as appropriate parameters to quantify structural damage. Story ductility ratio is defined as the peak relative displacement between adjacent floor levels normalized by the story height, and the maximum story drift ratio is defined as the peak relative displacement between adjacent floor levels.

In general, design lateral load patterns consist of two fundamental components: the relative distribution of design floor loads (i.e., story shear strength patterns) and their absolute values, which are a function of the base shear strength for the given ground motion level of interest. These two components were simultaneously obtained from an iterative procedure developed in this study. To derive for each structure and ground motion, the story shear strength distribution was required to achieve the same story ductility ratio in all stories. The story ductility ratios were calculated by conducting dynamic analyses (i.e., time-history analysis) with frame structures exposed to two different sets of ground motions: (1) ordinary ground motions (Medina 2003) without pulse-type characteristics; (2) near-fault ground motions (Fu 2005) with forward-directivity, pulse-type characteristics.

Statistical models were generated to provide estimates of the required story shear strength distribution to achieve uniform damage. The proposed design load patterns became a function of target story ductility ratios, total height, and mass. The base shear strength was a function of the ground motion hazard level of interest, fundamental period, and target story ductility level. Statistical models for ordinary and near-fault ground motions were obtained separately. Therefore, the design floor loads proposed in this study are also the function of frequency contents of the ground motions. The proposed load patterns were implemented into a conceptual seismic design methodology developed in this study. The applicability of this methodology to the design of regular moment-resisting frames was verified by evaluating story ductility and drift ratios of these frames with those obtained from frames whose member strengths were tuned to the lateral load patterns of the ELF procedure of building codes in the U.S.

The results from this study show that the proposed load patterns can produce fairly uniform distributions of story ductility and story drift ratios and can delay the onset of dynamic instability of regular, special moment-resisting frame structures prone to experience significant P-delta effects. This observation is primarily applicable to medium-to-tall frame structures (i.e., $N = 9 \sim 18$).

7.2 CONCLUSIONS

The main conclusions of this dissertation are as follows:

- Seismic lateral load patterns from various standards from the United States, Europe, Japan, and Mexico are reviewed in this study. The review of those standards shows a very similar shape of load distributions along the height of regular moment-resisting frames, which are mainly influenced by the fundamental period of the

structures and their mass and are based on elastic dynamic concepts. However, the required story strength distributions to achieve a constant story ductility ratio along the height are significantly different from the code-compliant story shear strength distributions. Thus, the expected level of inelastic behavior should be considered in the development of seismic lateral load patterns.

- The seismic base shear strength for moment-resisting frames exposed to ordinary and near-fault ground motions is obtained from the relative intensity (RI_P) estimated from the μ_T-T_1-RI_P relationship. For ordinary ground motions, the relative intensity strongly depends on the target story ductility ratio (μ_T = 1 ~ 5) and the fundamental period of structures (T_1 = 0.6 s. ~ 3.0 s.). For the same moment-resisting frames exposed to near-fault ground motions, the variation of the proposed μ_T-T_1-RI_P relationship also strongly depends on the ratio T_1/T_p, as well as the target story ductility ratio (μ_T). The best estimates of the proposed μ_T-T_1-RI_P relationship of MDOF systems are significantly different from those from previous studies for MDOF systems.
- Proposed load patterns for moment-resisting frames strongly depend on the target level of inelastic behavior, their mass, and the total height of structure. The load patterns corresponding to the ELF procedure are very sensitive to the frequency content of ground motions: far-field and near-fault ground motions. However, the proposed load patterns provide quite constant story ductility ratios and more uniform story drift ratios along the height for both sets of ground

motions. For near-fault ground motions the proposed load patterns are an improvement over currently used design load patterns because they are also a function of the ratio T_1/T_p, which considers the pulse-type characteristics of such ground motions.

- Frame structures with T_1 = 1.2 s. and 1.8 s. that are exposed to near-fault ground motions within the range $T_1/T_p > 1$ provide similar proposed load patterns as those corresponding to frame structures exposed to ordinary ground motions. This implies that for this family of generic frames within this fundamental period range, the structural response is not significantly affected by the pulse-type characteristics of near-fault ground motions.
- If regular moment-resisting frames are exposed to ordinary ground motions, the frames designed based on the proposed load patterns require stronger base shear strength, when compared to the frames designed based on the ELF procedure. This observation is prominent if the fundamental period of a structure is within the range (1.2 s. ~ 3.0 s). When the pulse period of the near-fault ground motion is greater than the fundamental period of structures, the use of proposed load patterns mostly requires larger base shear strength as compared to the load patterns from the ELF procedure for frames with fundamental periods within the range of periods utilized in this study.
- The shape of story ductility ratio distributions of frame structures designed based on the current approach significantly varies along the height corresponding to the total height of the structure as well as the target story ductility ratio. In addition, relatively large story ductility

ratios are found in bottom stories, but smaller story ductility ratios are found in middle stories of flexible frame structures (i.e., $T_1 = 0.2\ N$) designed based on the current approach. For the frame structures designed based on the proposed load patterns, the small story ductility ratios are found in the bottom stories. The proposed load patterns also help control story drift ratios at the top and bottom stories when compared to those experienced by frames designed based on the ELF procedure. The conceptual seismic design methodology developed in this study is particularly beneficial for tall buildings (i.e., the number of stories greater than or equal to 9) because of increased protection against potential dynamic instability problems due to P-delta effects.

- The proposed lateral load patterns for frames designed based on the set of near-fault ground motions with $T_1/T_p < 1$ also provide an increased protection for the bottom stories by limiting the story ductility ratio to values close to the target value. In most cases, story ductility ratios at the bottom stories of frame models designed based on the proposed approach show smaller demands when compared to those from frame models designed based on the ELF procedure. For longer periods (e.g., T_1 = 1.5 s. ~ 3.0 s.) of frame structures designed based on the ELF procedure, which are exposed to near-fault ground motions for $T_1/T_P > 1$, significantly large values of story ductility ratios are found in higher stories.
- Incremental Dynamic Analysis (IDA) generally provides "dynamic capacity" curves for different ground motion levels and characterizes the variation of maximum story drift ratio. The IDA curves for frame

models designed based on the proposed approach more slowly the onset of dynamic instability as the ground motion intensity increases. For near-fault ground motions for $T_1/T_P < 1$, both moment-resisting frame structures designed according to the current and proposed approaches reach the onset of global dynamic instability in a similar fashion. This implies that structural capacity against collapse is also strongly dependent on the ratio T_1/T_P.

7.3 SUGGESIONS FOR FUTURE WORK

- The proposed lateral load patterns introduced in this study are developed by tuning various strength distributions. They still prevent excessive story drift demands to some extent, but changing stiffness distributions may provide additional improvement to limit the story drift demands. Thus, future studies should focus on the development of lateral load patterns by changing stiffness and strength distributions simultaneously.
- The proposed design procedure should be verified by additional parametric studies utilizing various soil types (e.g., rock site) and larger sets of ground motions. Appendix A presents sample cases of this verification. The results show that the inelastic structural response of structures at rock sites is quite different from the structural response of structures at stiff or soft rock sites.
- One-bay frame models are not sufficient to comprehensively verify the application of the proposed methodology to the design of multibay steel and reinforced-concrete frame structures. More realistic steel and

concrete frame configurations designed based on the proposed and ELF procedures need to be investigated while taking into account global overstrength, as well as the variation of overstrength along the height of structural systems.

- This study utilized non-degrading structural models. Future studies should verify the application of the proposed load patterns with degrading models.
- Lateral load patterns for other type of lateral-load resisting sytems (e.g., eccentrically and concentrically braced frame structures, dual systems, base isolation systems, truss systems, etc) should also be developed based on the concepts proposed in this study for moment-resisting frames.

Appendices

Appendix A – Deformation Demands for Frames Designed Based on Seismic Design Lateral Load Patterns from Europe, Japan, and Mexico Subjected to Ground Motions with Different Site Classifications

INTRODUCTION

Seismic lateral load patterns as described in the standards from other parts of the world (i.e., Europe, Japan, and Mexico) are reviewed in Chapter 2 along with the lateral load patterns in the Equivalent Lateral Force (ELF) force procedure as described in NEHRP 2003, UBC 1997, and IBC 2006. Nonlinear time history analyses are conducted in order to evaluate the seismic performance of frame structures designed based on these provisions along with those designed based on the proposed lateral load patterns. A fifteen-story frame model with the fundamental period of 1.5 s. is selected as a representative model, and 174 ground motion records are utilized to generate time-history results. The large set of ground motions are the ground motions without pulse-type characteristics, corresponding to NEHRP (NEHRP 2003) Site Classes A (hard rock), B (rock), C (very dense soil and soft rock), and D (stiff soil). The base shear strength coefficient utilized in this appendix 1 is equal to 0.08 corresponding to the target story ductility equal to 4.0.

GROUND MOTIONS

The ground motions utilized in these analyses are shown in Tables A.1, A.2, and A.3 for the NEHRP site classes A and B; C; and D, respectively. For rock sites, the median spectral values are compared to the response spectral attenuation relationship for rock site developed by Abrahamson and Silva (1997). As shown in Figure A.1, the median spectral values of 37 ground motions for rock sites are fairly matched with the Abrahamson and Silva's attenuation relationship. Thus the given set of ground motions is presumed to be representative of the conditions described above..

Table A.1 Earthquake ground motions recorded in site classes A and B (37 records)

Year	Earthquake Name	Magnitude (M_w)	Station Name	Dist. [km]
1971	San Fernando	6.6	Lake Hughes, Array Station 4	19.6
1971	San Fernando	6.6	Lake Hughes, Array Station 9	23.5
1984	Morgan Hill	6.2	Gilroy Array #1	16.2
1986	Coyote Lake	5.7	Gilroy Array #1	9.3
1986	N. Palm Springs	6.0	Silent Valley - Poppet Flat	25.8
1986	N. Palm Springs	6.0	Winchester, Bergman Ranch	57.6
1986	N. Palm Springs	6.0	Murrieta Hot Springs, Collings Ranch	63.3
1986	N. Palm Springs	6.0	Anza Fire Station	46.7
1987	Whittier Narrows	6.0	San Gabriel-E Grand Av	9.0
1989	Loma Prieta	6.9	Gilroy Array #1	11.2
1989	Loma Prieta	6.9	SAGO South - surface	34.7
1989	Loma Prieta	6.9	Monterey, City Hall	44.8
1989	Loma Prieta	6.9	South San Francisco, Sierra Point	68.2
1989	Loma Prieta	6.9	San Francisco, Dimond Heights	77.0
1989	Loma Prieta	6.9	Piedmont, Piedmont Jr. High Grounds	78.3
1989	Loma Prieta	6.9	San Francisco, Rincon Hill	79.7
1989	Loma Prieta	6.9	San Francisco, Pacific Heights	81.6
1989	Loma Prieta	6.9	San Francisco, Cliff House	84.4
1989	Loma Prieta	6.9	San Francisco, Telegraph Hill	82.0
1989	Loma Prieta	6.9	Point Bonita	88.6
1992	Landers	7.3	Twentynine Palms Park Maintennance Bldg	42.2
1992	Landers	7.3	Silent Valley, Poppet Flat	51.7
1992	Landers	7.3	Amboy	69.2
1994	Northridge	6.7	Vasquez Rocks Park	24.2
1994	Northridge	6.7	Lake Hughes, Array Station 9	26.8
1994	Northridge	6.7	Los Angeles, Temple & Hope	32.3
1994	Northridge	6.7	Lake Hughes Array#4-Camp Mend	32.3
1994	Northridge	6.7	Mt Wilson, CIT Seismic Station	36.1
1994	Northridge	6.7	Los Angeles, City Terrace	37.0
1994	Northridge	6.7	Antelope Buttes	47.3
1994	Northridge	6.7	Leona Valley #3	37.8
1994	Northridge	6.7	L.A.- Wonderland Ave.	22.7
1994	Northridge	6.7	Mt. Baldy-Elementary School	71.5
1994	Northridge	6.7	San Gabriel-E. Grand Ave.	41.7
1994	Northridge	6.7	Sandberg-Bald Mtn.	43.4
1994	Northridge	6.7	Rancho Cucamonga-Deer Can	80.0
1994	Northridge	6.7	Littlerock-Brainard Can	46.9

Table A.2 Earthquake ground motions recorded in site class C (52 records)

Year	Earthquake Name	Magnitude (M_w)	Station Name	Dist. [km]
1952	Kern County	7.4	Santa Barbara, Courthouse	87.0
1952	Kern County	7.4	Pasadena, CIT Athenaeum	127.0
1952	Kern County	7.4	Taft Lincoln School	41.0
1971	San Fernando	6.6	Lake Hughes #12	20.3
1971	San Fernando	6.6	Castaic Old Ridge Route	24.9
1971	San Fernando	6.6	Pearblossom Pump Plant	38.9
1979	Livermore	5.8	APEEL 3E Hayward CSUH	31.0
1979	Imperial Valley	6.5	Parachute Test Site	14.2
1981	Westmoreland	5.8	Parachute Test Site	**24.1**
1984	Morgan Hill	6.2	Gilroy #6, San Ysidro Microwave Site	11.8
1984	Morgan Hill	6.2	Gilroy Gavillan college Phys Scl Bldg	16.2
1986	N. Palm Springs	6.0	Hesperia	75.9
1986	N. Palm Springs	6.0	Puerta La Cruz	71.9
1986	N. Palm Springs	6.0	Anza-Tule Canyon	55.4
1987	Whittier Narrows	6.0	Pasadena-CIT Athenaeum	15.4
1987	Whittier Narrows	6.0	Arleta, Nordhoff Av. Fire Station	38.9
1987	Whittier Narrows	6.0	L.A.-116 th. St School	22.5
1987	Whittier Narrows	6.0	LA - N Figueroa St	11.4
1987	Whittier Narrows	6.0	LA-N Westmoreland	16.6
1987	Whittier Narrows	6.0	Panorama City-Roscoe	33.0
1987	Whittier Narrows	6.0	Sylmar-Sayre St.	38.6
1989	Loma Prieta	6.9	Gilroy, Gavillan college Phys Sch Bldg	11.6
1989	Loma Prieta	6.9	Saratoga - Aloha Ave.	13.0
1989	Loma Prieta	6.9	UCSC Lick Observatory	17.9
1989	Loma Prieta	6.9	Gilroy 6, San Ysidro Microwave site	19.9
1989	Loma Prieta	6.9	Coyote Lake Dam, downstream	21.7
1989	Loma Prieta	6.9	Woodside, Fire Station	22.3
1989	Loma Prieta	6.9	Fremont, Mission San Jose	43.0
1989	Loma Prieta	6.9	Hayward, CSUH Stadium	57.1
1989	Loma Prieta	6.9	Berkeley, Lawrence Berkeley Lab.	83.6
1989	Loma Prieta	6.9	SAGO South-Surface	34.7
1989	Loma Prieta	6.9	APEEL 9-Cristal Springs Res	46.9
1989	Loma Prieta	6.9	Golden Gate Bridge	85.1
1989	Loma Prieta	6.9	Hayward - BART Station	58.9
1989	Loma Prieta	6.9	Belmont - Envirotech	49.9
1989	Loma Prieta	6.9	APEEl 10-Skyline	47.8
1992	Landers	7.3	Desert Hot Springs	23.2
1992	Landers	7.3	Puerta La Cruz	95.9
1994	Northridge	6.7	LA - Baldwin Hills	31.3
1994	Northridge	6.7	LA - Cypress Ave.	32.8
1994	Northridge	6.7	Beverly Hills - 14145 Mulhol	19.6
1994	Northridge	6.7	LA - Century City CC North	25.7
1994	Northridge	6.7	LA - Chalon Rd	23.7
1994	Northridge	6.7	LA - N. Faring Rd.	23.9
1994	Northridge	6.7	Malibu - Oint Dume Sch	35.2
1994	Northridge	6.7	Castaic Old Ridge Route	22.6
1994	Northridge	6.7	Alhambra, 900 S. Fremont	35.7
1994	Northridge	6.7	Lake Hughes #1, Fire station #78	36.3
1994	Northridge	6.7	Inglewood, Union Oil Yard	44.7
1994	Northridge	6.7	L.A.-116 th. St School	41.9
1994	Northridge	6.7	Beverly Hill-12520 Mulhol	20.8
1994	Northridge	6.7	Rolling Hills Est-Rancho Vista	46.6

Table A.3 Earthquake ground motions recorded in site class D (85 records)

Year	Earthquake Name	Magnitude (M_w)	Station Name	Dist. [km]
1942	Borrego Mtn	6.5	El Centro Array #9	49
1968	Borrego Mtn	6.5	El Centro Array #9	46.0
1971	San Fernando	6.6	Los Angeles, Hollywood Storage Bldg.	21.2
1971	San Fernando	6.6	Gormon-Oso Pump Plant	48.1
1973	Point Mugu	5.8	Port Hueneme	25
1979	Imperial Valley	6.5	Calexico, Fire Station	10.6
1979	Imperial Valley	6.5	El Centro Array #11 (McCabe Union School)	12.6
1979	Imperial Valley	6.5	El Centro Array #3 (Pine Union School)	9.3
1979	Imperial Valley	6.5	El Centro Array #12 (907 Brockman Road)	18.2
1979	Imperial Valley	6.5	El Centro Array#13 (Strobel Residence)	21.9
1979	Imperial Valley	6.5	El Centro Array #1(Borchard Ranch)	15.5
1979	Imperial Valley	6.5	Coachella, Canal #4	49.3
1979	Imperial Valley	6.5	Chihuahua	28.7
1979	Imperial Valley	6.5	Westmoreland Fire Station	15.1
1979	Imperial Valley	6.5	Compuertas	32.6
1979	Imperial Valley	6.5	Niland Fire Station	35.9
1979	Imperial Valley	6.5	Plaster City	31.7
1979	Imperial Valley	6.5	Victoria	54.1
1980	Livermore	5.8	San Ramon-Eastman Kodak	17.6
1980	Livermore	5.8	San Ramon Fire Station	21.7
1984	Morgan Hill	6.2	Hollister City Hall	32.5
1984	Morgan Hill	6.2	Gilroy #2, Hwy 101/Bolsa Road Motel	15.1
1984	Morgan Hill	6.2	Gilroy #7, Mantnilli Ranch,Jamison Rd	14.0
1984	Morgan Hill	6.2	Gilroy #3 Sewage Treatment Plant	14.4
1984	Morgan Hill	6.2	Gilroy Array #4	12.8
1984	Morgan Hill	6.2	San Juan Bautista	30.3
1984	Morgan Hill	6.2	Capitola	38.1
1986	N. Palm Springs	6.0	San Jacinto Valley Cementery	39.6
1986	N. Palm Springs	6.0	Indio	39.6
1987	Whittier Narrows	6.0	Studio City - Coldwater Can	28.7
1987	Whittier Narrows	6.0	Fountain Valley - Euclid	35
1987	Whittier Narrows	6.0	Downey, County Maintennance Bldg	18.3
1987	Whittier Narrows	6.0	Los Angeles, Hollywood Storage Bldg.	25.2
1987	Whittier Narrows	6.0	Century City, LA Country Club South	31.3
1987	Whittier Narrows	6.0	Compton-Castlegate St.	16.9
1987	Whittier Narrows	6.0	LA-W 70th St.	16.3
1987	Whittier Narrows	6.0	Carson-Water St.	24.5
1987	Whittier Narrows	6.0	Downey-Birchdale	56.8
1987	Whittier Narrows	6.0	Terminal Island - S Seaside	35.7
1987	Whittier Narrows	6.0	Northridge-Saticoy St.	39.8
1987	Superstition Hills	6.7	Brawley	18.2
1987	Superstition Hills	6.7	El Centro Imp. Co. Cent.	13.9
1987	Superstition Hills	6.7	Plaster City, Storehouse	21.0
1987	Superstition Hills	6.7	Westmoreland Fire Station	13.3
1989	Loma Prieta	6.9	Gilroy 7, Mantelli Ranch Jamison Rd.	24.2
1989	Loma Prieta	6.9	Gilroy 2, Hwy 101 Bolsa Road Motel	12.7
1989	Loma Prieta	6.9	Gilroy 3, Sewage Treatment Plant	14.4
1989	Loma Prieta	6.9	Agnews, Agnews State Hospital	28.2
1989	Loma Prieta	6.9	Agnews, Agnews State Hospital	28.2
1989	Loma Prieta	6.9	APEEL 2E Hayward John Muir School	57.4
1989	Loma Prieta	6.9	Oakland-Title & Trust	77.4
1989	Loma Prieta	6.9	Richmond, City Hall Parking lot	93.1
1989	Loma Prieta	6.9	Capitola	14.5
1989	Loma Prieta	6.9	Gilrroy Array #4	16.1
1989	Loma Prieta	6.9	Hollister City Hall	28.2
1989	Loma Prieta	6.9	Sunnyvale-Colton Ave.	28.8
1989	Loma Prieta	6.9	Fremont-Emerson Court	43.4
1989	Loma Prieta	6.9	Halls Valley	31.6
1989	Loma Prieta	6.9	Salinas-John & Work	32.6
1989	Loma Prieta	6.9	Palo Alto-SLAC Lab.	36.3
1992	Landers	7.3	Yermo, Fire Station	24.9
1992	Landers	7.3	Palm Springs, Airport	37.5
1992	Landers	7.3	Fort Irwin	64.2
1992	Landers	7.3	Baker, Fire Station	88.5
1992	Landers	7.3	Hemet, Stetson Av. Fire Station	69.5
1994	Northridge	6.7	Los Angeles, Hollywood Storage Bldg.	25.5
1994	Northridge	6.7	Canoga Park-Topanga Can	15.8
1994	Northridge	6.7	LA-N Faring Rd	23.9
1994	Northridge	6.7	LA-Fletcher Dr	29.5
1994	Northridge	6.7	Glendale-Las Palmas	25.4
1994	Northridge	6.7	La Crescenta-New York	22.3
1994	Northridge	6.7	LA-Centinela St	30.9
1994	Northridge	6.7	Downey-Birchdale	40.7
1994	Northridge	6.7	Bell Gardens-Jaboneria	46.6
1994	Northridge	6.7	Lake Hughes#1	36.3
1994	Northridge	6.7	Lawndale-Osage Ave	42.4
1994	Northridge	6.7	Leona Valley#2	37.7
1994	Northridge	6.7	Palmdale-Hwy 14 & Palmdale	43.6
1994	Northridge	6.7	LA-Pico & Sentous	32.7
1994	Northridge	6.7	Terminal Island-S Seaside	60.0
1994	Northridge	6.7	LA-Vernon Ave	39.3
1994	Northridge	6.7	West Covina-S Orange Ave	54.1
1994	Northridge	6.7	Lakewood-Del Amo Blvd	59.3
1994	Northridge	6.7	Compton-Castlegate St	49.6
1994	Northridge	6.7	LA - S Grand Ave	36.9
1994	Northridge	6.7	Leona Valley#6	38.5

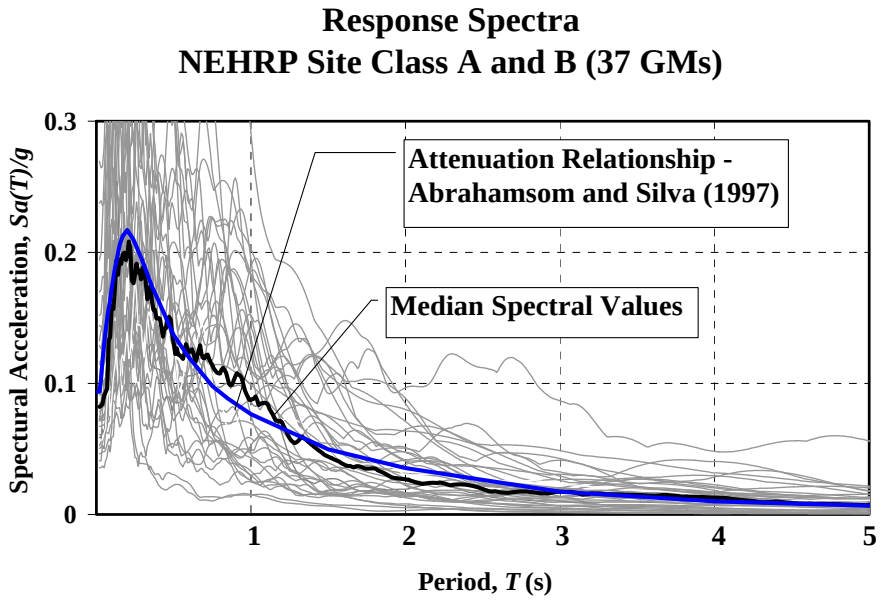

Figure A.1 Acceleration response spectra in rock sites (NEHRP site classes A and B)

TIME HISTORY RESULTS

Six different seismic design load patterns from various standards are considered in this application example case along with the proposed load pattern: EuroCode 8 (EC8); Japanese Seismic Design Code (BCJ); Mexico City Building Code 2003; IBC 2006; UBC 97; and PROPOSED. Figure A.2 and A.3 present the lateral load patterns and story shear strength distributions corresponding to these code provisions. The story shear strength distributions for the proposed load patterns are significantly different from those of other load patterns. These distinctive design inputs also provide quite different dynamic analysis results as shown in Figures A.4 ~ A.11. The inelastic dynamic response of the structues at rock sites provide more significant damage in the bottom stories when compared to the structures located at very dense and stiff soil sites. This implies that, for rock-type site classifications, new load patterns to achieve a uniform distribution of damage

along the height need to be developed. This is of particular importance to prevent a realtively large concentration of damage at the bottom stories. On the other hand, the proposed load patterns for the NEHRP site class D can be utilized for the design of moment-resisting frame structures located in the NEHRP site class C.

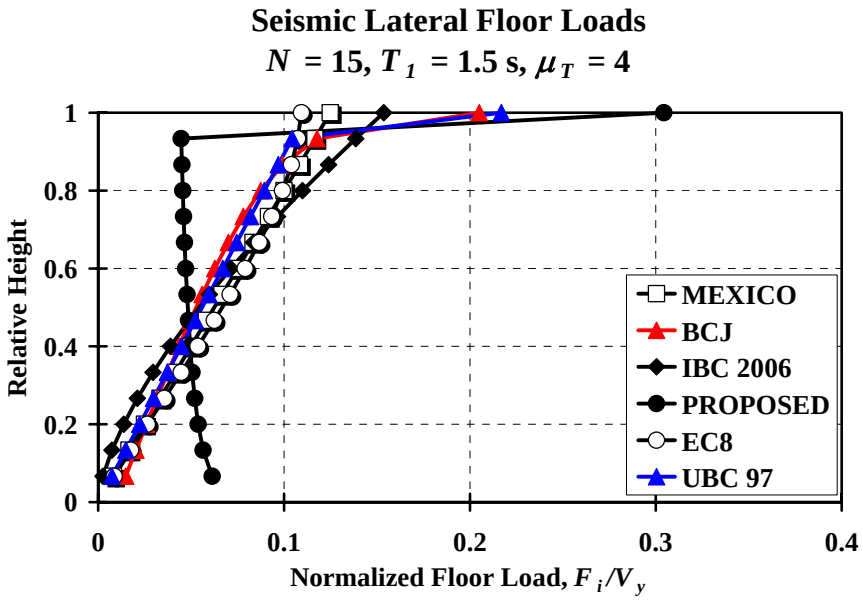

Figure A.2 Seismic lateral floor loads, 15-story frame with T_1 = 1.5 s. for μ_T = 4

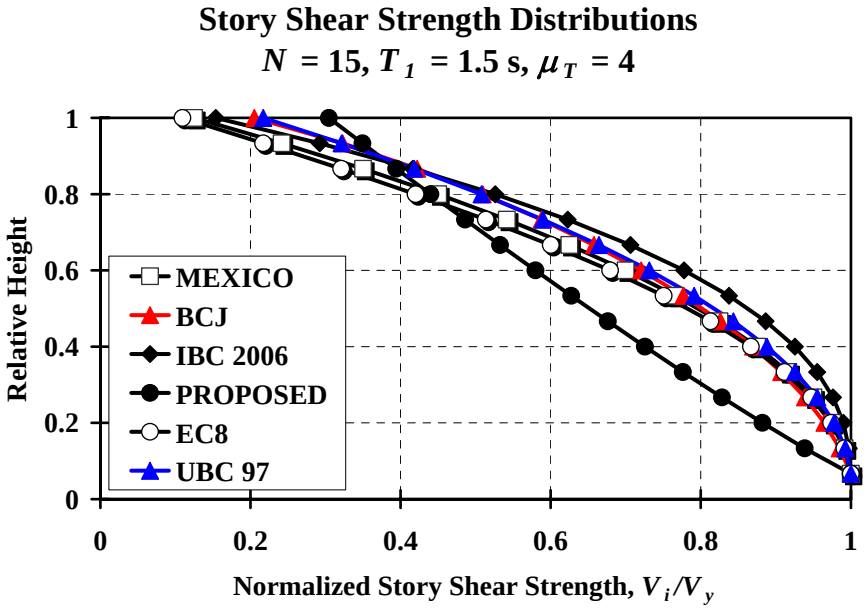

Figure A.3 Story shear strength distributions, 15-story frame with T_1 = 1.5 s. for μ_T = 4

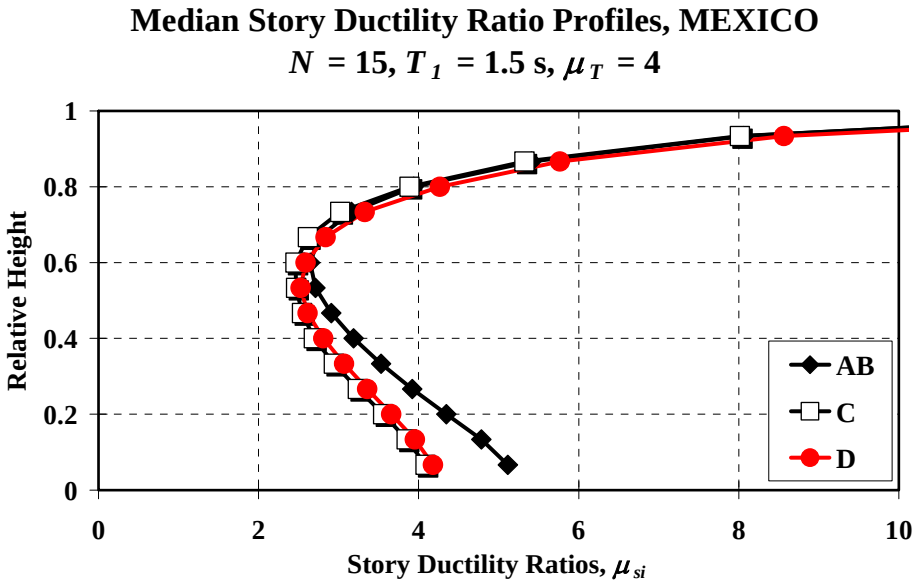

Figure A.4 Median story ductility ratio profiles, 9-story frame model designed based on Mexico City Building Code 2003

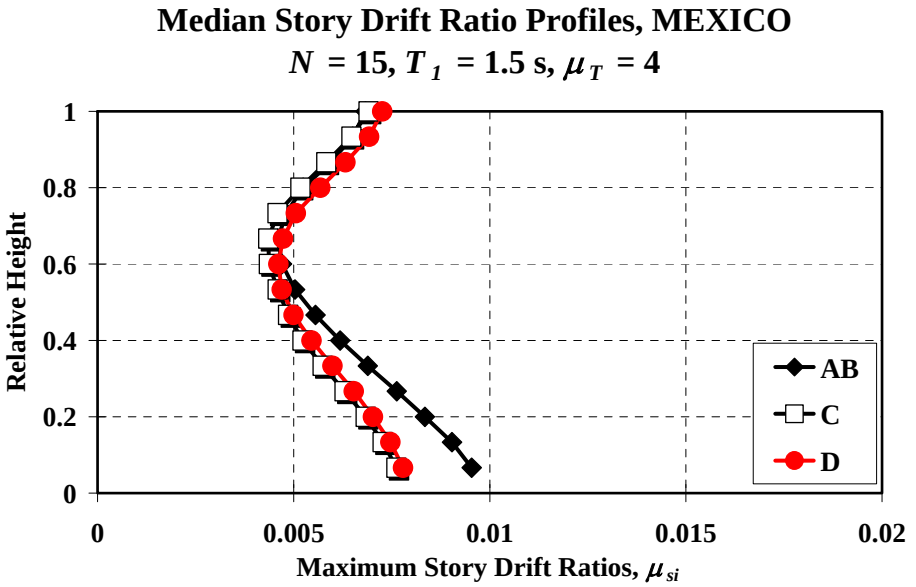

Figure A.5 Median story drift ratio profiles, 9-story frame model designed based on Mexico City Building Code 2003

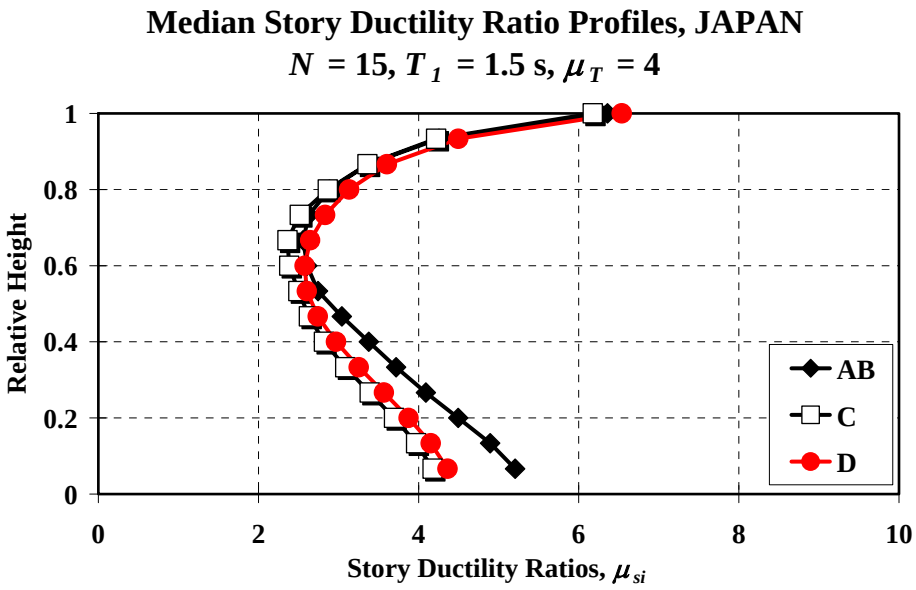

Figure A.6 Median story ductility ratio profiles, 9-story frame model designed based on Japanese Seismic Design Code

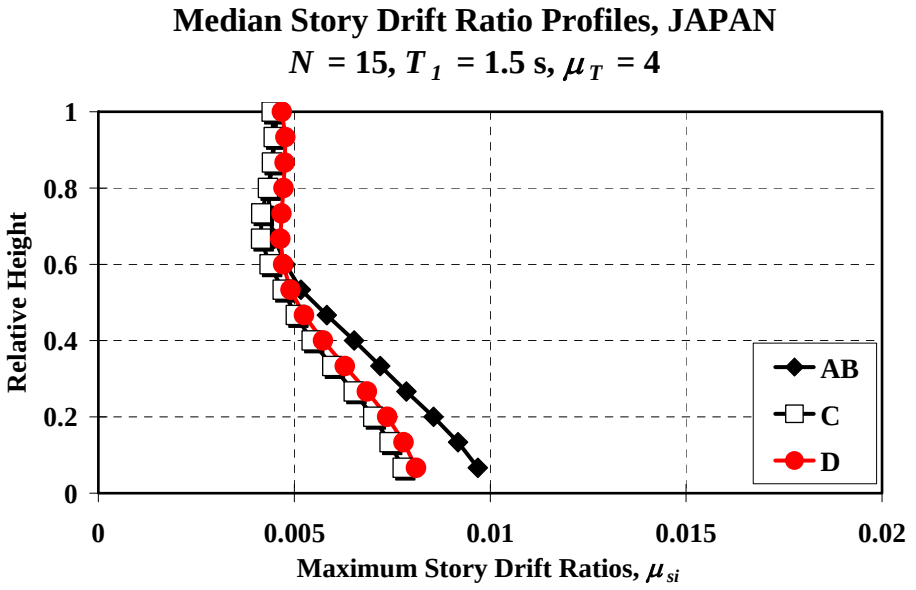

Figure A.7 Median story drift ratio profiles, 9-story frame model designed based on Japanese Seismic Design Code

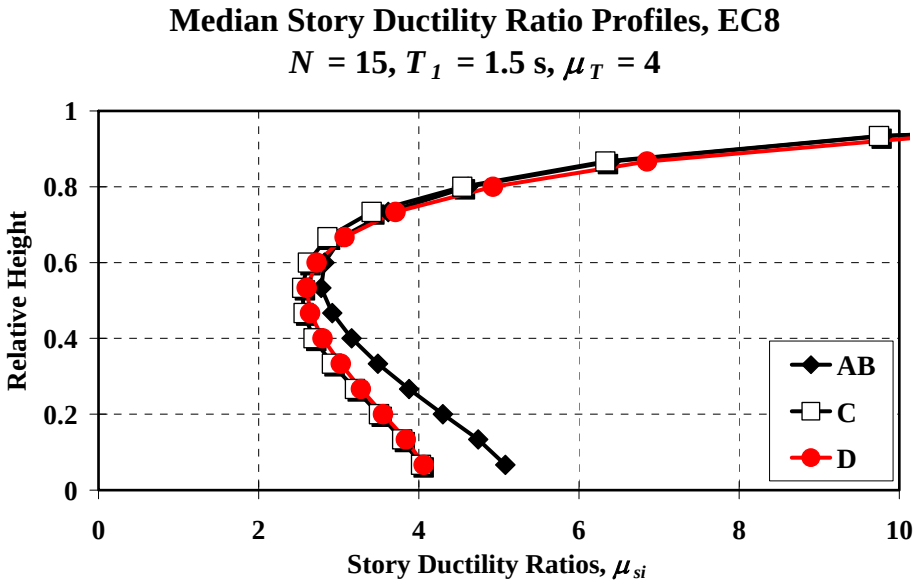

Figure A.8 Median story ductility ratio profiles, 9-story frame model designed based on EuroCode 8

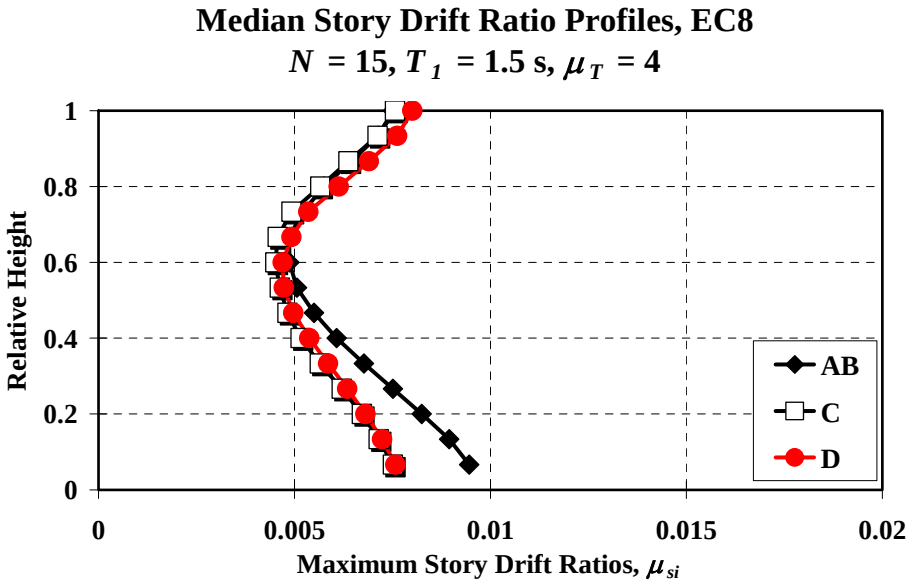

Figure A.9 Median story drift ratio profiles, 9-story frame model designed based on EuroCode 8

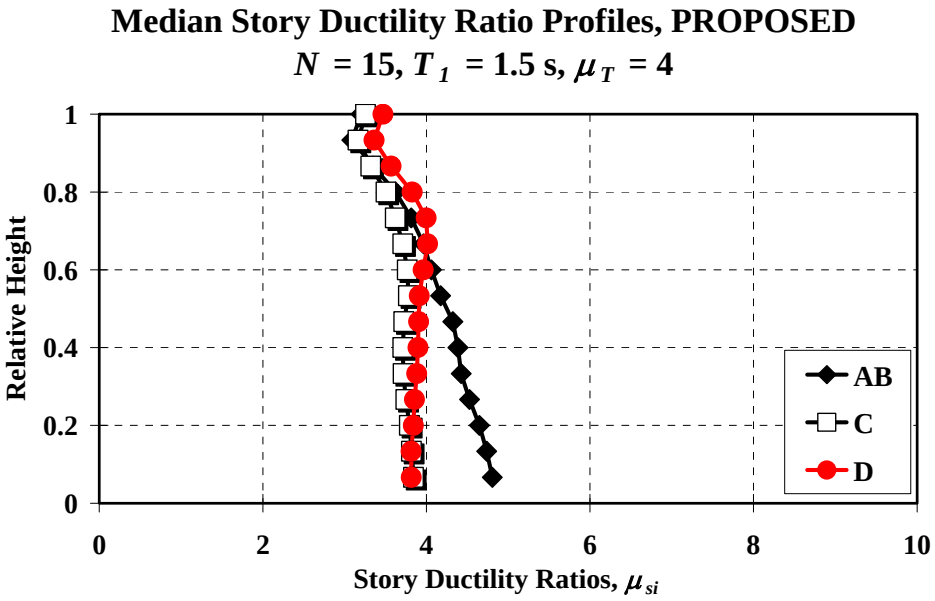

Figure A.10 Median story ductility ratio profiles, 9-story frame model designed based on the proposed load pattern

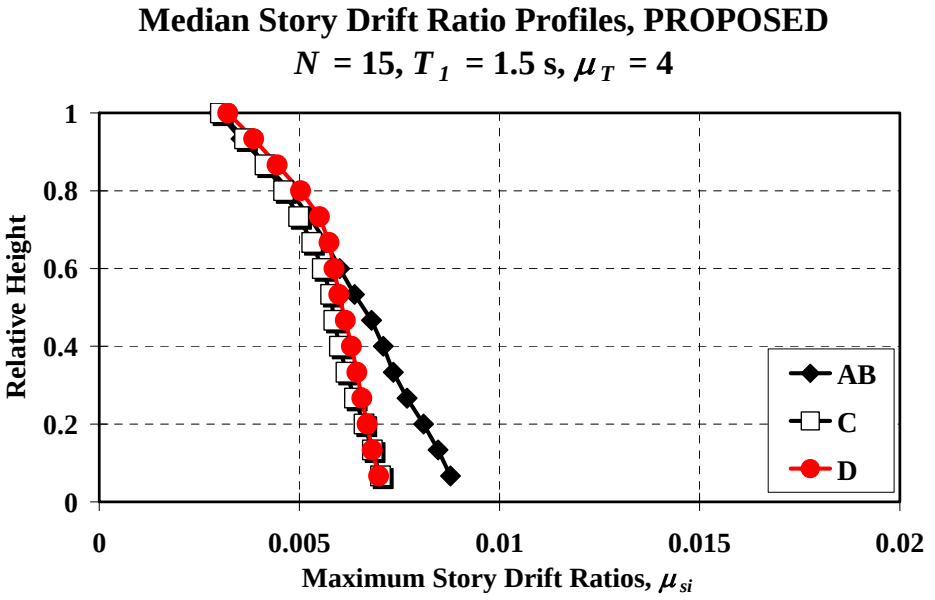

Figure A.11 Median story drift ratio profiles, 9-story frame model designed based on the proposed load pattern

Bibiliography

1. Alavi, B. and Krawinkler, H., (2001). "Effects of near fault ground motions on frame structures." *Report No. 138*, John A. Blume Earthquake Engineering Center, Stanford University, Stanford, CA.
2. BCJ. (1997). Structural provisions for building structures. 1997 edition – Tokyo; Building Center of Japan.
3. BSL. (2000). Building standard law. Japan.
4. BSSC. (2003). *NEHRP recommended provisions for the development of seismic regulations for new buildings,* Buidling Seismic Safety Council, Washington, D.C.
5. CEN. (2003). EuroCode 8: Final draft of EuroCode 8: Design of structure for earthquake resistance – Part 1: General rules for buildings. *Bruxelles: European Committee for Standardization*.
6. Chao, S.H., Goel, S.C., and Lee, S.S. (2007). "A seismic design lateral force distribution based on inelastic sate of structures." *Earthquake Spectra*, Vol. 23, No. 3, 547-569, August.
7. Chopra, A.K. and Goel, R.K. (2002). "A modal pushover analysis procedure for estimating seismic demands for buildings." *Earthquake Engineering and Structural Dynamics*, 31:561-582.
8. Elghadamsi, F.E. and Mohraz, B. (1987). "Inelastic earthquake spectra," *Earthquake Engineering and Structural Dynamics*, Vol. 15, pp. 91-104.
9. Englekirk, R. (1994). "Steel structures controlling behavior through design." *John Wiley & Sons, Inc*, pp. 441-448.
10. Fu, Q. and Menun, C. (2004). "Seismic-environment-based simulation of near-fault ground motions", *Proceedings of 13th World Conference on Earthquake Engineering*, *Vancouver, Canada*, pp. 15
11. Fu, Q. (2005). Modeling and prediction of fault-normal near-field ground motions and structural response. *Department of Civil and Environmental Engineerin*g. Stanford, CA, Stanford University. Doctoral Dissertation.
12. Garcia, J. R. and Miranda, E. (2004). "Performance-based assessment of existing structures accounting for residual displacements." *Ph.D. dissertation*, John A. Blume Earthquake Engineering Center, Stanford University, CA.
13. Goel, R.K. and Chopra, A.K. (2002). "Extension of modal pushover analysis to compute member forces." *Earthquake Spectra*, Vol. 21, No. 1, pages 125-139, February.

14. Gupta, A., and Krawinkler, H. (2000). “Dynamic P-Delta Effects for Flexible Inelastic Steel Structures,” *Journal of Structural Engineering, ASCE*, Vol. 126, No. 1, Jan.
15. Hidalgo, P.A. and Arias, A. (1990). “New Chilean Code for earthquake-resistant design of buildings.” *Proc. 4th U.S. National Conference Earthquake Engineering*, Palm Springs, CA, Vol 2, pp. 927-936.
16. IBC, 2003. International building code, *International Code Council, Inc.*, Falls Church, VA.
17. Jain, S.K., and Navin, R. (1995). “Seismic overstrength in reinforced concrete frames.” *Journal of Structural Engineering,* 121 (3), 580-585.
18. Krawinkler, H. and Nassar, A. (1992). “Seismic design based on ductility and cumulative damage demands and capacities.” Nonlinear Seismic Analysis and Design of Reinforced Concrete Buildings, edited by Krawinkler, H. and Faifar, P., Elsevier Applied Science, 95-104.
19. Krawinkler, H. and Seneviratna, G.D.P.K. (1998). “Pros and cons of a pushover analysis for seismic performance evaluation.” *Engineering Structures*, 20, 452-464.
20. Krawinkler, H. (1999). "Challenges and progress in performance-based earthquake engineering." *International Seminar on Seismic Engineering for Tomorrow - In Honor of Professor Hiroshi Akiyama, Japan.*
21. Krawinkler, H. (1999). "Structural engineering issues in performance based earthquake engineering." *PEER White Paper.* http://peer.berkeley.edu/research.
22. Krawinkler, H., Zareian, F., Medina, R. A. and Ibarra, L. F. (2006). "Decision support for conceptual performance-based design." Earthquake Engineering &n Structural Dynamics, 35(1), 115-133.
23. Lai, S. P. and Biggs, J.M. (1980). “Inelastic response spectra for a seismic building design.”, *Journal of Struct. Div.*, ASCE, Vol. 106, No. ST6, pp. 1295-1310.
24. Lee, D.G., Choi, W.H., Cheong, M.C., and Kim, D.K. (2006). “Evaluation of seismic performance of multistory building structures based on the equivalent responses.” *Engineering Structures* 28, 837-856.
25. Marino, E. M., Nakashima, M. and Mosalam, K. M. (2005). “Comparison of European and Japanese seismic design of steel building structures.” Engineering Structures 27 (2005) 827-840.
26. Masumi, A., Tasnimi, A.A., and Saatchoglu, M. (2004). “Prediction of seismic overstrength in concrete moment resisting frames using incremental static and dynamic analysis.” *Proc. of 13th World Conference on Earthquake Engineering*,

Vancouver, B.C., Canada.

27. Medina, R. A. (2003). "Seismic demands for nondeteriorating frame structures and their dependence on ground motions. " *PEER Report 2003/15, Stanford University*, CA
28. Medina, R. A. (2004). "Story shear strength patterns for the performance based seismic design of regular frames." *ISET Journal of Earthquake Technology,* 41 (1), 101-125.
29. Medina, R.A. and Krawinkler, H., (2005). Evaluation of drift demands for the seismic performance assessment of frames, *ASCE Journal of Structural Engineering* 131(7), 1003-1013.
30. Medina, R. A. and Krawinkler, H., (2005). "Strength demand issues relevant for the seismic design of moment-resisting frames." *Earthquake Spectra*, Vol. 21, No. 2, pp. 415-439.
31. Menum, C. and Fu, Q., (2002). "An analytical model for near fault ground motions and the response of SDOF systems." *Proc. 7th U.S. National Conf. on Earthquake Engineering*, Boston, MA.
32. Mexico City Building Code (2003)
33. Miranda, E. (1993). "Site-dependent strength reduction factors." *Journal of Structural Engineering* ASCE, Vol. 119, No.12, pp. 3 505-3 519
34. Miranda, E. (1997). "Strength reduction factors in performance-based design." *EERC-CUREe Symposium*, Berkeley, CA.
35. Moghaddam, H. and Hajirasouliha, I. (2006). "Fundamentals of optimum performance-based seismic design." *1st European Conference on Earthquake Engineering and Seismology*, Paper Number: 100, Geneva, Switzerland, September
36. Nassar, A.A. and Krawinkler, H. (1991). "Seismic demands for SDOF and MDOF systems." *Report No. 95*, John A. Blume Earthquake Engineering Center, Stanford University, CA.
37. Newmark, N.M. and Hall, W.J. (1973). "Seismic design criteria for nuclear reactor facilities." *Report No. 46*, Building Practices for Disaster Mitigation, National Bureau of Standards, U.S. Department of Commerce, pp. 209-236.
38. Osteraas, B. and Krawinkler, H. (1990). "Strength and ductility considerations in seismic design." Report No. 90, *Stanford University*, Stanford, CA.
39. Park, K. and Medina, R.A. (2006). "Lateral load patterns for the conceptual seismic design of frames exposed to near-fault ground motions." *Proc. of 8th National Conference of Earthquake Engineering*, San Francisco, CA, USA.
40. Park, K. and Medina, R. A. (2007). "Conceptual seismic design of regular frames

based on the concept of uniform damage." *Journal of Structural Engineering,* 133 (7), 945-955.

41. Riddell, R., and Newmark, N.M. (1979). "Statistical analysis of the response of nonlinear systems subjected to earthquakes." *Structural Research Series* No. 468, Dept. of Civ. Engrg, University of Illinois, Urbana.
42. Riddell, R., Hidalgo, P., and Cruz, E. (1989). "Response modification factors for earthquake resistant design of short period structures." *Earthquake Spectra*, Vol. 5, No. 3, pp. 571-590.
43. Riddell, R. (1995). "Inelastic design spectra accounting for soil conditions." *Earthquake Engrg. And Struct. Dynamics*, Vol 24, pp. 1491-1510.
44. SEAOC Vision 2000 Committee, Performance-Based Seismic Engineering, Report prepared by Structural Engineers Association of California, Sancramento, California, 1995.
45. Shome N. and Cornell, C.A. (1999). "Probabilistic seismic demand analysis of nonlinear structures." Reliability of Marine Structures Program Report No. RMS-35, Dept. of Civil and Environmental Eng., Stanford Univ., Calif.
46. Somerville P, Smith N, Graves R, Abrahamson N. (1997). "Modification of empirical strong ground motion attenuation relationships to include the amplitude and duration effects of rupture directivity." *Seismological Research Letters*, 68:180-203.
47. Somerville P. (2000). "Characterization of near-fault ground motions." Proceedings of the US-Japan Workshop on Effects of Near-Fault Earthquake Shaking, San Francisco, CA, March
48. Takada, T., Hwuang, H.H.M., and Shinozuka, M. (1988). "Response modification factor for multiple-degree-of-freedom systems." *Proc. of 9th World Conference on Earthquake Engineering*, Tokyo, Kyoto, Japan.
49. Teran-Gilmore, A. (1997). "Energy concepts and damage indices.", Berkeley, CA. (http://nisee.berkeley.edu/lessons/teran-gilmore.html)
50. Teran-Gilmore, A. (2004). "On the use of spectra to establish damage control in regular frames during global predesign." *Earthquake Spectra*, 20 (3), 995-1020
51. Teran-Gilmore, A. and Jirsa, J.O. (2005). "A damage model for practical seismic design that accounts for low cycle fatigue." *Earthquake Spectra*, Vol. 21, No. 3, 803-832
52. Uang, C. M., (1991). "Establishing R (or Rw) and Cd factors for building seismic provisions." *Journal of Structural Engineering,* 117 (1), No. 25439.

53. Vamvatsikos, D. and Cornell, C. A. (2002). “Incremental dynamic analysis.” *Earthquake Engineering and Structural Dynamics*, Vol. 31, pp. 491-514.

54. Vidic, T., Fajfar, P. and Fischinger, M. (1992). “A procedure for determining consistent inelastic design spectra.” *Proc. Workshop on Nonlinear Seismic Analysis of RC Structures*, Bled, Slovenia, July.

55. Whittaker, A. and Moehle, J. and Higashino, M. (1998). "Evolution of seismic building design practice in Japan." *Struct. Design of Tall Buildings,* 7, 93-111